INSIDE THE BLUE COLOR: SOCIAL AND METHODOLOGICAL INVESTIGATION OF THE TURQUOISE COLORED BEADS FOUND IN NEOLITHIC BARCIN HÖYÜK IN NW ANATOLIA

By

AYŞE BURSALI

A thesis submitted to the

Graduate School of Social Sciences and Humanities

in Partial Fulfillment of the Requirements for

the Degree of

Master of Arts
in

Archaeology and History of Art

Koç University

August 2017

Koç University

Graduate School of Social Sciences and Humanities

This is to certify that I have examined this copy of a master's thesis by

Ayşe Bursalı

and have found that it is complete and satisfactory in all respects,

and that any and all revisions required by the final

examining committee have been made.

Committee Members:

_____

Asst. Prof Rana Özbal

_____

Prof. Hadi Özbal

_____

Asst. Prof. Emma Baysal

Date: _____

ABSTRACT

Items of personal ornamentation can reveal much about past societies. This thesis investigates turquoise-blue colored beads found in the seventh millennium BCE site of Barcın Höyük in northwest Anatolia, to reveal the raw material and the techniques involved in the manufacture of the artificially-produced turquoise color. Similar beads are also found in nearby contemporaneous Neolithic and/or Early Chalcolithic sites, sometimes along with genuine turquoise-stone. Considering the similarity in color and shape with beads of turquoise stone, and that turquoise sources lie long distances away from Anatolia, the possibility of imitation is examined. Possibility for imitation also leads to a consideration of imbalances with regard to access to raw materials, and what this could mean for social differentiation in Neolithic Anatolia.

A range of different instrumental analyses was conducted on Barcın beads, including optical microscopy, Raman, FTIR (Fourier transform infra-red spectroscopy) and SEM with EDX (Scanning electron microscopy with energy-dispersive X-ray spectroscopy). The analyses revealed that the beads were made of fluorapatite, resulting from the natural transformation of the bone matrix. Laboratory experiments were further conducted on modern and archaeological bones and similar materials, to attempt to replicate the turquoise-blue color of the beads and to understand the production process.

Keywords: beads; Barcın Höyük; Neolithic period; turquoise; personal ornamentation items; instrumental analyses; apatite; heat treatment.

ÖZET

Kişisel süslenme eşyaları geçmiş toplumlar hakkında bir çok bilgi verebilir. Bu çalışmada M.Ö. yedinci binyıla tarihlenen ve kuzeybatı Anadolu'da bulunan Barcın Höyük yerleşiminde ortaya çıkarılan turkuaz renkli boncuklar incelenmektedir. Çalışmanın amacı bu boncukların hammaddesini ve insan eliyle elde edildiği görülen turkuaz rengin imal edilmesini sağlayan metotları ortaya çıkarmaktır. Benzer boncuklar, bazen turkuaz taşından yapılmış boncuklarla birlikte, Anadolu ve Orta Doğu'da Neolitik ve/veya Erken Kalkolitik döneme tarihlenen başka yerleşimlerde de ortaya çıkarılmıştır. Turkuaz taşından yapılan boncuklarla aralarındaki renk ve şekil benzerliği, ve turkuaz taşı kaynaklarının Anadolu'dan coğrafi olarak uzak olduğu düşünülürse, turkuaz renkli (fakat taş olmayan) boncukların, bu taşı taklit amaçlı yapılmış olma ihtimali de bu çalışmada ele alınacaktır. Taklit ihtimali ayrıca Neolitik dönemde Anadolu'da, hammaddeye erişim açısından bir dengesizlik olabileceğini düşündürür, ve bu durumun bu dönemde sosyal farklılaşma açısından ne anlama gelebileceğini değerlendirmeye yöneltir.

Barcın Höyük boncukları üzerinde optik mikroskopi, Raman, FTIR (Fourier dönüşümlü kızılötesi spektroskopisi), ve SEM-EDX (enerji dağılımlı X-ışını spektroskopisiyle birlikte taramalı elektron mikroskopisi) gibi aletli analizler yapılmıştır. Bu analizler boncukların, kemik matriksinin doğal dönüşümünden meydana gelen flüorapatit maddesinden oluştuğunu ortaya çıkarmıştır. Bu sonuç üzerine, boncuklardakine benzer bir turkuaz rengi elde edebilmek ve boncukların üretim sürecini anlayabilmek için, modern ve arkeolojik hayvan kemikleri ve benzer materyaller üzerinde laboratuvar deneyleri yapılmıştır.

Anahtar Kelimeler: boncuk; Barcın Höyük; Neolitik dönem; turkuaz; kişisel süs eşyaları; aletli analiz; apatit; ısıl işlem.

ACKNOWLEDGEMENTS

Professor Hadi Özbal's guidance and knowledge made it possible for this study and thesis to become what it is now; he has advised me on problems and subjects I would not have been able to grasp and investigate if it was not for his help. I am highly indebted to him, and I highly appreciate how he always made time for my endless questions, and his willingness to help me along.

Rana Özbal has been the best mentor, advisor and teacher I could ask for, and I feel lucky to have been able to work with her, to receive her insights and to have known her. She has been as patient with me as one can be. Her enthusiasm, resolve and guidance both set an example for me, and kept fuelling my interest in this subject and in archaeology. I think she has literally helped me begin to make my dreams come true as I slowly move towards a career in archaeology. I am forever indebted.

Emma Baysal initiated me to the subject at hand and opened up the world of personal ornaments to me. Her expertise in the field and her eagerness to transfer her knowledge were crucial in the realization of this study. She has been extremely supportive through my thesis process and her positivity helped me push forward in the most difficult of times. I am grateful that I had the chance to be advised by her.

Bilge Uluocak at Boğaziçi University Chemistry Department Laboratories, and Barış Yağcı, Ceren Yılmaz Akkaya, and Gülsu Şimşek at KUYTAM Laboratories of Koç University have all been very generous with their help, and I very much appreciate the time and effort they put aside for all the experiments that were done under the scope of this study.

The first steps of this thesis were undertaken in a course given by Professor Aslıhan Yener, and I would like to thank her for giving me the opportunity to explore this subject, as well as her comments and advice on a draft version of this study.

I would also like to express my gratitude to all my professors at the Archaeology and History of Art Department of Koç University for their guidance, and the staff at Koç University's Graduate School of Social Sciences and Humanities who have always been helpful with many kinds of problems I encountered.

I am very glad to have been a part of the Barcın Höyük team. Barcın Höyük excavations were where I had some of the most enjoyable moments of my life. I am thankful to everyone who has been a part of and has shaped my experience there. I especially would like to thank Fokke Gerritsen for making this possible. His guidance and knowledge are very valuable to me; and I am grateful to him for teaching me to try to think in different ways.

I can never thank my friends enough, who put up with me throughout this long and arduous journey. I'm grateful that they were there to support me and keep my spirits high. They are the best friends and colleagues I could hope for.

And lastly I'd like to thank my family. If it weren't for my parents, whose support I have no words to define, and their belief in me, none of this would have been possible. Their capacity for patience amazes me to no end. I am grateful for their influence on my life. And my grandparents, whom I like to dedicate this thesis to; I hope to come close to the example you set for me. I am very glad to have known your love and I know you would be proud. I love you. Thank you.

TABLE OF CONTENTS

LIST OF TABLES

LIST OF FIGURES

CHAPTER 1: INTRODUCTION

This thesis investigates turquoise-blue colored beads recovered from the seventh millennium BCE Neolithic levels of Barcın Höyük excavations in Yenişehir, Bursa, Turkey. Although all have the same color, except for difference in tones from cobalt to greenish, these beads seem to be divided into two categories by their color scheme and material. The main visual difference that led to this conclusion was that while some beads sport a homogenously turquoise-blue color, both on the exterior and interior as well as all the way through; others only sport this color on their exterior, including the piercings through which they were strung, but are colored white in their interiors as can be visible by chips and breaks in the beads. Some beads display this white color through bandings and blotches on their exterior surfaces as well. Coupled with the more stone-like and crystalline qualities of the homogenously turquoise-blue beads observed in the breaks, this led us to tentatively conclude that the wholly blue beads are made of stone, whereas others were made of a clay-like material, possibly man-made and painted (with an initial categorization of 85 as clay/plaster and 149 as stone (Baysal, personal comm. 2017)). The similarity in color, and finds of beads made of this stone in few Anatolian and Near Eastern Neolithic sites brought to mind the possibility that the (tentatively-called) stone beads may have been made of turquoise stone, though they seemed to be missing

some other visual cues, such as veins, that are characteristic of the semi-precious turquoise stone. However to be able to further comment on this issue, the raw material of the two different categories of beads had to be established with certainty. Thus, the aim of this thesis is to find out the material of these beads and to look into the possible coloring techniques of the beads, as well as to comment on what social implications the certain special coloring of the beads may have.

To establish the material of the beads for certain, a number of beads were subject to instrumental analysis, and experimental analyses were made on other materials to try to understand the technology used for their production. In total 20 beads and bead fragments were tested. Some of these bead fragments were categorized as samples, and were given separate BH numbers than the bead they belong to. Throughout this thesis, the BH number that is mentioned refers exclusively to the artefact that has been tested, be it a fragment or whole bead. However the actual BH number of the bead that the fragment belongs to, is also reported whenever possible. A table showing which fragment belongs to which bead can be seen in Table 1, for the ease of the reader.

BH # of the analyzed artefact	BH # of the bead it belongs to
BH 37394	**BH 34381**
BH 37395	**BH 32761**
BH 37398	**BH 5463**
BH 37400	**BH 17320**
BH 37622	**BH 31179**
BH 37399	**BH 30875**
BH 17556	**-**

BH 22451	**-**
BH 21476	**-**
BH 18294	**-**
BH 17299	**-**
BH 32714	**-**
BH 18358	**-**
BH 37621	**BH 24875**
BH 37393	**BH 30868**
BH 37397	**BH 14263**
BH 37617	**BH 37502**
BH 37620	**BH 20702**
BH 37629	**BH 36173**
BH 37627	**BH 26720**

Table 1 - BH numbers of the analyzed bead fragments and the corresponding beads where applicable

Optical microscopy, scanning electron microscopy (SEM) coupled with energy dispersive X-ray spectroscopy, Fourier transform infrared spectroscopy (FT-IR) and Raman were the techniques used in the scope of this thesis. The details of these methods and their results can be found in Chapters 4, 5, and 6. As per the results of these instrumental analyses, experimental analyses were also undertaken to re-create the color of the beads on different kind of materials, such as modern and ancient bone, and fossilized tooth. The experiment design was mostly borrowed from Taniguchi et al's (2002) work with similar material.

XRF and XRD analyses were also conducted on the blue beads, however the results of these tests were acquired after the analysis phase of this thesis, and are outside the scope of this thesis. The XRD results are included in Appendix G.

The XRF results are included in Appendix H, and pXRF results are included in Appendix I, for future work.

Apart from Barcın Höyük, the turquoise-blue beads with white interiors are found in many other Neolithic and/or Early Chalcolithic sites across the Anatolian and the Near Eastern landscape. A review of published material and unpublished research shows that so far they seem to have been discovered in nine other sites: Aktopraklık (Baysal 2016), Demircihöyük (Baykal-Seeher & Obladen-Kauder 1996: 308; Durgun 2012), Çukuriçi Höyük (Baysal, Emma; Barbara Horejs ERC Prehistoric Anatolia Project - personal comm. 2015), Can Hasan I (Baysal 2017), Yumuktepe (Caneva 2012: 25), Çatalhöyük (Bains 2012: 63, 84.), Köşk Höyük (Öztan 2012: 54, 58), Tepecik-Çiftlik (Bıçakçı, Godon, and Çakan 2012: 134), and Tell el-Kerkh (in Syria) (Taniguchi et al. 2002). The presence of the beads at these sites indicates that these blue beads were a widespread phenomenon during this period in Anatolia and the Near East, and that the Barcın occurrence was part of a larger trend. In two of these sites, Tell el Kerkh (Taniguchi et al. 2002) and Çatalhöyük (Bains 2012: 63), there is also evidence that genuine turquoise stone beads exist, alongside the beads with white interiors.

One book chapter (Bursalı et al. 2017) and one conference proceeding (of the Raw Materials 2016 Conference in Faro, Portugal, submitted) written beforehand about the subject matter of this thesis and co-authored by the author of the thesis are extensively used in this thesis.

1. 1 Turquoise as an Exotic Good?

There are no known turquoise sources in Anatolia (Khazeni 2014). One would think that real turquoise must have been difficult to obtain in Anatolia and the Near East, as the closest source of turquoise, the Sinai Peninsula, lies roughly 2,300 km away from northwestern Anatolia, followed by Nishapur in Iran, which is approximately 3,400 km away. The difficulty in the access to genuine turquoise stone in the area could imbue it with importance and meaning – per the writings of Mary Helms (1988) –, and make these products "exotic".

The power of goods that come from long distances and the influence of geographical distance are discussed by Mary Helms in *Ulysses' Sail* (1988). Helms is primarily concerned with how knowledge of distant lands becomes "part of the corpus of esoteric knowledge controlled by political-religious specialists as an attribute and legitimation of their status, power and authority" (Helms 1988:11). The special meaning ascribed to things that travel long geographical distances is not only limited to knowledge however, but is extended to objects as well: "The curious and unfamiliar objects that are most marked by cosmic power are frequently those that are not immediately at hand, but must be obtained by some exceptional effort… It is no accident that material goods that come from a distance – like those that are extracted from the earth or sea – are likely to be considered as unique and powerful, as containing exceptional potency and magical strengths and abilities" (Helms 1988: 114). Turquoise stone is one item that would have been extracted from the earth – from its ores in Sinai or Nishapur. Coincidentally, Helms illustrates her point with the trade of turquoise beads by the Navajo people: "[T]he ceremonial and special status goods sought by the Navajo in foreign trade included turquoise beads…"

(Helms 1988: 119-120). Additionally, the Navajo believed the beads to be "particularly dangerous because of foreign association" and ritually purified them so they could be handled safely (Hill 1948: 391; Ford 1972: 44; both as cited in Helms 1988:120).

In her investigation of possible inequalities in Çatalhöyük based on household goods, Wright similarly posits that "an artefact type may have had special value (1) if it is made of material imported from a considerable distance; (2) if there were difficulties associated with importing; and (3) if manufacture was unusually labor intensive" (Wright 2014: 12). Building on this assumption, we can propose that turquoise was a valuable material at the very least based on the distance it had to be transported to Anatolia.

Evaluating these items merely by their "exoticness or economic value" however, would be an entirely incomplete and narrow perspective of the vast array of information that we can actually extract from an item of personal ornamentation (Baysal and Miller 2016: 25). Investigation of such items can reveal much about the past societies, as can be seen in Section 1.2.

1.2. Personal Ornamentation in the Neolithic and Associated Problems

Beads, as items of personal ornamentation, can be interpreted as implying a variety of things. Worn attached to clothing items, or even directly on the bare body, beads function as a symbolic means of displaying identity and can be used as markers of age, affiliation, power or social status, revealing information without having to communicate with others (Kuhn and Stiner 2007: 45-54). Investigating the

origins and manufacture of ornamentation may also reveal connections of trade and exchange between groups, recreating links between past societies.

Neolithic period is a time of change with the beginning of farming and animal husbandry. During this period, beads may have also gained different meanings. Several studies, only a few of which are summarized below, show how bead studies can be helpful in answering important questions about the Neolithic society in Anatolia and the nearby regions.

Wright and Garrard (2003) theorize that appearance of farming and herding communities in Jordan coincides with an expansion in stone bead production due to changes in lifestyles and economic ways. Moreover, as people came into contact with new groups from far areas that were unreachable before, they felt a more urgent need to mark themselves as individuals and as a group to create social boundaries, and they did this with personal ornamentation items. Baysal (2013) examines the bead assemblages of Neolithic Pınarbaşı and Boncuklu in terms of technology, sense of personal expression and interactions with the wider landscape. Baysal concludes that some aspects of the bead traditions were influenced from foreign sources, while some stayed local. She also comments that the two sites shared the same values in choosing to preserve their beads. Healey and Campbell (2014) compare the obsidian artifacts of adornment from Neolithic sites of Domuztepe in Turkey and Tell Arpachiyah in Iraq, in terms of expertise in the production. Looking at different techniques of production, they conclude that the assemblages with higher standardization of obsidian suggest a centralized system of production, acquisition, and dispersal, at least in terms of values and skill, if not of the physical product. Bar Yosef and Porat (2008) take a more interpretive approach and comment that the

appearance of green stone beads at the beginning of the Neolithic is a rather symbolic reflection of the growing importance of agriculture in the lives of the Neolithic people.

Research on beads of the Neolithic period shows that beads and ornamentation are prolific areas for examining changes in a society, in identities, social dynamics and relationships. However, Neolithic research on ornaments hosts some inherent problems in its approach to examining these materials (Baysal and Miller 2016). As advocated by Baysal and Miller (2016), an individual-bead centered perspective of beads that considers each bead's own context and properties, rather than group them by typology and adhere to a rigid terminology, would provide a much better framework to study these items. The authors also turn to ethnographic studies of beads to establish a better methodology to examine them. In doing so they discover that the current methods of investigation overemphasize the visual or decorative purposes of ornamentation items to the detriment of other purposes. Current approaches also seem to overemphasize the economic value of the materials in lieu of the individual life-history of an item, considering the economic value over individual value, which hinders the unearthing of information about the cultural attitudes concerning personal ornamentation items in a society (Baysal and Miller 2016).

CHAPTER 2 – NORTH-WESTERN ANATOLIAN NEOLITHIC AND BARCIN HÖYÜK

2.1. Northwestern Anatolian Neolithic

Settlements in northwest Anatolia begin to appear towards the middle of the seventh millennium BCE around the Marmara Sea (Sagona 2009: 103). The Marmara region is frequently termed as a "stepping stone" in the spread of farming to Europe (Düring 2011: 195), and for a long time research has been plagued by prejudice in this direction (Özdoğan 2005). Interpretations on the Neolithic of northwest Anatolia traditionally focus on how there seem to be two distinctive cultures within the region, differentiating the coastal and inland sites (Özdoğan 2013). The coastal culture, represented by sites such as Pendik, Yenikapı and Fikirtepe, is characterized by round structures and more evidence of fishing (Düring 2011: 194-195). These sites are also claimed to be settled by the descendants of local hunter-gatherers who lived in the region before farming spread, based on the difference in subsistence (Özdoğan 2013). The inland sites, represented by Ilıpınar, Menteşe and Barcın Höyük, are claimed to be characterized by rectangular structures and more intense farming practices, whereas fishing is not of importance (Düring 2011: 194). These inland sites on the other hand, are settled by incoming farmers from the East (Düring 2011, 194). Both these cultures are still characterized by the existence of animal husbandry and dairy consumption (Düring 2011: 194). However more recent research may have begun to prove some of these theories wrong. Both

types of sites are revealed to have "identical portable material culture, including lithics, pottery and bone implements (Gerritsen and Özbal 2016: 206). Moreover, zooarchaeological research done by Çakırlar suggests that marine resources were not as dominant in the coastal sites as was believed (Çakırlar 2013: 70-73). Ongoing research and excavations in the region is sure to shed more light on these debates.

2.2. Personal Ornamentation in northwest Anatolian Neolithic

In Baysal's evaluation, personal ornamentation items in Neolithic Anatolia show great variation between and within regions (Baysal 2016), which Özdoğan attributes to "intramural traditions and grave goods" (Özdoğan 2016: 144). Baysal pinpoints a change in the ornamentation traditions in the second half of the 7th millennium BCE, where the earlier periods see individual items of long-term use (Baysal 2016: 52; Baysal and Miller 2016). Marine shells were also present even in inland sites (Baysal 2016: 52). In the Late Neolithic, repeated production became more prevalent; and the emphasis shifted to larger size, the color white and more complex production technologies (Baysal 2016: 53; Baysal 2017). In this later era, shells continued to be used but shifted to types that could be used as food sources unlike earlier ones that could not (Baysal 2016: 53).

The Northwestern Anatolian Neolithic personal ornamentation tradition involves materials such as marine shells, various stones (including marble) and bone-like material (Baysal 2016: 53). Instances of specific typologies being associated with specific materials are also witnessed (Baysal 2016: 53). This is best exemplified with the personal ornamentation assemblage of Barcın Höyük, which will be detailed

below. Bracelets are also part of the ornamentation assemblages of the area especially around the Eskişehir area (Baysal 2016: 53). Özdoğan moreover, mentions that sites around the Bosphorus in İstanbul area, such as Pendik, Fikirtepe and Yenikapı "show a number of variations" in items of personal ornamentation (Özdoğan 2016: 146). Shells seem to be prominently featured in the assemblages of Pendik and Yenikapı, whereas "no find resembling beads" have been found in Fikirtepe (Özdoğan 2016: 146).

2.3. Barcın Höyük

Barcın Höyük is a mainly seventh-millennium BCE Neolithic mound in Northwestern Anatolia in Yenişehir, Bursa. The site covers an area of 0,5 ha consisting of two mounds, and also has Late Chalcolithic, Early Bronze Age and Byzantine levels. However, these are not as extensive as the seventh millennium BCE Neolithic levels (Gerritsen, Özbal and Thissen 2013: 93-100). Barcın Höyük has been first recorded by James Mellaart and David French in the 1960s (Mellaart 1955: 53-80; French 1967: 49-100). It was later surveyed by Mehmet Özdoğan in the 1980s (Özdoğan 1986). The site was investigated under the scope of Netherlands Institute of Archaeology's (NIT) Early Farming Communities Research Project, under the direction of Jacob Roodenberg in 2005-6, and then of Fokke Gerritsen and Rana Özbal between 2007 and 2015 (Gerritsen and Özbal 2012). Study seasons continue.

The Early Farming Communities Research Project aims to study the westward spread of agriculture from the Near East to Europe. Through the

archaeological evidence in the Eastern Marmara region, where Barcın is also located, the role of the region in the spread of farming is documented (Gerritsen and Özbal 2012). These investigations in the past few years revealed that Barcın Höyük housed the earliest sedentary inhabitants of the Marmara region (Gerritsen and Özbal 2016) that belong to the initial wave of agricultural pioneers.

The Neolithic layers of Barcın Höyük date to between 6600 BCE and 6000 BCE. Five main Neolithic phases have been identified based on stratigraphical information and pottery analyses. Throughout all these phases one observes how Neolithic lifestyle takes its full shape. Agriculture and animal husbandry with domesticated species were practiced in the settlement beginning from even the earliest phase (Gerritsen, Özbal and Thissen 2013: 93-100). Barcın has further proved substantially helpful in providing information about the beginnings of milk production and consumption, through many analyses done on the animal fat lipids found inside the ceramic material (Thissen et al. 2010).

2.4. Overview of Items of Personal Ornamentation in Barcın Höyük

More than 700 beads were unearthed at Barcın Höyük (Baysal 2016: 53). Baysal find the range of bead types at Barcın "remarkably diverse" with stone and shell being the dominant materials (Baysal 2014: 9). According to Baysal's publication at the end of the 2014 season, Barcın beads included beads of turquoise blue color thought to be made of stone and manufactured materials (41%), beads of marine shells (31%), various types of stone (24%), clay (2%) and bone (2%) (Baysal 2014: 2). The stone bead typology is limited to seven bead forms and one pendant type, and the majority of the beads are simple short forms and basic disc beads (72% of the assemblage) (Baysal 2014: 2). Limestone and marble of different colors are

the most used stone materials, and "most stone procurement was probably on a local basis and related to locally available materials" (Baysal 2014: 3). Shell beads and pendants, both of freshwater and marine species, make up 30% of the bead assemblage of Barcın (Baysal 2014: 5-6). In terms of shapes, Baysal groups the shell beads into "those used in their natural form and those where shell is used as a raw material for the production of shapes unrelated to natural form" (Baysal 2014: 6). Clay and bone beads were found in very low numbers. The blue beads of the assemblage will be detailed in Chapter 3, "The Beads".

Due to the "relatively consistent production practices" of Barcın, Baysal identified the core types, and also found "relatively low level of overlap between the typologies of different materials", though the disc bead was the most common (Baysal 2014: 9). Baysal's findings demonstrate that "different values were attributed to different bead forms and materials" (Baysal 2014: 9). At Barcın the shell beads, Spondylus sp. being one example, show more similarity to the Balkan practices than Anatolian, which reflects the proximity of Barcın to the Balkans, though long-lived traditions that are common to Anatolia and the Near East are also witnessed (Baysal 2014: 9). Barcın can be said to have "participated in wider material culture practices of the Neolithic" and the stone disc beads is one of the most extensive of these traditions (Baysal 2014: 9)

CHAPTER 3 – THE BEADS

3.1. The Barcın Blue Beads

Figure 1 Selection of blue colored beads from Barcın Höyük (courtesy of Barcın Höyük Excavation Archive).

The turquoise-blue beads (see Fig. 1 and Fig. 2) comprise the largest single-material group in the Barcın Höyük bead assemblage and come in a range of tones of blue and turquoise. They constitute approximately one third of the bead assemblage discovered during the 2007-2015 excavation seasons, which amounts at least 236 blue beads (Baysal 2014: 2). The beads are made in a range of forms and sizes, and the most common type is the long and ovoid one (Baysal and Belcher 2016). Short and flat shapes are also encountered frequently, but disc beads are relatively rare (Baysal 2014: 5).

Both polished and matte looking examples can be found. The beads have a hardness level of 5 on Mohs scale, "which is harder than most of the stone used at the site and would therefore have required more effort to work" (Baysal 2014: 5). Baysal further reports that piercing these beads must have been challenging, as the "difficulty that was encountered in getting the bi-directional piercing to meet in the middle of the bead" can be visibly seen in the broken examples (Baysal 2014: 5).

Figure 2 Barcın blue beads in varying shades of blue and possible bead blanks (courtesy of Barcın Höyük Excavation Archive).

Even though the exterior of some of the beads are turquoise in color, the white material possibly used their production becomes visible in chips and breaks (Fig. 2). White areas and bands on the outer surface also often betray that these beads are not of turquoise stone (Bursalı et al. 2017). However, this difference in color is not always the case with the blue beads of Barcın, as beads that are all the way blue (both inside and outside) are also frequently encountered in the blue bead assemblage. Due to the difference in their coloring and textures of the material, the beads were initially thought to be made of two different materials, stone (64%) (149)

and clay/clay-like material (%36) (85) (Baysal 2014, 4). This categorization was made based on observations on the color, piercing type, surface characteristics (shiny, matt, smooth), material characteristics (striated or homogenous), and inner color (Baysal, personal comm. 2017).

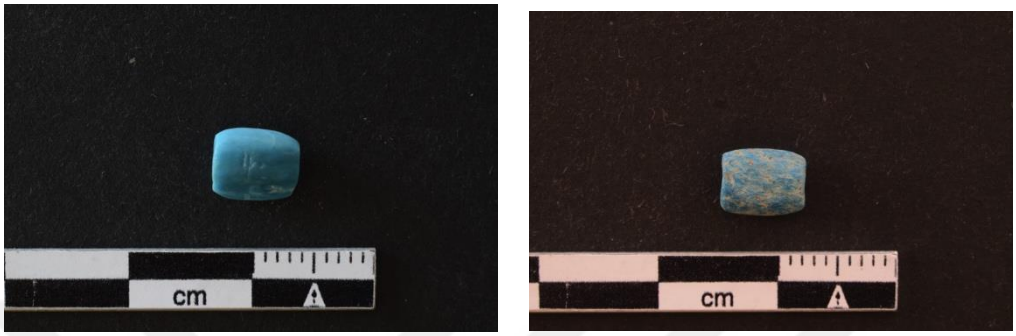

Figure 3 Barcın blue beads (courtesy of Barcın Höyük Excavation Archive).

Except for few burials yielding clusters, the beads are found individually. They are not typically reserved to a single context and appear in almost all kinds of deposits. We believe that some evidence of their production may exist considering the discovery of a few bead blanks that follow the same typology of the blue beads but feature solely a white color. However more work would be necessary to reach conclusive information on whether their production took place at Barcın (Bursalı et al .2017).

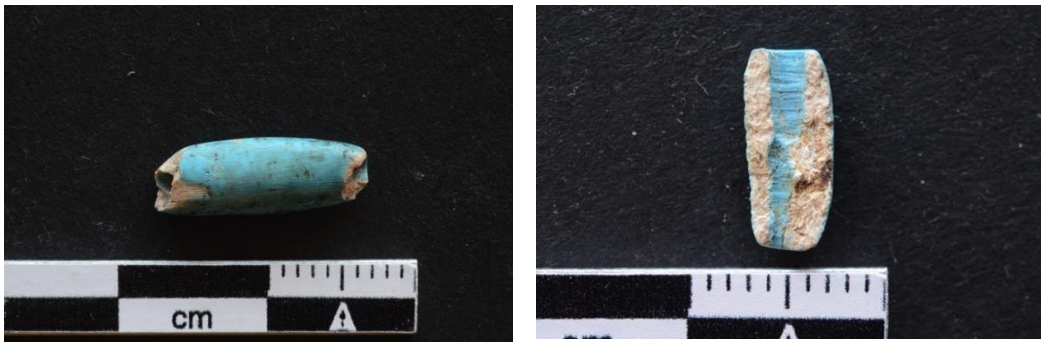

Figure 4 Barcın beads with white interiors (courtesy of Barcın Höyük Excavation Archive).

The relative rarity of the blue disc beads in the blue bead assemblage compared to the ratios of the beads made of other stones "suggests that the blue beads were distinguished from other stone beads" according to Baysal (2014: 5). Moreover, according to Baysal's analyses, the blue bead typology "includes a variety of forms that are unique to blue colored beads, regardless of material. These are the chip, long bead with round section, long with lenticular section, very long with lenticular section, short wide with lenticular section and bell-shape with wide lenticular section" (Baysal 2014: 5). Flattened lenticular forms are especially associated with blue coloring, and this is not seen in stone or shell beads (Baysal 2014: 5). In addition, "[t]he average length of blue beads is twice that of stone beads…, and the average piercing diameter is also much smaller" at 1.36 mm compared to the 2.55 mm of the general stone beads (Baysal 2014: 9).

Figure 5 Barcın blue beads (courtesy of Barcın Höyük Excavation Archive).

When considering the blue beads, Baysal (Baysal 2016: 56) puts forth that they "are a manifestation of one of the largest technological and stylistic trends of the end of the Neolithic period" due to their geographical and temporal prevalence and consistence. Baysal who has worked extensively on the blue beads also calls attention to the very limited number of forms these beads seem to come in, and to the fact that these forms are not usually encountered in other bead materials at the site (Baysal 2016: 56). Thus, the blue beads have non-local forms. To her, "[t]his suggests that these beads share either a common source or a culturally reinforced expectation about the forms suitable for a blue bead" (Baysal 2016: 56). Following this, Baysal reasons that the specific repertoire of shapes of the beads may suggest they originated from a single, and possibly foreign, source. Personal communication with Hala Alarashi further reveals the blue beads have forms connected with forms to the east, with bead forms from 7th millennium Euphrates region (Alarashi, personal comm. 2016). The only other possible explanation would be a specific "meaning associated with the forms" that is shared across the landscape, which leads to the exact reproduction of the bead forms (Baysal 2016: 56). For Baysal, "[t]he apparent skeuomorphism within the blue bead assemblage indicates that the blue color took precedence over material" (Baysal 2014: 5).

Figure 6 Barcın blue beads (courtesy of Barcın Höyük Excavation Archive).

3. 1.1. The Beads Used in this Study

In total, 20 beads and bead fragments were in the scope of the research undertaken for this study. Photographs for each bead can be found in Appendix A.

Reflecting the trend observed in the totality of the beads, the beads that were used in the study also come from various different contexts. 45% (9 out of 20) come from fill layers. 15% (3 out of 20) come from pits, 10% (2 out of 20) come from surfaces, and the rest come as single beads from an oven, a basin, a platform-bench, a post-hole row, and an exploratory context.

The breakdown of which bead went through which analyses can be seen in Table 2 in Chapter 4 – Methods and in Appendix B.

In the optical microscope and scanning electron microscope (coupled with energy dispersive x-ray) analyses, the main aim was to see if the beads were made of different raw materials, so the beads were chosen for the blatant differences in their appearances – in terms of properties that would signal whether they were of stone or clay – especially for the visible differences in their textures. These analyses were non-destructive so we had a certain amount of freedom when choosing the samples.

Even though the questions that we asked did not change, FTIR analyses required a different kind of sampling technique because FTIR is a destructive analysis that requires the sample to be in a powdered form. Since this would mean that the part of the bead that is sampled would be lost forever, we had to choose the bead fragments that were large enough to be available for further analyses in the future, even when parts of them were broken off and crushed into a powder. The six beads that were used in the FTIR analyses were chosen with this idea in mind, but attention was still paid to make sure there was a difference in the color of these beads, both within one bead as well as between the beads. To be able to get reliable results, and to be able to compare the differently-colored parts of a single bead, two different samples were taken from each bead that was to be analyzed under FTIR, whenever possible.

3.2. Similar Finds from Other Sites

3. 2. 1. Tell el-Kerkh

Tell el-Kerkh is a Neolithic mound occupied from around 6500 BC to 5000 uncal. BC near Idlib in Northwestern Syria (Taniguchi et al. 2002:175). Excavations at sixth-millennium levels of Tell el-Kerkh yielded blue beads with "lustrous light-blue surfaces", resembling the ones found at Barcın Höyük, and the first scientific analyses on these artificially colored blue beads were conducted here. However, beads of turquoise stone are also found at this site. Moreover, the turquoise stone comprised the majority of the beads of blue coloring; of the 32 turquoise-colored beads, only eight exhibited a whitish core. These were all "lozenge-section beads,

having an oval-shaped or square-shaped plan, which [was also] quite popular and typical among the stone beads of Tell el-Kerkh" (Taniguchi et al. 2002: 176). Seven of the eight blue beads were found in layers dated to 5700-5300 uncal. BC and the other one from layers dated to 5300-5000 uncal. BC (Taniguchi et al. 2002: 176). The excavators note that the turquoise is the farthest traveled material for stone beads found at the site, with a distance of either 600 km (to Sinai) or 1000 km (to Iran and Afghanistan). The authors interpret these blue colored beads as imitations; given that real turquoise is difficult to obtain in this region the inhabitants must have supplemented their supply of true turquoise with these "imitation" beads (Taniguchi et al. 2002: 176).

Figure 7 Blue beads with white cores from Tell el Kerkh, from Taniguchi et al. 2002: 176.

The researchers subjected three beads to scientific analyses such as binocular microscope, spectrophotometer, scanning electron microscope, X-ray fluorescence spectrometer, X-ray diffraction, and Fourier transform infrared spectroscopy (Taniguchi et al. 2002: 176-7). In their analysis, the researchers discovered that one of the beads had a "peculiar ivory-like texture" and as a result associated the beads with "ivory or fossil mastodon such as 'odontolite'". XRD analysis revealed the most common mineral in the 3 beads as fluorapatite or hydroxyapatite, but a distinction

between the two materials was not possible (Taniguchi et al. 2002: 177). FTIR analysis also identified apatite, and neither FTIR nor XRD was able to provide information on the blue areas or any kind of dye that could have been used to color the bone (Taniguchi et al. 2002: 177). On the other hand, the XRF analysis revealed that calcium and phosphate were the main components of the white cores, which led the researchers to believe that these may have substituted calcium during fossilization (Taniguchi et al. 2002: 178). XRF further revealed the blue surfaces of the beads to have "MnO (0.13-0.22wt%), Fe_2O_3 (0.06-0.09wt%), MgO (3wt%), Al_2O_3 (3wt%), SiO_2 (7wt%) and K_2O (0.8wt%), with high amounts of titanium and minor amounts of copper, zinc and strontium as trace elements" (Taniguchi et al. 2002: 178). The researchers interpret alumina and silica as associated with environmental contamination, and believe that minor elements such as arsenic and lead could have been used for substitution during fossilization (Taniguchi et al. 2002: 178). Taking this information into account, the Tell el-Kerkh researchers conclude that "the core of the blue beads may be interpreted as fossilized animal teeth or tusks" (Taniguchi et al. 2002: 179).

Figure 8 Cross section of blue bead 'Bead 1' found in Tell el Kerkh excavations, from Taniguchi et al. 2002: 179.

Spectral reflectance curves showed only one broad band, which means that the color of the beads "did not result from a mixture of blue with yellow" (Taniguchi et al. 2002: 178). The optical microscope revealed a pattern resembling annual rings, and SEM analysis found "no distinct interface between the colored blue layer and the white core" and that "the blue layer is not as distinct as a glaze or a paint layer" (Taniguchi et al. 2002: 178). The only elements that may be related to coloring which showed up in XRF analysis can be manganese and iron, according to the researchers (Taniguchi et al. 2002: 179). Analyses of the blue exteriors of the three beads also consistently yielded elevated elemental results for manganese and iron when compared with the cores. (Taniguchi et al. 2002: 178) Given these factors and the fact that they also lacked the vitreous surface of a glaze under SEM, the beads were identified as being ivory or fossil mastodon ivory, known as odontolite (Taniguchi et al. 2002: 178-9). Furthermore, the researchers believe that the color

"was obtained possibly by heating with transition metal compounds including manganese or iron", and because blue color was observed even in small cavities, it is also assumed that the colorant was applied after forming and piercing the beads (Taniguchi et al. 2002: 180). After their experimental analysis however, which will be detailed further below in the Methods section, the researchers remark that heat treatment makes bone/tusk too weak to be shaped into beads (Taniguchi et al. 2012: 181). Their experimental production of the blue color (Taniguchi et al. 2002) will be detailed in the Chapter 4 – Methods.

3. 2. 2. Aktopraklık

Aktopraklık is a Neolithic and Early Chalcolithic site in the city of Bursa in northwest Turkey, dating to between 7th and 6th millennia BCE, though not based on radiocarbon dates (Karul and Avcı 2013: 52). In total, 13.000 beads have been recovered from Aktopraklık, and the blue beads comprise the second largest group of beads in the assemblage (Baysal 2016: 53-4). The beads can be seen to be both matte and polished (Baysal 2016: 54). Baysal further reports that these beads, like the Barcın ones, range in color from "pale washed-out blue to a deep cobalt shade" and that the "most common shape is an elongated and lenticular-profiled barrel form. There are also some shorter versions of this same form as well as disc beads and flat 'chip' shapes" (Baysal 2012: 54). The specific forms of the blue beads are not seen in beads made of other materials.

Figure 9 – Blue beads found in Aktopraklık, from Baysal 2016: 55.

3. 2. 3. Çukuriçi Höyük

Çukuriçi Höyük is a mound in İzmir in Western Anatolia dated to the Late Chalcolithic (4th millennium BCE), and Early Bronze Age periods (Horejs 2014: 15). Although there is no published material on the blue colored beads found at Çukuriçi, personal communication with Dr Emma Baysal, (courtesy of Barbara Horejs and ERC Prehistoric Anatolia Project) who investigates the beads at the site informs as that blue colored beads do exist at the site.

3. 2. 4. Demircihöyük

Demircihöyük is a Chalcolithic and Early Bronze Age mound in Eskişehir in Northwestern Turkey, with also traces of a Neolithic settlement (Korfmann 1983: 242 as cited in Durgun 2012: 23). In Demircihöyük, 6 beads with light blue or turquoise exteriors and white interiors were unearthed (Baykal-Seeher & Obladen-Kauder 1996: 308). (Although a later study reports that there are 10 bone beads in total at Demircihöyük (Durgun 2012: 209), the coloring of the other 4 beads is not known from the information given.) This was noticed from the broken beads, where the interior was "always white and fractured surface uneven" (Baykal-Seeher & Obladen-Kauder 1996: 308). Baykal-Seeher and Obladen-Kauder report that the analysis on one of the beads revealed the chemical composition of ivory, and argue that the color may be due to the deposition of the beads in a copper or cobalt solution. However, they do add that this is not an exact result, as the color layer is too thin on the sampled beads (Durgun 2012: 308). The Demircihöyük beads are 0.5-0.7 cm long with a round or oval cross-section, and the diameter of the hole is 0.1 cm (Durgun 2012: 308). Unlike at other sites, the Demircihöyük reports provide context information: Out of the six beads discussed in the Demircihöyük volume, only 3 are well-stratified and are from "Room 109 (Phase E2F1), from Room 108 (Phase H) and from the courtyard (Phase IK1)" (Durgun 2012: 209). It is possible that this material dates to before the Bronze age since few blue beads have been found in Demircihöyük, and no Bronze Age examples of such beads have been so far found in any other site. We can be suspicious that this is residual material from earlier contexts, as Demircihöyük also hosts Neolithic and Chalcolithic layers as well (Korfmann 1983: 242 as cited in Durgun 2012: 23).

3.2. 5. Çatalhöyük

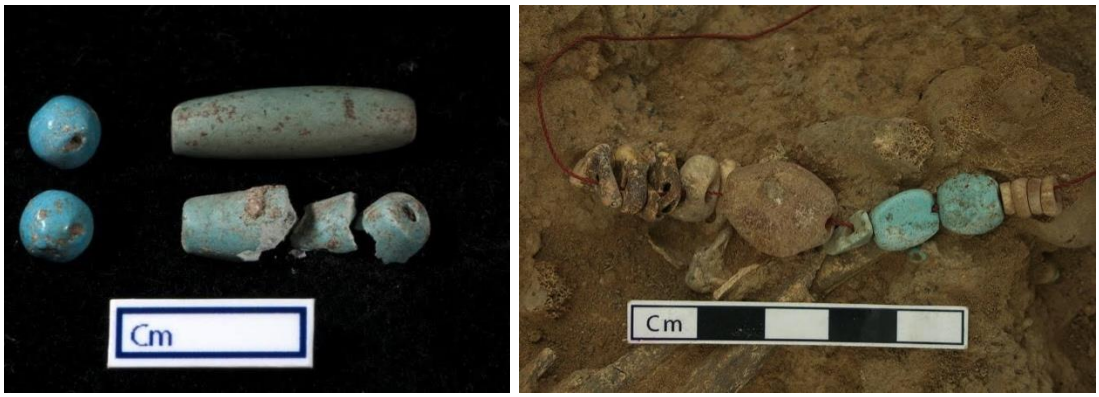

Figure 10 Blue "apatite" beads from Çatalhöyük (courtesy of Çatalhöyük Research Project, Jason Quinlan, licensed under CC BY-NC-SA 3.0).

Similar turquoise-blue colored beads at the Neolithic Çatalhöyük excavations in central Anatolia were identified as "fluorapatite" by Roseleen Bains. Bains writes that because some of the Çatalhöyük beads sport white blotches or banding, or appear altogether lighter, it is possible that they were made of a material other than fluorapatite, and most possibly odontolite (Bains 2012: 219). However, no further research was done to establish their material and Bains' conclusions have not been experimentally confirmed. Çatalhöyük also yielded beads of turquoise stone with smooth textures and a vitreous or dull luster. However, the "fluorapatite" beads with white interiors had "a much larger presence than turquoise" in Çatalhöyük and in fact, that they formed a "significant" portion of the stone bead assemblage (Bains 2012: 218). Fluorapatite beads are "found in all contexts except for in fills, such as pits, posts or bins or burials", whereas turquoise beads, which is one of the less common of the raw materials in the stone beads assemblage, are only found in burial fills or external middens and were never broken (Bains 2012: 218). Fluorapatite beads also seem to come in their own typology: "they are never featured as rings or

discs; instead they commonly take the form of lenticular (30.3% of fluorapatite), long elliptical beads (15.2%), and rectangular double perforation beads (13.6%)" (Bains 2012: 82-3). In a later publication Bains and colleagues further report that in Çatalhöyük "[i]n terms of forms, blue fluorapatite only appears in bead types that are individually made and therefore more labour intensive. The same can also be said for turquoise, the only other blue-colored raw material" (Bains et al. 2013: 340). Even though "pale to dark blue beads are such a small proportion of the assemblage", "they are found in all different context categories (Bains 2012: 93). Blue beads also have the highest breakage percentage "but do not appear to be intentionally broken", which Bains interprets possibly as an indication of blue beads being used "for longer or until broken more so than other coloured beads" (Bains 2012: 271-2). These all suggest that the color blue was considered to be of some importance. In light of the evidence that seems to render blue beads special, Bains argues that

> "[B]lue beads may be quintessential examples of stone beads illustrating a safe form of personal expression or individual identity during this time at Çatalhöyük…" as well as being "early examples of individuals or households conspicuously demonstrating their personal or household wealth, in a socially acceptable manner, all within the conservative framework of a conformist and unstratified Neolithic society. … [S]tone beads may be used as a means of initiating and differentiating oneself or a household from the community, in a non-threatening and benign manner. … Differentiating oneself or aligning oneself with a household, lineage, or ancestry through bead use may have been one of many potential steps towards asserting control or influence within the community, especially during the late Neolithic." (Bains 2012: 273)

Bains reports that fluorapatite beads are also featured prominently on skeletons in burials (Bains 2012: 206). An important note about blue-colored beads, a category which includes both fluorapatite and turquoise, is that in burials they are only found in adolescent and older adult burials, and never in neonate, infant or child burials (Bains 2012: 207). Moreover, they are never found in male burials, but only "in

female, indeterminate, or child burials", which Bains loosely theorizes that may be due to a connection with fertility or protection from death by childbirth (Bains 2012: 276).

3. 2. 5. 1. Possible Evidence for Production at Çatalhöyük

Bains also argues for evidence of production of fluorapatite beads, based on 4 instances of "preforms" (12826.H2 (Bains 2012: 124), 16253.H4 (Bains 2012: 125), possibly 12972.H7 (Bains 2012: 130), 13174.X4 (Bains 2012: 134)) and 2 instances of "roughouts" (12988.H9 (Bains 2012: 131), 14120.H7 (Bains 2012: 134)) (see Fig. 11). She puts forth that the presence of sandstone abraders and schist abrader knives, along with a finished fluorapatite bead next to preform 16253.H4 in Space 129 may mean that this is a production context (Bains 2012: 125). Likewise, she believes that unit 14120 where roughout 14120.H7 was found can also be a production context as one steatite preform, chert flakes and sixteen finished beads were also found in this context (Bains 2012: 134). The only other evidence Bains offers for production of fluorapatite beads is the presence of "linear abrasion manufacturing marks" on a lenticular bead, which she thinks "are likely due to a lack of final polishing" possibly due to time constraints that stopped it from being completely finished "before being buried as a necklace in an adolescent burial" (Bains 2012: 279). The SEM images of the said preform could possibly help identify manufacturing techniques (Bains 2012: 183). None of this however, provides conclusive evidence that production of such beads did actually take place at Çatalhöyük.

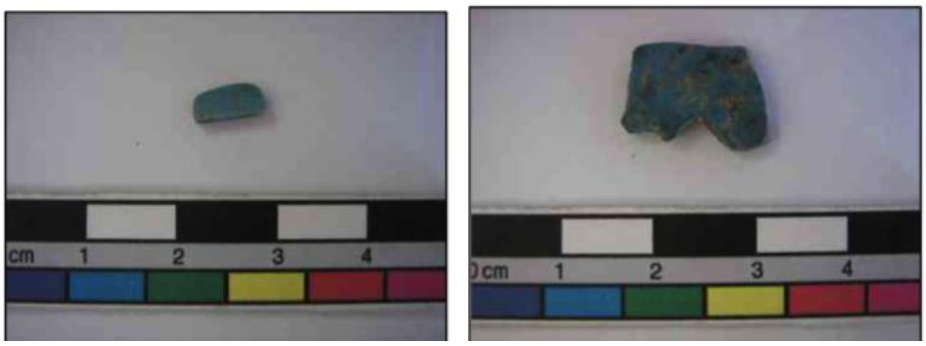

Figure 11 – Bains (2012) argues the fragments found in Çatalhöyük (pictured) may be preforms and may be evidence for production of such beads at Çatalhöyük, 16253.H3 on the left is defined as "half fragment of a finished lenticular square fluorapatite bead" and 16253.H4 on the right is defined as "fluorapatite preform", from from Bains 2012: 125.

3.2.5.2. Blue Pigment at Çatalhöyük

Çatalhöyük excavations also yielded blue colored pigments. PLM and Raman analyses of the pigments done by Duygu Çamurcuoğlu revealed them to be azurite "which could be the earliest known example of azurite in pigment form" (Çamurcuoğlu 2015: 147). With the chemical formula ($Cu_3(CO_3)_2(OH)_2$), azurite is copper-based. The blue azurite pigment was only found as grave goods in the burials of Çatalhöyük, and not in the numerous wall paintings, beginning from approximately 6700 cal. BC (Çamurcuoğlu 2015: 147). Interestingly, it was found particularly in the female and infant burials (Çamurcuoğlu 2015: 232). Since azurite, and the green pigment malachite have not been found in middens and fills, Çamurcuoğlu suggests "this may indicate the rarity and importance of these pigments, as they would not be regularly discarded, but only specially treated and used in certain contexts" (Çamurcuoğlu 2015: 234).

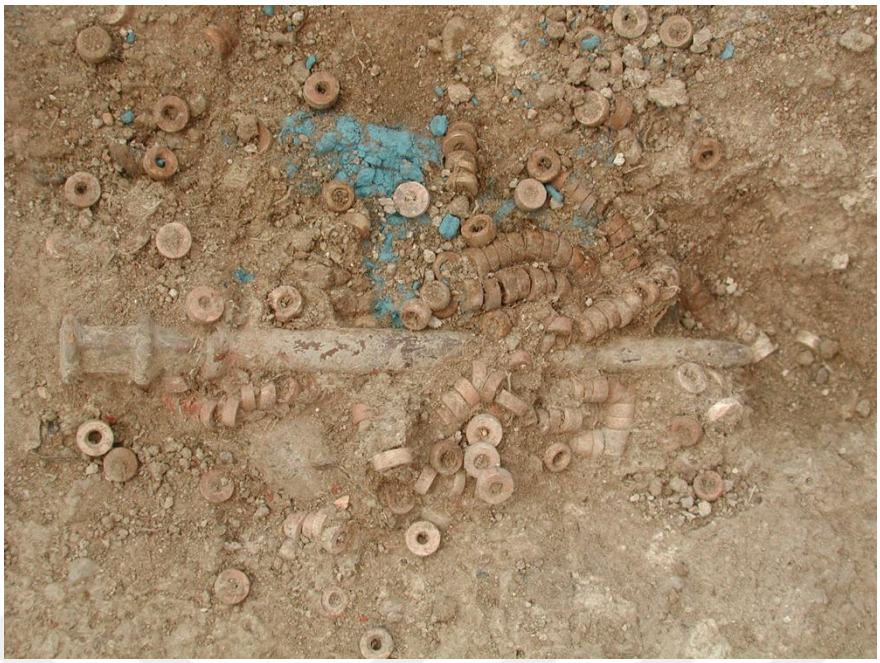

Figure 12 -Blue pigments from burial unit 7575 in Çatalhöyük, found in 2003 (courtesy of Çatalhöyük Research Project, licensed under CC BY-NC-SA 3.0).

3. 2. 6. Canhasan I

Canhasan I is a Late Neolithic and Chalcolithic site in Central Anatolia in Karaman (Baysal 2017). Excavations at Canhasan I yielded 224 beads in total and only ten were blue-colored beads (Baysal 2017: 3). David French initially characterized these as azurite in 1966 (French 1966: 172; Baysal 2017: 3). Baysal's recent examination revealed two of these to be jadeite, and the rest to be the kind of artificially colored beads with white interiors, the likes of which are known from Barcın (Baysal 2017: 3-4) Baysal reveals that at Canhasan I, there are "two discs, three short lenticular-form beads and three chip-form beads" of blue color (Baysal 2017: 4).

3. 2. 7. Mersin - Yumuktepe

Yumuktepe is a Neolithic mound with Early, Middle, Late and Final Neolithic phases in the city of Mersin on the Turkish Mediterranean (Caneva 2012). Based on the figures (Caneva 2012: 25) of the Yumuktepe publication in the Neolithic in Turkey (see Fig. 13), it can be noticed that the blue beads labeled as "disk stone beads" bear a likeness both in color and form to the blue-colored beads found in other sites. Although no chemical or otherwise analysis has been done on these beads, it is possible to argue that they are the same kind of beads as the ones in Barcın, considering their proximity in time. These blue beads belong to the Late Neolithic phase of Yumuktepe, and were unearthed from child graves that were scattered between structures (Caneva 2012: 7-8).

Figure 13 Blue beads can be seen among Late Neolithic beads from Yumuktepe, from Caneva 2012: 25.

3. 2. 8. Tepecik-Çiftlik

Tepecik-Çiftlik is a Neolithic and Chalcolithic mound located in the Southern part of the Central Anatolian plateau (Bıçakçı et al. 2012). The figures in the publication in the Neolithic in Turkey series feature photographs of blue beads (see Fig 14) that can be seen strung on a necklace (Bıçakçı et al. 2012: 134). A close-up of one blue bead (Bıçakçı et al. 2012: 134) (seen Fig 14) shows striations of a lighter color, that suggest that this is also of a similar nature with the artificially colored blue beads encountered in other sites. Although we do not learn specific information about the blue beads, the beads and ornamental pieces at Tepecik-Çiftlik are generally recovered as "stray finds" from open areas, refuse deposits or from building rubble (Bıçakçı et al. 2012: 102). In one rare occasion of a recovery in a primary context, we witness the use of blue beads as part of a necklace (Bıçakçı et al. 2012: 102, 134). The authors mention the use of "copper-derived mineral formations such as turquoise, malachite, and azurite" as the raw materials of ornaments at Tepecik-Çiftlik (Bıçakçı et al. 2012: 102). These materials have similar colors to the range of colors we see in the assemblage of blue beads elsewhere, so the identification of turquoise, malachite and azurite may be false unless further chemical analyses were conducted. Further on when authors mention "small amounts of precious minerals could easily have come from the Taurus mountains or even from Iran" (Bıçakçı et al. 2012: 102) it may be safe to assume that they imply turquoise.

Figure 14 Striations can be seen in one blue bead from Tepecik-Çiftlik, Bıçakçı et al. 2012: 134.

3. 2. 9. Köşk Höyük

Köşk Höyük is a Late Neolithic and Chalcolithic mound in the Central Anatolian city of Niğde (Öztan 2012: 31-70). The Köşk Höyük publication in the Neolithic in Turkey series mentions the discovery of clay beads that were painted turquoise in a bead cache, interpreted as a possible bead workshop area in Level IV, which dates to the Neolithic period according to the authors (Öztan 2012: 34-5). The authors further report that "[s]imilar terracotta beads from Levels III and II, unearthed in previous years, were found to have been painted with molybdenum powder" based on analyses by Prof Dr Yusuf Kaan Kadıoğlu (Öztan 2012: 35). More examples of these same beads were also discovered in an infant burial, the only burial found in Level IV at the time of the publication (Öztan 2012: 37). The

turquoise colored beads were found around the wrists of the infant, interpreted as bracelets (Öztan 2012: 37, 58). They were also interpreted as parts of a necklace, found together with other beads made of marble, stone and mollusc shells, which make us think they were found around the neck of the child, however the skull is reportedly much damaged (Öztan 2012: 37). Two feeding bowls and fresh water molluscs were also found in the burial, which was covered with lime plaster (Öztan 2012: 37).

Figure 15 Blue beads found in grave M.07-12 in Köşk höyük, from Öztan 2012: 58.

In one figure of the publication (see Fig. 16) (Öztan 2012: 54) it can be noticed that these blue colored beads also have white interiors, visible in the broken pieces, and white bands and striations. This could have given the impression of a clay raw material and blue paint covering the bead. The bead photos in the publication also show a variety of shades of blue, from greenish to light blue (Öztan 2012: 54, 58). These shared characteristics also imply that these are the same beads we are dealing with.

Figure 16 - Blue beads are seen among the beads and bone tools found in the Köşk höyük workshop, from Öztan 2012: 54.

3.2.10 Pendik

Özdoğan in her analysis of Neolithic beads in Anatolia, mentions "blue beads of faience (coloured, high-fired, baked clay)" and a bead made of "a blue stone that cannot be identified" in the site of Pendik, citing Baran-Çelik and Kiraz 2007 (Özdoğan 2016: 146). Pendik is a Neolithic site dated to late 7th millennium and early 6th millennium BCE in Istanbul in Northwest Anatolia (Özdoğan 2013: 175, 270). Faience beads, produced in Egypt, are indeed blue. However the earliest example of faience is dated to around 3200 BC (Aspinall et al. 1972: 27; Nicholson 2009), which makes it quite improbable that they would be found in Pendik especially at this date. The observation that the beads seem to be made of clay and have been painted, seem similar to our observations of the Barcın beads. Hence I believe that the beads named as faience in Baran-Çelik and Kiraz 2007, may actually be the same as our beads. The bead of "blue stone that cannot be identified"

(Özdoğan 2016: 146) may also be the same as the blue beads categorized as stone in Barcın. Personal communication with Emma Baysal (2017) concerning Pendik beads supports this argument that the beads from Pendik are similar to the beads at Barcın Höyük, with white interiors and blue exteriors.

3.2.11 Other Sites

Based on personal communication with Dr Ellen Belcher (2016), similar blue beads with blue exteriors and white interiors are also found in the Neolithic Domuztepe in southeast Turkey. Personal communication with Dr Rana Özbal (2015) informs us that similar beads are found in the Neolithic levels of Ulucak Höyük excavations in Western Turkey. Even though they are close in terms of geographical distance, personal communication with Emma Baysal (2017) revealed that the Neolithic site of Yenikapı where extensive excavations were carried out, did not have such beads.

3. 3. The Raw Materials

3.3.1. Turquoise

Semi-precious turquoise stone has the chemical formula $Cu(Al,Fe^{3+})_6(PO_4)_4(OH)_8 \bullet 4H_2O$ (Krzemnicki et al. 2011) and is encountered in several certain localities on earth. The closest turquoise sources to northwestern Anatolia are in the southwest Sinai in Egypt; in Wadi Magarah, Gebel Adeida and Serabit el-Khadim (Hauptmann 2004:173; Bloxam 2006: 278 as cited in Alarashi 2014: 561). The mineral otherwise originates from Nishapur in Iran and Afghanistan; Tibet, Mongolia, China and the Americas (Krzemnicki et al. 2011: 296).

Turquoise beads are reported from Domuztepe in southeast Turkey (Campbell and Carter 2006 as cited in Bains 2012: 16). Alarashi reports turquoise beads from Tell Hallula (Alarashi 2016: 497; Alarashi 2014: 76, 78, 102), Tell Aswad (Alarashi 2016: 497; Alarashi 2014: 97) and Dja'de el Mughara (Alarashi 2014: 646), all in Syria, that first appear in the early PPNB period and become more numerous in late PPNB period. Other reports of turquoise beads from other Neolithic sites in the Near East come from Ain Ghazal, Jordan (Rollefson 1993), Kfar HaHoresh, Israel (Goring-Morris 2007: 911), Nahal Hamar, Israel (Bar-Yosef 2013), Jilat and Shkarat Msaied, Jordan (Wright et al. 2008). Joyce Marcus also records the discovery of statuettes with turquoise bead inlays from Tell es-Sawwan, Iraq (Marcus 2008).

3.3.2. Odontolite and Apatite

Odontolite has been used as a substitute for the turquoise stone or as a decorative item extensively throughout history, at least since the Middle Ages, when its color changing properties were known and the material was used to decorate reliquary objects (Astre 1949 as cited in Reiche et al. 2001). Historic documents report that Cistercian monks in medieval France are known to have used heat treatment to turn this material blue and upon their transformation, mistakenly believe they created the semi-precious mineral turquoise stone (Réaumur 1715 as cited in Reiche et al. 2001; de La Brosse, 1626 as cited in Krzemnicki et al. 2011: 296). Réaumur (1715) reported that such "prepared turquoises originat[ed] from the region of Simorre (Gers, Southern France) as naturally white stones with some black inclusions" (Reiche et al 2000a: 625). It was Fischer in 1823 that concluded that the semi-precious mineral turquoise stone and the white material that turns blue are two

different mineral species; and it was also him that named the material odontolite (tooth stone in Greek) (Fischer 1823 as cited in Reiche et al. 2000a). Webster (1975) identified odontolite as not a real mineral (Reiche et al. 2000a). Finally, and more recently Baud (1985) stated "blue colour of bone and ivory is the result of a heat process that forms carbonised components in the material" (Reiche et al. 2000a: 626). Reiche et al report that since then, controversy kept surrounding the question of how blue color originated in such materials, relating the color to different inclusions such as vivianite (an iron phosphate) or copper salts (Reiche et al. 2000a: 626; Réaumur 1715, Fischer 1823, Webster 1986).

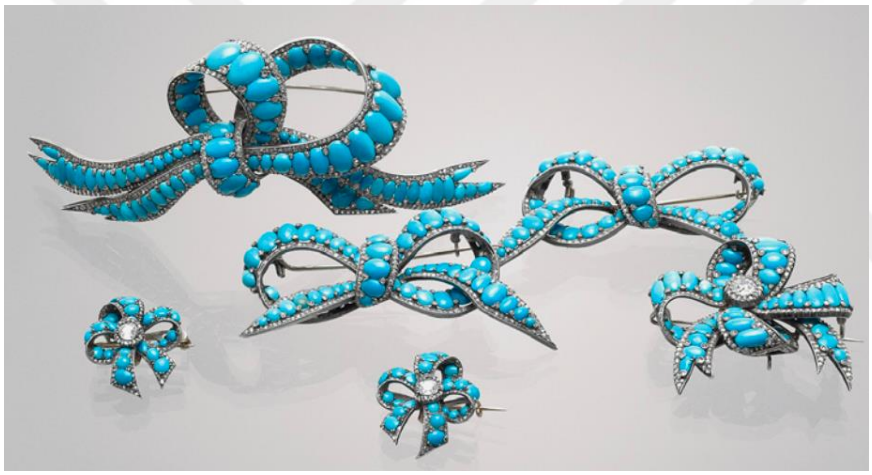

Figure 17 Odontolite jewellery from Krzemincki et al. 2011, 297.

Odontolite has been identified as fossilized Miocene mastodon ivory dated to 13-16 million years ago (Reiche et al. 2001: 1519), which is mineralogically relatively well-crystallized fluorapatite, with the chemical formula ($Ca_5(PO_4)_3F$) and with traces of Mn, Fe, Ba and U (Reiche et al. 2001: 1519; Reiche et al. 2000b). White-to-blue color changing materials have been vigorously investigated by Reiche

et al. in several articles that detail their work on green bone and tooth, 'odontolite' collection artifacts, white fossil mastodon ivory and modern elephant ivory, which are both reported to obtain a color similar to turquoise/blue when subject to heat (Reiche et al. 2000a, 2000b, 2001, 2002; Chadefaux et al. 2009). Their work revealed that it was the manganese found in these materials that causes the color change (Reiche, Vignaud, Champagnon et al. 2001).

Bone, ivory and teeth are originally made of a material called hydroxyapatite. Hydroxyapatite may undergo exchange reactions with various environmental compounds. The hydroxyl groups in the original raw material can be exchanged with F^{-1} to produce fluorapatite. Due to its more active properties, fluorine easily changes places with the hydroxyl (-OH) group present in the bone-tooth matrix. Similar exchange reactions and matrix deteriorations may change the proportions of calcium and phosphorus as well as introduce magnesium, and Sr, Fe, Zn, at trace levels (Bursalı et al., *submitted*). These processes take place during fossilization as well.

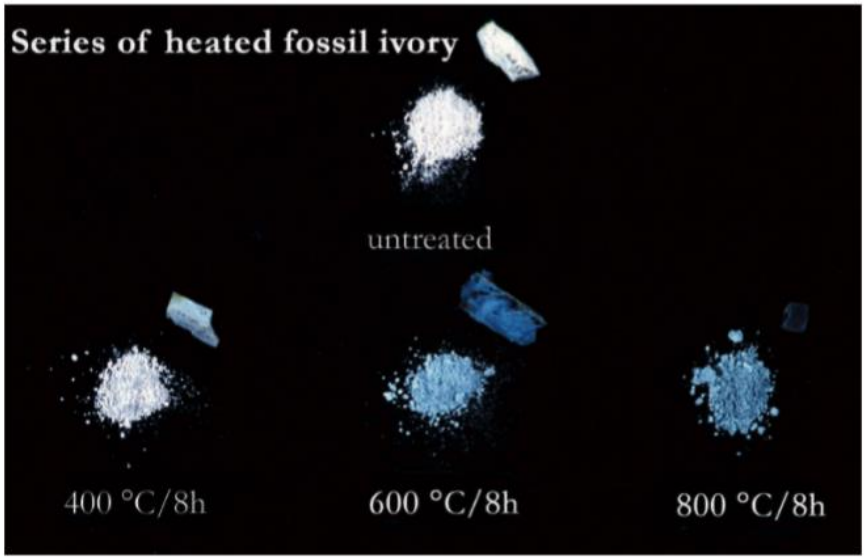

Figure 18 Change in color in fossilized mastodon ivories (from Rajegats in Gers, Southern France, found in a geological layer dating from the Middle Miocene (13-16 Ma)) heated under different temperatures for 8 hours, from Reiche et al. 2001: 1520.

The effect of heat treatment on ancient bone and ivory has long been investigated. Baer et al. in their 1971 research, show the changes in the color of ivory under different temperatures and durations, which obtains grey-blue coloration when subject to temperatures of 593 °C or higher, that they attribute to small quantities of free carbon in the sample (but not iron, vivianite, or trace metals) (Baer et al. 1971: 1, 3,5). Reiche and Vignaud et al. also studied the effects of heat on materials such as odontolite and bone. These researchers used Transmission Electron Microscopy, PIXE/PIGE analysis, EXAFS, Nuclear Reaction Analysis, XRD, XANES and FT-Infra red methods of analyses. In their earlier work the blue color in bones was attributed to copper, and blue color in odontolite was connected to an intake of iron, creating vivianite (Reiche et al. 2000a; 2000b). Later studies show, based on experiments on both archaeological and paleontological bones, which are all made of

apatite, the color change is usually due to an intake of Manganese during the fossilization process (Reiche and Chalmin 2008, Chadefaux et al., 2009). Specifically, on a molecular level, Reiche et al. explain that "[t]he energy degeneracy of the 3d electrons in Mn^{5+} is split due to the ligand-field splitting in a distorted tetrahedral environment of four O^{2-} ions (Oetliker et al. 1994). This splitting enables electronic transitions giving rise to the characteristic turquoise-blue color" (Reiche et al. 2001: 1523). The blue color in bones is a result by the presence of Manganese ions (Mn^{+5}) that bonds with material when heated under oxidizing conditions, suggesting that any bone material that has Mn^{+2} or Mn^{+3} inclusions can turn blue under favorable conditions. Thus this phenomenon does not seem to be reserved for odontolite. Here, the take-up of manganese ions into bones in archaeological and paleontological deposits becomes an important issue. Depositional and environmental conditions would be surely of upmost importance in determining whether (or possibly how much) a material would turn blue. Brügmann (2012), Dauphin (2007) and Henderson (1983) detail through what processes fossil bone and dentine chemically change in nature, and how manganese or other ions may be taken up into fossil bones in nature over time.

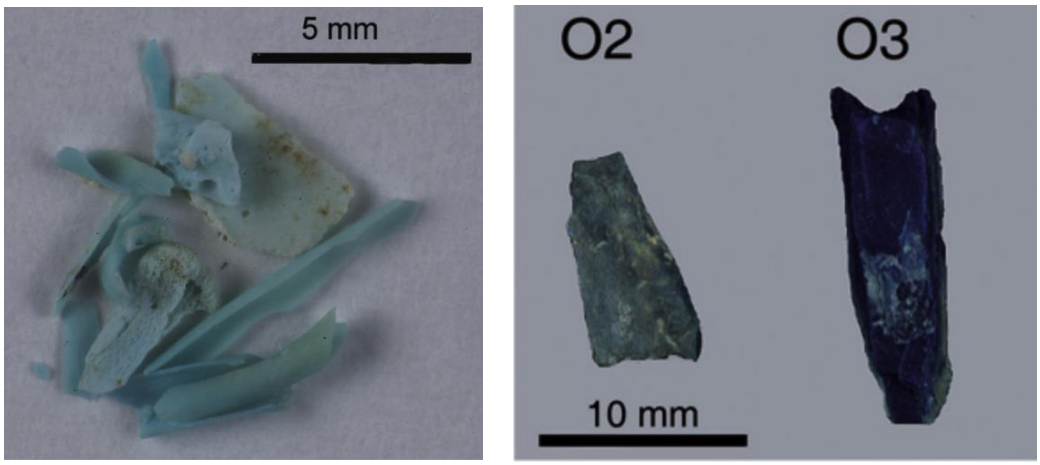

Figure 19 a) Blue colored paleontological bone fragments from stratum 770 of San Josecito Cave in Mexico, from Chadefaux et al. 2009: 28. b) Two traditional odontolite specimens from mineralogical collection of MNHN, Paris, France, from Reiche and Chalmin 2008: 800.

3.3.2.1 Geological Apatite

The apatite mineral is also found in nature as a rock. It can either be made up of hydroxylapatite, fluorapatite, or chlorapatite based on the existence of hydroxyl, fluorine or chlorine inside the crystals. The apatite rocks are known to come in blue colors as well (Johnson et al. 1963). The blue color of the natural apatite crystals is also frequently attributed to existence of Manganese, specifically to formation of formation of MnO_4^{3-} ions (Medina et al. 2016; Yubao et al. 1993; Johnson et al. 1963).

Figure 20 Blue apatite crystals (CaF) from Slyudyanka (Sludyanka), Lake Baikal area, Irkutskaya Oblast', Prebaikalia (Pribaikal'e), Eastern-Siberian Region, Russia, by Parent Géry (Own work) [CC BY-SA 3.0 or GFDL)], via Wikimedia Commons.

CHAPTER 4 – METHODS

In total, 20 beads and bead fragments were the in the scope of the research undertaken for this study. The breakdown of the analyses that the different beads went through is detailed in the table below.

BH # of bead fragment	**BH# of beads they belong to**	optical micro scope	SEM-EDX (polished not incl)	polished SEM	FTIR	Raman
BH 37398	BH 5463	x				
BH 37394	BH 34381	x	x (1)			x
BH 37395	BH 32761	x	x (1)			x
BH 37400	BH 17320	x	x (1)			x
BH 37622	BH 31179	x	x (1)			x
BH 37627	BH 26720	X (np)				
BH 17556	*BH 17556*		x (6)			
BH 22451	*BH 22451*		x (3)			
BH 21476	*BH 21476*		x (3)			
BH 18294	*BH 18294*		x (2)			
BH 17299	*BH 17299*		x (2)			
BH 32714	BH 32714		x (2)			
BH 18358	*BH 18358*		x (1)			
BH 37397	BH 14263			x(4)	x	
BH 37399	BH 30875			x(7)	x	
BH 37621	BH 24875				x	
BH 37393	BH 30868	X (np)			x	
BH 37617	BH 37502				x	
BH 37620	BH 20702				x	
BH 37629	BH 36173				x	

Table 2 The beads and the analyses they were subject to

4.1 Instrumental Methods

4.1.1. Optical Microscope

The optical microscope is used for magnifying the samples, by employing a mechanism of lenses that are arranged to achieve the expected view in terms of angle and magnification. The interiors and exteriors of five beads were analyzed under the optical polarizing light microscope Olympus BX5 under polarized light, with 2.5x, 5x, 10x, 20x, 50x and 100x magnifications. Two more beads were analyzed under the same microscope but under normal visual light. These seven samples were chosen because the appearance of their interiors led us to believe they were made of different materials: three of clay/plaster and four of stone.

4.1.2. Raman

Raman spectroscopy is a type of vibrational spectroscopy based on the molecular motion of a material, which is always characteristic of its structure (Yıldırım 2014). It is based on the inelastic scattering (Raman scattering) from a monochromatic excitation source, such as IR, red, green or blue lasers. In this technique, the photons sent from the excitation source interact with the sample, and due to this interaction, the energy of the returning photons shift up or down. This shift is related to the vibrational modes of the compound, which are unique to that compound. From this shift one can work backwards to find the compound (Yıldırım 2014).

Raman spectroscopy was done on 4 beads using Renishaw Invia - Raman Microscope in KUYTAM Laboratories by Barış Yağcı, to help compare the Raman

spectra of the bead samples with possible raw materials. 532 nm argon-ion laser power was used with 5% laser power, 5 seconds shooting time and 50x magnification. Each bead was tested under the laser ten times. The spectra were collected from 1400 to 100 cm^{-1} Raman shift so that it "include[s] the vibrational range of organic compounds, such as wax and artificial resin, used for turquoise impregnation" (Krzemnicki et al. 2011: 297).

4.1.3. Fourier Transform Infra-Red Spectroscopy

The Fourier transform infrared spectroscopy is a useful tool for identifying organic and inorganic materials, and determining the concentration of different parts of a mixture, with a long history of application in art and archaeology (Van Zelst et al. 1988, Margaris 2014). It creates the infrared spectrum of absorption, emission, photoconductivity or Raman scattering of a material. The infrared spectra are also unique to the material and help identify the compounds within. The Fourier transform turns the raw data gained into a spectrum (Griffiths and De Haseth 2007). FT-IR provides very quick and informative results and requires a very small amount of sample (in milligrams or even micrograms) for analysis (Margaris 2014; Weiner and Goldberg 1990). FTIR has also been preferable in archaeological analysis "as it can aid in determining the composition of such materials as fired clays, bone and tooth enamel, wood ash, fibers and dyes, plasters, and resins" (Margaris 2014).

In this technique, a beam that contains multiple frequencies is shone on the sample. The beam contains a broadband light source. The light from the beam shines into an alignment of mirrors, one of which moves, blocking and transmitting wavelengths periodically. This happens because of wave interference where waves

either amplify the signal or lower the amplitude of the signal. The FTIR machine measures which frequencies of the beam, and how much of the beam the material absorbs. Then a next beam is sent, this time modified to have a different combination of frequencies. This process is repeated, in our case 32 times. In our analyses, Thermo Scientific Nicolet 380 FTIR - Diamond 30,000-200 cm^{-1} was used. The computer program EZ OMNIC then works backwards and infers the absorptions at each wavelength.

4. 1. 3. 1. Samples

The FTIR analyses were done on 6 beads. We strove to take two different samples from two different spots of the bead, and to test the same sample at least 4 times. However these principles were not successfully followed for every bead as the sample amount was indeed very small and limited since this is a destructive analysis that requires the bead to be powdered.

To compare with the graphs of the beads, FTIR spectra of the specimens specified in Table 3 were collected.

modern	*lamb*	long bone
		metacarpal
	sheep	vertebra
		metacarpal
	cattle	long bone
		vertebra
neolithic	*sheep*	bone
		tooth
	pig	tooth
		tusk

	human	tooth
fossil	*equid*	tooth

Table 3 Specimens tested with FTIR

The Neolithic samples were taken from the Barcın excavations. The fossil equid tooth was obtained from the website www.fossilera.com . A soil sample from the excavations was also tested to account for background noise. The modern bone samples were acquired from the butcher's shop. Small pieces of the bone were cut and were physically cleaned. Then the samples were put in hydrogen peroxide solutions and were put into an ultrasound centrifuge. The tissue were thus cleaned off the bone. Then these pieces of modern animal bone were put in a muffle furnace for drying, before being powdered for the FTIR analysis.

4. 1. 3. 2. Procedure Followed for the FTIR Measurements

To get the best results from the FT-IR spectroscopy, the sample needs to be crushed into a fine powder. Fragments - approximately 0.2x0.2 cm - of 6 beads ranging from blue on the outside and white inside, to turquoise-blue all the way through, are powdered in an agate mortar for FTIR analysis (see Fig 21).

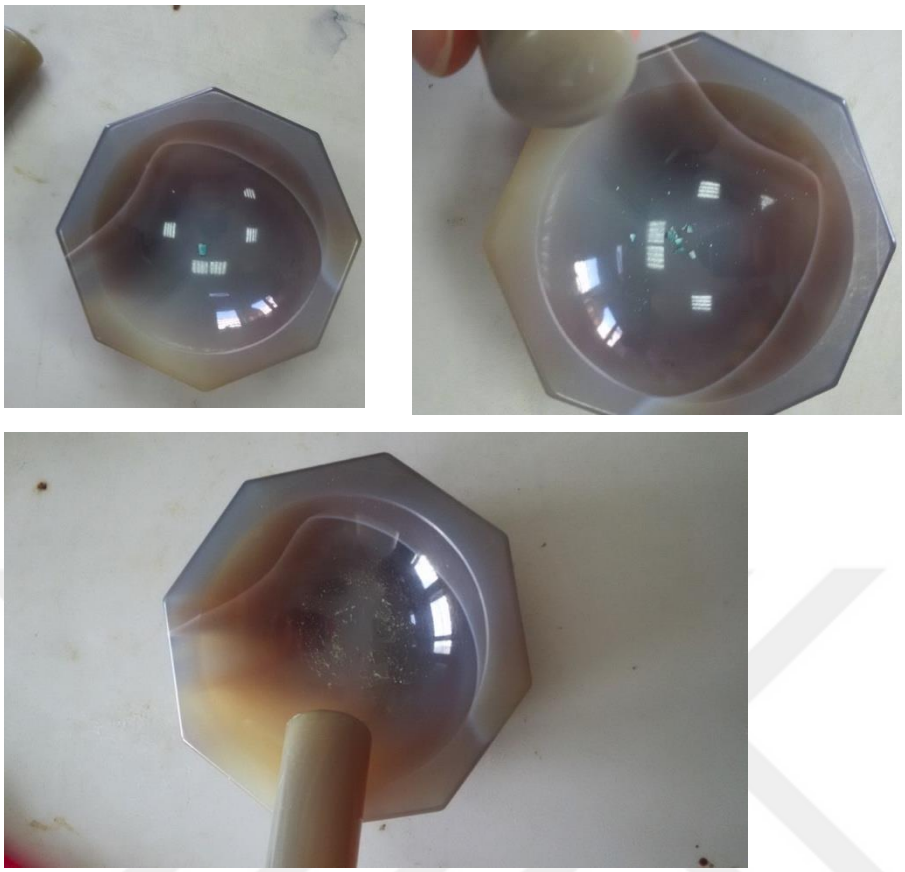

Figure 21 Crushing the bead samples for FTIR analysis

The EZ OMNIC program on the computer is opened. The FTIR needs to first collect a background sample with nothing placed under the Infrared Signal. Before the background collection, wiping the machine with acetone makes sure there is no contamination.

When the background collection is complete, the fine powder sample is placed in the eye of the machine under the tip that the signal is sent from. The powder should cover all of the eye, leaving no empty spots. The amount needed for the testing is the amount that covers this eye. After the fine powder sample is placed, the machine sends 32 signals through the sample, and the infra-red graph slowly takes shape on the program screen.

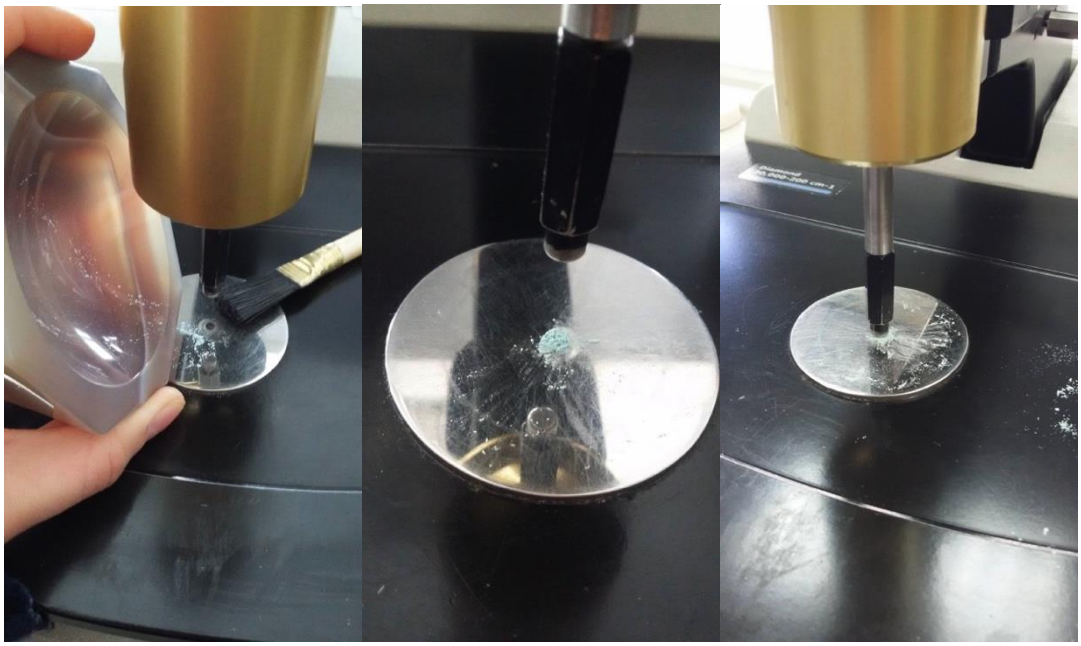

Figure 22 Placing the powdered bead sample in FTIR FTIR Thermo Scientific Nicolet 380 FTIR Machine

When the scans are completed, the graph obtained is modified to decrease the noise in the graph. We use the Smooth function with a value of 7. Then we apply Baseline Correction to the graph. Next we find the peaks automatically or using the T function. The peaks that were not identified through the EZ OMNIC software at

Boğaziçi, were identified later on with the free software Spectragryph 1.0 by Spekwin32.

4.1.4. Scanning Electron Microscopy with EDX

To understand the structural features of the beads as well as to obtain semi-quantitative elemental compositions, a scanning electron microscope was utilized. The SEM provides both surface topography imaging and an elemental analysis of the material through Energy Dispersive X-ray Spectroscopy. The SEM can fulfill these needs with the help of an electron gun "which produces a beam of electrons and accelerates them toward a specimen. The electron beam is focused onto a specimen by a series of apertures and electromagnetic lenses" (Frahm 2014: 6487-6488). These measurements happen under "a high vacuum to avoid beam scattering by air molecules and other effects" (Frahm 2014: 6488). When these electrons hit the sample, different kinds of "information-bearing signals" are produced: secondary electrons (SE), which have low energies, provide topographic details; backscattered electrons (BSE), which have higher energies, also help with topography but are affected by the atomic number of the specimen, so they provide images of compositional contrast. However, the elements inside the specimen can only be identified by measuring their X-ray emissions, which are unique to the specific elements. These "are measured using X-ray spectrometers to determine a specimen's elemental composition" however "the system is usually not sensitive enough to measure the tiny signals produced by trace elements" (Frahm 2014: 6488-9). Moreover with EDX, "the elemental composition is measured for only a small volume [that the electron beam is shone upon], just a few cubic micrometers, not the full specimen" (Frahm 2014: 6499). As our research question concerns the material

the beads are made from, the chemical signature obtained through EDX is helpful. However figuring out how the elements are bonded and reconstructing the chemical formula of the bead compound is difficult with this technique.

To conduct SEM analyses on archaeological materials, some extra steps also need to be taken. The sample needs to be polished flat to obtain successful imaging with a back-scattered detector, unless the sample is examined for its surface texture (Henderson 2013: 19). Moreover, the samples that do not conduct electrons, for example non-metals such as glass, glaze or obsidian in an archaeological case (and also in our case), "must be coated with an ultrathin layer (about 100 Å) of a conductive material, normally gold or carbon, to prevent an electric charge from building up on the specimen surface" (Frahm 2014: 6489) which would lead to the "distortion and deflection of the electron beam" (Henderson 2013: 20). However this can usually be removed later on (Frahm 2014: 6489).

4. 1. 4. 1.Conducting the Analyses

The first Scanning Electron Microscope tests were done in the KUYTAM Chemistry laboratory in Koç University by Barış Yağcı, with Zeiss Ultra Plus Field Emission Scanning Electron Microscope. Eleven bead samples with varying shades of blue as well as with white inner sections were selected and a total of 35 EDX analyses were carried out on various surface areas (see Figure 23). The samples used were comprised of both complete beads and broken fragments of beads. SEM and EDX measurements were first done without coating but when the samples got charged too much leading to distorted surface images, the samples were coated with carbon at the KUYTAM laboratories. Tests were done with carbon-coated samples. SEM and EDX were also done on archaeological cow bone and cow teeth from

Barcın Höyük. This analysis can be helpful in seeing if there is any similarity between the chemical compositions of discarded unworked animal bone and the blue beads.

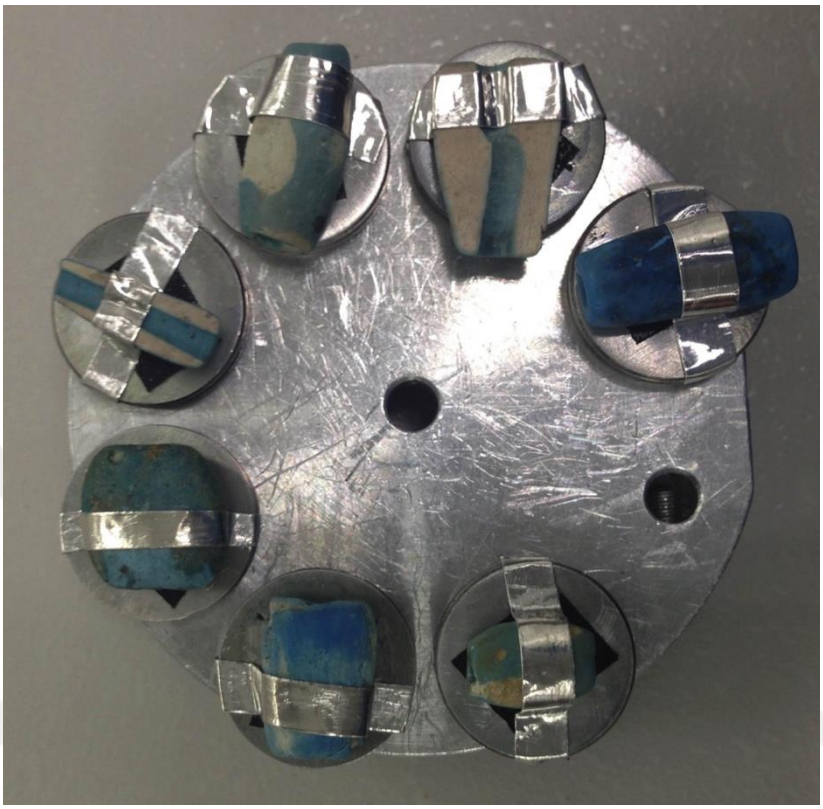

Figure 23 Blue beads ready for SEM analysis

In Boğaziçi University, a second round of SEM and EDX tests were carried out with the Philips XL30 ESEM-FEG/EDAX system by Bilge Uluocak. The analyses were carried out on beads BH 37399 and BH 37397, on one blue-colored archaeological bone from excavations, and on the bone samples that were subject to the coloring experiment. The polished cross sections of the two beads were analyzed under the SEM and elemental results were obtained with EDX. To get polished cross-sections, these two beads were first mounted in bakelite. Later they were cut

and their cross sections were polished. Elemental mapping of elements in the specimens was also carried out.

After the coloring experiments carried out in the Boğaziçi University's Archaeometry lab (which will be detailed in section 4.2) to try to achieve blue color through chemical and heat treatment of archaeological bone, SEM and EDX analyses were also conducted on one heat-treated and processed bone sample obtained in our experiments. These samples were also mounted in bakelite and polished. Along with these experiment samples, the archaeological blue-colored bone sample found in excavations was also subject to SEMEDX analysis after going through the same procedure.

4.2. Experimental Methods

In accordance with the prior scientific literature and the results of the instrumental analyses we carried out, laboratory experiments were also performed. The results of the instrumental analyses, which will be detailed in Chapter 5 -Results, led us to discover that the basic body of the beads are made of apatite.

4. 2. 1. Background on Experiments

Prior studies have also dealt with experimental production of blue color on materials such as ivory and teeth. Baer et al. in their 1971 work, subject ivories to temperatures between 149 °C and 871 °C (with 55.5 °C intervals) for one hour (Baer et al. 1971: 1-2), as well as investigate archaeological ivory samples with grey-blue coloration from museum collections (see Fig. 24). They come to the conclusion that

grey-blue coloration is achieved in oxidizing conditions at temperatures above 593 °C (649, 704 and 760 °C specifically) (Baer et al. 1971: 3).

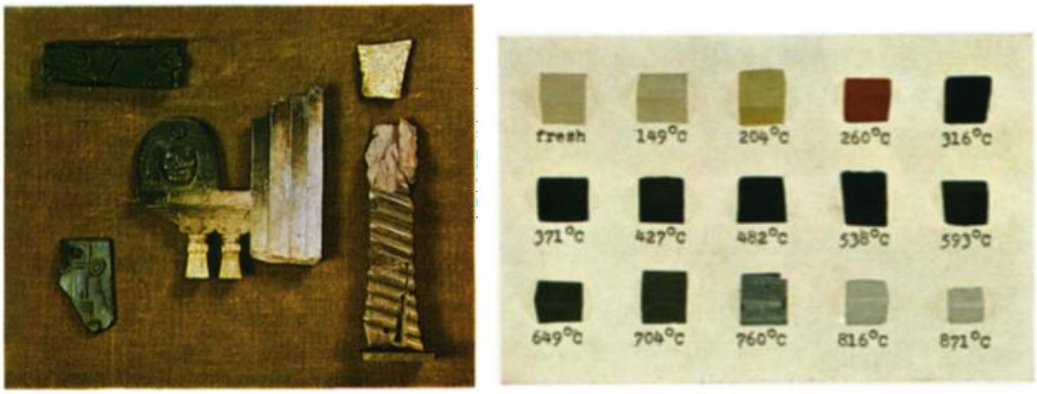

Figure 24a) Colored ivory in archaeological samples, 26b) Baer et al.'s results on the affect of heat treatment on ivory, both from Baer et al. 1971: 1.

In their research relating to the coloration of ivory or bone, Reiche et al. subject samples to heat treatment several times and achieve blue color under oxidizing conditions. In one 2000 article (2000a), they subject already-blue odontolite, as well as both modern and fossil ivory (13 million years-old samples with black inclusions, from Rajegats and Malartic both in Gers, France (Reiche et al. 2000a: 626; 2000b: 739)) to 400°C, 550°C, 600°C, 700°C, 800°C and 940 °C heat for 20 hours in air (Reiche et al. 2000a: 626-7). In this experiment the modern ivories do not show blue coloration although they do "chang[e] from beige at the unheated stage to black at 400 – 550°C, to grey at 700°C and to white above 800°C" (Reiche et al. 2000a: 633). On the other hand, the fossil ivory samples became blue all over the fragment above 550 °C; only slightly blue at 400°C, turquoise-blue at 600°C, and blue grey in one out of the two samples (the sample from Rajegats, Gers, France) at 800°C (Reiche et al. 2000a: 632-3). The blue odontolite samples also stayed

turquoise-blue after heating (Reiche et al. 2000a: 633). Reiche et al. repeated the same heating experiments in 400°C and 600°C for 20 hours also in nitrogen (N_2), rather than in air: however they achieved no color change under these conditions, except for the bright blue sample turning grey in 400°C; and the turquoise-blue sample turning black in 600°C (Reiche et al. 2000a: 633). In the 2000b article, the researchers subject yet another fossil ivory specimen without black inclusions, this time from En Pejouan, Gers-France to the same temperatures for the same duration in air, however this specimen does not turn blue at all (Reiche et al. 2000b: 739). Further tests show this specific fossil ivory specimen also does not have Manganese inclusions in it (Reiche et al. 2000b: 741). In their 2001 article, Reiche et al. subject fossilized mastodon ivory to heat at 400, 600, 800 and 940 °C, this time not for 20 but for 8 hours (see Fig 18), and reach blue color by heating it above 600 °C (Reiche et al. 2001).

Unlike the aforementioned research where the specimens are only subject to heat treatment to achieve color change, Taniguchi et al. (2002) employ additional chemical methods to achieve a blue color on wild pig tusk from Tell el Kerkh excavations and modern sea-mammal bone (Taniguchi et al. 2002: 180). The researchers report that these materials were specifically chosen for this experiment because “they displayed almost identical texture and chemical composition to the white core of the original beads” (Taniguchi et al. 2002: 180). Selecting materials that they believe would be “readily obtainable from natural resources” they prepared a “mixture of alkali and transition metals” consisting of 0.4 g of Manganese oxide, 0.1 g of Cupric oxide, 0.2 g of Iron, 1.0 g of Calcium carbonate and 1.2 g of Sodium chloride in 20 ml of water (Taniguchi et al. 2002: 180). The samples were left in the

solution for 24 hours and heated at 200, 300, 400, 500, 600, 700 and 800 °C for five hours. At 600 °C, the exteriors of the samples became similar to the exteriors of the Tell el Kerkh beads (see Fig. 25) (Taniguchi et al. 2002: 180). The FTIR spectra of the experimental blue pig tusk also provided a good match with that of the beads except for the OH frequency in the pig sample; the authors associate this spectrum with the apatite matrix (Taniguchi et al. 2002: 180). After the experiment however, the authors also note that the apatite matrix of the bone and tusk became fragile after heating, and suggest looking into methods that lack heat, or repeating the experiment on fossil material which they assume would be stronger (Taniguchi et al. 2002: 180, 181).

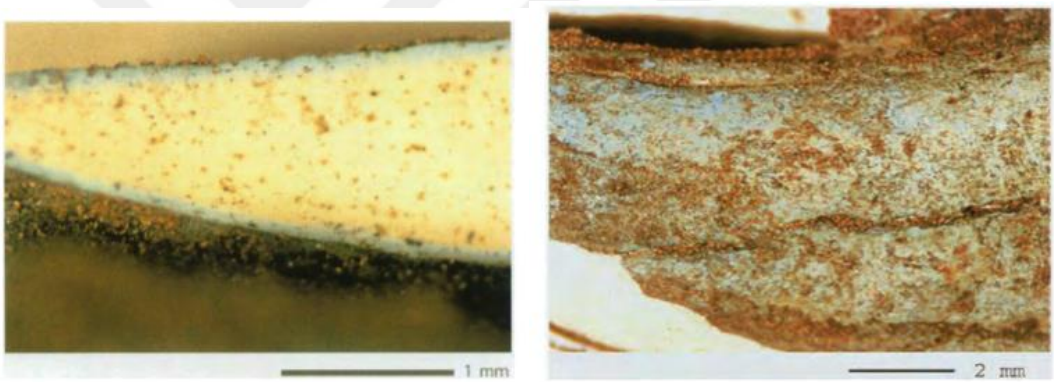

Figure 25 Color change attained in Taniguchi et al.'s experiments. Details from the synthesized blue bead made of ancient tusk of wild pig, Left, Taniguchi et al. 2002: 181. Right, Taniguchi et al. 2002: 180.

Borrowing from the research designs of these prior works, we also strove to reproduce the blue color experimentally on modern and archaeological bone, and archaeological and fossil tooth.

4. 2. 1. Procedure for the Experiments

An initial set of experiments was done to see if samples could turn turquoise or blue in color only by heating in the muffle furnace at around 600^0C. These samples included archaeological sheep/goat bone (white and blackened), fossil equid tooth, ancient cow tooth, ancient pig tusk, and modern bone samples such as modern sheep long bone, modern sheep vertebra and modern cow vertebra.

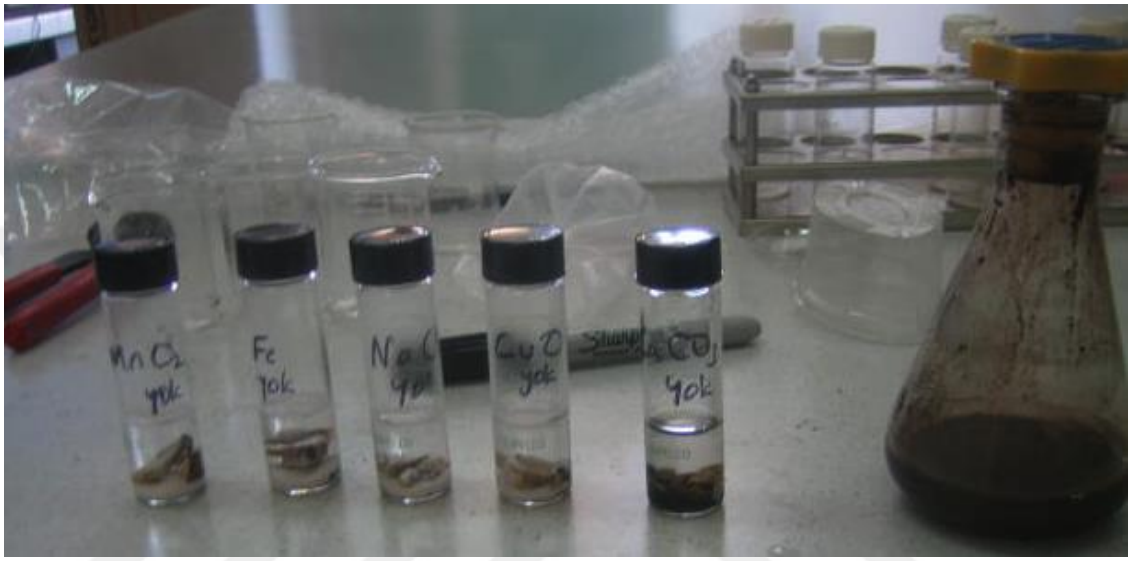

Figure 26 Solutions with one element ingredient missing seen on the left, full solution seen on the right

The second set of experiments employed the recipe published by Taniguchi et al. (2012) to replicate the color. Accordingly, an aqueous slurry containing iron metal (0.2g), manganese oxide (0.4g), copper oxide (0.1g), sodium chloride (1.2g), and calcium carbonate (1.0g) in 20 ml of water was prepared. In this set of experiments, only modern and archaeological sheep/goat bone, and archaeological pig teeth specimens were used as samples. The specimens were soaked with constant stirring in this aqueous solution for up to ten days. The samples then were removed from the solution, and cleaned with distilled water before being dried in a muffle

furnace at 110 °C for an hour. After getting dried, they were heated in the muffle furnace up to 44 hours at temperatures as high as 650^0C, over the course of five batches. The details of the batches can be seen in table 7 in the Results section 5.2.

The different batches served to try to answer several questions. The second batch was designed so it might allow us to see how modern and archaeological sheep/goat bones are affected differently from the solution. The third batch involved five different versions of the solution where one of the five ingredients was missing in each, and a full solution as control, all on archaeological sheep/goat bone samples. This third batch was also heat treated twice to see if more heat under a higher temperature (650^0C compared to 600^0C) would affect the color. The fourth batch of archaeological bone samples involved a full solution, as well as solutions with only Manganese, only Iron, and only Manganese and Iron, to see if we can identify if either element can be solely responsible for the coloring. In the fifth and final batch, the experiments were done on archaeological pig teeth from Barcın excavations as well as the usual archaeological sheep/goat bone.

CHAPTER 5 – RESULTS

5.1. Instrumental Results

5.1.1.Optical Microscope

The results of optical microscopy are given in Table 4 and exemplified here with micrographs (Figs 27-34). Generally the light microscopy revealed thin parallel lines under high magnification, grainy-looking surface texture, what looks like possible inclusions, and provided a closer look at the gradual color change from white to blue, the bone-like and stone-like structure of some beads, which are presented under the headline "Micrographs Relating to Material"; as well as drill marks and marks on the surface which are presented under the category "Other Micrographs".

BH # of bead fragment	BH# of beads they belong to	Initial category	lines	inclusions	stone structure	bone structure	grainy surface	gradual color change
BH37398	BH5463	clay		x		x?	x	
BH37394	BH34381	Stone						x
BH37395	BH32761	stone	x		x			
BH37400	BH17320	stone	x	x		x		
BH37622	BH31179	clay		x ?			x	
BH37627	BH26720	clay				x		x
BH37393	BH30868	stone			x			

Table 4 Table showing which characteristics were observed in which beads under optical microscope

5. 1. 2. 1. Micrographs Relating to Material

a) Under the optical light microscope under plane polarizing light, two beads (BH 37395 and BH 37400) exhibited very thin and parallel-ish light-colored lines along their surface, seen below. We cannot know for sure what these are yet, but tentatively suggest that they may be annual rings.

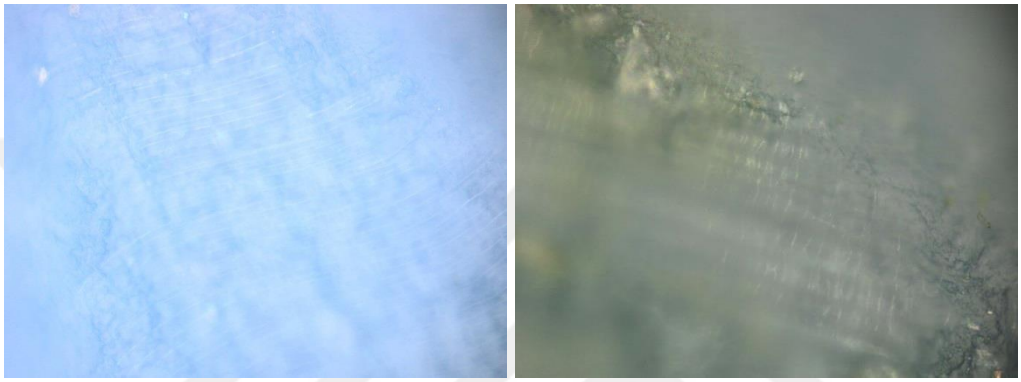

Figure 27 a) BH 37395 50x, interior (plane polarized light) b) BH 37400 100x, exterior (plane polarized light)

b) Some differently-colored specks that could possibly be inclusions were observed under plane polarizing light. However especially in the interior of BH 37398, it should be noted these may be what is essentially dirt stuck to the beads.

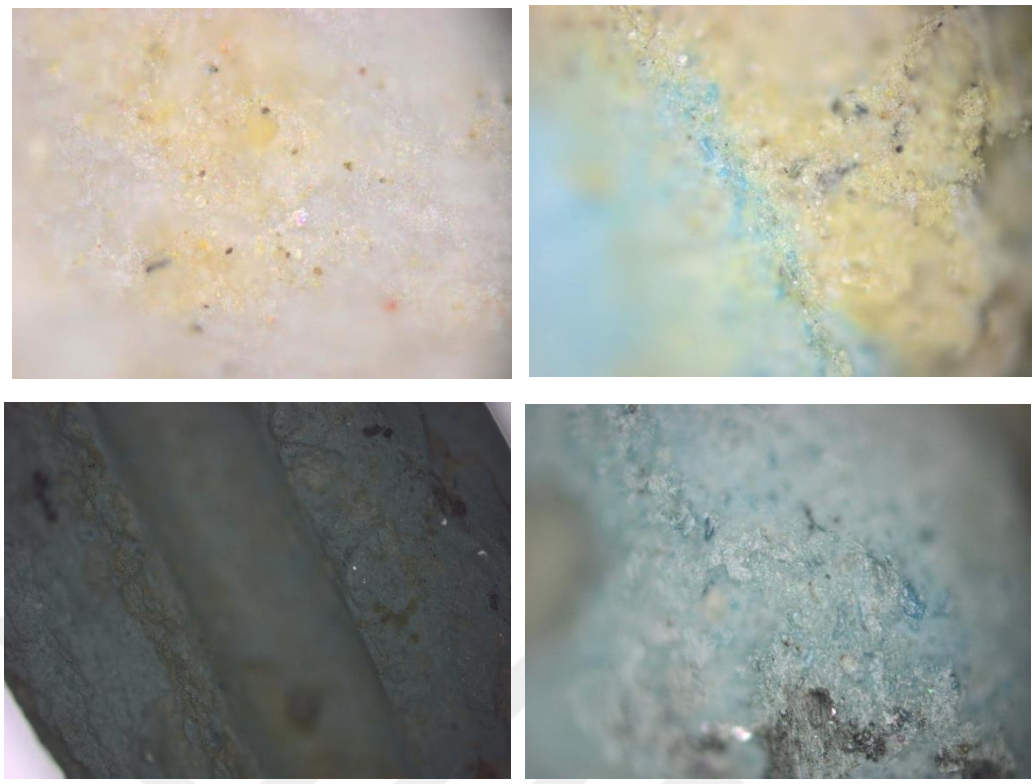

Figure 28.Clockwise a) 37394_100 x interior b) BH 37398 20x, interior c) BH 37398 20x, exterior d) BH 37622 5x, interior. All under plane polarized light

c) We were also able to confirm our macroscopic suspicions on the bone-like and stone-like structures of some of the beads thanks to microscope analysis. Stone-like structure was noticed in beads BH 37393 and BH 37395.

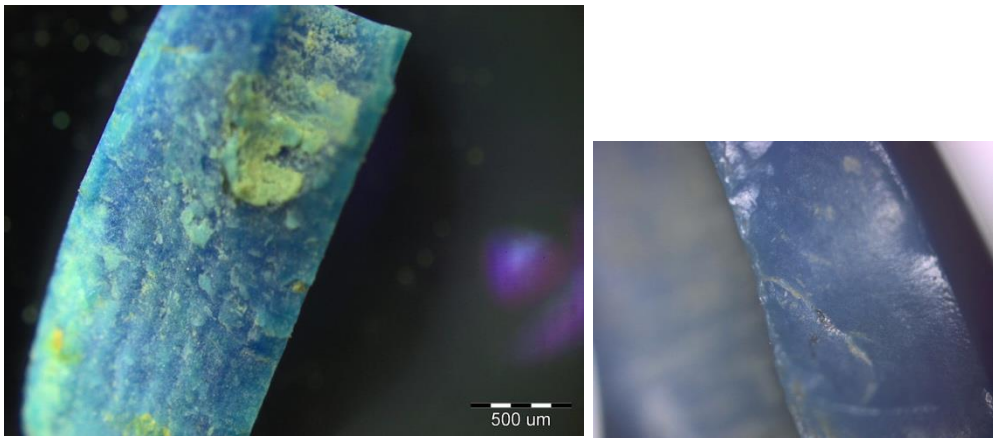

Figure 29 a) BH 37393 2,5x (normal light) interior b)BH 37395 5x interior (plane polarized light)

d) Bone-like structure in the interior of the beads was especially noticeable in two beads, BH 37627 and BH 37400. BH 37398 presented a more complicated image.

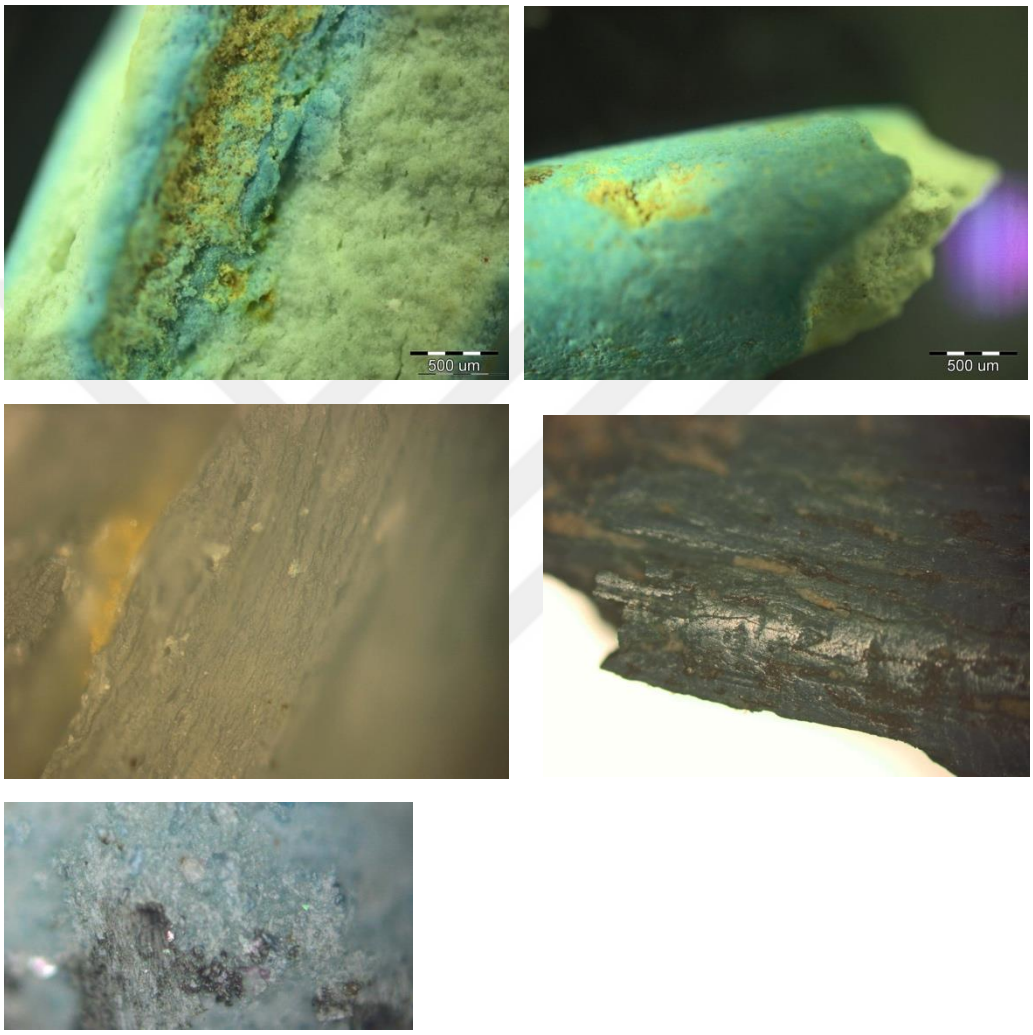

Figure 30 Left to Right. Top – a) BH 37627 5x, interior (under normal light) b) BH 37627 2,5x exterior (under normal light) Middle – c) BH 37400 50x, interior (under plane polarized light) d) BH 37400 5x, interior (under plane polarized light) Bottom e) BH 37398 20x, exterior (under plane polarized light)

e) A peculiar grainy surface was noticed in beads BH 37622 and BH 37398. This surface could be caused by the differential coloring on the surface of the exterior of the beads. On the other hand, it is worth nothing that the grainy textures could be caused by inclusions.

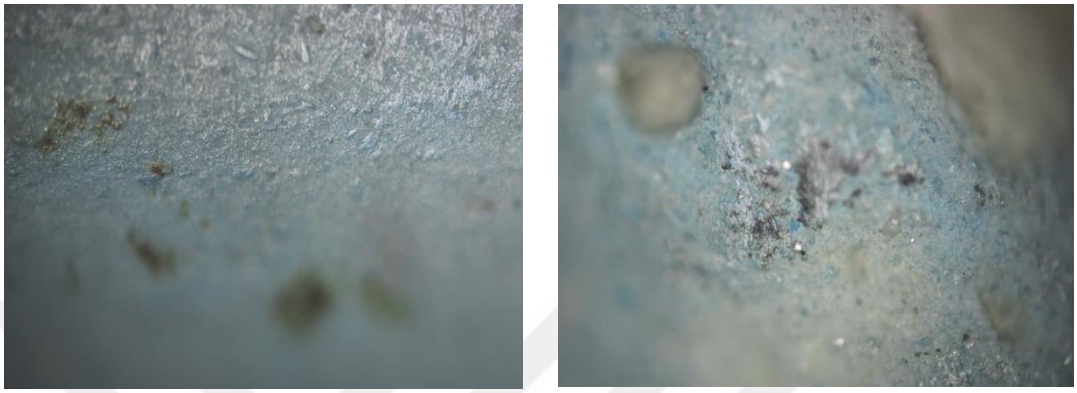

Figure 31 a) BH37622 10x, exterior. b) BH 37398 10x, exterior. Both under plane polarized light.

f) Gradual color change from white to blue was documented from close-up in beads BH 37394 and BH 37627.

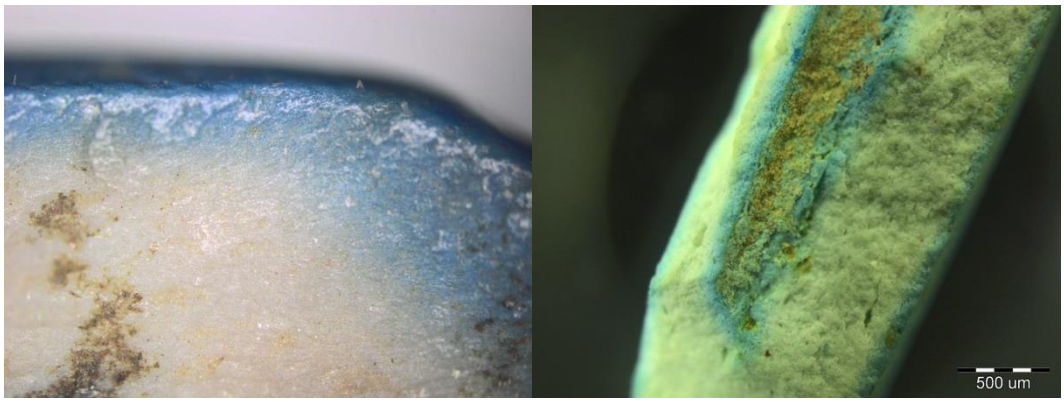

Figure 32 a) BH 37394 10x, interior (under plane polarized light) b) BH 37627 2,5x, interior(under normal light).

5. 1. 2. 2. Other Micrographs

We were able to take a closer look at the drill marks under plane polarized light:

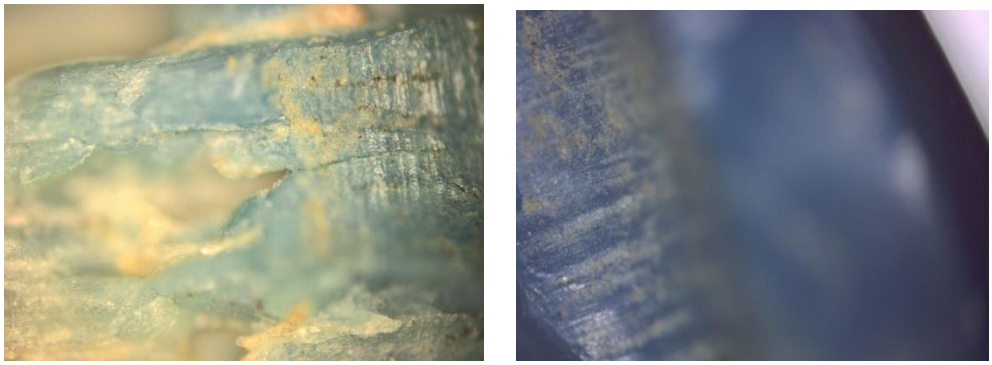

Figure 33 a) BH 37395 10x, interior. B) BH 37395 5x, interior.

We also were able to take a closer look at the marks on the surfaces:

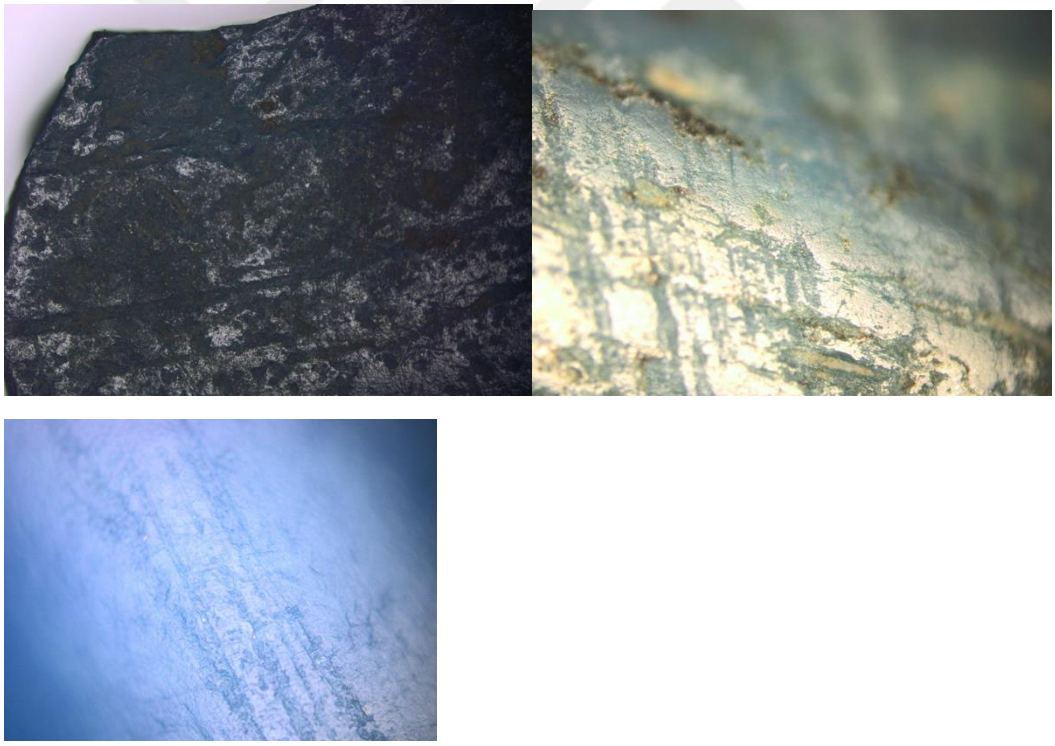

Figure 34 Left to Right. Top - a)BH 37394 5x, exterior b)BH 37400 10x, exterior. Bottom – c) BH 37395 20xx, exterior. All under plane polarizing light.

5. 1. 2. Raman

The Raman spectroscopy on the beads provided one peak in all spectra that is clearly identifiable. This peak at 960 cm^{-1} was sometimes weak and sometimes strong, according to Gülsu Şimşek from KUYTAM Laboratories, and belonged to calcium phosphate ($Ca_3(PO_4)_2$). The peaks were strongest in the spectra produced by beads BH37395 and BH37400 (Figs 35,36). The peaks in for BH 37622, BH 37394 and cow tooth were not well pronounced (Figs 37-39). When the Raman was carried out on the archaeological sheep/goat bone and tooth sample, the peaks were again not strong. The comparisons of the Raman graphs will follow in the Interpretation section, Section 6.1.2.

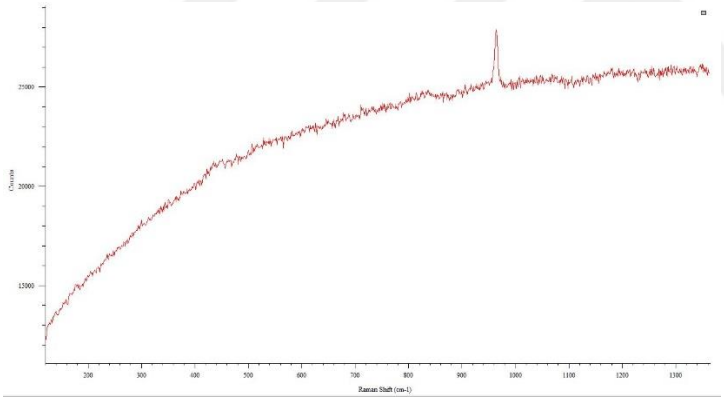

Figure 35 : Raman spectra for BH 37395, 532 nm, 5 seconds, 5% laser power, 50x magnification

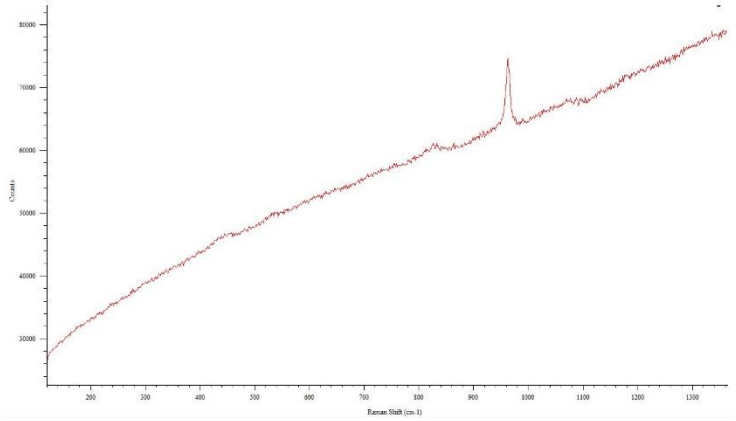

Figure 36 Raman Spectra for BH 37400, 532 nm, 5 seconds, 5% laser power, 50x magnification

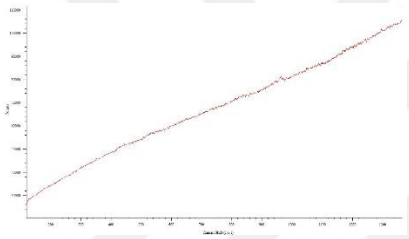

Figure 37 Raman Spectra for BH37622, 532 nm, 2 seconds, 1% laser power, 50x magnification

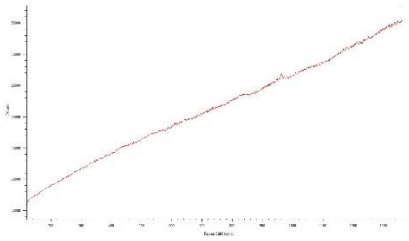

Figure 38 Raman Spectra for BH 37394, 532 nm, 3 seconds, 1% laser power, 50x magnification

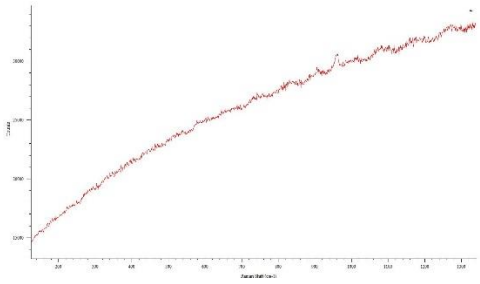

Figure 39 Raman Spectra for archaeological cow teeth, 633 nm, 1 second, 50% laser power, 50x magnification

5. 1. 3. FT-IR

5. 1. 3. 1. On Beads

FTIR was performed on 7 bead fragments. In 4 of the 7 bead fragments, we were able to use 2 different parts of the beads as samples (sample A from the blue part, sample B from the white part), amounting to 11 samples in total. More than 50 spectra were obtained on 11 samples from 7 beads, and only 50 were fit enough to be considered for interpretation. The measurements all revealed similar spectra, and six of these are provided in Figures 40-45 as examples. The breakdown of FTIR results with the exact points of the peaks in each spectrum, and the best matches for some beads can be found in Appendix E.

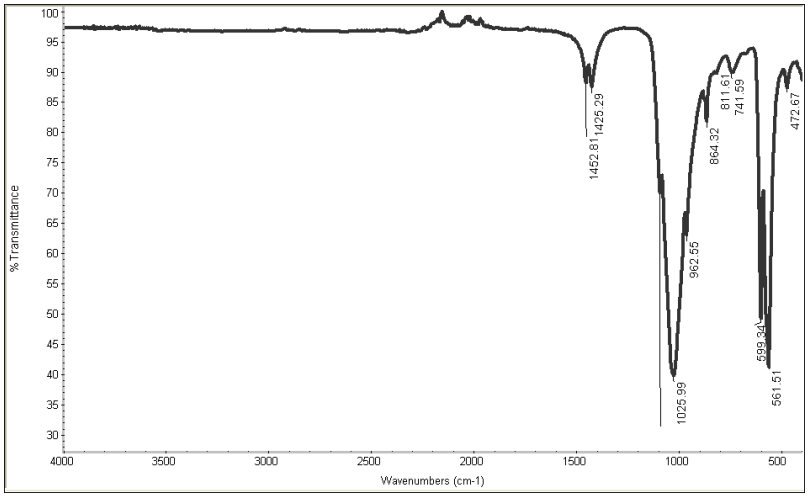

Figure 40 FTIR spectrum for BH 37397 - sample A - 4th take

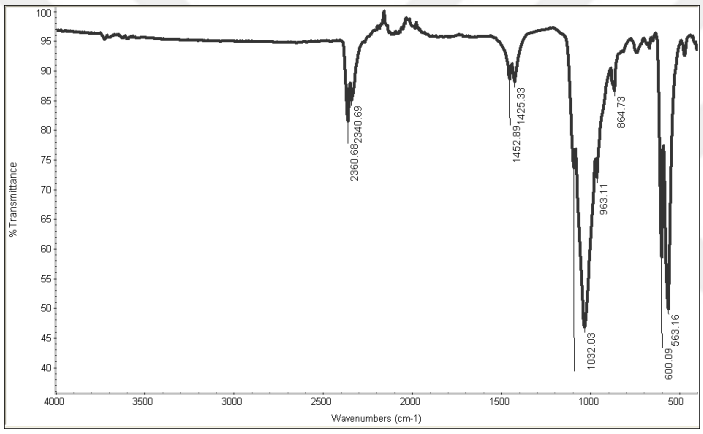

Figure 41 FTIR spectrum for BH 37393 - sample B – 1st take

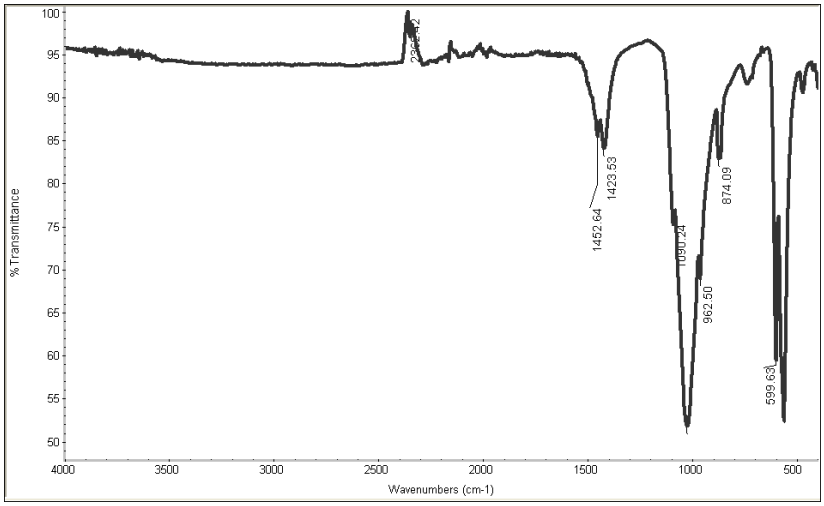

Figure 42 FTIR spectrum for BH 37399 - sample A - 1st take

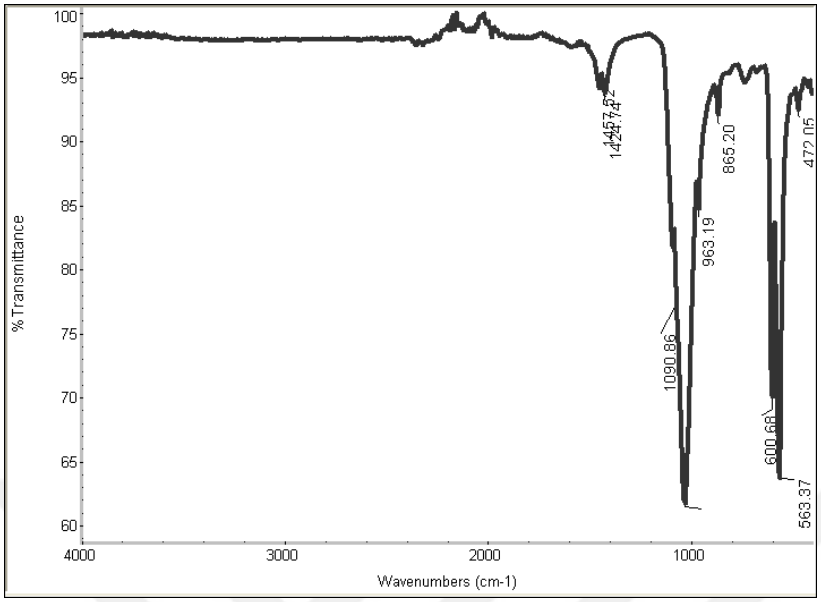

Figure 43 - FTIR spectrum for BH 37617 - sample B - 4th take

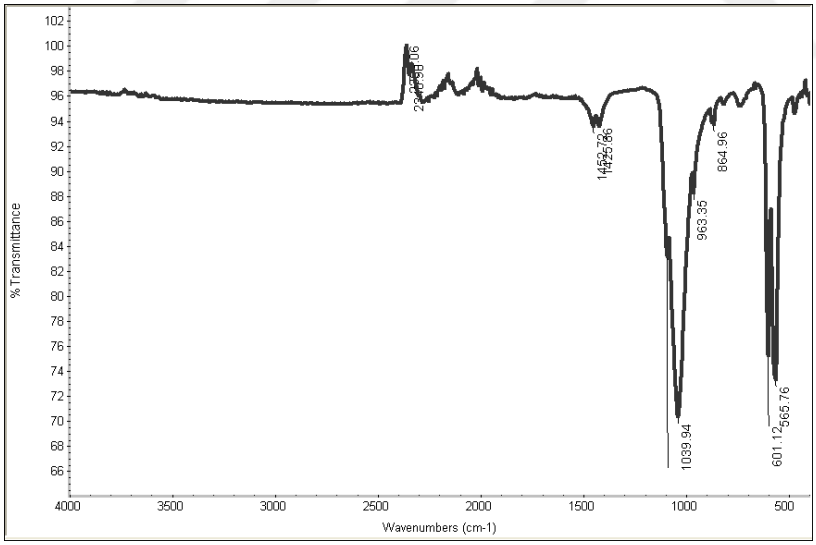

Figure 44 - FTIR spectrum for BH 37620 - sample A - 3rd take

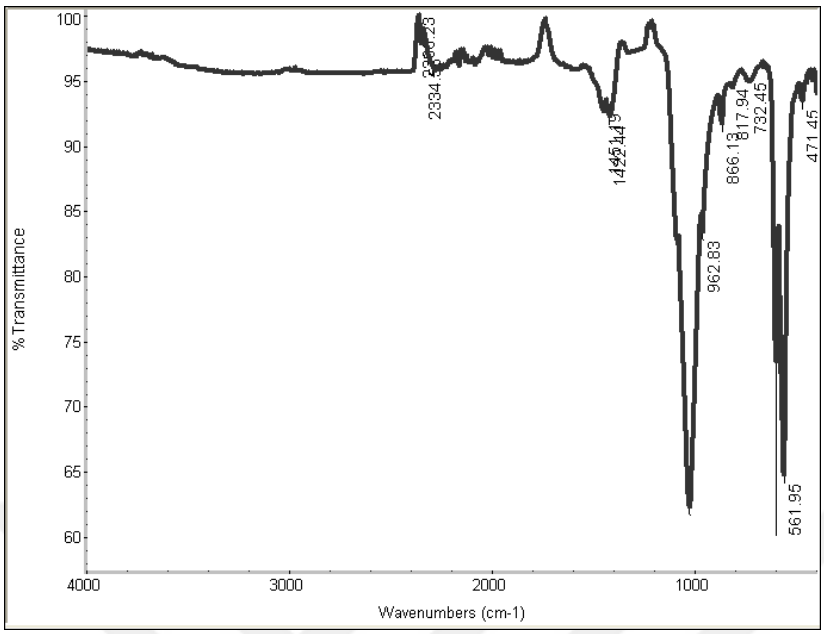

Figure 45 - FTIR spectrum for BH 37621 - sample B - 3rd take. Signal around 3400cm-1 indicates apatite.

There were no significant variations in the FTIR spectrum between the blue and white sections of the bead fragments, as the spectra for sample A's and sample B's from the same bead does not present differences. In the FTIR spectra of all bead samples we see a typical apatite FTIR spectrum with strong phosphate bands between 1094-962 cm^{-1} as ν3 (phosphate) antisymmetric stretching mode (Paz et al. 2012), and at 599 and 561 cm^{-1} as the bending mode of ν_4(phosphate) (Azami et al. 2011). At 470 cm^{-1} the bending mode of ν2 (phosphate) is noticeable in all beads as well (Paz et al. 2012). All samples also yielded minor amounts of carbonate signals at 864 cm^{-1} and between 1456 – 1427 cm^{-1} (NIST Chemistry Webbook), revealing the essential bone mineral made of carbonated hydroxyapatite (Field et al. 1974; Legros et al. 1987; Beasley et al. 2014). The two peaks seen around 2350 cm^{-1} (ca

2360 and 2340) are negligible as these are due to the carbon dioxide present in the air (Koreeda 2008).

Moreover, four samples belonging to bead fragment BH 37621 yielded an -OH signal around 3400 cm^{-1}, indicative of hydroxyapatite. In 17 other samples out of 50 that belong to all of the beads, we can also see a slight curve in the area around 3400 cm^{-1} (see Appendix E), but these are less pronounced than the signals seen in samples BH37621_A-1, BH37621_A-4, 4, BH37621_B-2, BH37621_B-3. The -OH signal was seen in samples collected from both the white and blue parts of the bead fragment.

When the IR spectra from the beads were matched with the mineral (HR Minerals) and inorganic library (HR Inorganics) of the EZ OMNIC instrument, the best match was seen with fluorapatite and isokite, the top two matches always being these two with match rates as high as 81.91% and 70.66% and as low as 34.8% and %63.97, respectively. Of 19 matches, ten have fluorapatite white as first match, and nine have isokite as first match. For the second highest matches, seven have fluorapatite blue, eight have fluorapatite white and three have isokite.

5. 1. 3. 2. On Bones

Number of bone samples	Number of tests run on each sample	Number of representative samples for each sample
14	4-6	1

Table 5 Breakdown of how FTIR spectra of bones were sampled

FTIR spectra of the archaeological sheep/goat bone samples are very similar to those of the beads (Fig. 46). Strong phosphate bands between 1094-962, at 599 and 561 cm^{-1}, and at 470 $cm^{-1;}$ as well as the carbonate signals at 864 and between 1456 – 1427 cm^{-1} are present. The only main differences are that the hydroxyapatite (-OH) signal is now present in every sample and is more noticeable, and that there is a new absorption band around 1640 cm^{-1}. The absorption bands around 1650, 1550 and 1235 cm^{-1} belong to amide carbonyl and point to presence of organic matter left in the material (Reiche et al. 2002b: 452; Baer et al. 1971: 6). The modern and archaeological bones are again very similar (Figures 47, 48), save for the intensity of the peaks, especially of the -OH signals at 3400 and 3300 cm^{-1}. Moreover in the modern bones, we see the other absorption bands that point to the presence of organic material at 1200 -1330 cm^{-1} (Lin et al. 2007: 4). The bands at 1740 cm^{-1} that can be seen in three samples, belong to aldehydic carbonyl group (Sastry et al. 2007: 910).

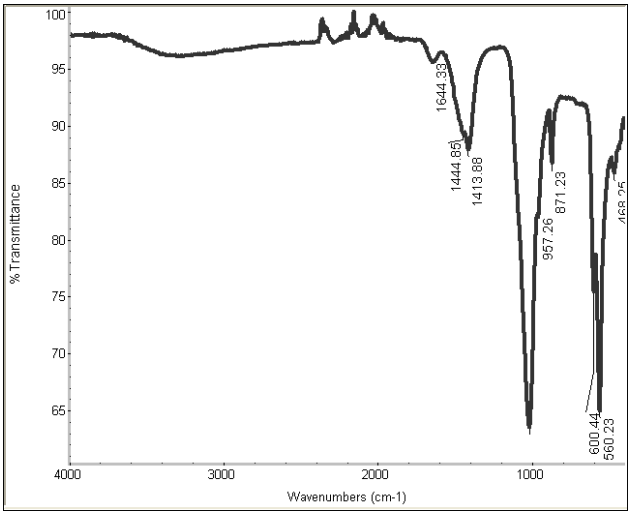

Figure 46 - FTIR spectrum for Archaeological sheep/goat bone - interior - sample 4 – take 2

Looking at the values in the table of the results of all FTIR tests, another noticeable difference between the beads and the bones (both modern and archaeological) is that the phosphate band at around 1090 cm-1 has disappeared in the bones, and the phosphate band at ca 1020-30 cm^{-1} has moved to around 1010 cm^{-1}.

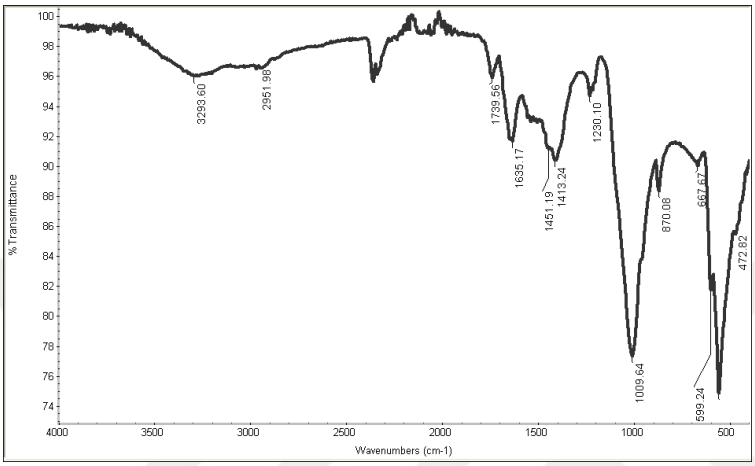

Figure 47 - FTIR spectrum for the modern sheep long bone - sample A - take 3

Unfortunately only one sample has been matched with the HR Inorganics and HR Minerals library of the EZ OMNIC software. This was the archaeological sheep/goat bone sample. The first match was Phosphate Sodium Dodecahydrate with 56.84 % match, and the second was Isokite with 54.81% match.

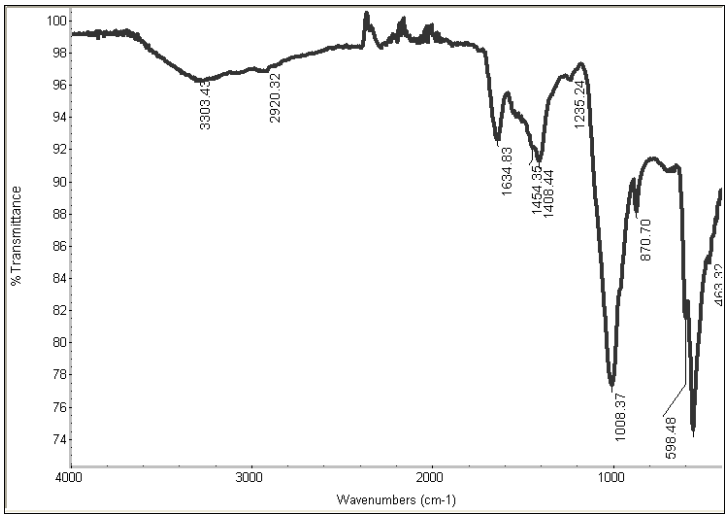

Figure 48- fTIR spectrum for Modern - cattle vertebra- sample B - take 4

5. 1. 3. 3. On Teeth, Tusk and Fossil Teeth

Four to six FTIR tests were run on each dentine, enamel, tusk and fossil tooth sample, however only one is chosen for each category as representative (Figures 49-52). These FTIR spectra are again very similar to those of the beads, with strong phosphate bands between 1094-962, at 599 and 561 $cm^{-1,}$ and at 470 cm^{-1}; and carbonate signals at 864 cm^{-1} and between 1456 – 1427 cm^{-1}. The amide carbonyl absorption bands around 1650, 1550, 1330 and 1235 cm^{-1} that point to presence of organic matter (Reiche et al. 2002b: 452; Lin et al. 2007: 4) are only present in the archaeological dentine (of sheep, human and cattle) and archaeological pig tusk samples. Interestingly -OH signal is not very noticeable in the teeth, tusk and fossil teeth samples except for in dentine, where it is quite intense in the dentine samples of sheep, human, and cattle. In terms of the -OH signal, dentine samples in fact seem to be closer to the bone samples. In the dentine spectra, the carbonate peaks around 1450 cm^{-1} seem to be more pronounced compared to the tusk, enamel and fossil

tooth samples. The bands at 1740 cm $^{-1}$ that can be seen in two samples belong to aldehydic carbonyl group (Sastry et al. 2007: 910).

The phosphate band at around 1090 cm^{-1} in the beads has disappeared in the tooth/tusk category as well, just like in bones. The phosphate band which was at ca 1020-30 cm^{-1} in the beads, and has moved to around 1010 cm^{-1} in bones, is found to be exactly in between those values for the tusk/teeth category, around 1015-1020 cm^{-1}.

Several samples in this category have been matched with the HR Inorganics and HR Minerals library of the EZ OMNIC software. Unlike the beads, fluorapatite is not one of the top matches for the samples in this category. The top two matches of this category consist of Isokite, Belovite and Phosphate-Sodium-Dodecahydrate.

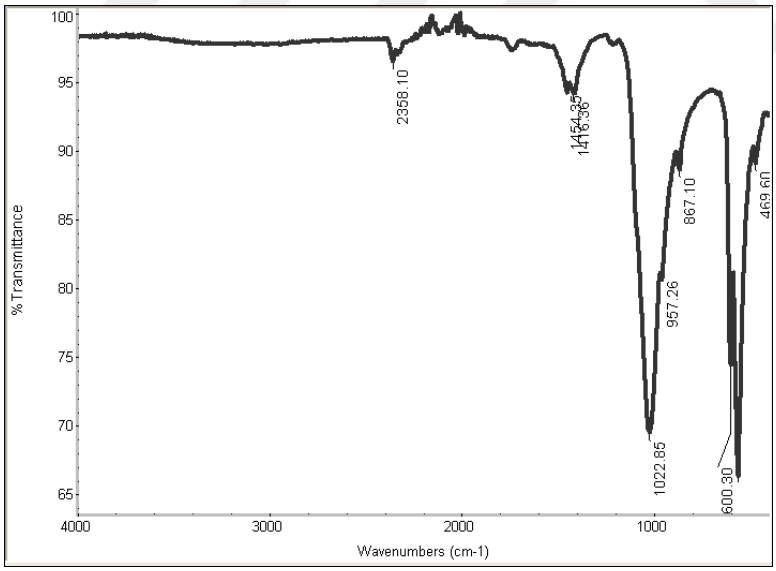

Figure 49 - FTIR spectrum for Equid Tooth Fossil 1 - take 5

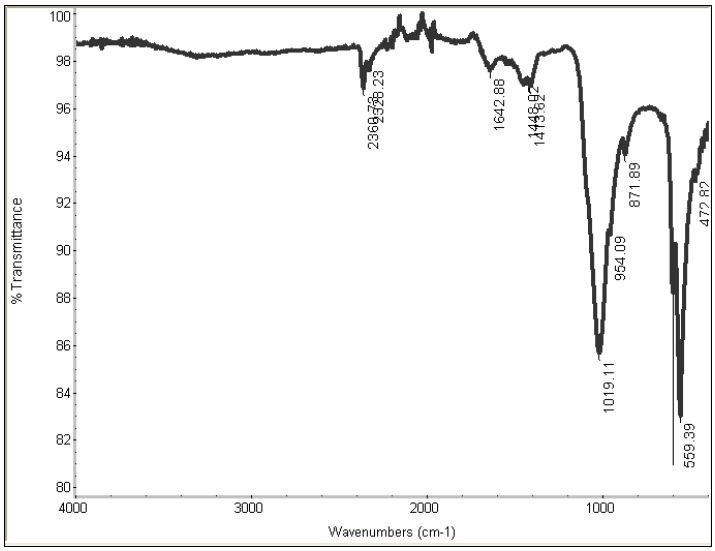

Figure 50 - FTIR Spectrum for archaeological pig tusk - take 4

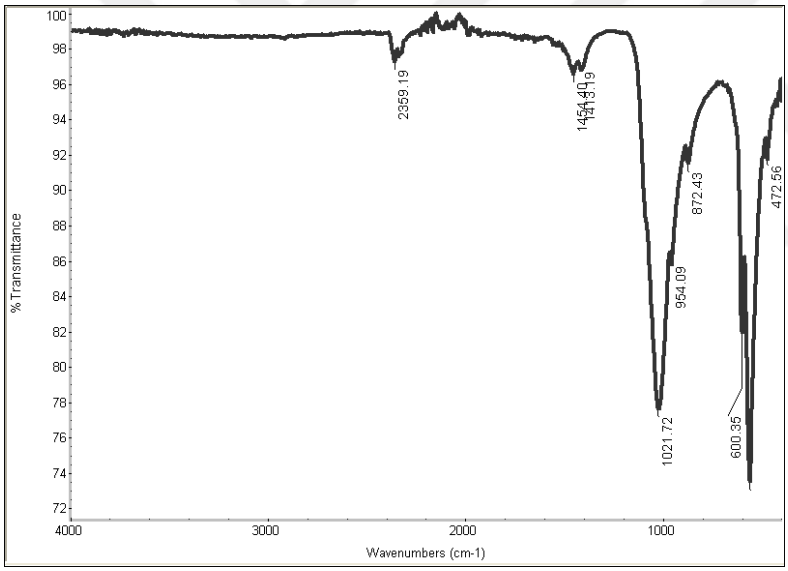

Figure 51 - FTIR Spectrum for the Enamel of Archaeological human tooth - take 5

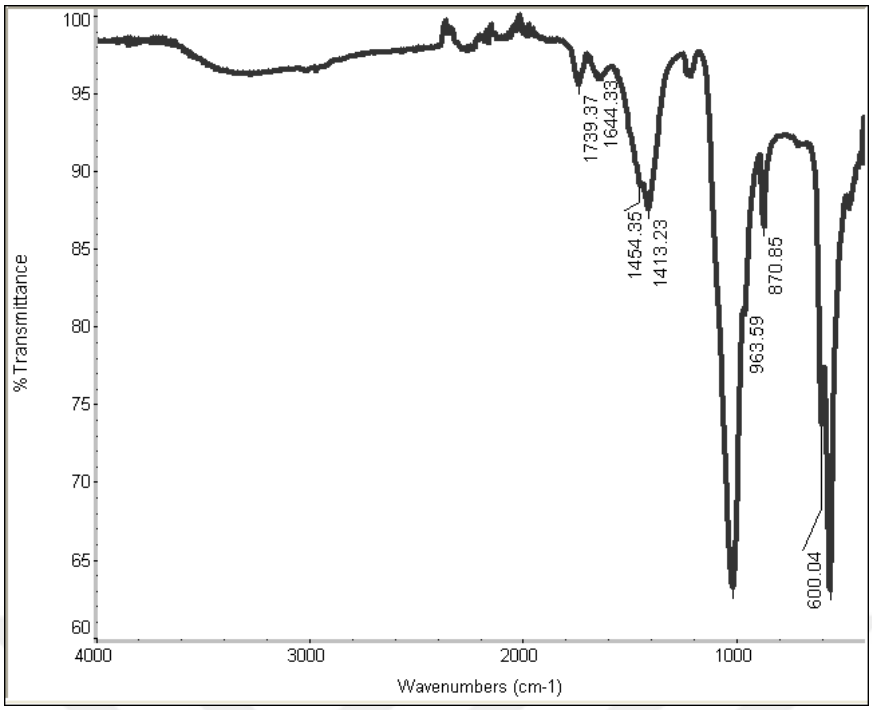

Figure 52 - FTIR Spectrum for the Dentine of Archaeological Sheep tooth - take 4

5. 1. 3. 4. On Heated Samples

Three samples (archaeological white-colored bone, archaeological black-colored bone, and pig tusk) were subject to a second round of FTIR tests after they went through heat treatment in solid and in powdered form, for 18 hours under 550 °C. These specimens were from the first batch of the experiments, and were not soaked in the solution. We aimed to see the affect of heat treatment on the archaeological samples.

The differences between the powder form of the original sample, the heat-treated solid sample, and heat-treated powdered sample can be seen below (Figs 53-55). The two heat-treated samples (both powder and solid) seem to be virtually the same. Even though they are similar to the original sample, we can see that the 1640-

50 cm^{-1} peaks in the modern bone samples, which point to the presence of organic matter, have disappeared after heat treatment.

Minor changes in the frequencies are also noticeable. In all cases we can see that the phosphate band at ca 950 cm^{-1} at the original sample, has moved higher in the heat-treated specimens (954 cm^{-1} became 957 cm^{-1} and 960 cm^{-1}; 954 became 961 cm^{-1}; 954 cm^{-1} became 960 cm^{-1}). The original carbonate peak around ca 870 cm^{-1} has moved towards 876 cm^{-1} in the heat-treated samples. In two cases (pig tusk and black bone) the carbonate peak at 1440 has moved higher towards 1450 cm^{-1} in the heat-treated samples.

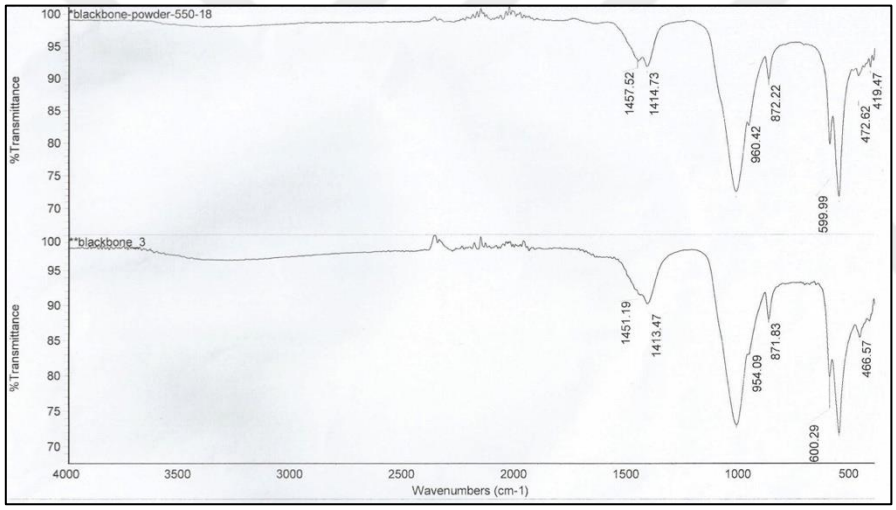

Figure 53 - Below, FTIR spectrum of black-colored archaeological sheep/goat bone before heat treatment. Above, FTIR spectrum of the same bone sample, heated in its powdered form

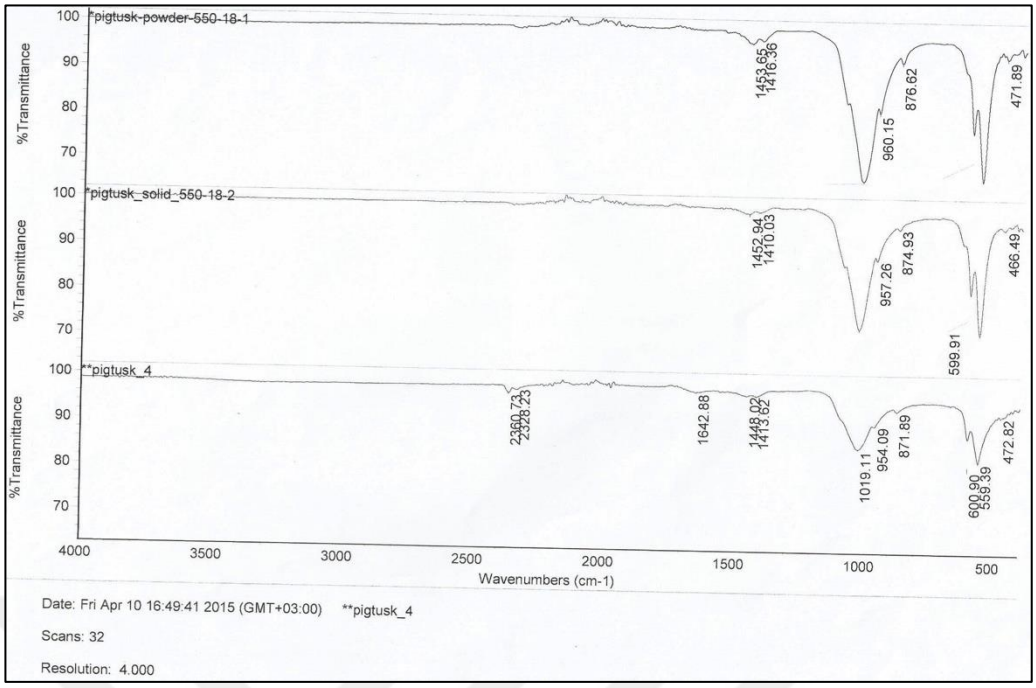

Figure 54 - Below, FTIR spectrum of white-colored archaeological sheep/goat bone before heat treatment. Middle, FTIR spectrum of the same bone sample, heated in its solid form. Above, FTIR spectrum of the same bone sample, heated in its powdered form

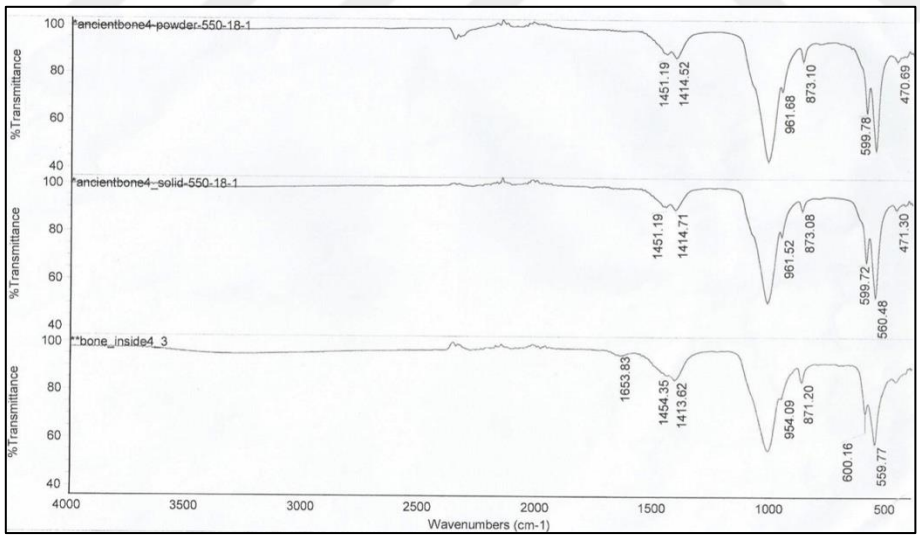

Figure 55 - Below, FTIR spectrum of white-colored pig tusk before heat treatment. Middle, FTIR spectrum of the same bone sample, heated in its solid form. Above, FTIR spectrum of the same bone sample, heated in its powdered form

5. 1. 4. SEM with EDX

Scanning Electron Microscopy on bead fragments revealed that the beads had textures similar to bone and teeth. Only a few SEM micrographs of the many taken for each bead provided images that show more clearly the inner structures of these materials. In terms of unpolished samples, BH37400 and BH37394 were the only samples that provided clear images of the exterior and interior surfaces of the beads. Many of these micrographs reveal canals that have fibers inside them (Figs 56-7). These canals are ca 1-2 macrons wide in some samples (BH37394, BH 37399), and are 6-8 macrons wide in others (BH37400). The images from the exterior surface of the beads generally did not give characteristic data.

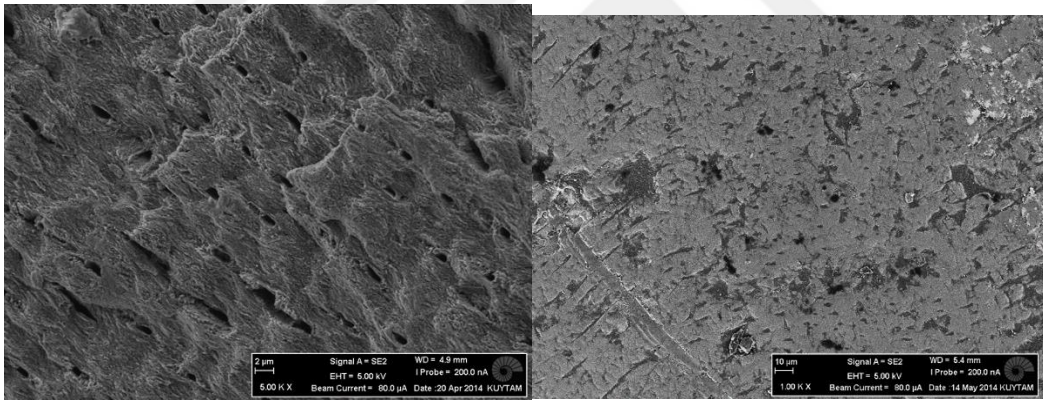

Figure 56 Micrographs from the interior of the beads vs the exterior. A) BH 37394 interior (500 times magnified surface) B) BH 373935 exterior

Cow teeth and bone from archaeological excavations were also examined under the SEM for comparison (figs 58-59). Polished cross-sections (of bead fragments BH 37399 and BH 37397) also proved useful in terms of obtaining images of the structure of the beads. In addition to providing a magnified surface topography of the beads, investigation of the polished cross section of the two beads with the scanning electron microscope (SEM) showed possible variations in structure.

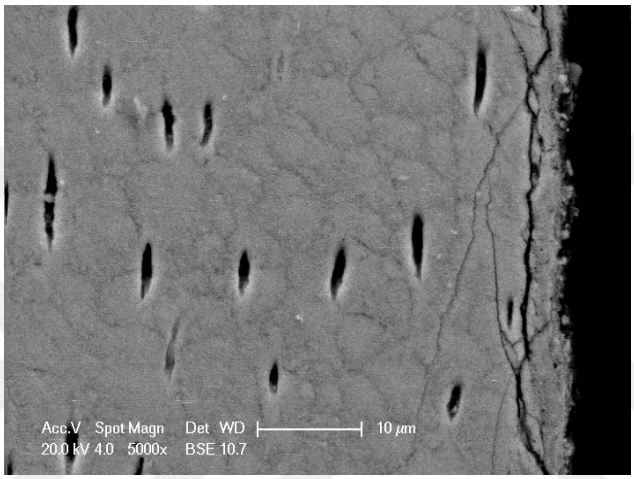

Figure 57 - SEM micrograph of the cross-section of bead fragment BH 37399

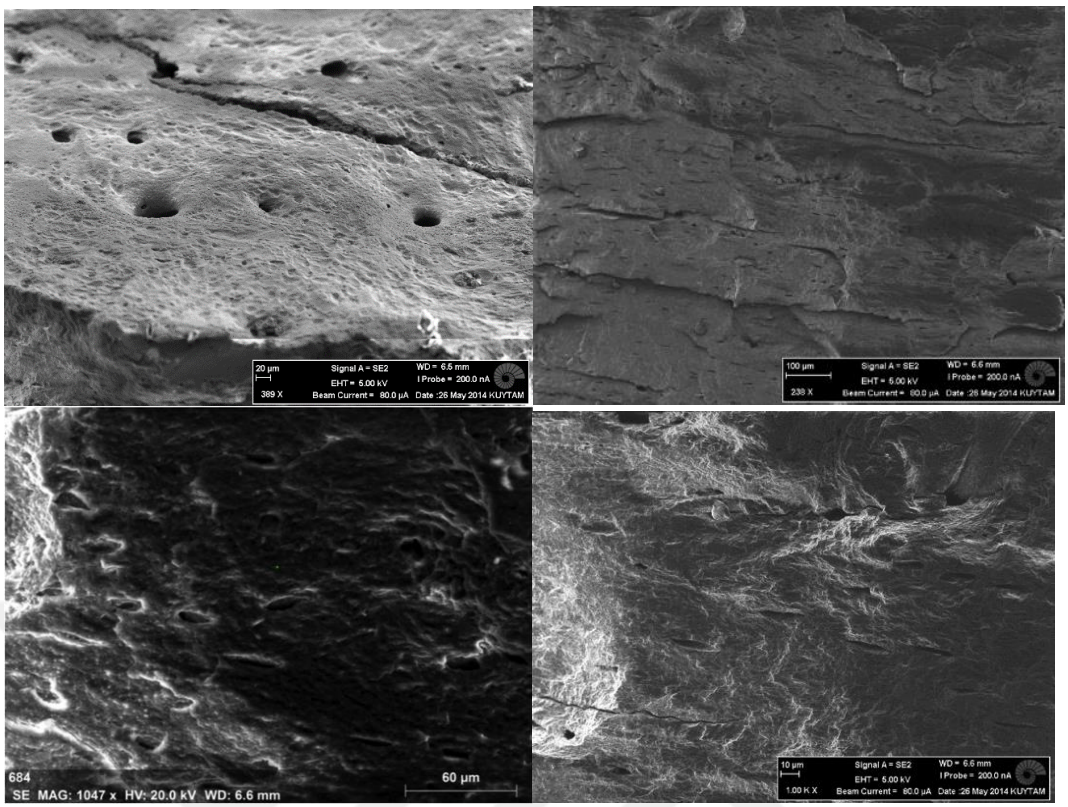

Figure 59 SEM of Archaeological cow long bone

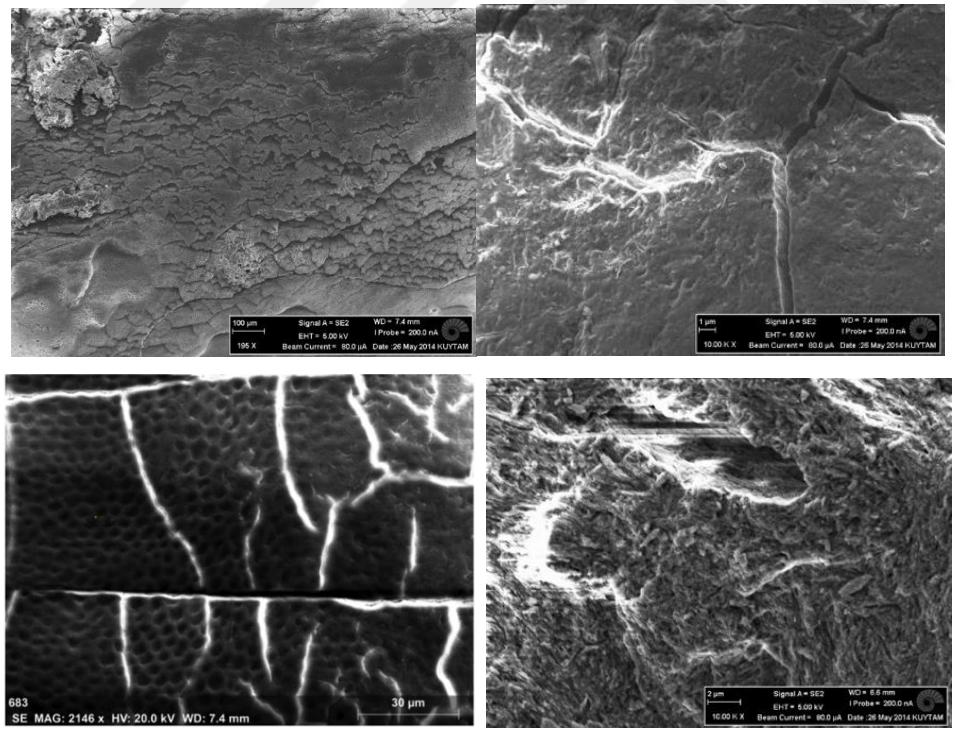

Figure 58 SEM of Archaeological cow teeth (top – dentine, bottom left – dentine, bottom right – enamel)

5. 1. 4. 1. Surface Layer on the Beads

In the back-scattered electron images of BH 37399 gathered from SEM analyses on the polished cross section, a thin distinctive crust layer of about 7-10 microns on the surface was noticed, shown in Figure 60. “Unfortunately, sections of this distinct thin layer were missing, which may be due to use, or to damage caused during the cutting or polishing operations of the cross section. The highly pitted and porous bone matrix is visible” (Bursalı et al. *submitted*). The backscattered electron image of bead BH 37397 is shown in Figure 63c. Similarly, the bead matrix here also displays excessive porosity, and reveals a surface layer of about 5 microns that is distinctly visible (Bursalı et al. *submitted*).

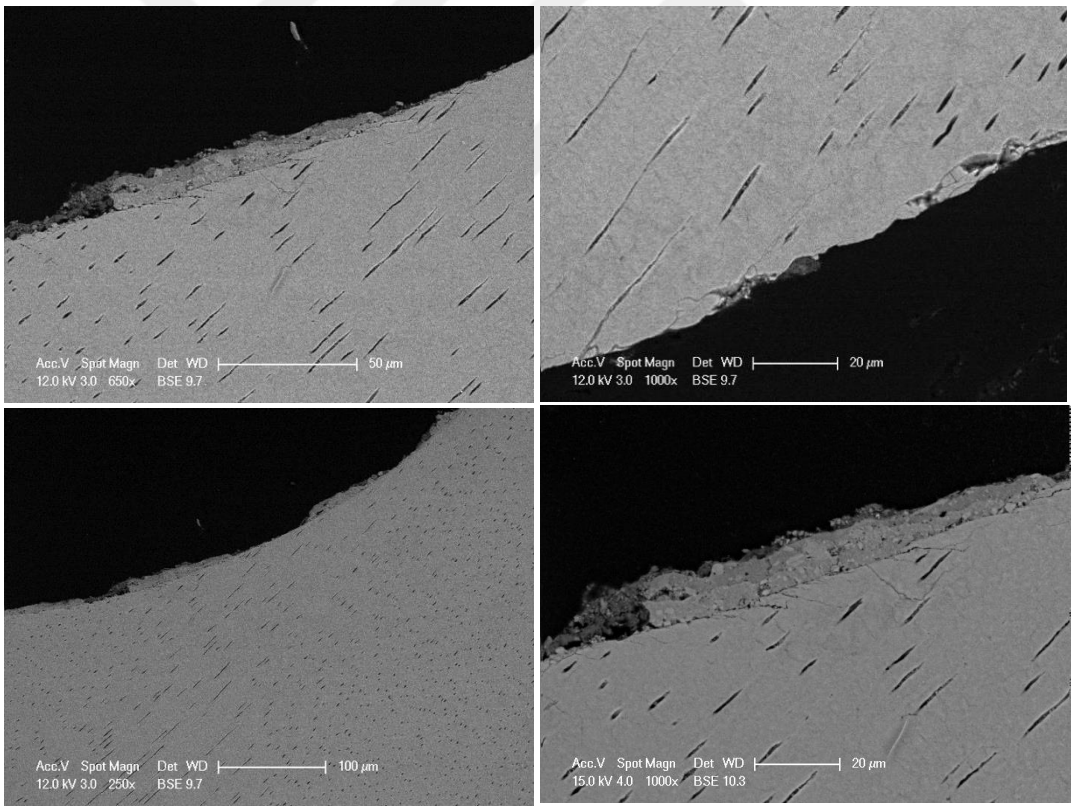

Figure 60 - Cross section SEM micrographs of bead fragment BH 37399, showing also the surface layer.

5. 1. 4. 2. Energy Dispersive X-Ray Analysis Results

Energy dispersive X-ray analysis (EDX) yielded elemental composition of the beads and the essential components were discovered to be CaO, P_2O_5, F, MgO, MnO, SiO_2, Al_2O_5 that constitute the composition of fluorapatite. These components as well as possible contaminations were focused on. However with the existing information it has been difficult to interpret all of our results comprehensively. The elemental compositions calculated at both KUYTAM and Boğaziçi labs were partly conducted including carbon, and partly excluding carbon. The reason for not including carbon was that all samples had to be carbon-coated to be scanned. Because carbon was introduced externally, the values would not present accurate information about the actual elemental distribution of our sample. In KUYTAM EDX analyses, when carbon was included, it stayed in a 4-7% range in the EDX results (see extended table in Appendix F), and it can be argued that this could be a negligible amount. However in Boğaziçi laboratory analyses, when carbon is included, it was in a 16-45% (see extended table in Appendix F), which would not be negligible. The stark difference in the carbon percentage of the samples tested at different laboratories, also suggests that the SEMEDX machines in the two labs may be configured differently. Evaluating the results obtained from them together would not provide accurate results. In light of this problem, the results were evaluated separately, and a summary follows. The EDX results of bead surfaces at KUYTAM both include and exclude carbon based on the sample. EDX results of the polished cross-sections at Boğaziçi all include carbon.

In the extended table in appendix F where the EDX results are detailed, the KUYTAM and Boğaziçi results are separated by their font colors, Boğaziçi results

dark red at top, KUYTAM black at bottom. The carbon-excluded results are italicized. For some Boğaziçi samples (2 bead samples and all the bone samples), both carbon included and excluded results exist, these are marked with a star. In parentheses are the carbon-excluded results.

In all bead samples, calcium, phosphorus and fluorine were the three most abundant elements. Sodium, magnesium, manganese, silicon, sulphur, potassium, chlorine, aluminum, titanium and iron were also detected in minor amounts in different beads. There does not seem to be a noticeable difference in the elemental composition of the beads between the blue and white sections. In the archaeological bone and tooth samples, fluorine was not present, calcium and phosphorus constituted most of the make-up of these materials. In only the blue-colored archaeological bone sample, manganese was also detected.

In total 35 analyses were made on 13 beads. A summary of the results of 23 elementary analyses on the surface of eleven beads, and 12 elementary analyses on the cross-section of two beads are presented in Table 6 as average and minimum/maximum of the respective components. The parentheses next to the average values represent the total number of results observed in the analysis for the particular compounds measured. The more detailed table where the results of each analysis on beads, bones, and experiment samples can be found is in Appendix F. Among the samples analyzed, two unique contrasting data are observed. One bead sample (BH 17556) yielded very low levels of calcium oxide (as low as 0,63%) but in contrast yielded nearly 20 times more than the average value observed for SiO_3 and Al_2O_3, namely 22,52% and 9,16% respectively. Samples like this one may have

undergone dramatic deterioration as well as been subject to compositional exchange due to environmental contaminations.

Average and range of data from SEM-EDX of surface analyses of beads and bone (some of the results used in the averages include carbon)								
Compounds	**CaO %**	**P_2O_5 %**	**F %**	**MnO %**	**MgO %**	**SiO_2 %**	**Al_2O_3 %**	**Fe %**
Average	28.18 (23)	10.41 (23)	3.08 (13)	0.39 (10)	0.75 (18)	5.77 (19)	2.56 (21)	2.51 (8)
Range	0.63 – 49.33	0.22 – 21.21	nd - 12.1	nd - 0.92	nd – 2.37	nd – 22.52	nd – 9,83	Nd – 6,1
Bone&Teeth	42.4	13.9	nd	nd	0,25	nd	nd	nd
	SEM-EDX data of polished cross section of bones and beads							
BH37399 (carbon incl)								
Surface layer (4)	27,19	11,71	1.03	1.52	0.62	2.53	1.16	0.49
Body (4)	30,58	13.12	1.81	1.41	0.60	4.19	1.42	0.33
BH37397 (carbon incl)								
Surface layer(1)	26.33	10.16	0,89	0,35	0.47	2,04	0,62	nd
Body (3)	29,88	11,45	1.22	0.29	0.81	5.54	4,02	nd
Experimental bone (5) (carbon exc)	43.8	20	nd	0.45	0.69	nd	Nd	nd

Table 6 The results of all elementary analyses presented in as average and minimum/maximum of the respective components. Numbers in the parenthesis show number of data used in determining the average, nd = not detected

Out of 23 surface analyses that belong to eleven beads, 11 samples that belong to six beads yielded a recordable quantity of MnO (with an average of 0.39%), the element believed to be responsible for the turquoise color (Reiche et al. 2001). One sample (BH 21476) had 10.9% manganese oxide in the surface layers and is not included in the averages. Interestingly, this at least 25-fold increase from the average MnO concentration of the rest of the bead was detected not on the dark blue section of the bead but on the light blue section, and we have at this time no possible explanation for this except that it may be due to intense accumulation of MnO at this given spot (Bursalı et al. *submitted*). It should be noted here that Fe, which was thought to be responsible for the blue color before more detailed research revealed it to be MnO (Reiche et al. 2001), was also detected 10 times, but in 2 beads, and on average in higher amounts than MnO.

Fluorine was detected 13 times out of 23 analyses on nine beads with an average of 3.08% (see Table 6). This is an important result as it confirms the results observed with FTIR analysis, where the majority of the samples were classified as fluorapatite, indicating that -OH of hydroxyapatite is exchanged with fluoride. Magnesium was detected in 18 analyses out of 23, in all beads except one with a 0.75% average which supports the idea as shown in FTIR library matches that even isokite ($CaMg(PO_4)F$) formation was in progress in these beads. To provide comparison, Table 6 also shows SEM EDX analyses of archaeological bone and teeth samples, indicating that such contamination and exchange processes as seen with the beads have not taken place even with these samples that have been exposed to almost identical depositional processes as the beads.

The results of twelve EDX analyses on the cross-section of two beads can also be seen in Table 6, however we should keep in mind that these results do include major amounts of carbon. The elemental compositions of both the surface layer (of 7-10 microns) and the inner bulk matrix of bead BH 37399 were analyzed by EDX. Interestingly, the surface layer revealed MnO levels as high as %4.21, which is more than 7 times the average Mn values of the bead matrix (Bursalı et al. *submitted*). Bead surfaces also had similarly revealed high levels of MnO under EDX analysis, just like the three beads analyzed from Tell el-Kerkh, which are the only other such beads subjected to scientific examination. On the other hand, this same point on the surface layer also contained 5,2% and 2,5% silicate and aluminum oxide respectively. As can be seen in the Mn distribution map in figure 61b, contrary to our expectations, there was only a slight excess of Mn in the surface layer compared to the bone matrix. This leads us to think that the MnO that was detected in the analysis must have been concentrated in a small area, as it probably was in the case of sample BH 21476. Distribution maps for calcium and phosphorus did not reveal any difference and can be seen in the appendices. The Mn distribution map of bead BH 37399 (Fig 61b) shows that Mn has penetrated evenly into the bone matrix as far as 40 microns (Bursalı et al. *submitted*). The Mn distribution map of the other bead, BH 37397 is shown in Figure 61d and reveals no extensive variations in the concentration of components between the surface and the matrix (based on EDX done on one point in the layer and two points in the matrix) (Bursalı et al. *submitted*). Distribution maps for calcium and phosphorus also did not reveal any difference and can be seen in the appendices. EDX analysis shows that the surface layer is slightly more concentrated with environmental contaminant, namely silicate and aluminum

oxide, with a slight decrease in calcium and phosphorus levels (Bursalı et al. *submitted*).

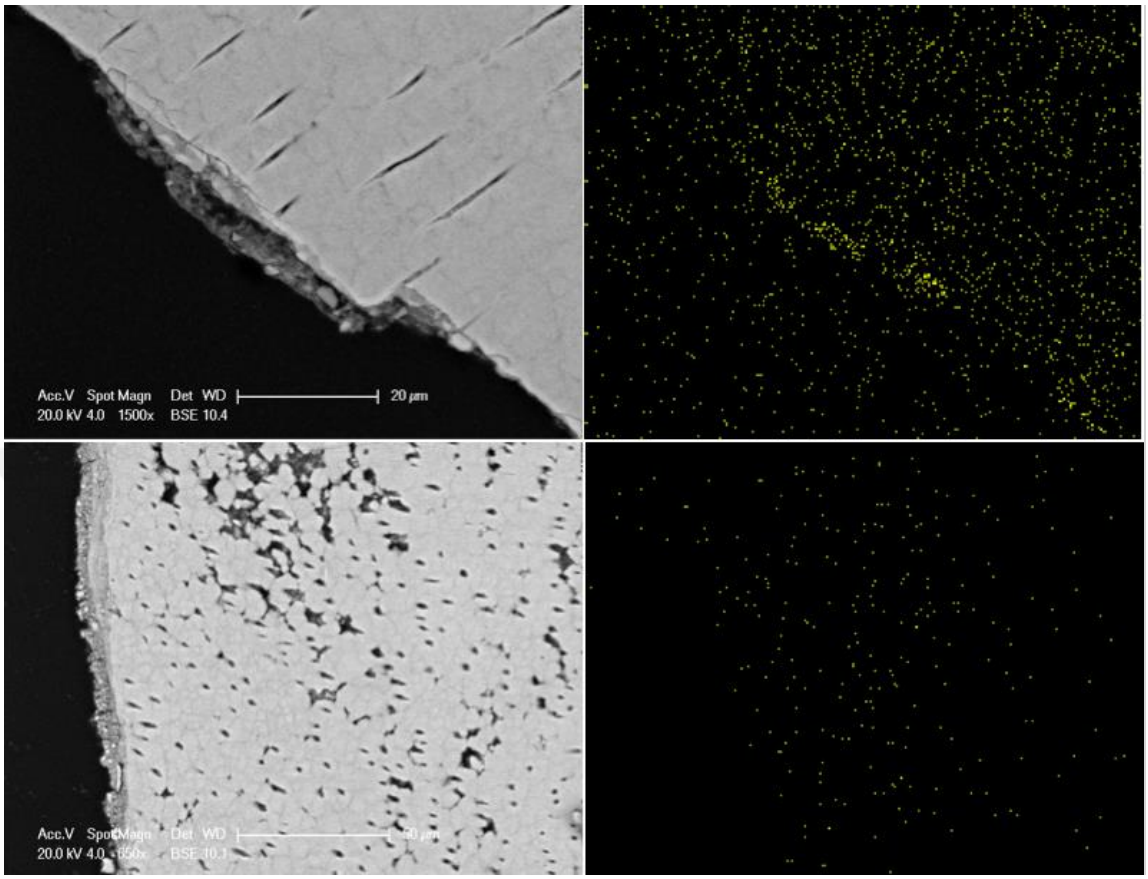

Figure 61 (top left) back-scattered electron images of BH 37399, showing a layer of about 5-7 microns on the surface,
Fig. 61b (top right) Mn distribution map of BH 37399. The layer is seen to be richer in terms of MnO,
Fig. 61c (bottom left) SEM image of BH 37397,
Fig. 61d (bottom right) Mn distribution map of BH 37397

The Mn average for the surface layers of the two beads was 0,54% compared to the 0,7% in the body of the beads. Fluorine was again detected, in all bead samples, with an average of 0,96% in the surface layers and 1,52% in the body of the beads. Fe was again detected in one bead, 0.49% on the surface layer and

0.42% in the body. The calcium average for these beads were 30,23% in the body and 26,76% in the layer; and phosphorus 12,28% in the body and 10,93% in the surface layer.

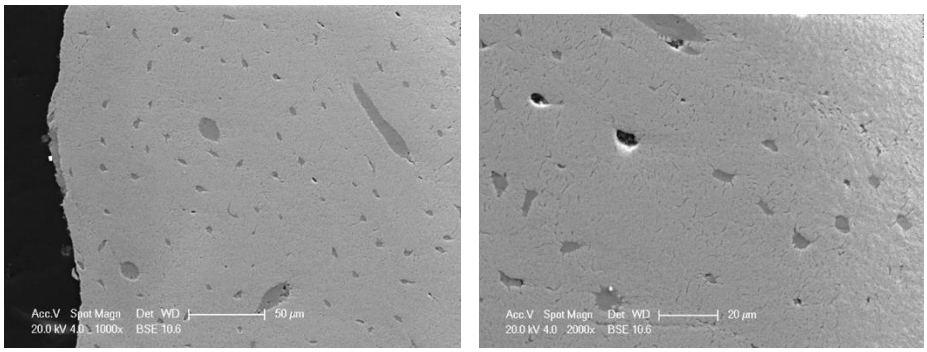

Figure 62 - SEM micrographs of archaeological blue bone found in excavations – BH 44499

SEMEDX analysis further led to an interesting revelation about the archaeological blue-colored bone found in the excavations (see Fig 63 and Appendix F). This bone fragment was discovered in a burnt context and was found stuck in burnt loam, presumably turning blue due to the heat it was exposed to. This bone fragment was also investigated with SEMEDX, and unlike the normal white-colored bone and teeth samples, it was found to contain Mn, in amounts of 0.4% on the pores and 0.73% on the matrix section. This was higher than the average value of Mn observed in the bead samples, and the Mn amounts observed in the experimented bone samples, the results of which will be detailed in section 5.2.1. The presence of Mn in the archaeological blue bone, and at such amounts, suggests a connection between the blue color and Manganese.

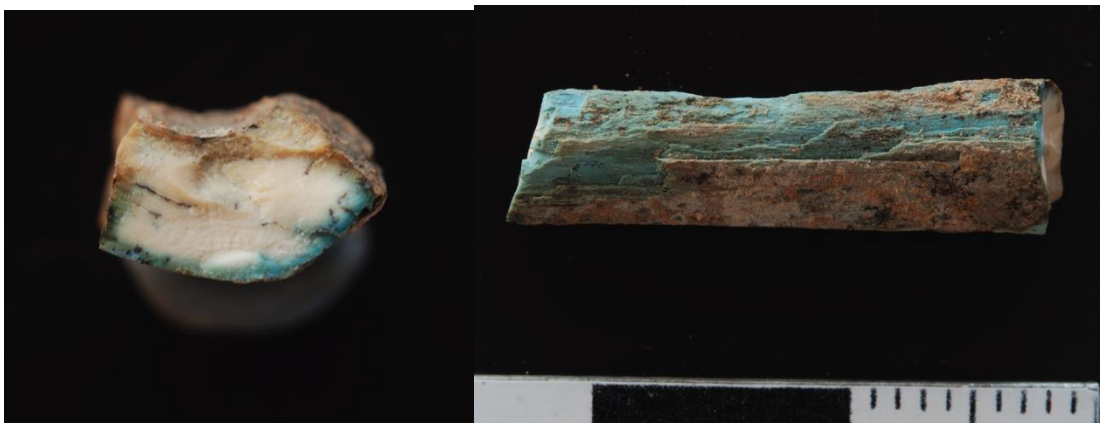

Figure 63 Archaeological blue bone found in excavations, BH44499

5. 2. Experimental Results

By using Taniguchi et al. (2012)'s recipe, and then employing heat treatment, we achieved positive results. Blue color was best achieved with archaeological Neolithic animal bone from the Barcın excavation when bones are kept in solution for nearly 5 days and then heated in an oven for 26 hours at 600 °C. Application of the same procedure on archaeological teeth as well as on modern bone yielded green and dark blue hues, but not a full color change. Results are detailed in Table 7 and can be seen in Figs 64-7.

Table 7 Results of coloring experiments:

Results	Slight color change to bluish hues in only few specimens. Most specimens became darker brown or gray colors compared to their unheated versions.	Modern sheep bones (vertebra and long bone) only became dark yellow. Cow vertebra had yellow color with green tints. Archaeological sheep/goat bone became blue and dark brown.	Some had reached turquoise color. But only few photos exist. The versions with missing ingredient are mostly white.	Full solution – when taken out at 94 hours, they were more brownish/ blackish at parts compared to at 50 hours, but still kept their turquoise color. In versions with the missing ingredient, the samples are more light turquoise /green compared to at 26 hrs.	We reached brown and light turquoise/blue colors with the full solution. The solution with only Mn was a much lighter turquoise/white color. The solutions with only Fe and only Mn + Fe produced light blue colors which are closer to green than blue. much as the first try of the first batch. (Only one kind of bone turned the brightest turquoise color and only some parts of it)	The bone did not have a full turquoise color but was light turquoise. On the pig teeth, we reached gray/blackish and brown coloring. Some very small spots on the brown colored tusk could be interpreted as dark turquoise.
Oven temp	550 °C	600 °C	600 °C	650 °C	600 °C	550 °C
How long in oven	18 hours	24 hours	26 hours	26+18 = 44 hours	24 hours	21 hours
Solution properties	-	Full solution	Full solution,		Full solution, solution with only Mn, solution with only Fe, solution with only Mn +	Full solution
How long in Solution	-	100 hours	110 hours		190 hours	144 hours
What are the samples	Archaeological sheep/goat bone samples from different bones, fossil equid tooth, archaeological cow tooth, archaeological pig tusk, modern animal bone (cow Vertebra, sheep vertebra)	Archaeological sheep/goat bone (from one bone), modern sheep long bone, modern sheep vertebra, modern cow vertebra.	Archaeological bone from the one bone that seems to give the best results based on previous experiments		Archaeological sheep/goat bone samples from the one bone that seems to give the best results based on previous experiments	Archaeological sheep/goat bone (same bone as before), archaeological pig teeth
	1st	**2nd**	**3rd**		**4th**	**5th**

1st batch, 550 °C, 18 hours, no solution:

Figure 64 Samples that belong to the 1st batch. a) archaeological sheep/goat bone heated for 18 hours at 550 °C without the solution b) archaeological pig tusk heated for 18 hours at 550 °C without the solution,

2nd batch, 600 °C, 24 hours:

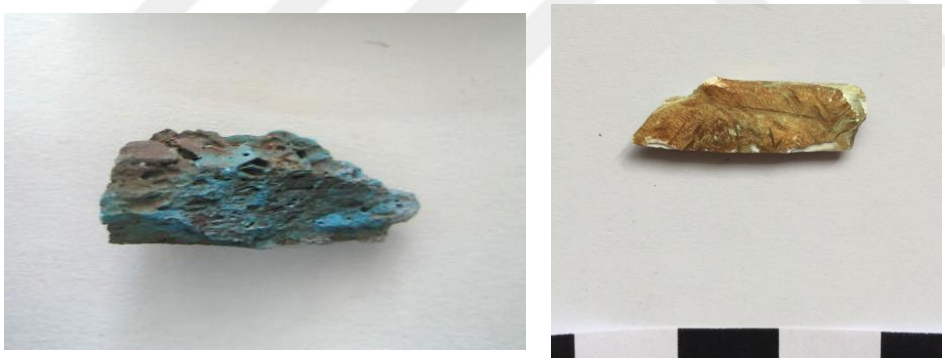

Figure 65 Samples that belong to the 2nd batch that have been subject both to the solution and heat treatment
*a) archaeological sheep/goat bone heated for 24 hours at **600** °C b) archaeological modern cow vertebra heated for 24 hours at **600** °C*

3rd batch, 600 °C, 26 hours (left), 44 hours (right)

Figure 66 The same piece of archaeological sheep/goat bone sample part of the 3rd batch that has been subject both to the solution and heat treatment. A) When heated at 600 °C for 26 hours. B) Same piece of bone heated for 18 hours more at 650 °C, totaling 44 hours.

After our experiments, we noticed that the matrix of the heated samples had weakened, and that the blue bone pieces were easily chipped upon handling, even when gently placing in plastic bags. We attributed this weakening to the heating process. However when we went back to our experiment samples 2 years later, we noticed that it was mainly the samples that were soaked in the solution with NaCl that were affected by this phenomenon. This was easily seen when comparing the samples that were put in the solution without NaCl, with the other samples (Fig 67). The samples without NaCl also had small chips. However the NaCl samples had become almost fully powdered (see Fig 67). Thus we can attribute this phenomenon mostly to the presence of NaCl in the samples.

Figure 67 All samples belong to the 3rd batch, heated for 44 hours (26 hours at 600 °C, 18 hours at 650 °C) a) (top-left) 2 years after the experiments took place, looking at the experiment samples put in solution without NaCl b) (top-right) 2 years after the experiments took place, the results of the experiment samples put in solution without MnO, c) (bottom) 2 years after the experiments took place, the results of the experiment samples put in full solution.

5. 2. 1. Results of SEM with EDX on Experiment Samples

The polished cross section of one bone sample which was subject both to the solution and heat treatment was investigated with SEM-EDX analysis which revealed the typical bone matrix as well as about 1-2 micron of thin surface layer (Figure 68). EDX analyses from the surface layers (2 tests) as well as from the

matrix (3 tests) of the sample yielded practically the same compositional data. The average values for the components are listed in Table 6 and are detailed in Appendix F. Similar to the bead samples, calcium and phosphorus constituted the main components, however unlike those samples, no fluorine, silicate and aluminum oxide were detected in the experimented sample. The average MnO value of the experiment sample was 0.45%, which is within the range of the average MnO value of the beads. “Finally, experimental blue bone contained an average of 0.92% chlorine, which must be due to exchange of hydroxide of apatite with the chlorine ions present in the impregnation slurry” (Bursalı et al. 2017 *submitted*).

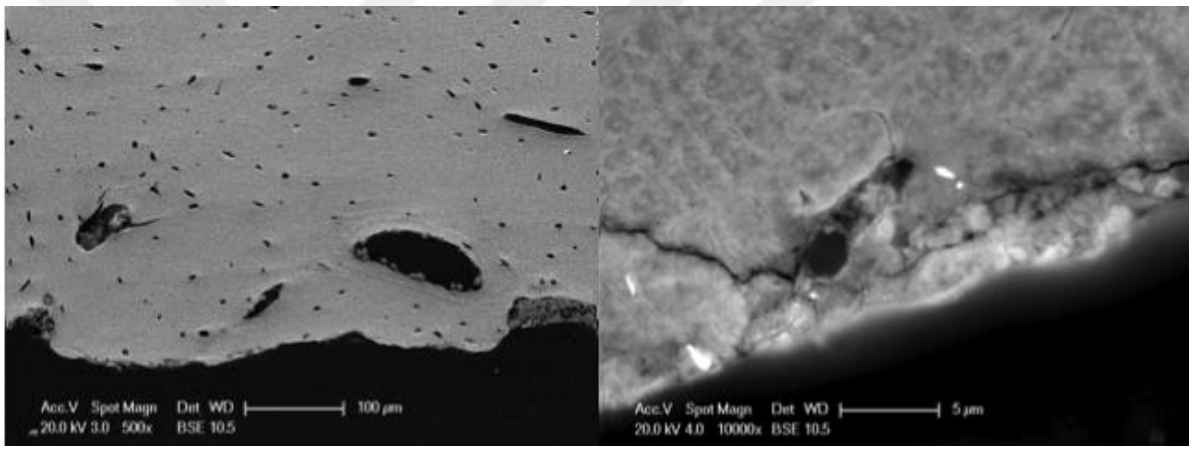

Figure 68 Cross section SEM images of experimental bone.

CHAPTER 6 – INTERPRETATION OF THE RESULTS

Taken together, the data in hand suggests that the material is either bone, tooth or ivory, and that at least some specimens are the fossilized versions of bone, tooth or ivory, or are in the process of becoming fossilized. Going back to our initial hypothesis, we can safely say that none of the beads that we analyzed were made of turquoise stone, clay or plaster. The fossilized material however could be classified as stone.

It is difficult to chemically distinguish between bone, tooth or ivory; and not possible through the analyses we have conducted. However based on the decrease in hydroxyapatite and intake of materials such as fluoride we can guess at the fossilization of the material. To help with our understanding, in this section we also turned to other literature on odontolite and blue-colored bone/ivory for comparison.

6.1 Instrumental Analysis

6.1. 1. Optical microscope

The optical microscope images show that some beads have bone-like and others stone-like structure. Parallel lines similar to annual rings found in teeth or tusk have also been noticed. However these lines could exist in unfossilized and fossilized material alike, so they do not help distinguish between bone or stone/fossilized material. In fact they do exist in a bead with stone-like structure as well as a bead with a bone-like structure.

Comparisons with similar beads from Tell el Kerkh, as well as with odontolite found in Krzemnicki et al. are made (Figs 69-71). However nothing optical microscope provides should be taken for certain as it merely provides an assessment of the appearance of the beads. More semi-quantitative scientific analyses that reveal a closer look at the structure and the elemental composition are needed to reach more conclusive results.

The Tell el-Kerkh beads were also investigated with optical microscope (Fig 69) and the researchers describe the beads to display "a regular pattern with annual rings, characteristic features of an animal tusk, ivory, or a molar tooth of a herbivorous animal" (Taniguchi et al. 2002: 178). Although reminiscent, these do not seem very similar to the parallel lines seen in our investigation.

Figure 69 Parallel pattern seen in one Tell el Kerkh bead, Bead 1, interpreted as annual rings by Taniguchi et al, from Taniguchi et al. 2012: 179.

Krzemincki et al., who investigate a historic jewelry set with odontolite pieces set in it alongside turquoise stone, provide optical micrographs of odontolite. The banding seen in the first figure (Fig 70 - left) is also not similar to our bead samples, however the texture seen in the third figure (Fig 70 - right) is slightly

reminiscent of the grainy surface observed in the Barcın beads, though this one is admittedly more homogenous, more turquoise-colored, and lacks the bone-like texture observed in the some of the grainy surfaces.

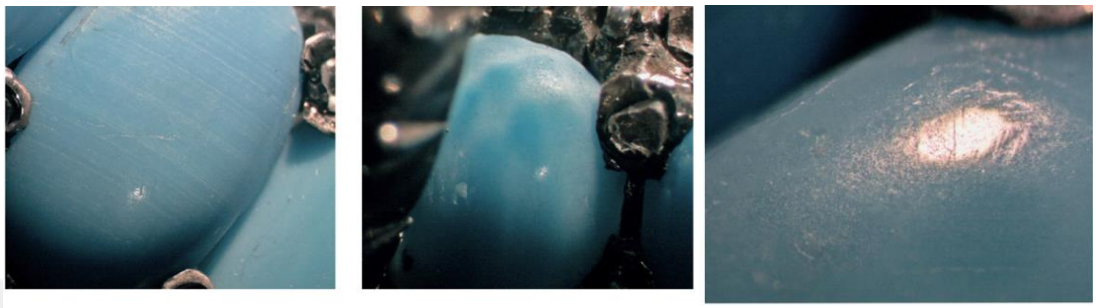

Figure 70 – Optical microscope images of 3 odontolite beads, from Krzemincki et al 2011, 298. Left – 15x magnifies photomicrograph "displays weak banding in odontolite". Middle – 20x magnified photomicrograph shows "characteristic curved intersection bands…on several of the odontolite cabochons". Right – 30x magnified micropores observed on the surface of the odontolite cabochons".

6.1.2. Raman

The Raman shift spectra of the beads and tooth sample that we obtained showed the presence of calcium phosphate ($Ca_3(PO_4)_2$), with strong or weak peaks at 960 cm^{-1} which point to a bone-like composition in the beads. Here we compare the Raman shift spectra of odontolite published in Krzemnicki et al., 2011 to see if any similarities with our results exist. Krzemnicki et al. used a 514 nm argon-ion laser and collected the spectra "from 1800 to 100 cm^{-1} Raman shift, to include the vibrational range of organic compounds, such as wax and artificial resin, used for turquoise impregnation. In a few cases, spectra were collected up to 5000 cm^{-1} to

check for OH bands in the dentine" (Krzemnicki et al. 2011: 297). The odontolite specimen they analyzed had a distinct peak at 964 cm^{-1} , smaller peaks at about 1090, 580, and 430 cm^{-1} , and a weak, broad OH band at about 3540 cm^{-1} (Fig 71) (Krzemnicki et al. 2011: 298). The authors report that the pattern they obtained "showed a perfect correlation with fluorapatite spectra taken from the SSEF reference mineral collection…" (Krzemnicki et al. 2011: 298).

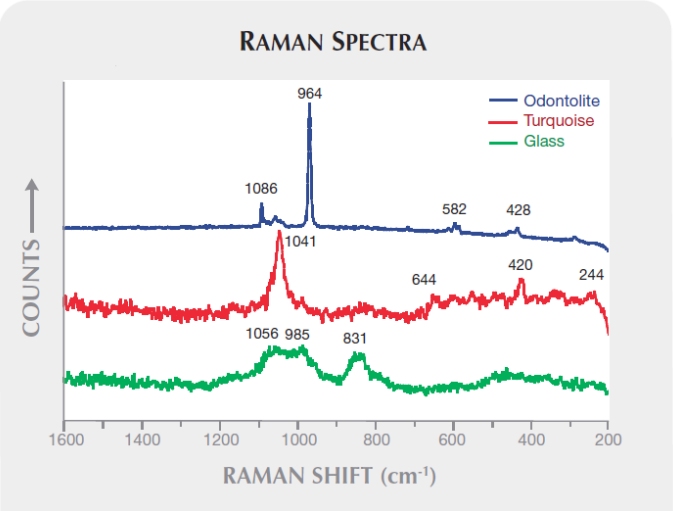

Figure 71 Raman spectra for odontolite after Krzemnicki et al. 2011: 299.

The laser power used in KUYTAM was different than in the aforementioned study, as the one mentioned is not found in KUYTAM, however it was the closest laser power possible (532 nm). In the Raman spectra for beads BH 37395 and BH 37400 (figs 35 and 36 respectively), the highest peak does seem to fit with the peak at 964 cm^{-1}, which is also visible but with much less intensity at in the Raman spectra of beads BH37622 and BH37394 (figures of 37 and 38 respectively) Raman spectra for beads BH 37395 and BH 37400 (figs 35 and 36 respectively), also

provide very minor peaks around 400 cm^{-1} and 500 cm^{-1}. If the exact laser as was used in the study could be used, more pronounced and accurate results could have been achieved. However so far only minimal similarities exist, which may be enough to suggest that the beads are made of a bone-like material, but not enough to make any identification as odontolite or any other certain material.

6.1. 3. FTIR

The infrared spectra of the beads presented a typical apatite spectrum with strong phosphate bands between 1094-962 cm^{-1}, as ν3 (PO) antisymmetric stretching mode (Paz et al. 2012), at 599 cm^{-1} and 561 cm^{-1} as the bending mode of ν_4(PO) (Azami et al. 2011), and at 470 cm-1 the bending mode of ν2 (PO) (Paz et al. 2012). All samples also yielded minor amounts of carbonate signals at 864 cm^{-1} and between 1456 – 1427 cm^{-1} (NIST Chemistry Webbook), revealing the essential bone mineral made of carbonated hydroxyapatite (Field et al. 1974; Legros et al. 1987; Beasley et al. 2014).

Four samples belonging to bead fragment BH 37621 yielded an –OH signal around 3400 cm^{-1}, indicative of hydroxyapatite. In 17 other samples out of 50 that belong to all of the beads, we can also see a slight curve in the area around 3400 cm^{-1} (see Appendix E). This hydroxyapatite signal was present and more pronounced in all modern and archaeological bone samples. In fossil teeth and enamel however the -OH signal was again much less pronounced. An amide carbonyl signal pointing to the presence of organic materials was seen in some bone and teeth samples. “Hydroxyapatite may undergo exchange reactions with various environmental

compounds especially under acidic conditions. Thus, the -OH groups in the original raw material has likely been exchanged with F^{-1} to produce fluorapatite. Due to its more active properties, fluorine easily changes places with the hydroxyl (-OH) group present in the bone-tooth matrix. Similar exchange reactions and matrix deteriorations may change the proportions of calcium and phosphorus as well as introduce magnesium, as in the case of isokite ($CaMg(PO_4)F$). Likewise, elements like Sr, Fe, Zn, at trace levels may be introduced which are not detectable with FT-IR" (Bursalı et al. *submitted*). The phosphate band at 1090 cm^{-1} does not exist in bones and teeth, and at this time we do not know the cause for this.

Unfortunately, no specific variation in the FTIR spectrum between the beads and known samples (of archaeological bone deriving from sheep/goat, teeth of pigs, cows, ovicaprines and humans, as well as a fossilized equid tooth) can be observed, to definitely identify the specific raw material of the beads. Seeing the hydroxyapatite peaks in archaeological bones and teeth, and seeing minor traces of the peak in beads goes to support our conclusions that the -OH group in the original material of the beads has been exchanged with fluoride, becoming fluorapatite.

The turquoise-blue beads of Tell el Kerkh have also been subjected to FTIR analysis and provide us with a point of comparison. The spectra they obtained are provided in Fig 72. Taniguchi et al. also found the material of the beads, based on samples from both the bulk and blue areas, to be apatite and did not identify any signal pertaining to a dye or colorant (Taniguchi et al. 2002: 177). The spectra showed absorption bands at 1100-960 cm-1 (specifically at 1094 cm^{-1}, 1040 cm^{-1} and 960 cm^{-1}) that belong to phosphates, and at 1456 cm^{-1}, 1427 cm^{-1} and 860 cm-1 that belong to carbonates, as well as bands at 603 cm^{-1} and 574 cm-1 (Taniguchi et

al 2002, 177). The authors attribute the broadness of the phosphate region partly to the “counter ions by diagenesis reaction and ionic exchange in F- for -OH of apatite” (Taniguchi et al. 2002: 177).

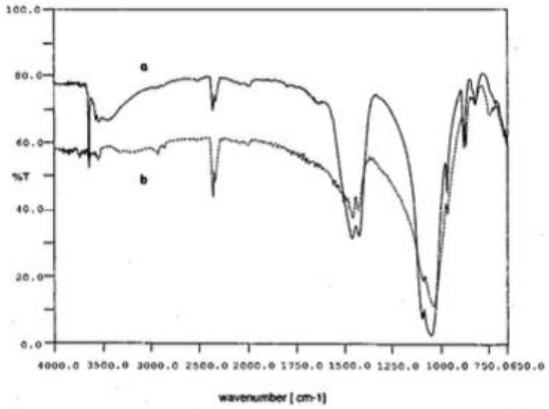

Figure 72. FTIR Infrared absorption spectra of the blue part bead of bead 2 (a) from Tell el Kerkh excavations, along with the FTIR spectra of the reproduced blue ancient tusk (b), from Taniguchi et al. 2002: 177.

While researching the transformation of ivory to odontolite and investigating the origin of the blue/green color, Ina Reiche et al. (2000a), use FT-IR on green bones and non-treated and heated ivory samples (Reiche et al. 2000a: 628, 633). The green bones showed “typical absorption bands of bone or ivory corresponding to an organic and an apatite fraction (3540 cm − 1 (w OH, apatite), 3440 cm − 1 (w OH, water), 1634 cm − 1 (remaining collagen), 1455 and 1428 cm− 1 (w3CO23 −), 1094 and 1040 cm− 1 (w3PO34 −), 875 cm− 1 (w3CO23 −), 565 and 605 cm− 1 (w4PO34 −), 470 cm− 1 (w2PO34 −))”, which is identical to our results on bones as well, and different from beads in its apatite and collagen contents. (Reiche et al. 2000a: 627-8) Fossil samples present the same absorption bands except for lacking in collagen, which is again visible in modern ivory samples (Reiche et al 2000a, 633). Chadefaux et al use FT-IR to investigate the differences between blue colored and

gray colored bones, which are both made of apatite; however one can note (Fig 73) that -OH and carbonate intensities are a lot less in the blue bone (Chadefaux et al. 2009: 29).

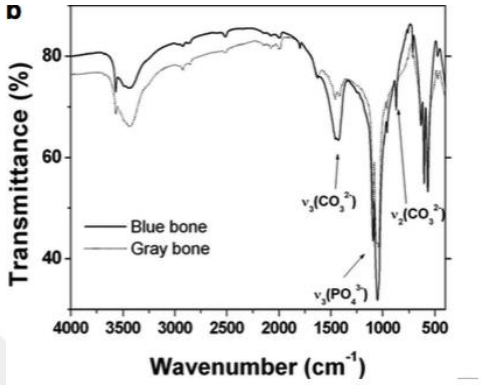

Figure 73 – FTIR spectra of blue bone and gray bone from Chadefaux et al. 2009: 29.

6.1.4. SEMEDX

We asked for Dr. Alfred Galik's help in interpreting the SEM micrographs, mainly to try to understand if the micrographs present a bone or tooth structure. Alfred Galik, from the Austrian Academy of Sciences and Austrian Archaeological Institute, is the archaeozoology specialist of the Barcın Höyük excavations. Galik remarked that the structures seen in the micrographs are complicated and are not very clear. He explained that the matrix in the micrographs seems very dense and amorphous, and that if often looks like stone or fossilized material. The pores at first resembled the Haversian canals in the bone matrix, however "a clear bone structure like an Osteon with a central canal, and the Havers canals and the bone lamellae are not clearly visible" (Galik, personal comm. 2017). Galik further added that such

pores or “canals/tubuli” can be found in the dentine part of the tooth, and that he favors interpreting the material as tooth rather than bone (Galik, personal comm. 2017). Some of the interpretations Galik provided of the micrographs can be found seen in Figs 74-79.

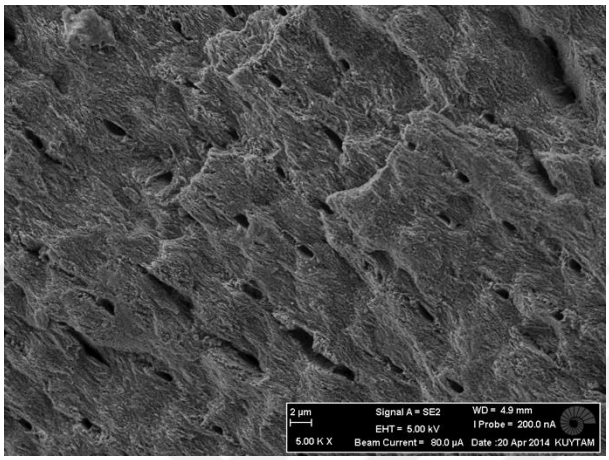

Figure 74 Scanning Electron Micrograph of BH 37394 - interior

In Figure 74 Galik notes that the fibrous structure and the pores speak for bone rather than tooth, but that these may also be dentine canals.

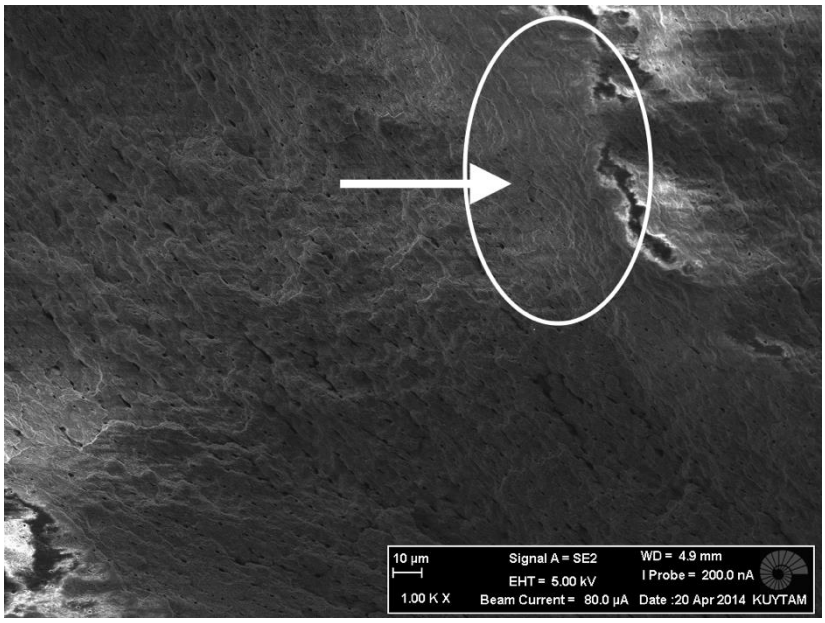

Figure 75 - Scanning Electron Micrograph of BH 37394 interior

In figure 75, Galik notes that there are very fine pores and an amorphous structure. The section inside the circle might represent layers, and if that is the case, Galik says he would interpret this as tooth rather than bone.

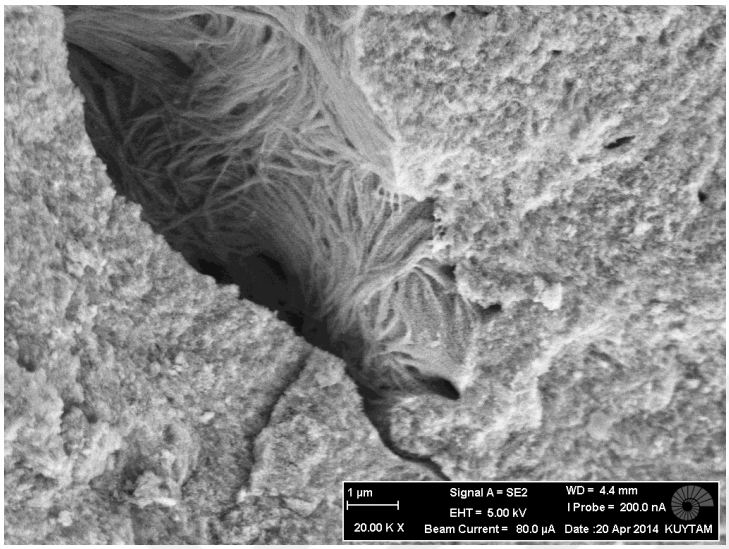

Figure 76 - Scanning Electron Micrograph of BH 37400 interior

In figure 76, Galik notes that while the outside is very amorphous and crystalline, the fibers inside the cavity look like the structures called “dentinal tubules” that can be found in the canals of dentine.

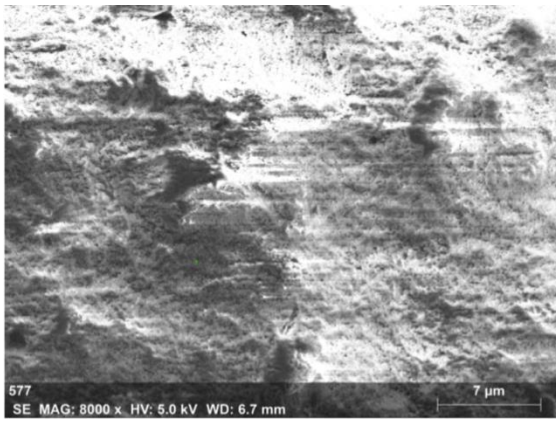

Figure 77 Scanning Electron Micrograph of BH37622 exterior

In figure 77, Galik says that the layer structure such as the one seen in this micrograph is more similar to tooth than bone.

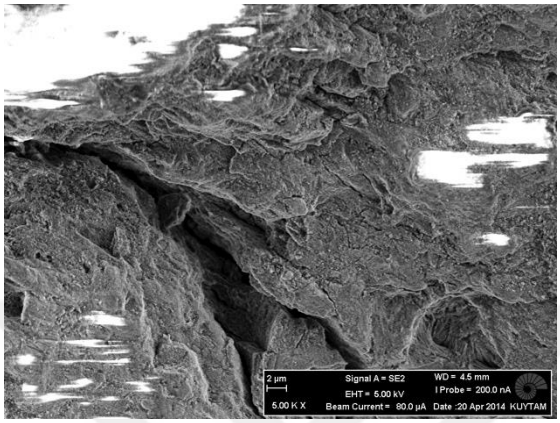

Figure 78 Scanning Electron Micrograph of BH37400 exterior - the blue section

In figure 78, Galik says that the amorphous structure and lack of pores make the structure look like tooth, but that this is not certain.

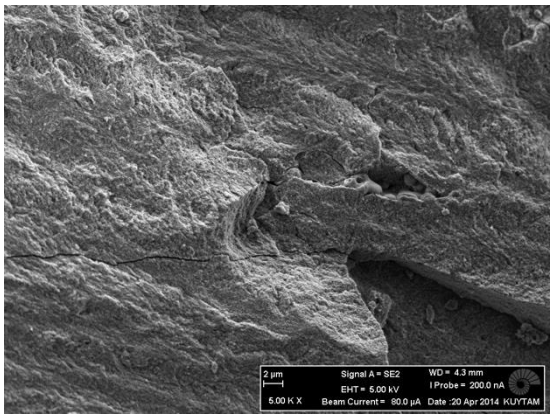

Figure 79 Scanning Electron Micrograph of BH 37400 exterior

In figure 79, Galik interprets this structure as amorphous and adds that it looks like a fossilized specimen or stone.

The Tell el Kerkh team have also applied SEM to the blue colored beads found at Tell el Kerkh, and the micrographs seen in fig. 80, also revealed a similar structure to the Barcın beads.

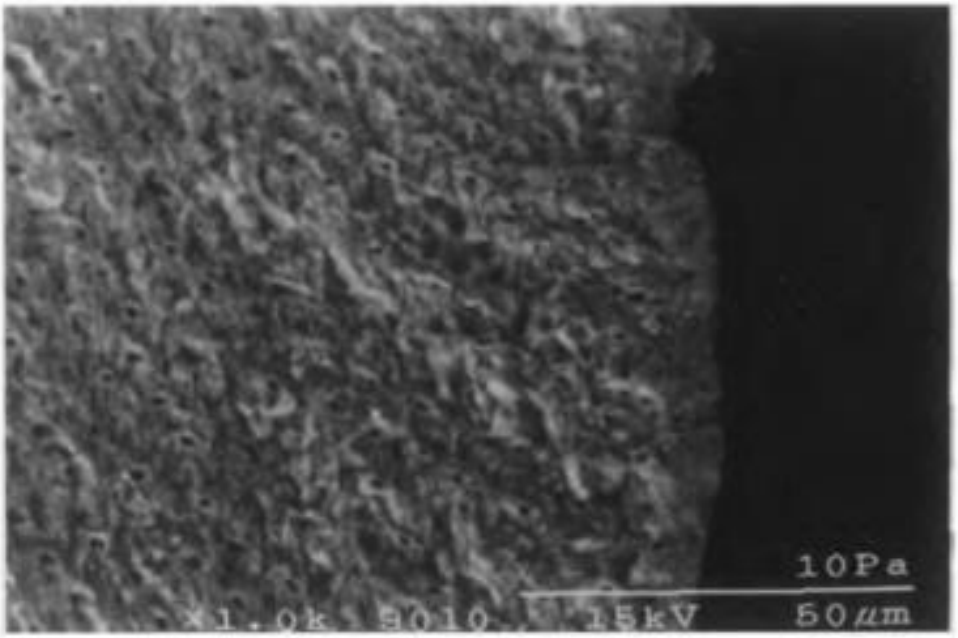

Figure 80 – Scanning electron micrograph of Surface of bead 1 from Tell el Kerkh excavations from Taniguchi et al. 2002: 179.

The Tell el Kerkh team use SEM to see if any structural difference exists between the blue and white parts of the bead, but come across none, as can be seen in fig 81.

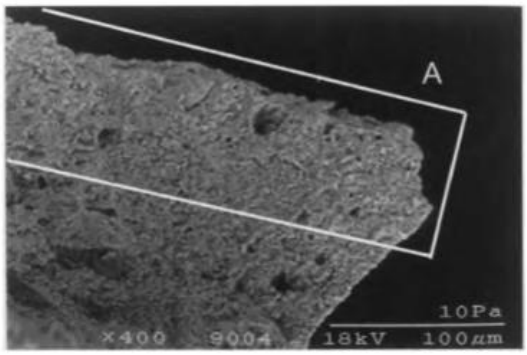

Figure 81 SEM micrograph focusing on the border of white and blue sections of the blue bead Bead 3 from Tell el Kerkh excavations, from Taniguchi et al. 2002: 179. "No clear boundary between the white matrix and coloured surface was observed. The texture is quite coarse. A shows the blue area." Taniguchi et al. 2002: 179.

In light of this information, we turned to our SEM micrographs of bone and dentine that we obtained at KUYTAM and ones that are found in other literature to make comparisons. Sample micrographs taken at KUYTAM of archaeological cow bone and tooth are provided in figure 82.

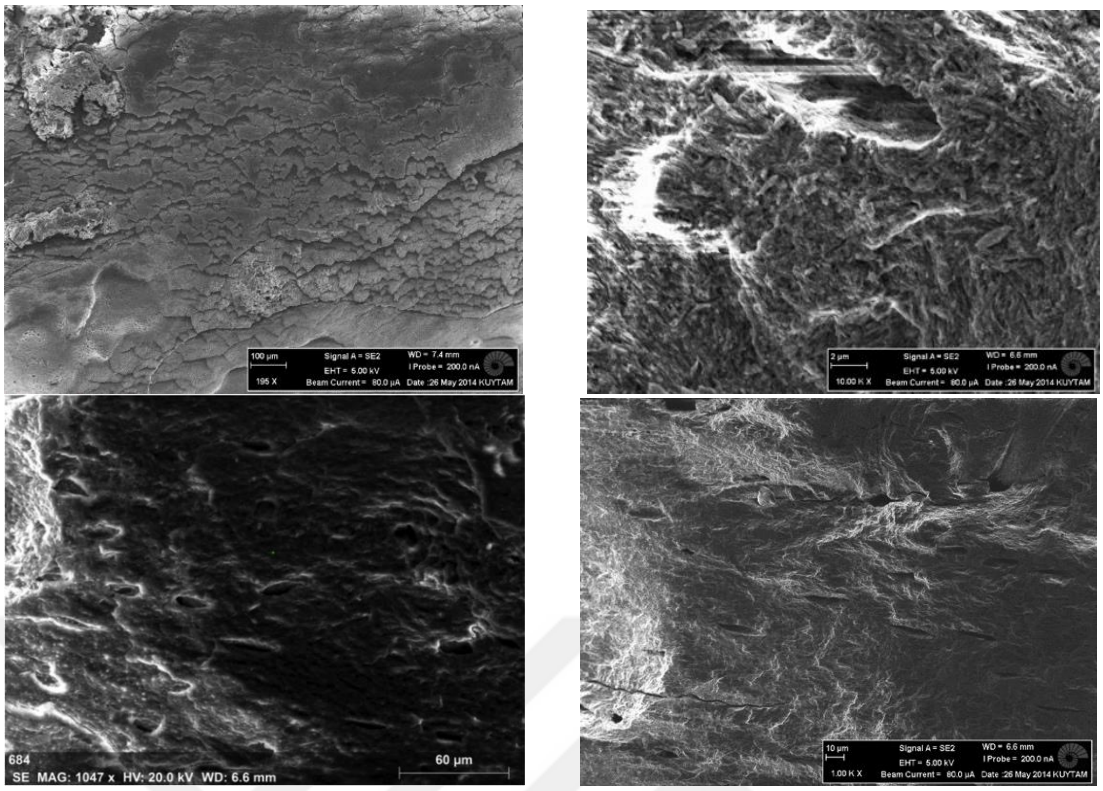

Figure 82 – A) top line - SEM micrograph of archaeological cow teeth B) bottom line - SEM micrograph of archaeological cow bone

The micrographs of archaeological cow (fig 82a) teeth seem to echo the amorphous structure seen on the exterior of bead BH 37400, that Galik also categorized as possibly tooth. The layer structure seen on fig 82, top right, is the layer structure Galik mentions as being characteristic of the tooth.

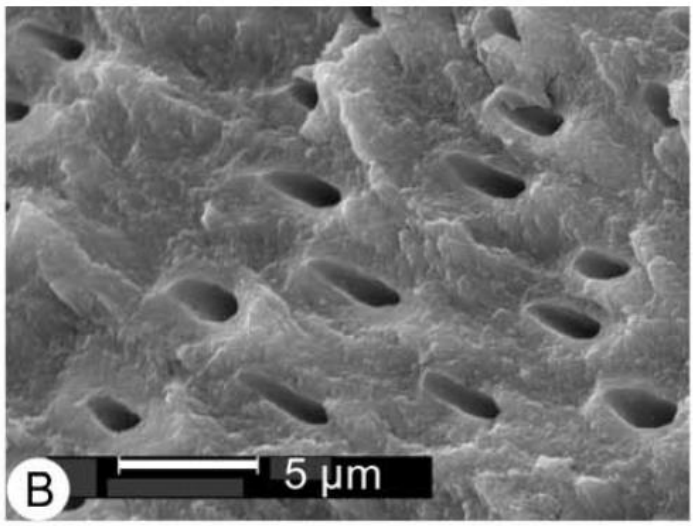

Figure 83 SEM image from modern mammal teeth, peritubular dentine structure, from Dauphin and Williams 2007, 1254

However, archaeological cow bone seen in fig 82b is more similar to the porous structure seen in bead BH37394 (fig. 74), and also in the Tell el Kerkh beads (fig. 80). However Galik had advised that this porous structure could be seen in the dentine of the tooth as well. Following this advice we researched the structure of dentine and came across the SEM micrograph of the peritubular dentine structure of untreated modern mammal teeth in Dauphin and Williams 2007 (1254), seen in Figure 83. Dentinal tubules of ivory were also researched (Fig. 84) (Liaqat et al. 2015: 2113), as well as demineralized bone matrix from various specimens (Fig 85) (Schweitzer et al. 2007: 190).

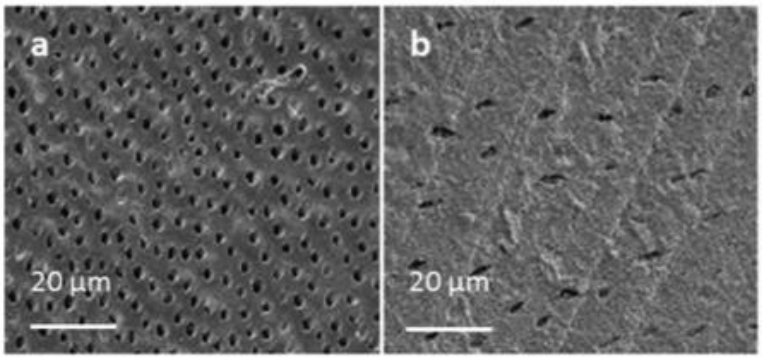

Figure 84 – SEM images of human dentinal tubules (a) near the pulp, and tubules in ivory (b), from Liaqat et al. 2015: 2113.

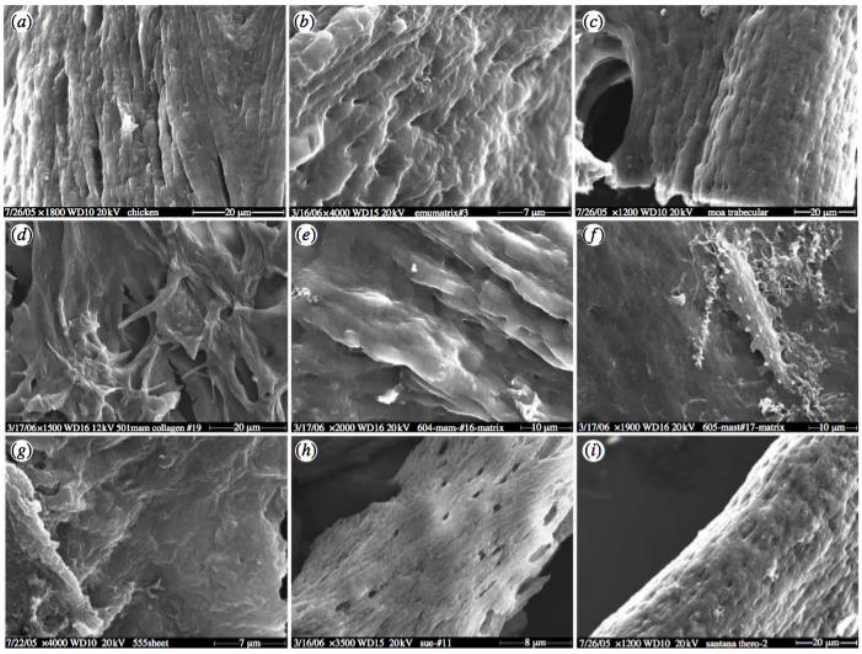

Figure 85 – SEM images of demineralized modern and fossil bones, from Schweitzer et al 2007, 190: "(a) Fresh chicken showing fibre bundles. Crossbanding is not within SEM resolution capability. (b) Emu matrix, with fibre bundles at higher magnification. (c) Moa trabecular bone (MOR OFT255). (d) Mammoth (MOR 91.72) (e) Mammoth (MOR 604). (f) Mastodon (MOR 605). Featureless matrix is impossible to image without also imaging osteocytes (centre). (g) Tyrannosaurus rex (MOR 555). (h) Tyranossaurus rex (FMNH- PR 2081). (i)Theropod indeterminant (MN 4802-V). Magnifications and scale bars are as indicated."

It is possible to find similarities between the beads with all of these micrographs (Figs 82-85), and the information at hand still does not allow us to categorize these beads as one or the other. Although I would argue that the SEM micrographs, coupled with optical micrographs bring up the possibility that some beads are made of bone (BH37394?), and others of fossilized tusk/tooth (BH37400?), we cannot safely assume a conclusion by these micrographs, a point also heavily stressed by Dr. Alfred Galik.

6.1.4.1. Polished SEMEDX

Identification of a crust/layer of on the exterior of the polished cross section of the beads suggests that manganese might have been added later (see fig 86). Such a feature was not identified in the Tell el-Kerkh beads, which are the only other such beads that scientific analyses were conducted upon. Even though in one bead, this layer seems to be richer in manganese based on the Manganese distribution map (fig 86b), we cannot suggest that this is a paint layer.

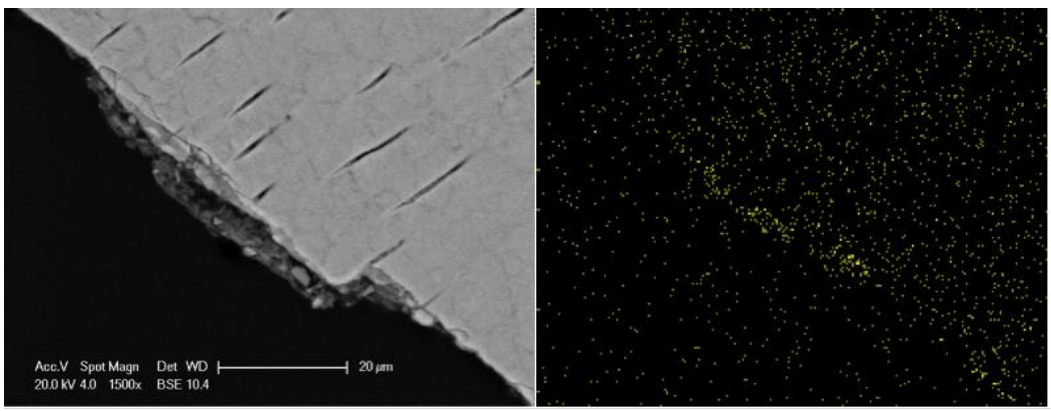

Figure 86 a) (left) back-scattered electron images of BH 37399, showing a layer of about 5-7 microns on the surface. b) (right) Mn distribution map of BH 37399. The layer is seen to be richer in terms of MnO,

6.1.4.2. EDX results

EDX analysis revealed a typical bone or tooth elementary composition. The existence of fluorine is fitting with the assumption that they are made of bone or tooth, indicating that -OH of carbonated hydroxyapatite that makes up the bone was exchanged with fluoride. Discovery of manganese helps us connect the blue color to this element. In terms of bone and teeth samples, manganese was only found in the blue-colored archaeological bone sample.

Reiche et al. (2000a) conduct EDX analysis on odontolite and in these samples obtain "between 3.7 and 4.2 wt.% of fluorine, 42.5 $\pm$ 2.5 wt.% of oxygen, 17.0 $\pm$ 2.5 wt.% of phosphorus and 36.5 $\pm$ 2.5 wt.% of calcium and on dark zones iron and manganese", and other trace elements (Reiche et al. 2000a: 632), similar to our results in Table 6.

Further supporting the existence of fluorine in the beads, Chadefaux, Vignaud et al.'s 2009 case study shows that Fluorine is not in modern bone, is most and quite abundant in blue bone, and relatively negligible in gray bone (Chadefaux et al. 2009: 30). Copper and manganese were also existent in the paleontological blue bone sample studied by the researchers (Chadefaux et al. 2009: 30-31).

6.2. Experimental Research

Our laboratory experiments have been successful in that we managed to obtain blue color on porous archaeological sheep/goat bones from Barcın Höyük. However one should be wary of this result, as it brings us no closer to understanding how Neolithic peoples might have reached this color 8000 years ago, nor to figuring

out if the beads were subject to chemical treatment (in a solution?) as well as heat treatment. Firstly it should not be forgotten that the blue color was only achieved on one specific bone, and samples from other bones did not undergo a full color change, although they had bluish hues. Secondly, EDX results of the experiment sample do not reveal copper or iron, the other candidates for the source of the color, in the makeup of the sample. This is due to the fact that these elements do not dissolve in water. However we also observed that the bones that were put in the solution with only Mn in it, did not turn out as blue as the bones that were put in the full solution (full solution had Mn, NaCl, Cu, Fe and CO_3 in it). In any case, as Neolithic people would not have used neither the materials nor the apparatus that we have during this experiment, unfortunately it fails to reveal information about their technology and methods for producing such beads and color, except for the involvement of heat treatment.

The Tell el-Kerkh team was the one who came up with and used the same chemical formula we had with successful results, but on ancient wild pig tusk and modern bone. Personal communication with the team informed us that they are now also considering techniques that do not involve heat, and thus would not weaken the texture of the material, for the coloring of the beads. In their experimental study, the heat treatment was found to make the bone/tusk weak too weak to be properly made into a bead (Taniguchi et al. 2002: 181). We initially believed that our experiment also confirms the conclusion that heat can not be involved, due to the fact that it seems to weaken the matrix. However now with the realization that at least in our experiments, the weak matrix is caused by the presence of NaCl, we do not fully agree with their conclusion that heat cannot be a part of the procedure.

6.3. Conclusion of Scientific Analyses

The turquoise-blue beads of unknown material from Neolithic Barcın Höyük were subject to various analytical, chemical and instrumental analyses, to try to identify their raw material and their coloring process. As a result of these analyses, we now know that none of the beads that were subject to analyses were actually made of the semi-precious turquoise stone or of a clay/plaster material. Even copper, which is in the chemical formula for turquoise ($Cu(Al,Fe^{3+})_6(PO_4)_4(OH)_8 \bullet 4H_2O$), has not been detected in any of our analyses. Rather, it has been discovered that the Barcın blue beads are formed from a bone matrix like apatite. However the analyses that we used were not able distinguish between similar materials such as bone, teeth, ivory or similar fossilized material that could possibly form the raw material of the beads. The presence of the element of Yttrium in some beads, revealed by the pXRF analysis (for Results see Appendix I) points to a possibility fossilized material preliminary result. The analyses that were conducted in the scope of the study moreover revealed that the bone matrix of carbonized hydroxyapatite has transformed to fluorapatite in these beads. SEM was used to determine both surface and cross section topography, which revealed bone-like matrix. Manganese, which is the compound responsible for the blue color in the beads, along with the elemental composition of apatite and possible exchange components were analyzed with the help of EDX, which also again yielded considerable amounts of fluoride, pointing to the existence of fluorapatite. On the cross-section SEM micrographs of one bead, a surface layer of about 5 microns was noticeable. Incidentally this layer contained higher levels of manganese compared to the inner core of the bead matrix. Experimental procedures were also employed to try to recreate the blue color of the

beads on bone and tooth samples. Blue color was obtained when manganese-(and other elements)-impregnated bone was heated to about 600 °C. However in the end, we still cannot claim to have conclusive information on the manufacturing and coloring technology of Barcın Höyük residents.

CHAPTER 7 – CONCLUSION

7.1 A Case for Imitation and Skeuomorphism

Skeuomorphism is the act of manufacturing a product usually made from a specific material using another material, and fashioning it in a way to reflect the physical properties of the original material. Skeuomorphism is frequently encountered in archaeology, and examples of it in terms of personal ornamentation have been unearthed as early as the early Upper Palaeolithic period in Europe (Conneller 2013: 125). Chantal Conneller suggests that beads made of ivory, antler and teeth found later in the inland Palaeolithic sites, are imitations that mimic the form and texture of shell beads found in the earlier coastal sites. The ivory beads are attempts to mimic high-status shell beads in a more readily available material. In her discussion of these materials, she argues that treating materials with different properties the same way, creates equivalence between different materials used for beads. She believes this is not to replicate, but to reveal the "sameness" of the materials through the properties they share (Conneller 2013: 129).

Several lines of evidence suggest that this may be the case with the turquoise colored beads found in Barcın and other sites; the artificially-colored beads may be skeuomorphs. Finding the two kinds of beads together at sites like Tell el-Kerkh and Çatalhöyük brings to mind that the non-stone beads may be made in imitation of the

genuine turquoise stone beads, mirroring their color, luster and shape. Another point to take into account in this respect, is that the artificially-colored apatite beads and turquoise stone beads all seem to belong to the same repertoire of shapes, distinct from beads made of other materials. This was observed on the two different raw materials in Çatalhöyük by Bains (Bains 2012; Bains et al. 2013). Bains further notes other similarities in the treatment of turquoise-stone and artificially-colored apatite beads, such as they both seem to appear "in bead types that are individually made and therefore are more labour intensive" (Bains et al. 2013: 340), and that they are both, only associated with female and indeterminate burials, and only with adolescent and older adult burials (Bains 2012: 207, 276). Blue-colored beads are never associated with male burials in Çatalhöyük, or with neonate, infant or child burials (Bains 2012: 207, 276). Unlike Çatalhöyük where apatite beads were a lot more common than turquoise stone beads, at Tell el Kerkh three times as many turquoise stone beads were found as apatite beads (Taniguchi et al. 2002: 176). Here too researchers believe the apatite beads to be in imitation of turquoise stone beads. Even though turquoise stone beads have not been discovered in sites such as Barcın and Aktopraklık, the specific forms of the apatite beads are not seen in beads of other materials, and still seems to follow the specific "blue bead typology", not seen in beads made of other materials (Baysal 2014; Baysal 2016). Knowing that the blue color of apatite beads was man-made, and that the Neolithic people intentionally preferred turquoise-blue color and the shape of turquoise-stone beads, reinforces the claim of skeuomorphism.

Could imitation be in effect within the assemblage of apatite beads themselves? When only assessed visually the apatite beads come in two types: all the

way blue and white in their interior. Even though we now know that these two materials are chemically the same, visually the structures look indubitably different, possibly resulting from the difference in the bone and tooth structures. Appearance however, is likely how Neolithic inhabitants would have evaluated these beads. If the turquoise apatite beads had a single (and most probably foreign) source, and the restricted repertoire of shapes would suggest so (Baysal, personal comm. 2017), then would the manufacturers of these beads value their products differently based on the difference in raw material? The differences within the blue apatite bead assemblage raise even more questions about the imitation of turquoise color.

Real turquoise must have been difficult to obtain for the inhabitants of Neolithic sites in Anatolia. The closest source of turquoise to this region is the Sinai Peninsula, and lies roughly 2,300 km away from northwest Anatolia, where Barcın is located. The second closest source would be in Nishapur in Iran, which is approximately 3,400 km away from northwest Anatolia. The difficulty in the access to the genuine turquoise stone may have made this material valuable and exotic, as Helms suggests for materials that travel long distances in her 1988 work *Ulysses' Sail* (Helms 1988). Given the innate power that exotic goods likely carried, Neolithic peoples might have desired to produce local imitations. One of the reasons why imitation may take place according to Choyke, is the presence of a more easily available medium to produce like goods (Choyke 2008: 13). Choyke links the concept of skeuomorphism with issues of prestige, rank and group identity. The widespread existence of the turquoise-blue "imitation" beads in Neolithic Anatolia suggests that they were a cheaper alternative for producing desired goods and that they were easily procured. The blue beads at Barcın may well be skeuomorphs made

to imitate turquoise. It seems the Barcın Höyük beads are part of a larger desire to imitate, which appears to have swept across Anatolia and beyond during this time.

7.2. Implications for Social Differentiation

The suggestion of inequality in the access to materials brings up the question of social differentiation in the Neolithic period in the seventh millennium BCE. Socio-economic inequality in this region is generally said to have started much later, in the third millennium BCE (Çevik 2007; Horejs 2014; Schoop 2014) but the disparity in access to turquoise, as well as the evidence for the desire to imitate this stone may urge us to rethink the timing of this phenomenon (Bursalı et al. 2017). Finding support from Brian Hayden's (Hayden 2001: 235) claims that social differentiation starts well before the Neolithic – in the Middle Palaeolithic -, it could be argued that the presence of imitation beads adds to the evidence for such social differentiation for the Neolithic period.

Other research also supports the possibility of rising inequalities in these earlier periods (Kuijt 2000; Kuijt and Goring-Morris 2002). Focusing on data from Çatalhöyük, Wright's analysis of house floors and household artifacts "reveals a mix of egalitarian features and emerging social complexity" in the site, revealing household differentiation and beginnings of inequality (Wright 2014: 23, 29).

The difficulty in the access to the original material, in this case turquoise, may also work to create distinctions between people. We can observe here that the blue beads may signal age, affiliation, power or social status, as Kuhn and Stiner (2007) suggest items of personal ornamentation items can do. By implying that this one person had the means to obtain the raw material whereas others may not, the

beads differentiate the wearer from others. This could possibly be one reason to explain the desire to imitate the original turquoise beads, and to explain the widespread distribution of the blue-colored beads, showing a shared desire for some certain objects. Working on Çatalhöyük beads, Bains moreover theorizes that blue-colored beads are more valuable and that they may even create social differentiation (Bains 2012: 273), expressing that "stone beads may be used as a means of initiating and differentiating oneself or a household from the community, in a non-threatening and benign manner" (Bains 2012: 273). What Bains puts forward concerning the blue colored beads then would undoubtedly put the society that used them into what Hayden would categorize as a "transegalitarian society", with "private ownership of resources and produce" and "low levels of sharing", even though admittedly missing "institutionalized hierarchies" (Hayden 2001: 232). It is, however, worth noting that Bains seems to consider only the economic value of the beads in her analysis. Besides lacking a holistic approach (a more holistic approach is proposed in Section 7.3), this analysis is also problematic as it implies that concepts such as wealth, money, hierarchies and status fully existed in the Neolithic (Baysal and Miller 2016).

Even though scholars such as Ulf Schoop (Schoop 2014), Tim Earle and Kristian Kristiansen (Earle and Kristiansen 2010) argue for Anatolia and Europe respectively that such social differentiation was not present before the Bronze Age, it also did not, as Bains says, begin overnight. It may well have roots going back to the expression of self already in the Neolithic, and beads are one of the best (and most practical) ways to align or differentiate oneself with or from given groups or affiliations (Bains 2012: 273).

7.3. Shared Materials and Beliefs in the Neolithic

The blue beads from different sites, and even made from possibly different materials, seem to come in a specific repertoire of shapes (Bains 2012; Baysal 2014; Baysal 2016). This suggests that they either had a single source of production and widely travelled, or that they are representative of a specific tradition that causes the form and color to be precisely copied without any change being introduced in different localities, be it Central, Western or Northwestern Anatolia or the Near East (Baysal, personal comm, 2017). Furthermore these shapes are generally not the local bead shapes of the sites they are found in (Baysal, personal comm., 2017). Hala Alarashi informs us that the forms of the blue beads are Northern Mesopotamian forms, from the Euphrates region in 7th millennium BCE (Alarashi, personal comm. 2016). If we take this to mean that the beads themselves were manufactured in the Northern Mesopotamia, the widespread distribution of the blue beads across the Near Eastern and Anatolian landscapes raises questions about the processes and means through which these items were moved along (Baysal, personal comm. 2017). Is this the result of well-connected Neolithic communities that transferred the beads amongst one another, or of the existence of traders that moved and distributed the beads along the landscape to different communities? How were these ties organized? In Wright's view, acquisition and importing processes are also other factors that could give an artifact special value (Wright 2014: 12).

If the beads did not have a single source, then the form and color of specific beads kept being copied in different communities from the Near East to as far as Istanbul in Anatolia, without introducing any change to the specific form. This could be due to shared traditions and beliefs systems (Baysal and Miller 2016); and could

reflect a willingness to keep up the same forms or resistance to change well-known forms due to long-lasting tradition (Baysal 2016: 56).

In either case, such a widespread distribution does not need to be explained solely by virtue of its economic value, as Baysal and Miller argue for the interpretation of personal ornaments in prehistory (Baysal and Miller 2016). This can be easily exemplified by observing the distribution of another blue-colored bead in the modern times, the evil eye bead (Baysal, personal comm. 2017). Also known as the Nazar bead, the evil eye bead is an eye-shaped bead or amulet that is believed to provide protection against the evil eye (Baysal and Miller 2016). The evil eye bead isn't only widely available and distributed in Anatolia, but in the whole world; hung inside or outside houses or shops, inside vehicles, on clothes and other fabrics (bags, tablecloths), as jewelry (both on humans or animals), as key chains, sometimes even embedded in concrete pavements in Turkey. These beads cannot be said to have any economic or monetary value; in fact most of the time they can be made of the cheapest materials and can be obtained at negligible prices, sometimes even given away for free. The evil eye beads do not bring monetary or economic value into mind – but the blue color is still shared and replicated (Baysal, personal comm. 2017). Similarly, they do not denote economic wealth; they simply imply adherence to belief systems, or sometimes are just used for decoration without any implication at all (in mostly urban contexts). Just like the evil eye beads, the blue beads in the Neolithic contexts may have belief, tradition or identity-related reasons for their wide distribution, possibly completely irrelevant to economic value or representation of status and/or wealth (Baysal and Miller 2016).

As a final note, it is worth considering that the beliefs or traditions concerning the blue colored beads in the Neolithic may actually be tied specifically to their color. Blue is a rare color to find in Neolithic contexts so it can be assumed that it was of some interest to the Neolithic peoples. The blue beads begin to appear in assemblages in Anatolia beginning from the middle of 7th millennium BC. The copper-based blue pigment azurite is unearthed from Çatalhöyük excavations beginning from 6700 cal. BC (Çamurcuoğlu 2015: 147). This can find a parallel in the Levant, with Bar Yosef and Porat's 2008 research on green-colored beads, where they argue that these beads become widespread by 11,500 cal. BC as farming begins to spread, and have symbolic ties to agriculture and fertility (Bar Yosef and Porat 2008: 8548). In considering the blue apatite beads, we can't ignore the impact of the blue color given its rarity and potential meaning.

7.4. Suggestions for Future Work

It was not possible to differentiate whether the materials are bone or ivory with the scientific analyses we conducted. However, other methods are known to be successful in making this differentiation, and they should be employed to be able to reach a clearer verdict on this issue. Reiche et al. make this differentiation by focusing on crystal size and crystallinity through the use of transmission electron microscope (TEM) (Reiche et al. 2000a; 2000b; 2001; Chadefaux et al. 2009). Employing such a method could also help us distinguish between these materials.

More recent work by Müller and Reiche (2011) aims to "[focus] on the evaluation of a non- destructive distinction method for ivory, bone and antler based on the chemical composition of the mineral part, which generally lasts longer than the organic fraction in the archaeological context" (Müller and Reiche 2011: 3235).

To look for slight differences in the chemical composition of the materials on the minor and trace levels, they use Micro-Proton Induced X-ray and Gamma-ray Emission (micro-PIXE/PIGE) (Müller and Reiche 2011: 3234). This could present another way to try to distinguish between the possible materials of the beads in the future.

Research on blue beads is still preliminary and reports of turquoise apatite beads from Anatolia and the Near East are still in the process of surfacing. These should be monitored, as these beads seem to appear in more localities when we especially look for them. Looking at the examples of Pendik, Köşk Höyük, Tepecik-Çiftlik and Mersin-Yumuktepe, it is obvious that some re-evaluation of excavated finds also needs to be made. Apart from a re-evaluation, instrumental analyses such as the ones conducted in the scope of this study, as well as XRF and XRD could also be conducted on the bead finds from other sites as well, to identify the materials.

When more information about their exact distributions across the Anatolian and Near Eastern landscape is achieved, we can begin to ask new questions on how and why these beads may have become so widely distributed. Did they imply shared beliefs about a Neolithic Anatolian society? How did the community of Barcın Höyük obtain these beads? If these beads have a single source, judging by the restricted repertoire of shapes they come in, where were they first manufactured? Where else did their journey take them? I hope that such questions can be answered in the future and shed a little light on the Neolithic trade and trade networks.

7.5. Concluding Remarks

The main aims of this study were to reveal the raw materials of the turquoise-blue colored beads found in Neolithic Barcın Höyük, and to investigate the process behind the change of color. The results of instrumental analyses such as optical microscopy, Raman, FTIR and SEM with EDX, as well as laboratory experiments conducted; show that the beads were made of organic materials such as bone, tusk or tooth, possibly in fossilized form. For the coloring mechanism, we can confidently say that manganese and possibly heat treatment were responsible.

This study also aimed to assess whether the imitation of beads made of turquoise stone took place at Barcın Höyük and at other settlements. Although no turquoise stone beads were discovered in Barcın Höyük, in Çatalhöyük and Tell el-Kerkh beads of both turquoise stone and apatite have been discovered. Similarity in color, luster and shape of the beads suggests that the apatite beads are skeuomorphs of the turquoise stone beads. Geniune turquoise would have been much more difficult to obtain, especially in Anatolia as the closest sources of the stone are in the Sinai and Iran. Nonetheless, the Neolithic inhabitants strove to achieve this turquoise-like effect on other materials.

Although tentative, skeuomorphism may suggest that the residents of Barcın Höyük and other settlements did not have access to the original material, but still desired it. Given their exotic nature, the blue beads may have been preferred only for aesthetic purposes or because they implied some kind of affiliation or status (Helms 1988; Wright 2014: 12). How some Anatolian Neolithic societies had access to the real turquoise, and why excavations in some sites yielded both stone and apatite beads raise questions about access to specific materials. In such societies where both

stone and apatite are found, this discrepancy can point to imbalances in the access and ownership of a material within the same society. The users of the "imitation" beads may have desired ownership of a likeness of something, the original of which they cannot afford, or they may have felt a need to identify with a group they aspired to be a part of. This suggests that the origins of inequalities extend into the seventh millennium as advocated by Hayden, Wright and Kuijt (Hayden 2001; Wright 2014; Kuijt 2000; Kuijt and Goring-Morris 2002). Still it should be recognized that the widespread distribution of the blue beads cannot only be tied to their possible economic value, but can also be caused by the prevalence of specific traditions and beliefs, similar to the evil eye beads in the modern world. The uniformity of the shape and color of the blue beads found in different locations suggests that they sprung from a single source; how they achieved such wide distribution in the Neolithic period 8,000 years ago would be a point worth researching further.

The claim for imitation remains impossible to prove with scientific data, but the theory is strengthened as more turquoise stone beads appear alongside apatite ones. Further research can inform us on what this possible imitation implies about social differentiation, possible trade routes, and shared identity or aesthetics across broad geographical areas.

The research on blue beads raises many questions on an array of different topics ranging from trade and economy to identities and beliefs. In this period of change, as concepts such as agriculture, animal husbandry and many others are introduced, a new tradition of blue-colored beads also seems to have swept across these regions. It is evident that the Neolithic was the backdrop for many innovations in many different areas of life.

BIBLIOGRAPHY

Alarashi, H. Personal Communication, 2016.

Alarashi, H. "Butterfly Beads in the Neolithic Near East: Evolution, Technology and Socio-cultural Implications." *Cambridge Archaeological Journal* 26.03 (2016): 493-512.

Alarashi, H. *La parure épipaléolithique et néolithique de la Syrie (12 e au 7 e millénaire avant J.-C.): Techniques et usages, échanges et identités*. Diss. Universidad Autónoma de Barcelona, 2014.

Aspinall, A., et al. "Neutron activation analysis of faience beads." *Archaeometry* 14.1 (1972): 27-40.

Astre, G. "Mastodontes à Gimont (Turquoises de Planselve) et à Bédéchan." *Bulletin de la Société d'Histoire Naturelle Toulouse* 84 (1949): 147-150.

Azami, M., et al. "Synthesis and solubility of calcium fluoride/hydroxy-fluorapatite nanocrystals for dental applications." *Ceramics International* 37.6 (2011): 2007-2014.

Baer, N., N. Indictor, J. Frantz, and B. Appelbaum. "The Effect of High Temperature on Ivory." *Studies in Conservation* 16, no.1 (1971): 1–8.

Bains, R., M. Vasić, D.E.B.-Y. Mayer, N. Russell, K.I. Wright, and C. Doherty. "A Technological Approach to the Study of Personal Ornamentation and Social Expression at Çatalhöyük." In *Substantive Technologies at Çatalhöyük: Reports from the 2000–2008 Seasons*, vol. 9, edited by I. Hodder. (2013): 331–63. London: British Institute of Archaeology at Ankara; Los Angeles: Cotsen Institute of Archaeology.

Bains, R.K. "The Social Significance of Neolithic Stone Bead Technologies at Çatalhöyük." Ph.D. diss. University College London, 2012.

Bar-Yosef Mayer, D. E. "Towards a typology of stone beads in the Neolithic Levant." *Journal of Field Archaeology* 38.2 (2013): 129-142.

Baran-Çelik, G.and Kiraz, M. "Maden ve Hulliyat Eserleri Koleksiyonu; Boncuk, Sarkaç, Amulet ve Heykelcikleri". In *Boncuk: İnanç, Güç ve Güzellik,* edited by Ş. Atik, G. Kongaz, H. Karadeniz, G. Baran-Çelik, M. Kiraz, A. Denker, G. Yağcı & T. Akbaytogan Hoşgör. Rezzan Has Müzesi- İstanbul Arkeoloji Müzeleri, İstanbul, (2007): 20-27.

Baud, Ch A., and H. J. Tochon-Danguy. "Les caractéristiques physico-chimiques de l'ivoire et leurs modifications par traitement thermique." *Bulletin l'association pro Aventico* 29 (1985): 49-52.

Baykal-Seeher, A. and Obladen-Kauder, J. "Demircihöyük IV. Die Kelinfunde. Teil A: Die Lithischen Kleinfunde. Teil B: Die Kelinfunde aus Ton, Knochen und Metall." Mainz:Philipp von Zabern, 1996.

Baysal, E. Personal Communication, 2017.

Baysal, E. "Reflections of Far Away Places: The Chalcolithic Personal Ornaments of Canhasan I". Anatolian Studies 67 (2017) *(in press).*

Baysal, E. "Beads at the Place of White Earth - Late Neolithic and Early Chalcolithic Aktopraklık Northwest Turkey". BEADS: Journal of the Society of Bead Researchers 28 (2016): 50-59

Baysal, E. "A Preliminary Typology for Beads from the Neolithic and Chalcolithic Levels of Barcın Höyük." Anatolia Antiqua 22 (2014):1–10.

Baysal, E. "A tale of two assemblages: Early Neolithic manufacture and use of beads in the Konya plain." *Anatolian Studies* 63 (2013): 1-15.

Baysal, E., Miller, H. "Teoride Süs Eşyaları: Arkeolojik Kontekstlerde Prehistorik Boncukların Yorumu" Journal of Anatolian Prehistoric Research 2 (2016): 11–32.

Baysal, E. and Belcher, E. "Beads", *Barcın Höyük Symposium, archaeological investigations of a Neolithic settlement, Netherlands Institute in Turkey*, Istanbul, 2016.

Baysal, E., Barbara Horejs, ERC Prehistoric Anatolia Project, Personal Communication, 2015.

Beasley, M. M., et al. "Comparison of transmission FTIR, ATR, and DRIFT spectra: implications for assessment of bone bioapatite diagenesis." *Journal of Archaeological Science* 46 (2014): 16-22.

Belcher, E. Personal Communication, 2016.

Bıçakçı, E., M. Godon, and Y.G. Çakan. "Tepecik-Çiftlik" In *The Neolithic in Turkey. Vol. 3: Central Turkey*, edited by M. Özdoğan, N. Başgelen, and P. Kuniholm, Istanbul: Archaeology and Art Publications (2012): 89–134.

Bloxam, E. "Miners and mistresses Middle Kingdom mining on the margins." *Journal of Social Archaeology* 6.2 (2006): 277-303.

Brügmann, G. et al. "Chemical composition of modern and fossil Hippopotamid teeth and implications for paleoenvironmental reconstructions and enamel formation-Part 1: Major and minor element variation." *Biogeosciences* 9.1 (2012): 119-139.

Bursalı, A., H. Özbal, R. Özbal, G. Şimşek, B. Yağcı, C. Yılmaz-Akkaya, E. Baysal, "Investigating the Source of Blue Color in Neolithic Beads from Barcın Höyük, NW Turkey" *Proceedings of the conference Raw Materials Exploitation in Prehistory in Faro 2016.* Cambridge Scholars Publishing. *(submitted)*

Bursalı, A., R. Özbal, E. Baysal, H. Özbal, H, B. Yağcı. "Neolithic Blue Beads in Northwest Turkey: the Social Significance of Skeuomorphism" Selected Papers in Ancient Art and Architecture vol. 3: Dress and Identity, edited by M. Cifarelli and L. Gawlinski. Boston, MA: Archaeological Institute of America, (2017): 123-142.

Campbell, S. and E. Carter. Domuztepe Excavations, Domuztepe. S. Campbell and E. Carter (eds.), (2006) *Open Context.* from the World Wide Web: http://www.opencontext.org/database/space.php?item=1_DT_Spatial

Caneva, I. "Mersin-Yumuktepe," In *The Neolithic in Turkey. Vol. 3: Central Turkey*, edited by M. Özdoğan, N. Başgelen, and P. Kuniholm, Istanbul: Archaeology and Art Publications (2012): 1–29.

Chadefaux, C., C. Vignaud, E. Chalmin, J. Robles-Camacho, J. Arroyo-Cabrales, E. Johnson, and I. Reiche. "Color Origin and Heat Evidence of Paleontological Bones: Case Study of Blue and Gray Bones from San Josecito Cave, Mexico." *American Mineralogist* 94, no.1 (2009): 27–33.

Choyke, A. M. "Shifting meaning and value through imitation in the European Late Neolithic." *Import and Imitation in Archaeology, Schriften des Zentrums für Archäologie und Kulturgeschichte des Schwarzmeerraumes* 11 (2008): 5-21.

Conneller, C. "Deception and (Mis) representation: Skeuomorphs, Materials, and Form." *Archaeology After Interpretation: Returning Materials to Archaeological Theory* (2013): 119.

Çakırlar, C. "Rethinking Neolithic subsistence at the gateway to Europe with new archaeozoological evidence from Istanbul." *Barely Surviving or More than Enough* (2013): 59-79.

Çamurcuoğlu, D. S. *The wall paintings of Çatalhöyük (Turkey): materials, technologies and artists*. Diss. UCL (University College London), 2015.

Çevik, Ö. "The Emergence of Different Social Systems in Early Bronze Age Anatolia: Urbanisation versus Centralisation." Anatolian Studies 57 (2007): 131–40.

Dauphin, Y., and C. T. Williams. "The chemical compositions of dentine and enamel from recent reptile and mammal teeth—variability in the diagenetic changes of fossil teeth." *CrystEngComm* 9.12 (2007): 1252-1261.

de La Brosse G. Livre sur la Nature, vertu et Utilité des Plantes. Bibliothèque Interuniversitaire de Médecine et d'Odontologie, Paris, 1626.

Durgun, P. "Social Organization In The Early Bronze Age Demircihöyük: A Re-Evaluation". Diss. Koç University, 2012.

Düring, B. S. *The prehistory of Asia Minor: from complex hunter-gatherers to early urban societies*. Cambridge University Press, 2011.

Earle, T., and K. Kristiansen. *Organizing Bronze Age Societies: Thee Mediterranean, Central Europe, and Scandinavia Compared*. Cambridge: Cambridge University Press (2010).

Field, R. A., et al. "Bone composition in cattle, pigs, sheep and poultry." *Journal of Animal Science* 39.3 (1974): 493-499.

Fischer, M.G. "Essai sur les turquoises". *Annales de Chimie, VIII*, (1823): 326.

Ford, R. I., 1972, "Barter, Gift, or Violence: An Analysis of Tewa Intertribal Exchange". In *Social Exchange and Interacti*on, edited by E.N. Wilmsen. University of Michigan Anthropological Papers 46. Ann Arbor, (1972) :21-46.

Frahm, E. "Scanning Electron Microscopy (SEM): Applications in Archaeology." Encyclopedia of Global Archaeology. Springer New York, (2014): 6487-6495.

French, D. H. "Prehistoric Sites in Northwest Anatolia: I. The İznik Area." Anatolian Studies (1967): 49-100.

French, D. H. "Excavations at Can Hasan, 1965: fifth preliminary report" Anatolian Studies 16 (1966): 113–23.

Galik, A. "Barcın Beads under SEM - Bone?" 8 May 2017. E-mail.

Gerritsen, F.A., and R. Özbal. "Barcın Höyük and the pre-Fikirtepe Neolithization of the Eastern Marmara Region in Anatolian Metal VII." Der Anschnitt, Beiheft, Bochum (2016): 199-208.

Gerritsen, F.A., and R. Özbal. "NIT Excavations at Barcın Höyük, 2012." *NINO-NIT Annual Report 2012,* (2012): 13–20. Istanbul: The Netherlands Institute in Turkey.

Gerritsen, F.A., R. Özbal, and L. Thissen. "Barcın Höyük. The Beginnings of Farming in the Marmara Region." In *The Neolithic in Turkey.* Vol. 5: *Northwestern Turkey*, edited by M. Özdoğan, N. Başgelen, and P. Kuniholm, (2013): 93–112. Istanbul: Archaeology and Art Publications.

Goring-Morris, N., and L. K. Horwitz. "Funerals and feasts during the Pre-Pottery Neolithic B of the Near East." *Antiquity* 81.314 (2007): 902-919.

Griffiths, P. R., and J. A. De Haseth. "Fourier Transform Infrared Spectrometry". Vol. 171. John Wiley & Sons, (2007).

Hauptmann, A. "Greenstones' from Basta. Their mineralogical composition and possible provenance." *Basta I. The human ecology. Bibliotheca Neolithica Asiae Meridionalis et Occidentalis & Yarmouk University, Monograph of the Faculty of Archaeology and Anthropology* 4 (2004): 169-176.

Hayden, B. "Richman, Poorman, Beggarman, Chief: The Dynamics of Social Inequality." In *Archaeology at the Millenium: A Sourcebook,* edited by G. Feinman and T. Price, New York: Kluwer Academic/Plenum, (2001): 231– 72.

Healey, E., and S. Campbell. "Producing adornment: Evidence of different levels of expertise in the production of obsidian items of adornment at two late Neolithic communities in northern Mesopotamia." *Journal of Lithic Studies* 1.2 (2014): 79-99.

Helms, M. W. "Ulysses' Sail: An Ethnographic Odyssey of Knowledge, Power, and

Geographical Distance." Princeton, NJ: Princeton University Press, 1988.

Henderson, J. “The science and archaeology of materials: an investigation of inorganic materials”. Routledge, (2013): 8-23.

Henderson, P., et al. "Patterns of chemical change during bone fossilization." Nature 306.5941 (1983): 358-360.

Hill, W. W. "Navaho trading and trading ritual: a study of cultural dynamics." *Southwestern Journal of Anthropology* 4.4 (1948): 371-396.

Horejs, B. “Proto-Urbanisation without Urban Centres? A Model of Transformation for the İzmir Region in the 4th Millennium BC.” In Western Anatolia before Troy: Proto- Urbanisation in the 4th millennium BC? Proceedings of the International Symposium Held at the Kunsthistorisches Museum Wien, Vienna, Austria, 21–24 November 2012, edited by B. Horejs and M. Mehofer. Vienna: Austrian Academy of Sciences Press, (2014): 15–42.

Johnson, P. D., J. S. Prener, and J. D. Kingsley. "Apatite: origin of blue color." *Science* 141.3586 (1963): 1179-1180.

Karul, N. and M. B. Avcı. “Aktopraklık In *The Neolithic in Turkey.* Vol. 5: *Northwestern Turkey,* edited by M. Özdoğan, N. Başgelen, and P. Kuniholm. Istanbul: Archaeology and Art Publications, (2013): 45-68.

Khazeni, A. *Sky Blue Stone: The Turquoise Trade in World History*. Vol. 20. University of California Press, 2014.

Koreeda, M. “211-400 Fall 08 Lecture Notes – Characteristic IR Peaks”. *www.umich.edu/~chem211/211-400%20F08-IR%20peaks.pdf.* September 23, 2008. Accessed: May 6, 2017.

Korfmann, M., and Deutsches Archäologisches Institut. “Demircihüyük: die Ergebnisse der Ausgrabungen 1975-1978”. *1 - Architektur, Stratigraphie und Befunde.* Ed. Manfred Korfmann. von Zabern, (1983).

Krzemnicki, M. S., F. Herzog, and W. Zhou. "A historic turquoise jewelry set containing fossilized dentine (odontolite) and glass." *Gems & Gemology* 47.4 (2011): 296-301.

Kuhn, S. L., and M. C. Stiner. "Body ornamentation as information technology: towards an understanding of the significance of early beads." *Rethinking the human revolution* (2007): 45-54.

Kuijt, I. "People and space in early agricultural villages: exploring daily lives, community size, and architecture in the Late Pre-Pottery Neolithic." *Journal of Anthropological Archaeology* 19.1 (2000): 75-102.

Kuijt, I., and N. Goring-Morris. "Foraging, farming, and social complexity in the Pre-Pottery Neolithic of the southern Levant: a review and synthesis." *Journal of*

World Prehistory 16.4 (2002): 361-440.

Legros, R., N. Balmain, and G. Bonel. "Age-related changes in mineral of rat and bovine cortical bone." *Calcified tissue international* 41.3 (1987): 137-144.

Li, Y., et al. "Relationship between the colour change of hydroxyapatite and the trace element manganese." Biomaterials 14.13 (1993): 969-972.

Liaqat, S., et al. "Characterization of dentine to assess bond strength of dental composites." *Materials* 8.5 (2015): 2110-2126.

Lin, SY., MJ. Li, and WT. Cheng. "FT-IR and Raman vibrational microspectroscopies used for spectral biodiagnosis of human tissues." *Journal of Spectroscopy* 21.1 (2007): 1-30.

Marcus, J. "The archaeological evidence for social evolution." *Annual review of Anthropology* 37 (2008): 251-266.

Margaris, A. V. "Fourier Transform Infrared Spectroscopy (FTIR): Applications in Archaeology." *Encyclopedia of Global Archaeology*. Springer New York. (2014) 2890-2893.

Mayer, D. E. Bar-Yosef, and N. Porat. "Green stone beads at the dawn of agriculture." *Proceedings of the National Academy of Sciences*105.25 (2008): 8548-8551.

Medina, E. A., et al. "Intense turquoise colors of apatite-type compounds with Mn 5+ in tetrahedral coordination." *Solid State Sciences* 52 (2016): 97-105.

Mellaart, J. "Some Prehistoric Sites in North-Western Anatolia." Istanbuler Mitteilungen 6 (1955): 53-88.

Müller, K., and I. Reiche. "Differentiation of archaeological ivory and bone materials by micro-PIXE/PIGE with emphasis on two Upper Palaeolithic key sites: Abri Pataud and Isturitz, France." Journal of Archaeological Science 38.12 (2011): 3234-3243.

National Institute of Standards and Technology Chemistry Webbook, US Department of Commerce. http://webbook.nist.gov/cgi/cbook.cgi?Spec=C471341&Index=0&Type=IR, 2016. Accessed May 7, 2017.

Nicholson, P. "Faience technology." *UCLA encyclopedia of Egyptology* 1.1 (2009): 1-11.

Özbal, R. Personal Communication, 2015.

Özdoğan, E. "Neolithic Beads of Anatolia: An Overview" in *Anatolian Metal VII – Anatolien und seine Nachbarn vor 10.000 Jahren / Anatolia and Neighbours 10.000 years ago.* Edited by Ü. Yalcin . Der Anschnitt, Beiheft 31, Bochum. (2016) 135-152.

Özdoğan, M. "Neolithic sites in the Marmara region." In *The Neolithic in Turkey. Vol. 5: Northwestern Turkey,* edited by M. Özdoğan, N. Başgelen, and P. Kuniholm. Istanbul: Archaeology and Art Publications, (2013): 167-269.

Özdogan, M. "The expansion of the Neolithic way of life: what we know and what we do not know." *How did farming reach Europe* (2005): 13-27.

Özdoğan, M. *1984 Yılı Trakya ve Doğu Marmara Araştırmaları Araştırma Sonuçları Toplantısı*. (1986): 3409–20.

Öztan, A.. "Köşk Höyük" In *The Neolithic in Turkey. Vol. 3: Central Turkey*, edited by M. Özdoğan, N. Başgelen, and P. Kuniholm. Istanbul: Archaeology and Art Publications, (2012): 31–70.

Paz, A., et al. "A comparative study of hydroxyapatite nanoparticles synthesized by different routes." *Química Nova* 35.9 (2012): 1724-1727.

Réaumur R. "Observations sur les mines de turquoises du royaume; sur la nature de la matière qu'on y trouve, et sur la matière dont on lui donne la couleur". Memoires de l'Académie Royale des Sciences (1715): 174–202.

Regnier, P., A.C. Lasaga, R.A. Berner, O.G. Han, K.W. Zilm. "Mechanism of CO_3^{-2} substitution in carbonate-fluorapatite: Evidence from FTIR spectroscopy, ^{13}C NMR and quantum mechanical calculations" *American Mineralogist*, 79 (1994): 809-818.

Reiche, I., and E. Chalmin. "Synchrotron radiation and cultural heritage: combined XANES/XRF study at Mn K-edge of blue, grey or black coloured palaeontological and archaeological bone material." *Journal of Analytical Atomic Spectrometry* 23.6 (2008): 799-806.

Reiche, I., C. Vignaud, and M. Menu. "The crystallinity of ancient bone and dentine: new insights by transmission electron microscopy." *Archaeometry* 44.3 (2002b): 447-459.

Reiche, I., G. Morin, C. Brouder, V.A. Solé, P.-E. Petit, C. Vignaud, T. Calligaro, and M. Michel. "Manganese Accommodation in Fossilised Mastodon Ivory and Heat-Induced Colour Transformation." *European Journal of Mineralogy* 14, no. 6 (2002a) :1069–73.

Reiche, I., C. Vignaud, B. Champagnon, G. Panczer, C. Brouder, G. Morin, V.A. Solé, L. Charlet, and M. Menu. "From Mastodon Ivory to Gemstone: The Origin of Turquoise Color in Odontolite." *American Mineralogist* 86, no. 11-12 (2001): 1519–24.

Reiche, I., C. Vignaud, and M. Menu. "Heat Induced Transformation of Fossil Mastodon Ivory into Turquoise 'Odontolite.' Structural and Elemental Characterisation." *Solid State Sciences* 2, no.6 (2000a): 625–36.

Reiche, I., C. Vignaud, T. Calligaro, J. Salomon, and M. Menu. "Comparative Analysis of Odontolite, Heated Fossil Ivory and blue Fluorapatite by PIXE/PIGE and TEM." *Nuclear Instruments and Methods in Physics Research Section B: Beam*

Interactions with Materials and Atoms 161 (2000b): 737–42.

Rollefson, G. O. "The origins of the Yarmoukian at'Ain Ghazal." Paléorient (1993): 91-100.

Sagona, A., and P. Zimansky. *Ancient Turkey*. Routledge, 2009.

Sastry, T. P., et al. "Comparative study of some physico-chemical characteristics of osteoporotic and normal human femur heads." *Clinical biochemistry* 40.12 (2007): 907-912.

Schweitzer, M. H., J. L. Wittmeyer, and J. R. Horner. "Soft tissue and cellular preservation in vertebrate skeletal elements from the Cretaceous to the present." *Proceedings of the Royal Society of London B: Biological Sciences* 274.1607 (2007): 183-197.

Schoop, U. "Weaving Society in Late Chalcolithic Anatolia: Textile Production and Social Strategies in the 4th millennium BC." In Western Anatolia before Troy: Proto-Urbanisation in the 4th millennium BC? Proceedings of the International Symposium Held at the Kunsthistorisches Museum Wien, Vienna, Austria, 21–24 November 2012, edited by, B. Horejs and M. Mehofer. Vienna: Austrian Academy of Sciences Press, (2014): 421–46.

Taniguchi, Y., et al. "The first fake? Imitation turquoise beads recovered from a Syrian neolithic site, Tell El-Kerkh." *Studies in conservation 47.3* (2002): 175-183.

Thissen, L, et al. "The Land Of Milk? Approaching Dietary Preferences Of Late Neolithic Communities In NW" Anatolia." (2010): 157-171.

Van Zelst, L., D. W. Von Endt, and M.T. Baker. "Non-destructive and micro-sample FTIR spectrometric analysis of organic materials in art objects." In *2nd international conference on non-destructive testing, microanalytical methods and environment evaluation for study and conservation of works of art, Perugia, 17-20 April 1988,* 30.1-30.17. Rome: Istituto Centrale per il Restauro – Associazione Italiana Prove Non Distrutive. 1988.

Webster, R. "Gems Their Sources, Descriptions and Identification". Butterworth, London, 1986.

Webster, R. "Turquoise." *Lapidary Journal* 16.8 (1962): 717-812.

Weiner, S., and P. Goldberg. "On-site Fourier transform-infrared spectrometry at an archaeological excavation." Spectroscopy 5.2 (1990): 46-50.

Wright, K. I. K. "Domestication and inequality? Households, corporate groups and food processing tools at Neolithic Çatalhöyük." *Journal of Anthropological Archaeology* 33 (2014): 1-33.

Wright, K. I., et al. "Stone bead technologies and early craft specialization: insights from two Neolithic sites in eastern Jordan." *Levant* 40.2 (2008): 131-165.

Wright, K. and A. Garrard. "Social identities and the expansion of stone bead-making in Neolithic Western Asia: new evidence from Jordan." *Antiquity* 77.296 (2003): 267-284.

Yıldırım, C. Lecture titled “Method and Theory in Archaeology: X-Ray Diffraction, Raman Spectroscopy, Infrared Spectroscopy”. Koç University, March 20, 2014.

APPENDICES

Appendix A – Photographs of Beads

BH # of sample	BH# of bead
BH 37398	BH 5463

BH # of sample	BH# of beads
BH 37394	BH 34381

BH # of sample	BH# of beads
BH 37395	BH 32761

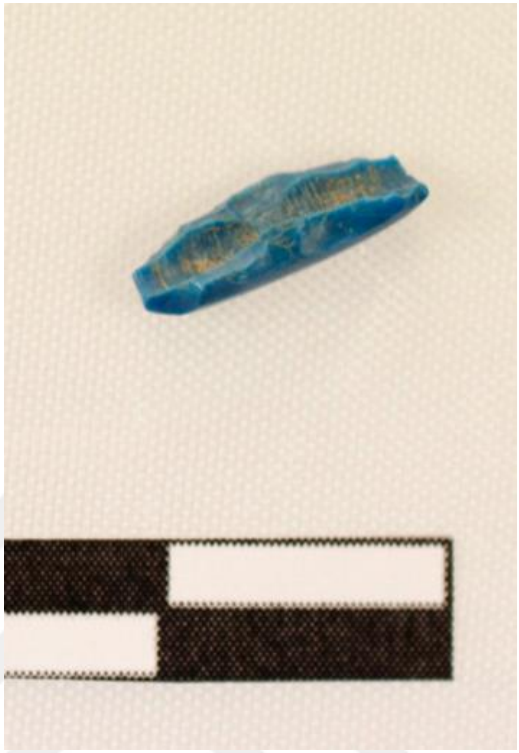

BH # of sample	BH# of beads
BH 37400	BH 17320

BH # of sample	BH# of beads
BH 37622	BH 31179

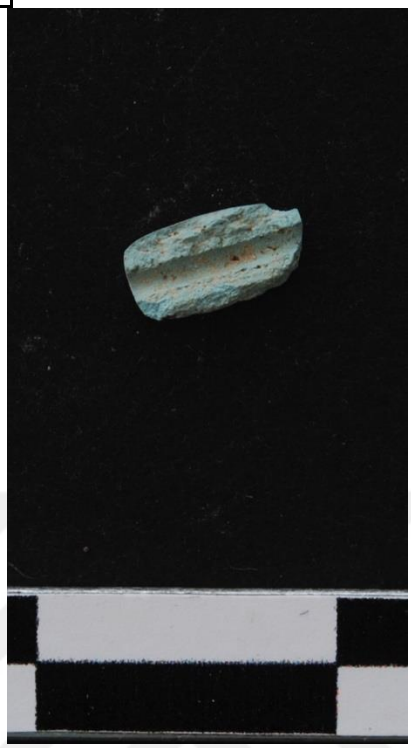

BH # of sample	BH# of beads
BH 37627	BH 26720

BH # of sample	BH# of beads
BH 17556	BH 16557

BH # of sample	BH# of beads
BH 22451	BH 22451

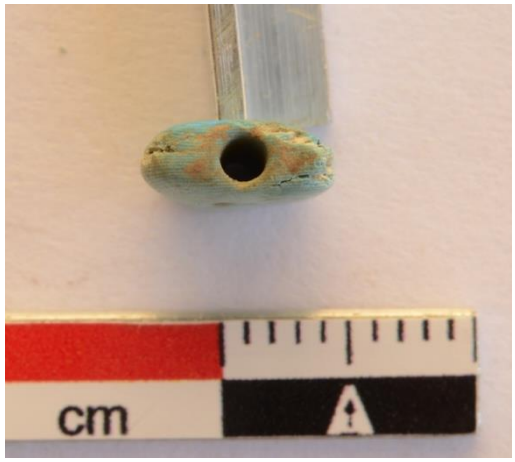

BH # of sample	BH# of beads
BH 21476	BH 21476

BH # of sample	BH# of beads
BH 18294	BH 18294

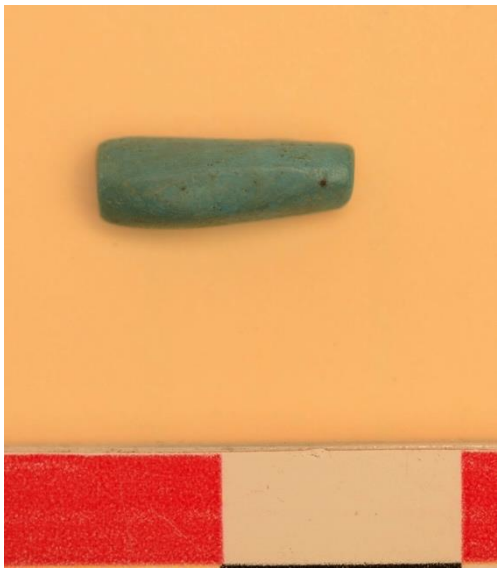

BH # of sample	BH# of beads
BH 17299	BH 17299

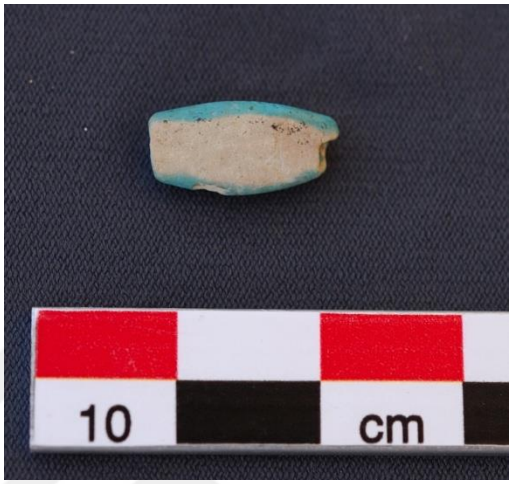

BH # of sample	BH# of beads
BH 32714	BH 32714

BH # of sample	BH# of beads
BH 18358	BH 18358

BH # of sample	BH# of beads
BH 37397	BH 14263

BH # of sample	BH# of beads
BH 37399	BH 30875

BH # of sample	BH# of beads
BH 37621	BH 24875

BH # of sample	BH# of beads
BH 37393	BH 30868

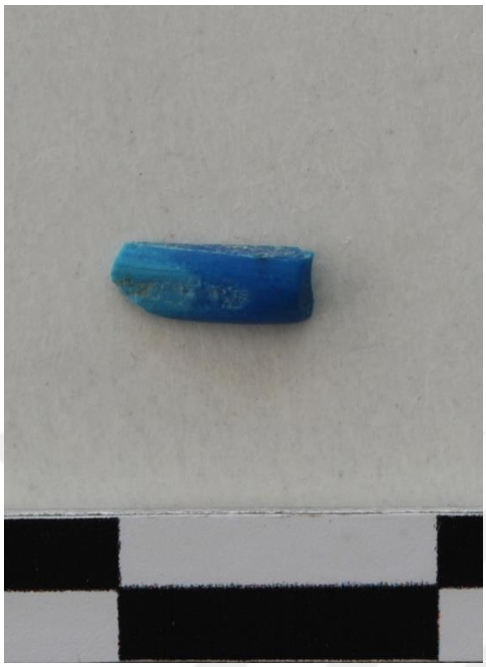

BH # of sample	BH# of beads
BH 37617	BH 37502

BH # of sample	BH# of beads
BH 37620	BH 20702

BH # of sample	BH# of beads
BH 37629	BH 36173

Appendix B - Table of Analyses Conducted on Beads

BH # of sample	BH# of beads	optical micro scope	SEM-EDX (polished not here)	polished SEM	FTIR	Raman
BH 37398	BH 5463	x				
BH 37394	BH 34381	x	x (1)			x
BH 37395	BH 32761	x	x (1)			x
BH 37400	BH 17320	x	x (1)			x
BH 37622	BH 31179	x	x (1)			x
BH 37627	BH 26720	X (np)				
BH 17556	BH 16557		X (6)			
BH 22451	BH 22451		x (3)			
BH 21476	BH 21476		x (3)			
BH 18294	BH 18294		x (2)			
BH 17299	BH 17299		x (2)			
BH 32714	BH 32714		x (2)			
BH 18358	BH 18358		x (1)			
BH 37397	BH 14263			x(4)	x	
BH 37399	BH 30875			x(7)	x	
BH 37621	BH 24875				x	
BH 37393	BH 30868	X (np)			x	
BH 37617	BH 37502				x	
BH 37620	BH 20702				x	
BH 37629	BH 36173				x	

Appendix C – SEM Distribution Maps

Phosphorus Distribution map for bead BH 37397

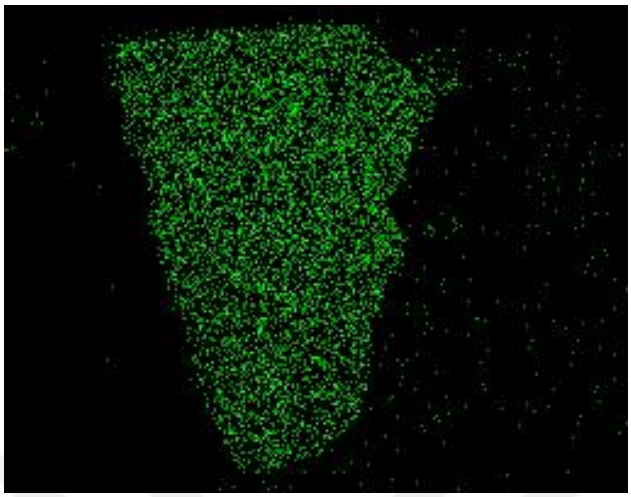

Calcium Distribution map for bead BH 37397

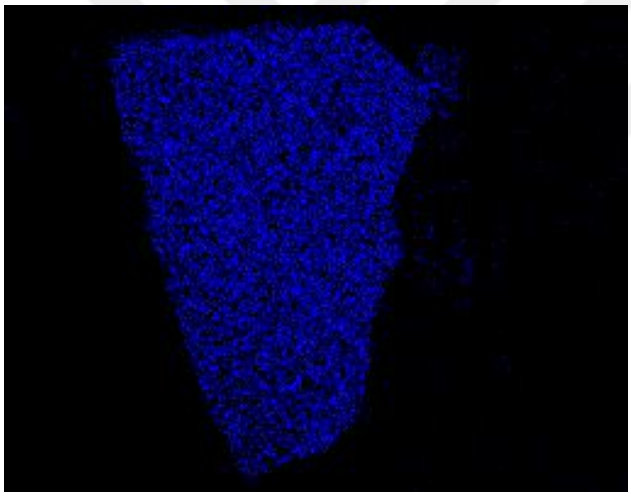

Manganese Distribution map for bead BH 37397:

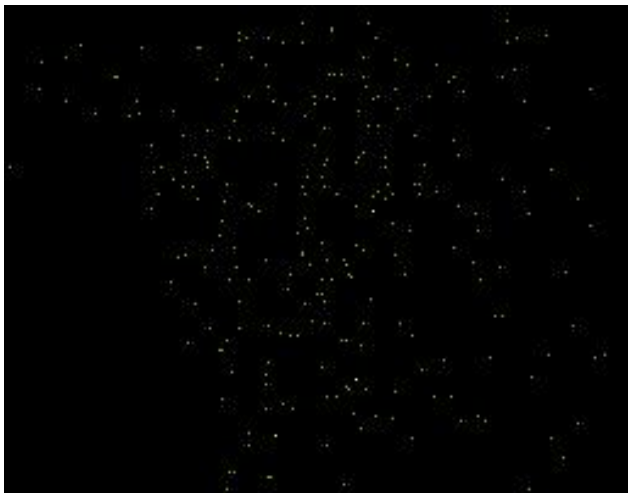

Phosphorus Distribution maps for bead BH 37399

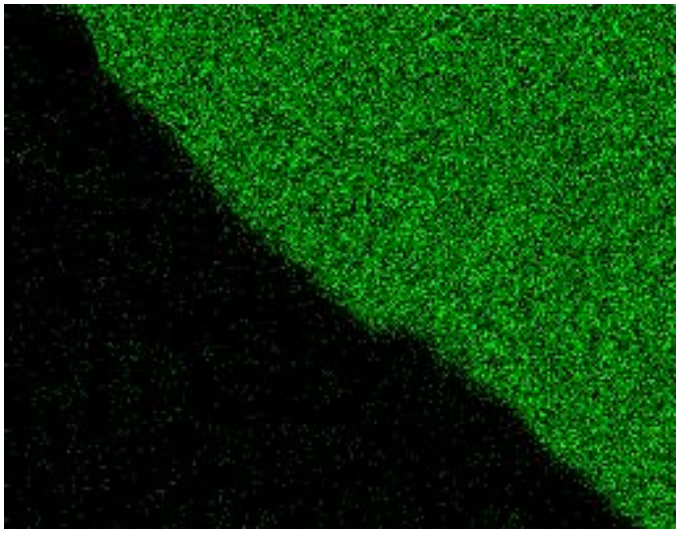

Calcium Distribution maps for bead BH 37399

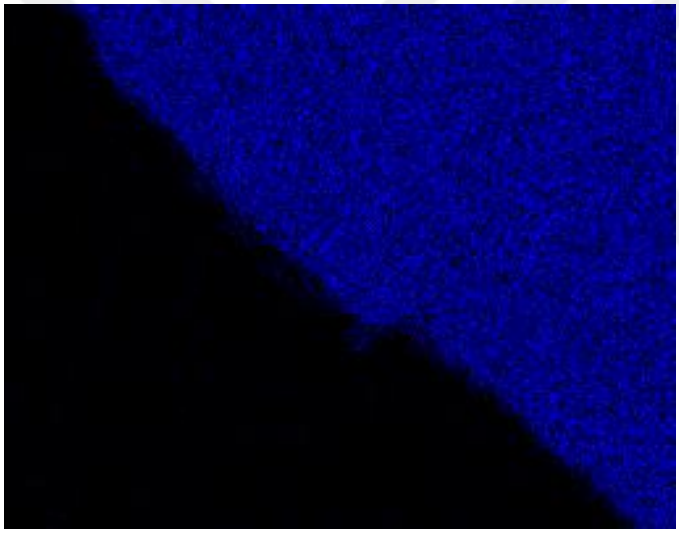

Manganese Distribution maps for bead BH 37399

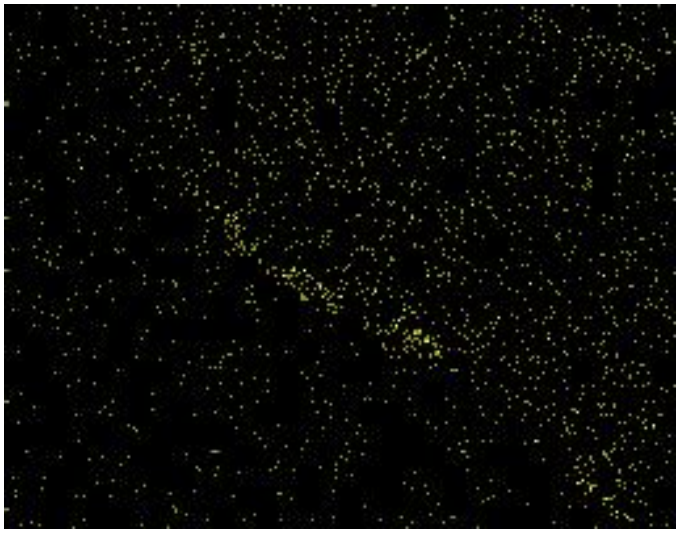

Appendix D – Catalogue of Beads

BH # of sample used	bead it belongs to	how much of the bead is sampled	supposed material	trench	locus	lot	properties of locus/lot	date	general form	size of sample used (cm)	weight of sample used (g)	complete-ness of actual bead	piercing diameter (cm)	colour	material characteristics	surface characteristics	inner colour	notes
BH 37394	**BH 34381**	100% sample	stone	L11W	504	1326	layer - white surface	06/08/13	Fragment	0,6* 0,38 *0,1	0,0674	<20	?	Blue	striated	shiny	white visible	probably part of a long flat bead, about a quarter remaining. Bright blue with very white inside. Striations from piercing visible
BH 37395	**BH 32761**	100% sample	stone	L12	368	1352	layer	28/07/13	Long flat - fragment	0,97* 0,30* 0,2	0,1366	40	0,15	Blue	homogenous	polished	blue throughout	definitely stone, consistent bright blue htroughout, drilled from both ends, bad meeting in middle, broekn in half along piercing, heavily shipped around broken edges. Chips have left percussion scars
BH 37398	**BH 5463**	50% sample	clay/ plaster	M10	115	401		30/07/09	Short flat - fragment	0,49* 0,28* 0,14	0,0423	90	0,14	Pale blue	homogenous	matt	white visible	reltively roughly shaped, quite worn, especially at ends. Grooves and breaks at the ends suggestive of damage from stringing
BH 37400	**BH 17320**	20% sample	stone	M10	252	1025	oven	05/08/11	Long round - fragment	0,8* 0,24* 0,11	0,0376	90	0,23	Blue	striated	shiny	interior pale	crystalline tooth-like structure, broken along one side, excellent view of fossil-ivory structure. Interior is greyish in colour. No flat areas at ends, relatively wide apertures to piercing
BH 37622	**BH 31179**	100% sample	clay/ plaster	L11S	456	1201	post hole row	22/07/13	Long flat - fragment	0,56* 0,27* 0,08	0,0287	20	?	Pale blue	homogenous	matt	blue throughout	fragment of lonf flat bead, pale blue throughout, straight piercing
BH 37399	**BH 30875**	50% sample	stone	L12	316	1270	layer	21/07/13	Long flat - fragment	0,7* 0,31* 0,24	0,1191	50	0,13	Blue	striated	shiny	white visible	very fine chert-like structure, very blue outside, very white inside, drilled piercing from both ends, meets badly, abrasion marks and faceting on outer surface. Broken along piercing

BH # of sample used	bead it belongs to	how much of the bead is sampled	supposed material	trench	locus	lot	properties of locus/lot	date	general form	size of sample used (cm)	weight of sample used (g)	complete-ness of actual bead	piercing diameter (cm)	colour	material characteristics	surface characteristics	inner colour	notes
BH 17556			clay/ plaster	L10	37	165	layer	14/08/11	Short flat - fragment	0,78 * 0,54 max 0,33 min	-	100	0,9	Pale blue	homogenous	matt	beige interior	neat shaping, flat ends, tiny piercing, serious chipping on outer surface showing glaze-like nature of coating and beige clay underneath
BH 22451			stone	M11	194	1185	layer or pit	06/08/12	Wide flat - fragment	1* 0,71 max 0,28 min	-	100	0,16	Blue	striated	matt smooth	white visible	laminated structure, damaged on one side with laminations split apart. Intense blue on one side, much paler on the other, quite large flat end areas
BH 21476			clay/ plaster	L11	346	883	surface	02/08/12	Wide flat - fragment	0,92* 0,92 max 0,37 min	-	100	0,13	Blue	homogenous	matt	no white visible	darkish turquoise surface colour, some areas of surface worn off, structure appears homogenous and molded
BH 18294			stone	M11	225	998	layer	19/08/11	Long flat - fragment	1,09* 0,39	-	50	0,14	Blue	striated	semi matt	white visible	split in half, clearly drilled from both ends, blue layer quite thin, then white inside. Slight faceting to outer surface, flattened end areas
BH 17299			clay/ plaster	L11	317	716	pit	06/08/11	Long flat - fragment	1,35 * 0,66 max 0,4 min	-	90	0,17	Pale blue	homogenous	matt	beige interior	both ends quite rounded, one quite irregular. In someplaces blue has worn off, in some it is chipped off and one patch has been abraded fairly hard over whole side to reveal inside material, looks like fine fired clay
BH 32714			stone	M13	53	544	pit	28/07/13	Flattened bell - fragment	1,24 * 0,82	-	50	0,19	Pale blue	striated	matt smooth	white visible	clear laminated structure, pale but shiny finish, pierced by drilling from both ends, piercings do not meet well
BH 18358			stone	M13	38	192	exploratory locus, sounding	16/08/11	Long flat - fragment	1,3 * 0,61 max 0,45 min	-	100	0,19	Blue	striated	matt	white visible	even shape, one end has a considerable groove, in groove white can be seen. Blue colour varies in intensity, some areas are very dense and bright, others more worn and paler, some of outer surface has chipping
BH 37621	**BH 24875**	100% sample	stone	M10	266	1236	layer but primary - deposited material	22/08.2012	Fragment	0,63* 0,35* 0,2	0,0512	<40	0,08	Pale blue	striated	shiny	white visible	laminated structure, fragmented through piercing and outer surface mostly missing. Glossy blue outside mostly eroded, thick layer of pale blue then white in the middle, drilled hole.

BH # of sample used	bead it belongs to	how much of the bead is sampled	supposed material	trench	locus	lot	properties of locus/lot	date	general form	size of sample used (cm)	weight of sample used (g)	complete-ness of actual bead	piercing diameter (cm)	colour	material characteristics	surface characteristics	inner colour	notes
BH 37393	**BH 30868**	100% sample	stone	L12	316	1270	layer	12/07/13	Fragment	0,6* 0,20* 0,08	0,04	<20	?	Blue	striated	shiny	blue throughout	Tiny chip of very bright blue elongated bead. Blue all through, striations visible in structure. Very shiny finish, faceting on outside
BH 37397	**BH 14263**	20% sample	stone	M10	230	919	platform bench ledge	18/07/11	Long flat - fragment	0,82* 0,27* 0,12	0,0605	90	0,13	Blue	striated	shiny	blue throughout	broken, 4 fragments remain. Relatively large flat ends, clear drilling from both ends seen in piercing cross section.
BH 37617	**BH 37502**	40% sample	clay/ plaster	L12	394	1548	surface	26/08/13	Long flat	0,56* 0,2* 0,08 // 0,45* 0,18* 0,09	0,024 / 0,0113	50	0,1	Pale blue	homogenous	matt	white visible	very worn outer colour, broken in half across its length, normal example
BH 37620	**BH 20702**	20% sample	stone	L12	117	1008	pit	27/07/12	Wide flat	0,54* 0,2* 0,19 // 0,47* 0,30* 0,1	0,0408 / 0,0355	100	0,14	Blue	striated	shiny	white visible	chipped on one side, seems to be striated in structure, almost chert like in appearance, blue colour goes quite deep, large flat ends, good blue colour and regular drilled piercing
BH 37629	**BH 36173**	30% sample	clay/ plaster	L12	376	1492	basin/bin installation	18/08/13	Long flat	0,65* 0,22* 0,21	0,0324	95	0,08	Pale blue	homogenous	matt	white visible	pale matt surface, white inside visible, ends falttened but edges slightly rounded.
BH 37627	**BH 26720**	20% sample	clay/ plaster	M11S	307	1363	secondary context	30/06/13	Long flat	0,74* 0,25* 0,21	0,0892	80	0,07	Pale blue	homogenous	matt	white visible	very worn surface, much interior white visible in broken areas, tiny piercing, very consistent consistency. Straight sided with flat ends

information in table adapted from database courtesy of Emma Baysal

Appendix E – FTIR Results Table

	1094cm-1 phosphate	1035cm-1 phosphate	962 cm-1 phosphate	599 cm-1 phosphate	561 cm-1 phosphate	470 cm-1 phosphate	1456cm-1 carbonate	1427cm-1 carbonate	864 cm-1 carbonate	OH-signal around 3400 cm-1	amide carbonyl /aldehyde	first match in library	percentage of match	second match in library	percentage of match
37393_1	1092	1036	960	601	566	479	1456	1424	865			fluorapatite w	35.94	fluorapatite b	34.80
37393_5	1092	1035	963	601	565	471	1453	1426	865			fluorapatite w	81.91	fluorapatite b	78.92
37393_b_1	1093	1032	963	600	563	472	1452	1425	865	slight curve		fluorapatite w	73.07	isokite	70.66
37393_B_2	1092	1033	963	600	564	472	1453	1425	865			fluorapatite w	77.03	fluorapatite blue	73.52
37393_B_3	1092	1033	963	600	564	471	1452	1425	865			fluorapatite w	75.28	fluorapatite blue	71.97
37393_B_4	1092	1031	963	600	563	473	1453	1425	865			isokite	71.76	fluorapatite white	70.76
37393_B5	1092	1035	963	601	565	471	1453	1426	865						
37397_2	1092	1028	963	600	562	473	1453	1425	864			fluorapatite w	70.13	isokite	69.24
37397_3	1091	1024	963	599	561	472	1453	1425	864			isokite	67.15	fluorapatite w	63.04
37297_4	1091	1026	963	599	562	473	1453	1425	864			isokite	68.74	fluorapatite w	66.21
37397_5	1092	1029	963	600	562	473	1453	1425	864			fluorapatite w	71.00	isokite	69.25
37397_6	1092	1027	963	600	562	472	1453	1425	864	slight curve		isokite	68.85	fluorapatite w	67.88
37397_7	1092	1026	963	600	562	472	1453	1425	864			isokite	68.81	fluorapatite w	67.42
37397_8	1091	1026	963	599	561	472	1453	1425	864	slight curve		isokite	68.67	fluorapatite w	66.28
37397_1	1092	1024	963	599	562	472	1453	1426	864			isokite	67.87	fluorapatite w	65.83
37399_2	1090	1040	962	600	563	472	1451	1425	864	slight curve					
37399_3	1090	1041	962	600	564	470	1454	1425	873						
37399_4	1092	1031	962	600	562	472	1460	1424	864						
37399_5	1087	1040	960	600	564	471	1458	1421	874	slight curve					
37399	1090	1024	963	600	562	473	1453	1424	874	slight curve		isokite	66.5	fluorapatite white	65.08
37617	1094	1036	964	602	566	467	1454	1428	864			fluorapatite w	37.98	fluorapatite b	36.63
37617_B2	1091	1027	963	600	563	473	1454	1425	865	slight curve					
37617_B-3	1090	1027	963	600	562	472	1453	1424	865						
37617_B-5	1091	1028	963	600	563	474	1451	1425	865						
37617-B_1	1091	1031	963	601	564	474	1458	1425	865	slight curve					
37617-B_4	1091	1030	963	601	563	472	1458	1425	865						
37620_1	1090	1038	no	601	567	468	1452	1420	865			fluorapatite w	50.63	fluorapatite b	48.21
37620_2	1091	1037	963	601	565	472	1454	1423	865						
37620_3	1092	1040	963	601	566	474	1453	1427	865						
37620_4	1091	1038	963	601	565	471	1453	1425	866	slight curve					
37620_5	1092	1036	963	600	564	472	1451	1425	865	slight curve					
37620_6	1091	1035	963	600	564	472	1453	1425	865	slight curve					

	1094cm-1 phosphate	1035cm-1 phosphate	962 cm-1 phosphate	599 cm-1 phosphate	561 cm-1 phosphate	470 cm-1 phosphate	1456cm-1 carbonate	1427cm-1 carbonate	864 cm-1 carbonate	OH-signal around 3400 cm-1	amide carbonyl /aldehyde	first match in library	percentage of match	second match in library	percentage of match
37620_7	1091	1037	963	601	565	472	1454	1425	865						
37620_8	1092	1037	963	601	565	473	1454	1425	865						
37620_B_2	1092	1035	963	600	564	471	1458	1424	875						
37620_B_3	1091	1034	963	600	563	471	1454	1425	875						
37620_B_4	1091	1032	963	600	564	473	1451	1425	875	slight curve					
37620_B_5	1091	1031	963	600	563	469	1460	1425	875	slight curve					
37620_b	1091	1035	963	600	564	472	1458	1425	875						
37621_2	1090	1032	963	601	563	473	1461	1423	866	slight curve					
37621_3	1090	1030	963	601	563	472	1461	1425	866						
37621_4	1090	1030	963	601	563	472	1454	1425	867	3400					
37621_5	1090	1031	963	601	563	472	1451	1424	866	slight curve					
37621_B_2	1089	1027	963	601	562	472	1451	1423	866	3400					
37621_b_3	1089	1027	963	601	562	472	1451	1422	866	3400					
37621_b_4	1089	1028	no	601	562	473	1458	1423	866	slight curve					
37621_B-5	1090	1029	963	601	562	471	1458	1423	865	slight curve					
37621_b1	1090	1026	963	601	562	473	1458	1422	866						
37621_1	1090	1023	963	600	561	471	1454	1423	866	3400		isokite	63.97	phosphate sodium dodecahydrate	57.02
37629	1093	1040	964	602	567	474	1457	1417	857			fluorapatite w	35.81	fluorapatite b	35.00
Bone samples															
black bone 1	no	1016	957	600	560	467	1444	1413	871	ca 3300	1647				
bone inside4_5	no	1018	957	600	560	468	1445	1414	871	ca 3300	1644				
bone2_insideA2	no	1016	957	600	560	470	1451	1413	871	ca 3300	1644				
bone2_out5	no	1018	954	601	561	468	1448	1414	872	ca 3300	1213, 1746	phosphate sodium dodecahydrate	56.84	isokite	54.81
cattle long_B_4	no	1011	957	600	557	466	1445	1409	871	3290, 2929	1242, 1654, 1543				
sheep long bone _B	no	1007	956	599	556	471	1446	1409	870	3271, 2922, 2853	1240, 1330, 1642				
cattle t bone A2	no	1012	957	599	558	466	1451	1412	871	3275, 2936	1230, 1642, 1537				

	1094cm-1 phosphate	1035cm-1 phosphate	962 cm-1 phosphate	599 cm-1 phosphate	561 cm-1 phosphate	470 cm-1 phosphate	1456cm-1 carbonate	1427cm-1 carbonate	864 cm-1 carbonate	OH-signal around 3400 cm-1	amide carbonyl /aldehyde	first match in library	percentage of match	second match in library	percentage of match
sheep vertebra A 4	no	1016	957	599	556	453	1446	1387	872	3290, 2968	1632, 1740, 1517, 1230, 1382				
sheep vertebra B2	no	1015	957	600	557	463	1442	1412	871	3271, 2923	1230, 1633, 1535, 1736				
cattle long bone A 3	no	1017	958	599	558	463	1448	1412	872	3274, 2927	1642, 1537,1236				
sheep long bone A 3	no	1008	958	598	556	463	1454	1408	871	3303, 2920	1235, 1634				
sheep feet B 1	no	1015	957	599	556	468	1451	1414	873	3289, 2927	1643, 1536, 1242, 1331				
cattle t bone B 4	no	1010	957	599	557	473	1451	1413	870	3294, 2952	1635, 1740, 1230				
sheep feet a 1	no	1010	957	599	557	466	1442	1413	871	3274, 2917	1624, 1540, 1239				
tooth/tusk samples															
equid fossil tooth 2	no	1023	959	602	562	471	1456	1415	868	no	no	isokite	60.99	phosphate sodium dodecahydrate	51.32
equid fossil tooth 1	no	1023	957	600	561	470	1454	1416	867	no	no	isokite	64.29		
pig tusk	no	1019	954	559	560	473	1448	1414	872	3308	1643				
pig enamel	no	1022	954	601	560	470	1453	1413	872	no	no	phosphate sodium dodecahydrate	58.98	isokite	57.67
sheep enamel	no	1020	957	601	560	470	1454	1413	872	3730, 2922	no				
cattle enamel	no	1021	954	601	560	473	1454	1413	872	no	1736				
human enamel	no	1021	954	600	560	473	1454	1413	872	no	no	isokite	63.05	belovite	56.60
human dentine	no	1012	954	599	557	468	1448	1413	870	ca 3300, 2900	no	belovite	49.26	phosphate sodium dodecahydrate	46.66
cattle dentine	no	1019	960	600	561	469	1451	1414	871	ca 3300	1647	isokite	65.21	phosphate sodium dodecahydrate	59.86
sheep dentine	no	1016	964	600	560	471	1454	1413	871	ca 3300, 2900	1739, 1644				

Appendix F – EDX Results Table

bead fragment BH#	bead BH#	O	Ca	P	C	Mg	Al	Na	Si	S	Mn	Ti	K	Fe	F	Cl
cross section of beads at Boğaziçi																
BH 37399	BH 30875															
Boncuk 2 (BU SEM)	6	19,85	11,15	4,46	45,47	0,34	2,5		9,77	0,25	4,16		0,83		0,96	0,27
	07 layer 1	21,74	32,49	13,88	26,78	0,53	0,47	0,52	1,09	0,23	0,55		0,44		1,07	0,22
	08 layer	18,28	34,36	14,31	27,06	0,72	0,54	0,63	1,3	0,46	0,57		0,68		0,71	0,38
	10 layer	15,45	18,91	7,47	42,27	0,64	2,47	0,36	5,2	0,43	4,21		0,99		1,33	0,28
	10bos	20,28	41,14	16,86	15,39	0,52	0,61	0,72	1,32	0,37	0,46		0,76		1,21	0,37
	10kanallı	19,40	37,73	15,43	18,45	0,98	1,14	0,97	1,49	0,67	0,44		0,79		2,01	0,49
	37399 layer	*25,90 (38,60)	*22,98 (36,22)	*11,17 (18,12)	*35,75 (carbon exc,)	*0,57 (1,01)		*0,62 (1,11)			*0,75 (1,17)		*0,54 (0,86)	*0,49 (0,77)	*1,01 (1,79)	*0,22 (0,36)
	37399 matrix	*29,31 (34,40)	*32,29 (38,61)	*15,71 (19,01)	*16,24 (carbon exc,)	*0,55 (0,69)		*0,93 (1,17)			*0,59 (0,71)		*0,71 (0,85)	*0,42 (0,71)	*3,06 (3,83)	*0,19 (0,23)
BH 37397	BH 14263															
Boncuk1 (BU SEM)	02bos	16,47	37,24	15,22	22,12	0,68	0,83	0,67	3,56	0,59	0,23		0,67		1,31	0,42
	02layer	13,65	26,33	10,16	43,85	0,47	0,62	0,51	2,04	0,32	0,35		0,43		0,89	0,38
	crack	25,00	16,62	4,98	30,78	1,08	10,34	0,63	7,94	0,46	0,34		0,5		0,96	0,36
	genel	15,56	35,78	14,15	23,64	0,67	0,89	0,73	5,11	0,57	0,29		0,77		1,4	0,44
surface analysis of beads and bone at KUYTAM																
BH 37394	*BH 34381*	*37,82*	*42,27*	*16,2*	Carbon Excluded	*0,18*	*0,27*	*0,24*	*0,42*	*0,2*	*0,92*				*1,47*	
BH 37395	*BH 32761*	*29,01*	*46,39*	*19,09*		*0,1*	*0,21*	*0,18*	*0,31*	*0,24*					*4,45*	
BH 37400	*BH 17320*	*34,79*	*45,43*	*16,3*		*0,07*	*0,02*	*0,11*	*0,04*						*3,25*	
BH 37622	*BH 31179*	*26,64*	*49,33*	*21,21*		*0,11*	*0,24*	*0,06*	*0,49*	*0,18*					*1,75*	
BH 17556																
1	*blue area*	*54,37*	*18,45*	*6,21*		*1,16*	*4,87*	*0,39*	*11,51*		*0,22*		*1,01*	*1,82*		
2	*blue area*	*54,90*	*11,04*	*3,46*		*1,68*	*7,05*	*0,37*	*16,05*		*0,27*	*0,19*	*1,83*	*3,15*		
3	*blue area*	*50,89*	*6,23*	*1,7*		*1,45*	*9,83*		*22,52*				*3,86*	*3,53*		
4	*bulk*	*59,87*	*4,18*	*1,55*		*1,95*	*8,82*	*0,72*	*18,1*				*1,85*	*2,96*		
5	*bulk*	*68,66*	*0,63*	*0,22*		*2,37*	*9,16*	*1,19*	*16,21*				*1*	*0,51*		
6	*bulk*	*63,70*	*1,14*	*0,36*		*2,07*	*8,86*	*0,86*	*19,53*				*1,68*	*1,81*		
BH 22451																
	light blue	39,28	39,7	13,54	4,03										3,45	
	light blue	38,70	41,26	13,17	4,71	0,03	0,03				0,18				1,92	
	dark blue	39,23	41,41	13,2	4,26	0,07	0,08	0,12			0,16				1,46	
BH 21476																
	light blue	50,06	19,11	7,59	8,46	1	0,62	0,61	0,76	0,12	10,86	0,49	0,32			
	light blue	27,67	45,43	20,03	4,27	0,35	0,85	0,34	0,54	0,2	0,33					
	dark blue	37,96	42,79	14,1	4,48	0,01	0,07	0,1	0,14		0,34					
BH 18294																
	blue	63,65	11,46	4,83	7,68		0,23	0,02							12,13	

bead fragment BH#	bead BH#	O	Ca	P	C	Mg	Al	Na	Si	S	Mn	Ti	K	Fe	F	Cl
	bulk	37,99	39,14	14,57	4,56		0,09	0,09	0,1						3,47	
BH 17299																
	blue	59,08	15,83	6,68	9,61	0,72	1,77	0,91	1,39					0,22	3,77	
	bulk	57,80	20,58	7,64	7,08		0,36	0,04	0,41					6,1		
BH 32714																
	blue	56,85	27,9	8,55	4,21	0,1	0,17	0,04	0,7	0,05	0,23		0,09		1,11	
	blue	45,62	35,06	12,53	4,28			0,03	0,13	0,11	0,75				1,5	
BH 18358																
	blue	34,36	43,46	16,72	4,1	0,13	0,26	0,03	0,2		0,5				0,32	
archaological cow long bone		48,33	34,66	11,04	5,38	0,12	0,08	0,38								
archaeological cow teeth		27,50	50,08	16,67	4,21	0,38	0,09	0,62								0,45
bone samples																
archaeological blue bone found in excavations - bone 101		37,90 (45,93)	42,11 (51,15)	0,34 (0,42)	17,72 (Carbon exc,)	1,00 (1,30)		0,50 (0,66)			0,32 (0,40)					0,11 (0,14)
archaeological blue bone found in excavations - bone 102		30,87 (35,80)	35,11 (41,18)	17,24 (20,41)	14,61 (Carbon exc,)	0,26 (0,32)		0,91 (1,22)			0,63 (0,73)					0,37 (0,45)
experiment sample - bone 202 - matrix		28,27 (31,79)	39,52 (44,59)	18,19 (20,68)	11,48 (Carbon exc,)	0,39 (0,45)		1,18 (1,39)			0,46 (0,52)					0,51 (0,58)
experiment sample - bone 203 - matrix		26,24 (29,41)	40,70 (45,70)	18,52 (20,95)	11,13 (Carbon exc,)	0,82 (0,95)		1,37 (1,60)			0,32 (0,36)					0,90 (1,03)
experiment sample - bone 204 - surface		28,06 (34,65)	35,32 (43,99)	14,98 (18,90)	19,73 (Carbon exc,)	0,08 (0,11)		0,62 (0,82)			0,48 (0,59)					0,74 (0,94)
experiment sample - bone 205 - surface		28,34 (33,56)	35,96 (42,95)	16,23 (19,61)	16,34 (Carbon exc,)	0,63 (0,79)		1,21 (1,52)			0,45 (0,54)					0,84 (1,03)
experiment sample - bone 207 - matrix		28,59 (33,80)	34,82 (41,64)	16,53 (20,02)	16,41 (Carbon exc,)	0,92 (1,16)		1,70 (2,14)			0,20 (0,24)					0,83 (1,01)
		O	Ca	P	C	Mg	Al	Na	Si	S	Mn	Ti	K	Fe	F	Cl

values are wt%

italic - carbon excluded

* - has carbon excluded results as well

Appendix G – XRD Results

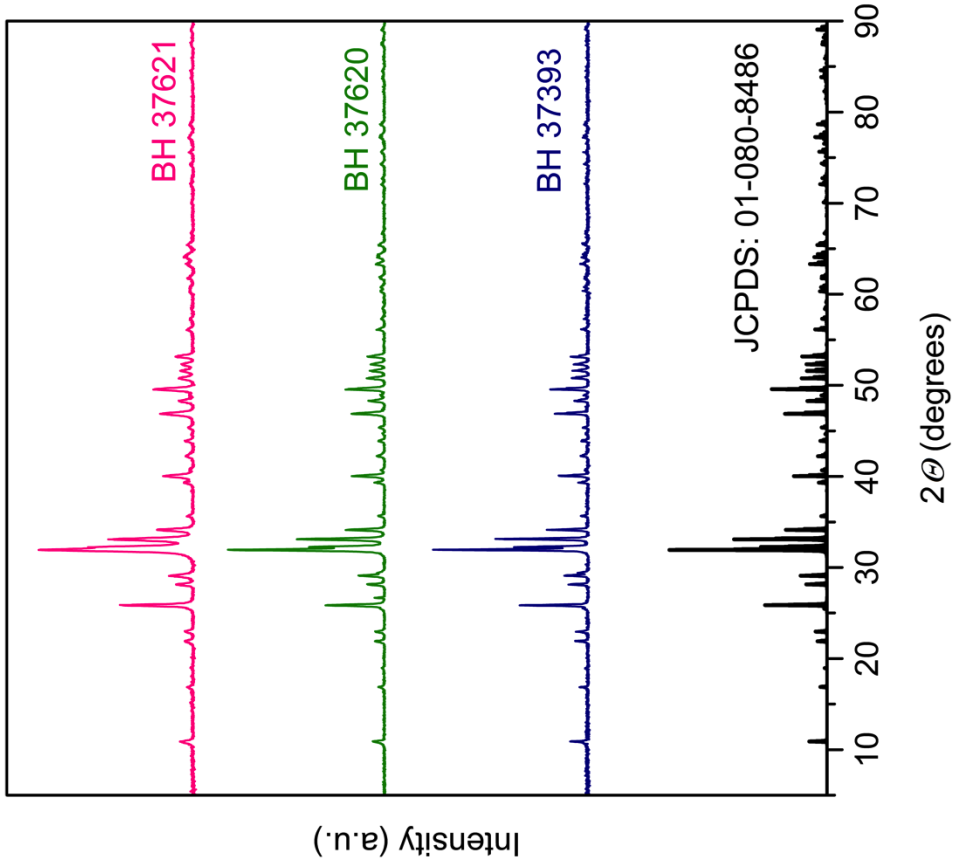

Measurements done and figures prepared by Dr Ceren Yılmaz Akkaya from KUYTAM Laboratories.

Pattern: PDF 01-080-8486 Radiation: 1.54060 Quality: Star (*)

Formula	Ca10 (P O4)6 F2
Name	Calcium Fluoride Phosphate
Name (mineral)	Fluorapatite, syn
Name (common)	decacalcium hexakis (orthophosphate) difluoride

Lattice:	Hexagonal	Mol. weight =	1008.62
S.G.:	P63/m (176)	Volume [CD] =	523.15
		Dx =	3.2
		Dm =	
		I/Icor =	1.110

a =	9.36723	alpha =	
b =		beta =	
c =	6.88445	gamma =	
a/b =	1.00000	Z =	1
c/b =	0.73495		

ANX: A3B5XY12
Analysis: Ca10 F2 O24 P6
Formula from original source: Ca10 (P O4)6 F2
ICSD Collection Code: 262707
Calculated Pattern Original Remarks: R = R(p)
Wyckoff Sequence: i h4 f a (P63/M)
Unit Cell Data Source: Powder Diffraction

Structure
Publication: J. Solid State Chem.
Detail: volume 184, page 2978 (2011)
Authors: Lim, S.C., Baikie, T., Pramana, S.S., Smith, R., White, T.J.
Primary Reference
Publication: Calculated from ICSD using POWD-12++

Radiation:	CuKα1	Filter:	Not specified
Wavelength:	1.54060	d-spacing:	
SS/FOM:	999.9 (0,31)		

d	2θ	I fix	h	k	l	d	2θ	I fix	h	k	l
8.11226	10.897	92	1	0	0	1.77024	51.588	130	1	4	0
5.24903	16.877	39	1	0	1	1.74734	52.315	124	4	0	2
4.68362	18.933	15	1	1	0	1.74734	52.315	124	3	0	3
4.05613	21.895	57	2	0	0	1.72111	53.174	150	0	0	4
3.87243	22.948	73	1	1	1	1.71447	53.397	15	4	1	1
3.49468	25.467	21	2	0	1	1.68364	54.454	5	1	0	4
3.44222	25.862	377	0	0	2	1.63712	56.136	73	3	2	2
3.16876	28.138	126	1	0	2	1.62245	56.690	5	5	0	0
3.06615	29.100	160	2	1	0	1.61549	56.956	6	1	1	4
2.80091	31.926	999	2	1	1	1.60658	57.301	32	3	1	3
2.77369	32.248	427	1	1	2	1.57919	58.390	17	5	0	1
2.70409	33.102	565	3	0	0	1.57426	58.590	6	4	1	2
2.62452	34.135	247	2	0	2	1.56121	59.129	8	3	3	0
2.51690	35.643	37	3	0	1	1.53307	60.325	45	2	4	0
2.34181	38.408	4	2	2	0	1.52255	60.786	40	3	3	1
2.28955	39.320	52	2	1	2	1.50083	61.761	35	1	2	4
2.24994	40.042	204	1	3	0	1.49642	61.963	24	2	4	1
2.21705	40.662	34	2	2	1	1.46760	63.319	102	5	0	2
2.20817	40.833	6	1	0	3	1.45700	63.834	15	5	1	0
2.13862	42.223	57	1	3	1	1.45196	64.082	76	3	0	4
2.12643	42.477	14	3	0	2	1.44548	64.404	56	3	2	3
2.06075	43.900	43	1	1	3	1.42543	65.422	60	5	1	1
2.02806	44.645	12	4	0	0	1.42180	65.610	18	3	3	2
1.99731	45.371	36	2	0	3	1.40166	66.674	19	2	4	2
1.93622	46.886	264	2	2	2	1.40166	66.674	19	1	4	3
1.88332	48.286	124	1	3	2	1.38684	67.481	2	2	2	4
1.86108	48.900	35	2	3	0	1.36701	68.595	5	3	1	4
1.83723	49.577	329	2	1	3	1.35748	69.145	2	1	0	5
1.79659	50.777	152	3	2	1	1.35204	69.463	4	6	0	0

d	2θ	I fix	h	k	l	d	2θ	I fix	h	k	l	d	2θ	I fix	h	k	l
1.34176	70.073	23	1	5	2	1.14741	84.341	17	0	0	6	1.02569	97.355	16	7	1	2
1.33365	70.562	5	4	3	0	1.14478	84.580	32	2	4	4	1.02439	97.521	7	2	4	5
1.32479	71.105	3	5	0	3	1.13916	85.095	2	4	0	5	1.02216	97.806	20	3	6	0
1.32099	71.341	4	1	1	5	1.13610	85.378	6	1	0	6	1.02216	97.806	20	1	3	6
1.31226	71.889	7	4	0	4	1.13045	85.908	15	5	2	3	1.01403	98.865	9	8	0	0
1.30931	72.076	41	4	3	1	1.12497	86.429	3	2	6	0	1.01097	99.271	19	6	3	1
1.30382	72.428	3	2	0	5	1.11445	87.449	32	1	1	6	1.00453	100.139	22	1	6	4
1.29900	72.740	30	5	2	0	1.11204	87.687	18	5	1	4	1.00073	100.661	17	5	1	5
1.29081	73.276	4	3	3	3	1.11024	87.866	5	2	6	1	0.99866	100.948	12	4	0	6
1.27648	74.236	24	5	2	1	1.10853	88.036	6	4	4	2	0.99439	101.547	9	5	4	2
1.27477	74.352	35	2	4	3	1.10689	88.200	22	2	3	5	0.99107	102.017	7	7	2	0
1.26360	75.122	9	2	3	4	1.10408	88.483	4	2	0	6	0.98096	103.488	6	7	2	1
1.25845	75.483	13	6	0	2	1.09832	89.070	61	3	5	2	0.97977	103.664	26	3	6	2
1.25606	75.652	48	2	1	5	1.08895	90.044	4	1	6	3	0.97670	104.124	7	1	0	7
1.24357	76.549	21	3	4	2	1.08684	90.267	2	4	1	5	0.97670	104.124	7	3	2	6
1.23711	77.021	22	6	1	0	1.07450	91.597	19	1	7	0	0.97270	104.730	31	1	7	3
1.23401	77.251	67	1	4	4	1.06931	92.170	12	6	2	2	0.97270	104.730	31	8	0	2
1.23003	77.547	33	5	1	3	1.06321	92.855	6	6	0	4						
1.22699	77.775	4	3	0	5	1.06164	93.033	2	7	1	1						
1.21761	78.489	12	6	1	1	1.05625	93.652	2	3	0	6						
1.21534	78.664	56	2	5	2	1.05420	93.890	5	4	3	4						
1.18693	80.930	6	2	2	5	1.04981	94.404	4	5	0	5						
1.18059	81.456	10	5	0	4	1.04298	95.217	2	4	4	3						
1.17443	81.975	7	1	3	5	1.03867	95.739	2	5	4	0						
1.17090	82.275	18	4	4	0	1.03683	95.965	10	5	2	4						
1.16420	82.853	8	1	6	2	1.03447	96.255	6	7	0	3						
1.15889	83.317	9	7	0	0	1.03266	96.479	11	3	3	5						
1.15635	83.541	10	3	3	4	1.03037	96.765	19	2	2	6						
1.15307	83.832	37	4	3	3	1.02705	97.183	12	4	5	1						

Appendix H – XRF Results

BH 37393 - normalized															
Formula	Z	Concentration	Status	Line 1	Calc. concentration	Net int.	Analyzed layer	Line 2	Calc. concentration	Net int.	Analyzed layer	Line 3	Calc. concentration	Net int.	Analyzed layer
Ca	20	75.1	XRF 1	Ca KA1-HR-Tr	75.1	17.13	35 um	Ca KB1-HR-Tr	79.8	2.183	44 um				
P	15	22.3	XRF 1	P KA1-HR-Tr	22.3	4.933	13.7 um								
Si	14	0.38	XRF 1	Si KA1-HR-Tr	0.38	0.05270	9.5 um	Si KB1-HR-Tr/El	2.2	0.00847	11.0 um				
S	16	0.28	XRF 1	S KA1-HR-Tr	0.28	0.08395	10.6 um								
Sr	38	0.152	XRF 1	Sr KA1-HR-Tr	0.152	0.5305	0.32 mm	Sr KB1-HR-Tr	0.22	0.3407	0.45 mm	Sr LA1-HR	0.16	0.00851	10.5 um
Cr	24	0.13	XRF 1	Cr KA1-HR-Tr	0.13	0.02965	22.7 um	Cr KB1-HR-Tr	0.35	0.01323	29.1 um	Cr LA1-HR		0.0	0.64 um
Fe	26	0.11	XRF 1	Fe KA1-HR-Tr	0.11	0.05114	35 um	Fe KB1-HR-Tr	0.18	0.01550	46 um	Fe LA1-HR		0.0	1.03 um
As	33	0.085	XRF 1	As KA1-HR-Tr	0.085	0.1643	140 um	As KB1-HR-Tr	0.045	0.01655	189 um	As LA1-HR	0.023	0.01210	4.3 um
Zr	40	0.028	XRF 1	Zr KA1-HR-Tr	0.028	0.3407	0.44 mm	Zr KB1-HR-Tr	0.080	0.05159	0.61 mm	Zr LA1-HR	0.36	0.02882	14.3 um
BH 37393 - not normalized															
Formula	Z	Concentration	Status	Line 1	Calc. concentration	Net int.	Analyzed layer	Line 2	Calc. concentration	Net int.	Analyzed layer	Line 3	Calc. concentration	Net int.	Analyzed layer
Ca	20	29.4	XRF 1	Ca KA1-HR-Tr	29.4	17.13	81 um	Ca KB1-HR-Tr	30.9	2.183	102 um				
P	15	10.6	XRF 1	P KA1-HR-Tr	10.6	4.933	34 um								
Si	14	0.16	XRF 1	Si KA1-HR-Tr	0.16	0.05270	23.9 um	Si KB1-HR-Tr/El	0.97	0.00847	27.5 um				
S	16	0.13	XRF 1	S KA1-HR-Tr	0.13	0.08395	24.5 um								
Mn	25	0.087	XRF 1	Mn KA1-HR-Tr	0.087	0.08569	71 um	Mn KB1-HR-Tr	0.067	0.01260	91 um	Mn LA1-HR		0.0	2.04 um
Sr	38	0.0588	XRF 1	Sr KA1-HR-Tr	0.0588	0.5305	0.81 mm	Sr KB1-HR-Tr	0.085	0.3407	1.12 mm	Sr LA1-HR	0.099	0.00851	26.4 um
Cr	24	0.040	XRF 1	Cr KA1-HR-Tr	0.040	0.02965	57 um	Cr KB1-HR-Tr	0.10	0.01323	72 um	Cr LA1-HR		0.0	1.61 um
Fe	26	0.036	XRF 1	Fe KA1-HR-Tr	0.036	0.05114	88 um	Fe KB1-HR-Tr	0.059	0.01550	114 um	Fe LA1-HR		0.0	2.57 um
As	33	0.030	XRF 1	As KA1-HR-Tr	0.030	0.1643	0.35 mm	As KB1-HR-Tr	0.016	0.01655	0.47 mm	As LA1-HR	0.076	0.01210	10.9 um
Zr	40	0.022	XRF 1	Zr KA1-HR-Tr	0.022	0.3407	1.10 mm	Zr KB1-HR-Tr	0.033	0.05159	1.53 mm	Zr LA1-HR	0.27	0.02882	36 um
BH 37617 - normalized															
Formula	Z	Concentration	Status	Line 1	Calc. concentration	Net int.	Analyzed layer	Line 2	Calc. concentration	Net int.	Analyzed layer	Line 3	Calc. concentration	Net int.	Analyzed layer
Ca	20	74.8	XRF 1	Ca KA1-HR-Tr	74.8	15.58	36 um	Ca KB1-HR-Tr	74.3	1.853	45 um				
P	15	22.7	XRF 1	P KA1-HR-Tr	22.7	4.607	14.1 um								
Mn	25	0.46	XRF 1	Mn KA1-HR-Tr	0.46	0.1288	29.3 um	Mn KB1-HR-Tr	0.32	0.01769	38 um	Mn LA1-HR		0.00192	0.84 um
Fe	26	0.17	XRF 1	Fe KA1-HR-Tr	0.17	0.06982	36 um	Fe KB1-HR-Tr	0.46	0.03598	47 um	Fe LA1-HR		0.00130	1.05 um
Sr	38	0.16	XRF 1	Sr KA1-HR-Tr	0.16	0.3757	0.33 mm	Sr KB1-HR-Tr	0.13	0.06894	0.46 mm	Sr LA1-HR	0.26	0.01272	10.7 um
K	19	0.11	XRF 1	K KA1-HR-Tr	0.11	0.02836	27.1 um	K KB1-HR-Tr	0.31	0.00839	34 um				
Zn	30	0.060	XRF 1	Zn KA1-HR-Tr	0.060	0.06724	82 um	Zn KB1-HR-Tr	-0.092	-0.01752	109 um	Zn LA1-HR-Tr	-0.50	0.00139	2.43 um
BH 37617 - not normalized															
Formula	Z	Concentration	Status	Line 1	Calc. concentration	Net int.	Analyzed layer	Line 2	Calc. concentration	Net int.	Analyzed layer	Line 3	Calc. concentration	Net int.	Analyzed layer
Ca	20	26.1	XRF 1	Ca KA1-HR-Tr	26.1	15.58	92 um	Ca KB1-HR-Tr	25.6	1.853	115 um				
P	15	9.84	XRF 1	P KA1-HR-Tr	9.84	4.607	40 um								
Mn	25	0.13	XRF 1	Mn KA1-HR-Tr	0.13	0.1288	81 um	Mn KB1-HR-Tr	0.093	0.01769	105 um	Mn LA1-HR		0.00192	2.34 um
Sr	38	0.060	XRF 1	Sr KA1-HR-Tr	0.060	0.3757	0.93 mm	Sr KB1-HR-Tr	0.048	0.06894	1.28 mm	Sr LA1-HR	0.15	0.01272	30 um
Fe	26	0.049	XRF 1	Fe KA1-HR-Tr	0.049	0.06982	102 um	Fe KB1-HR-Tr	0.14	0.03598	131 um	Fe LA1-HR		0.00130	2.94 um
K	19	0.044	XRF 1	K KA1-HR-Tr	0.044	0.02836	69 um	K KB1-HR-Tr	0.12	0.00839	85 um				
Zn	30	0.019	XRF 1	Zn KA1-HR-Tr	0.019	0.06724	228 um	Zn KB1-HR-Tr	-0.030	-0.01752	0.30 mm	Zn LA1-HR-Tr	-0.066	0.00139	6.8 um
BH 37620 - normalized															
Formula	Z	Concentration	Status	Line 1	Calc. concentration	Net int.	Analyzed layer	Line 2	Calc. concentration	Net int.	Analyzed layer	Line 3	Calc. concentration	Net int.	Analyzed layer

Ca	20	75.4	XRF 1	Ca KA1-HR-Tr	75.4	20.68	37 um	Ca KB1-HR-Tr	72.5	2.381	46 um				
P	15	22.4	XRF 1	P KA1-HR-Tr	22.4	5.969	14.2 um								
Si	14	0.34	XRF 1	Si KA1-HR-Tr	0.34	0.05683	9.8 um	Si KB1-HR-Tr/El	2.5	0.01140	11.2 um				
Fe	26	0.29	XRF 1	Fe KA1-HR-Tr	0.29	0.1561	36 um	Fe KB1-HR-Tr	0.43	0.04402	47 um	Fe LA1-HR		0.0	1.05 um
S	16	0.27	XRF 1	S KA1-HR-Tr	0.27	0.09578	10.8 um								
Al	13	0.19	XRF 1	Al KA1-HR-Tr	0.19	0.01931	6.5 um	Al KB1-HR-Tr/El	8.3	0.00825	7.3 um				
Mn	25	0.19	XRF 1	Mn KA1-HR-Tr	0.19	0.06927	29.2 um	Mn KB1-HR-Tr	0.035	0.00298	38 um	Mn LA1-HR		0.00105	0.84 um
Zr	40	0.102	XRF 1	Zr KA1-HR-Tr	0.102	0.6408	0.45 mm	Zr KB1-HR-Tr	0.15	0.1289	0.63 mm	Zr LA1-HR	0.54	0.05079	14.7 um
Ti	22	0.075	XRF 1	Ti KA1-HR-Tr	0.075	0.01048	14.5 um	Ti KB1-HR-Tr	0.44	0.00948	18.2 um				
Sr	38	0.066	XRF 1	Sr KA1-HR-Tr	0.066	0.2954	0.33 mm	Sr KB1-HR-Tr	0.0433	0.6408	0.46 mm	Sr LA1-HR	0.17	0.01111	10.8 um
Zn	30	0.033	XRF 1	Zn KA1-HR-Tr	0.033	0.05155	82 um	Zn KB1-HR-Tr	0.010	0.00279	109 um	Zn LA1-HR-Tr	0.40	0.00564	2.43 um
As	33	0.024	XRF 1	As KA1-HR-Tr	0.024	0.05763	143 um	As KB1-HR-Tr	0.004	0.00175	193 um	As LA1-HR	0.085	0.00908	4.4 um
BH 37620 - not normalized															
Formula	Z	Concentration	Status	Line 1	Calc. concentration	Net int.	Analyzed layer	Line 2	Calc. concentration	Net int.	Analyzed layer	Line 3	Calc. concentration	Net int.	Analyzed layer
Al	13	0.085	XRF 1	Al KA1-HR-Tr	0.085	0.01931	13.1 um	Al KB1-HR-Tr/El	3.8	0.00825	14.7 um				
As	33	0.011	XRF 1	As KA1-HR-Tr	0.011	0.05763	287 um	As KB1-HR-Tr	0.002	0.00175	0.39 mm	As LA1-HR	0.081	0.00908	9.0 um
Ca	20	36.9	XRF 1	Ca KA1-HR-Tr	36.9	20.68	69 um	Ca KB1-HR-Tr	35.4	2.381	87 um				
Fe	26	0.12	XRF 1	Fe KA1-HR-Tr	0.12	0.1561	73 um	Fe KB1-HR-Tr	0.18	0.04402	95 um	Fe LA1-HR		0.0	2.12 um
Mn	25	0.077	XRF 1	Mn KA1-HR-Tr	0.077	0.06927	58 um	Mn KB1-HR-Tr	0.015	0.00298	76 um	Mn LA1-HR		0.00105	1.68 um
P	15	12.7	XRF 1	P KA1-HR-Tr	12.7	5.969	28.6 um								
S	16	0.15	XRF 1	S KA1-HR-Tr	0.15	0.09578	20.6 um								
Si	14	0.18	XRF 1	Si KA1-HR-Tr	0.18	0.05683	19.7 um	Si KB1-HR-Tr/El	1.3	0.01140	22.7 um				
Sr	38	0.032	XRF 1	Sr KA1-HR-Tr	0.032	0.2954	0.67 mm	Sr KB1-HR-Tr	0.109	0.6408	0.92 mm	Sr LA1-HR	0.12	0.01111	21.8 um
Ti	22	0.028	XRF 1	Ti KA1-HR-Tr	0.028	0.01048	29.0 um	Ti KB1-HR-Tr	0.17	0.00948	36 um				
Zn	30	0.014	XRF 1	Zn KA1-HR-Tr	0.014	0.05155	164 um	Zn KB1-HR-Tr	0.004	0.00279	219 um	Zn LA1-HR-Tr	0.25	0.00564	4.9 um
Zr	40	0.0539	XRF 1	Zr KA1-HR-Tr	0.0539	0.6408	0.91 mm	Zr KB1-HR-Tr	0.076	0.1289	1.27 mm	Zr LA1-HR	0.44	0.05079	29.8 um
BH 37621 - normalized															
Formula	Z	Concentration	Status	Line 1	Calc. concentration	Net int.	Analyzed layer	Line 2	Calc. concentration	Net int.	Analyzed layer	Line 3	Calc. concentration	Net int.	Analyzed layer
Ca	20	72.7	XRF 1	Ca KA1-HR-Tr	72.7	12.80	35 um	Ca KB1-HR-Tr	69.6	1.478	44 um				
Fe	26	0.14	XRF 1	Fe KA1-HR-Tr	0.14	0.05068	37 um	Fe KB1-HR-Tr	0.22	0.01502	48 um	Fe LA1-HR		0.0	1.07 um
Mn	25	0.41	XRF 1	Mn KA1-HR-Tr	0.41	0.09905	29.7 um	Mn KB1-HR-Tr	0.29	0.01398	38 um	Mn LA1-HR		0.00007	0.85 um
P	15	24.2	XRF 1	P KA1-HR-Tr	24.2	4.160	14.2 um								
S	16	0.31	XRF 1	S KA1-HR-Tr	0.31	0.06866	10.5 um								
Si	14	0.30	XRF 1	Si KA1-HR-Tr	0.30	0.03191	9.8 um	Si KB1-HR-Tr/El	3.6	0.01077	11.3 um				
Sr	38	0.122	XRF 1	Sr KA1-HR-Tr	0.122	0.4912	0.34 mm	Sr KB1-HR-Tr	0.10	0.1153	0.47 mm	Sr LA1-HR	0.50	0.02104	10.8 um
BH 37621 - not normalized															
Formula	Z	Concentration	Status	Line 1	Calc. concentration	Net int.	Analyzed layer	Line 2	Calc. concentration	Net int.	Analyzed layer	Line 3	Calc. concentration	Net int.	Analyzed layer
Ca	20	20.4	XRF 1	Ca KA1-HR-Tr	20.4	12.80	105 um	Ca KB1-HR-Tr	19.1	1.478	131 um				
Fe	26	0.030	XRF 1	Fe KA1-HR-Tr	0.030	0.05068	125 um	Fe KB1-HR-Tr	0.047	0.01502	162 um	Fe LA1-HR		0.0	3.6 um
Mn	25	0.086	XRF 1	Mn KA1-HR-Tr	0.086	0.09905	100 um	Mn KB1-HR-Tr	0.063	0.01398	130 um	Mn LA1-HR		0.00007	2.90 um
P	15	8.99	XRF 1	P KA1-HR-Tr	8.99	4.160	49 um								
S	16	0.11	XRF 1	S KA1-HR-Tr	0.11	0.06866	32 um								
Si	14	0.097	XRF 1	Si KA1-HR-Tr	0.097	0.03191	34 um	Si KB1-HR-Tr/El	1.2	0.01077	39 um				
Sr	38	0.0688	XRF 1	Sr KA1-HR-Tr	0.0688	0.4912	1.15 mm	Sr KB1-HR-Tr	0.065	0.1153	1.59 mm	Sr LA1-HR	0.26	0.02104	37 um

Measurements were done with Bruker Tiger XRF by Dr Gülsu Şimşek from KUYTAM laboratories.
Analysis method: Elements, Mylar 2.5 micron powder sample holder, He mode 5mm filter, best detection method 17 min.

Appendix I - pXRF Results from ARTAX software

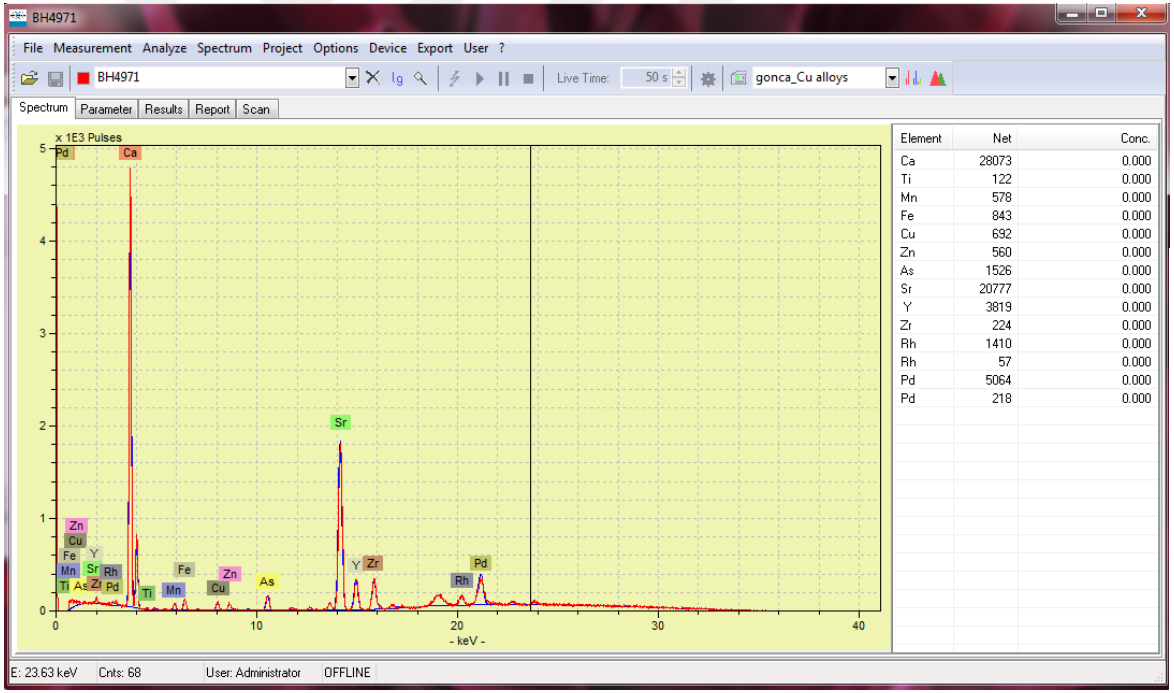

Element	Net	Conc.
Ca	28073	0.000
Ti	122	0.000
Mn	578	0.000
Fe	843	0.000
Cu	692	0.000
Zn	560	0.000
As	1526	0.000
Sr	20777	0.000
Y	3819	0.000
Zr	224	0.000
Rh	1410	0.000
Rh	57	0.000
Pd	5064	0.000
Pd	218	0.000

ARTAX - ELEMENT ANALYSIS

Listed at 11/8/2016 9:49:51 AM

Serial number:
Meas.date: 8/8/2016 9:31:42 AM
Live time: 181 s
Dead time: 0.0 %
Current: 40 µA
Filter: Ti/Al/Cu
Atmosphere: Air

Spectrum: BH4971
Method: gonca_Cu alloys (Bayes)
Count rate: 846 cps
Voltage: 40 kV
Anode:
Optic:

Element	Line	Sigma/	Net area	Backgr.
Ca	K12	0.00	28073	670
Ti	K12	0.00	122	212
Mn	K12	0.00	578	156
Fe	K12	0.00	843	147
Cu	K12	0.00	692	193
Zn	K12	0.00	560	198
As	K12	0.00	1526	175
Sr	K12	0.00	20777	419
Y	K12	0.00	3819	343
Zr	K12	0.00	224	433
Rh	K12	0.00	1410	1989
Rh	L1	0.00	57	895
Pd	K12	0.00	5064	2415
Pd	L1	0.00	218	860

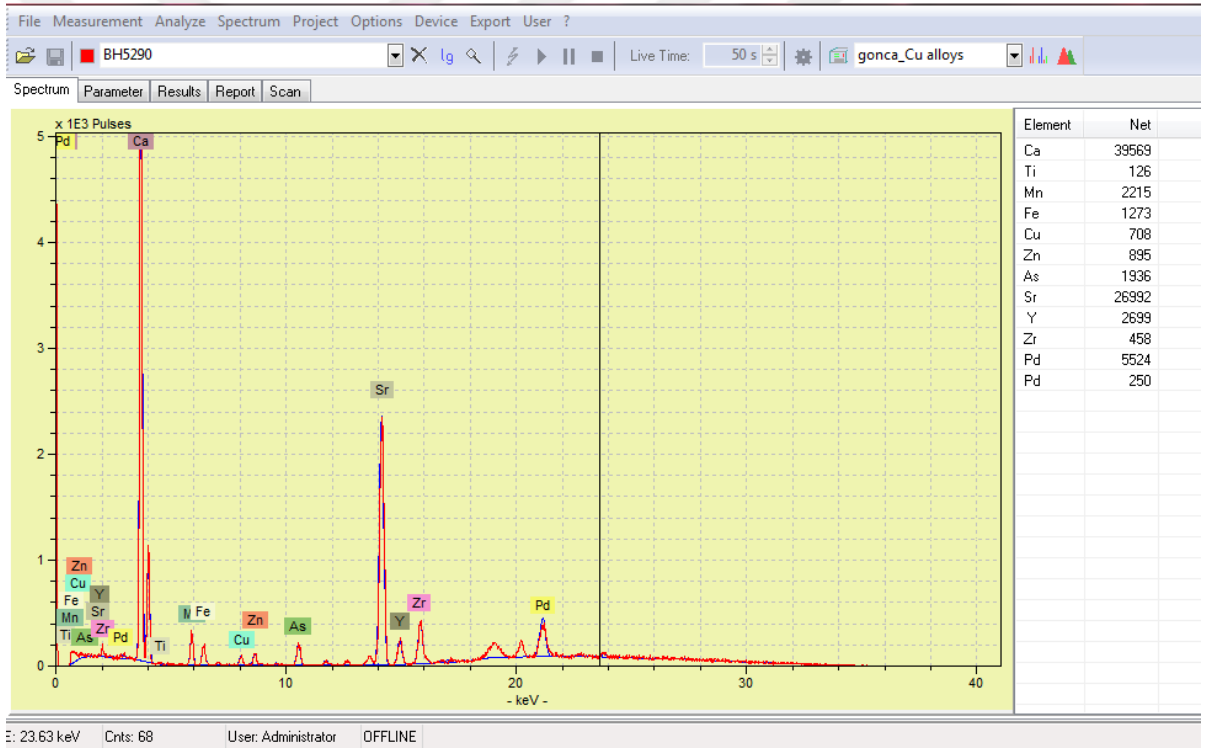

ARTAX - ELEMENT ANALYSIS

Listed at 11/8/2016 9:53:39 AM

Serial number:
Meas.date: 8/8/2016 10:17:20 AM
Live time: 182 s
Dead time: 0.0 %
Current: 40 µA
Filter: Ti/Al/Cu
Atmosphere: Vacuum

Spectrum: BH5290
Method: gonca_Cu alloys (Bayes)
Count rate: 1049 cps
Voltage: 40 kV
Anode:
Optic:

Element	Line	Sigma/	Net area	Backgr.
Ca	K12	0.00	39569	778
Ti	K12	0.00	126	259
Mn	K12	0.00	2215	202
Fe	K12	0.00	1273	202
Cu	K12	0.00	708	206
Zn	K12	0.00	895	231
As	K12	0.00	1936	170
Sr	K12	0.00	26992	399
Y	K12	0.00	2699	397
Zr	K12	0.00	458	619
Pd	K12	0.00	5524	3159
Pd	L1	0.00	250	1020

Element	Net	Conc.
Ca	22787	0.000
Mn	2049	0.000
Fe	1587	0.000
Cu	715	0.000
Zn	733	0.000
As	2122	0.000
Sr	24450	0.000
Y	256	0.000
Zr	335	0.000
Ba	139	0.000
Ba	3142	0.000

ARTAX - ELEMENT ANALYSIS

Listed at 11/8/2016 9:55:02 AM

Serial number:
Meas.date: 8/8/2016 10:25:58 AM
Live time: 181 s
Dead time: 0.0 %
Current: 40 µA
Filter: Ti/Al/Cu
Atmosphere: Air

Spectrum: BH5291
Method: gonca_Cu alloys (Bayes)
Count rate: 905 cps
Voltage: 40 kV
Anode:
Optic:

Element	Line	Sigma/	Net area	Backgr.
Ca	K12	0.00	22787	748
Mn	K12	0.00	2049	240
Fe	K12	0.00	1587	183
Cu	K12	0.00	715	171
Zn	K12	0.00	733	180
As	K12	0.00	2122	165
Sr	K12	0.00	24450	360
Y	K12	0.00	256	313
Zr	K12	0.00	335	448
Ba	K12	0.00	139	1232
Ba	L1	0.00	3142	364

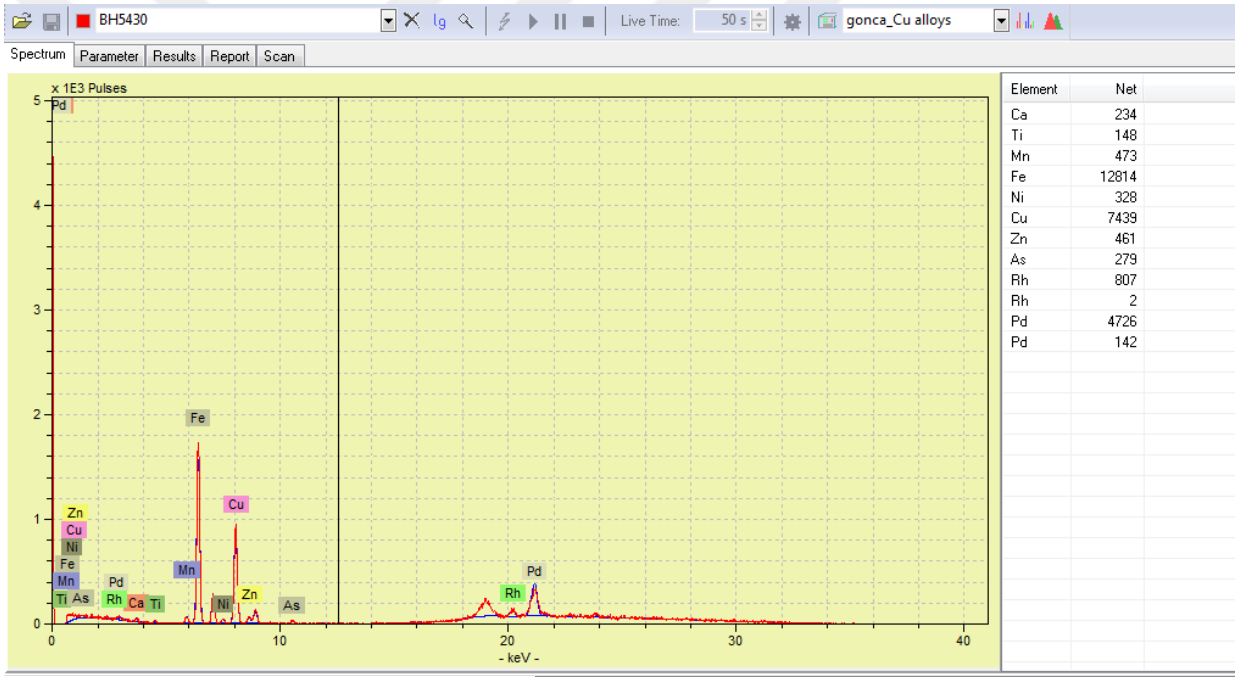

ARTAX - ELEMENT ANALYSIS

Listed at 11/8/2016 9:57:16 AM

Serial number:
Meas.date: 8/8/2016 9:51:39 AM
Live time: 181 s
Dead time: 0.0 %
Current: 40 µA
Filter: Ti/Al/Cu
Atmosphere: Air

Spectrum: BH5430
Method: gonca_Cu alloys (Bayes)
Count rate: 568 cps
Voltage: 40 kV
Anode:
Optic:

Element	Line	Sigma/	Net area	Backgr.
Ca	K12	0.00	234	310
Ti	K12	0.00	148	165
Mn	K12	0.00	473	147
Fe	K12	0.00	12814	169
Ni	K12	0.00	328	143
Cu	K12	0.00	7439	208
Zn	K12	0.00	461	219
As	K12	0.00	279	95
Rh	K12	0.00	807	2395
Rh	L1	0.00	2	651
Pd	K12	0.00	4726	2662
Pd	L1	0.00	142	608

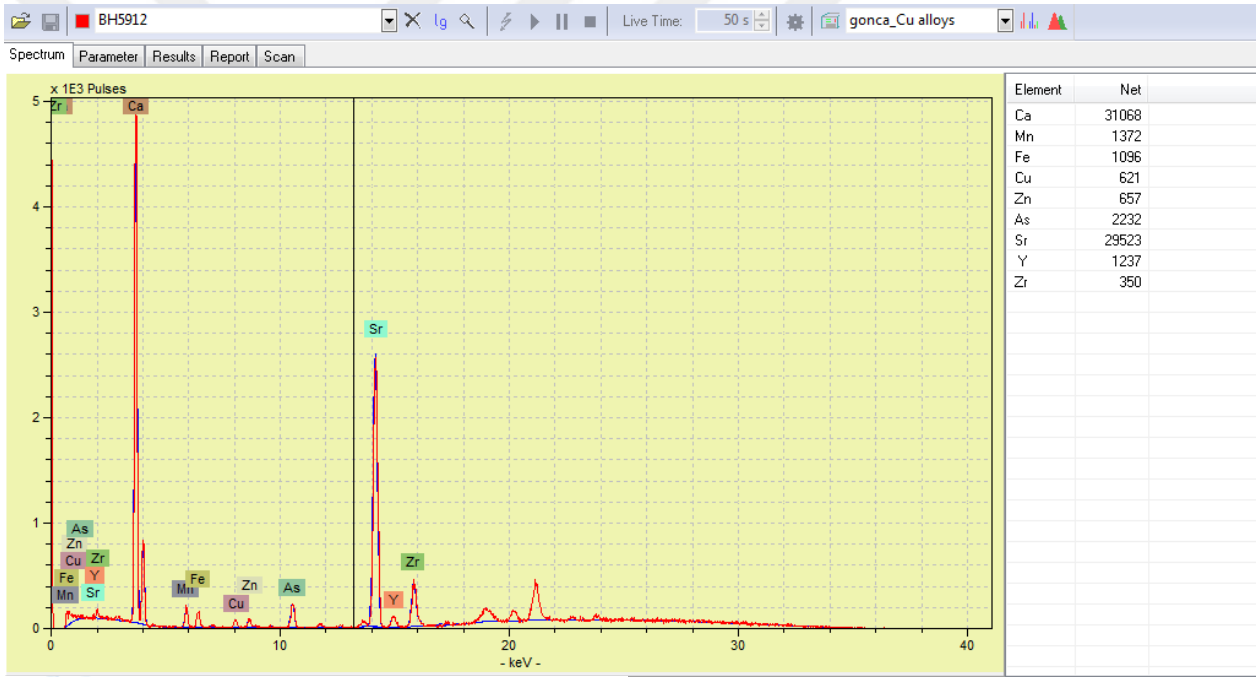

ARTAX - ELEMENT ANALYSIS

Listed at 11/8/2016 10:00:00 AM

Serial number:
Meas.date: 8/8/2016 9:18:57 AM
Live time: 180 s
Dead time: 0.0 %
Current: 40 µA
Filter: Ti/Al/Cu
Atmosphere: Air

Spectrum: BH5912
Method: gonca_Cu alloys (Bayes)
Count rate: 1002 cps
Voltage: 40 kV
Anode:
Optic:

Element	Line	Sigma/	Net area	Backgr.
Ca	K12	0.00	31068	845
Mn	K12	0.00	1372	207
Fe	K12	0.00	1096	181
Cu	K12	0.00	621	199
Zn	K12	0.00	657	202
As	K12	0.00	2232	188
Sr	K12	0.00	29523	448
Y	K12	0.00	1237	354
Zr	K12	0.00	350	479

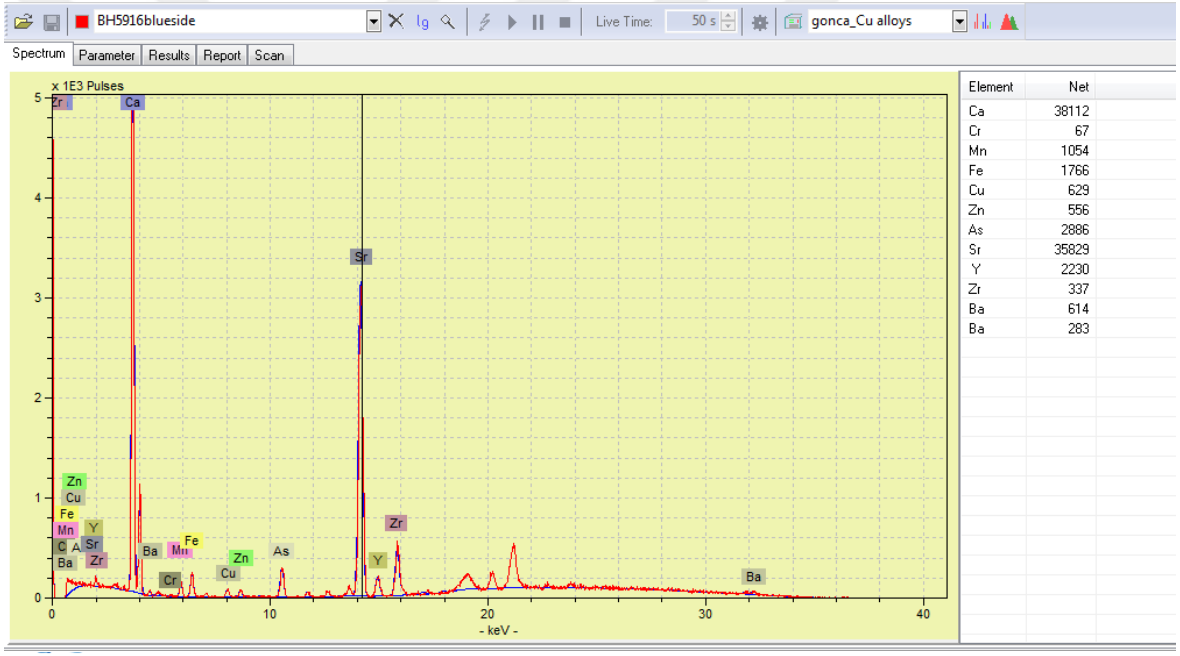

ARTAX - ELEMENT ANALYSIS

Listed at 11/8/2016 10:01:46 AM

Serial number:
Meas.date: 8/8/2016 9:06:53 AM
Live time: 180 s
Dead time: 0.0 %
Current: 40 µA
Filter: Ti/Al/Cu
Atmosphere: Air

Spectrum: BH5916blueside
Method: gonca_Cu alloys (Bayes)
Count rate: 1237 cps
Voltage: 40 kV
Anode:
Optic:

Element	Line	Sigma/	Net area	Backgr.
Ca	K12	0.00	38112	983
Cr	K12	0.00	67	260
Mn	K12	0.00	1054	241
Fe	K12	0.00	1766	233
Cu	K12	0.00	629	255
Zn	K12	0.00	556	255
As	K12	0.00	2886	244
Sr	K12	0.00	35829	541
Y	K12	0.00	2230	480
Zr	K12	0.00	337	693
Ba	K12	0.00	614	1912
Ba	L1	0.00	283	400

ARTAX - ELEMENT ANALYSIS

Listed at 11/8/2016 10:02:57 AM

Serial number:
Meas.date: 8/8/2016 9:02:45 AM
Live time: 180 s
Dead time: 0.0 %
Current: 40 µA
Filter: Ti/Al/Cu
Atmosphere: Air

Spectrum: BH5916whiteside
Method: gonca_Cu alloys (Bayes)
Count rate: 1276 cps
Voltage: 40 kV
Anode:
Optic:

Element	Line	Sigma/	Net area	Backgr.
Ca	K12	0.00	39207	918
Mn	K12	0.00	1146	272
Fe	K12	0.00	1936	221
Cu	K12	0.00	694	269
Zn	K12	0.00	603	276
As	K12	0.00	3069	243
Sr	K12	0.00	37550	573
Y	K12	0.00	2417	517
Zr	K12	0.00	367	679
Ba	K12	0.00	826	1842
Ba	L1	0.00	302	371

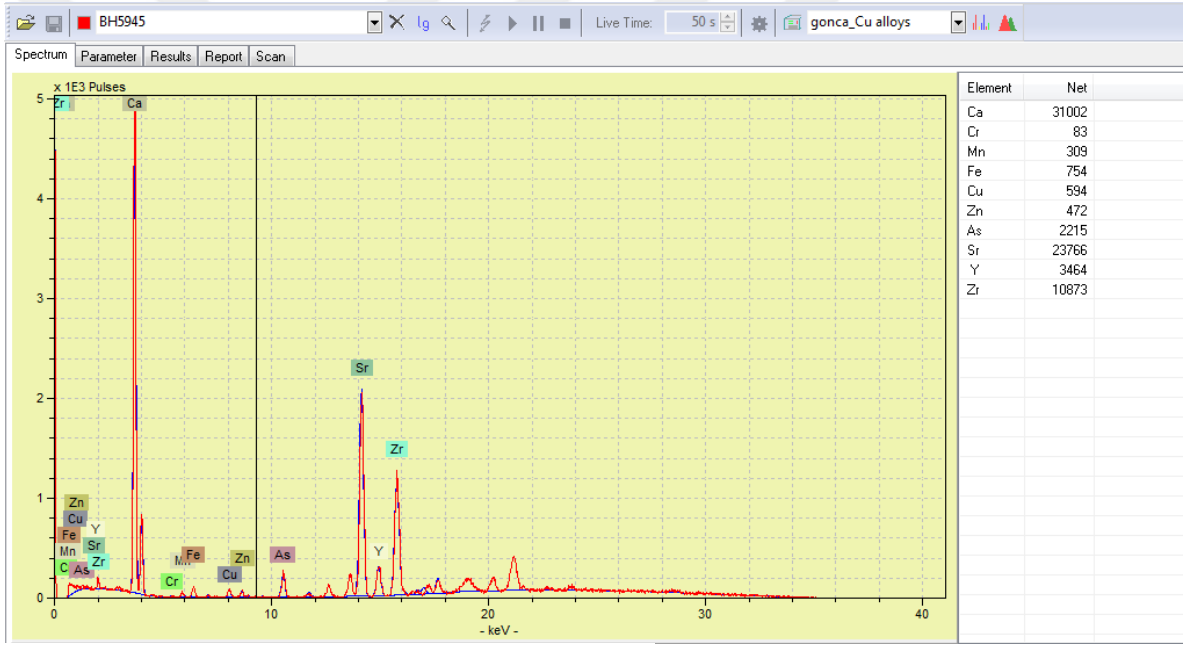

ARTAX - ELEMENT ANALYSIS

Listed at 11/8/2016 10:03:57 AM

Serial number:
Meas.date: 8/8/2016 9:22:40 AM
Live time: 180 s
Dead time: 0.0 %
Current: 40 µA
Filter: Ti/Al/Cu
Atmosphere: Air

Spectrum: BH5945
Method: gonca_Cu alloys (Bayes)
Count rate: 1055 cps
Voltage: 40 kV
Anode:
Optic:

Element	Line	Sigma/	Net area	Backgr.
Ca	K12	0.00	31002	801
Cr	K12	0.00	83	180
Mn	K12	0.00	309	174
Fe	K12	0.00	754	171
Cu	K12	0.00	594	234
Zn	K12	0.00	472	245
As	K12	0.00	2215	207
Sr	K12	0.00	23766	531
Y	K12	0.00	3464	572
Zr	K12	0.00	10873	829

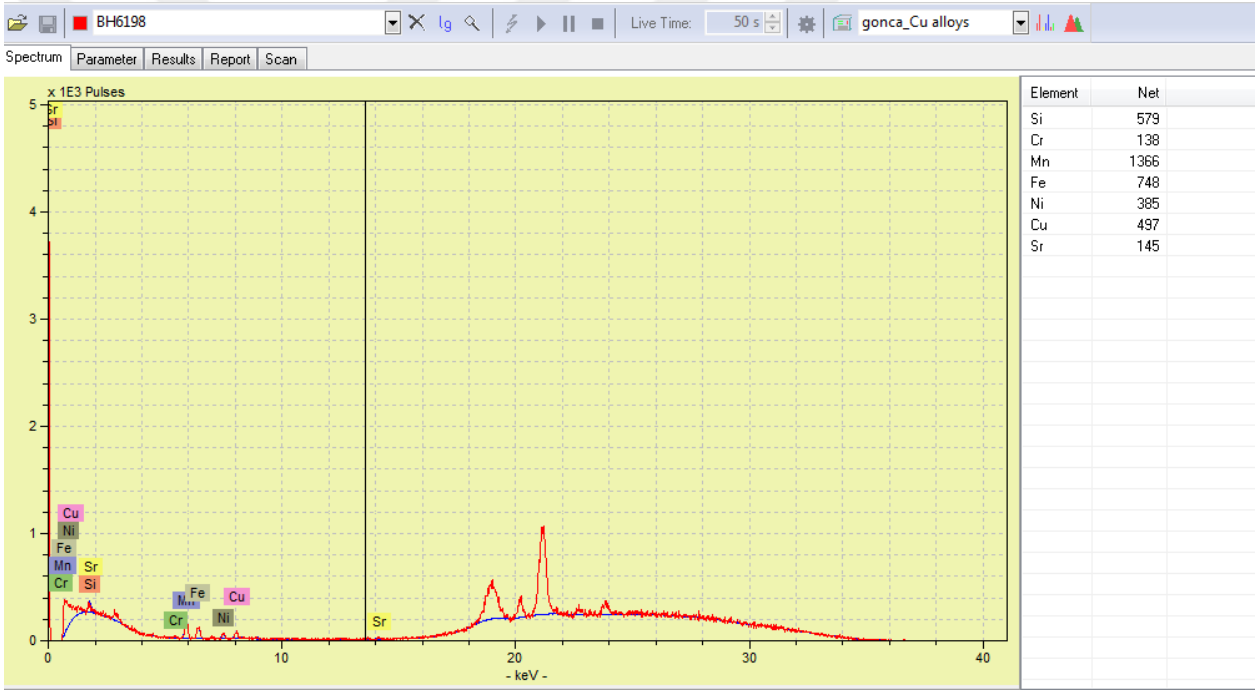

ARTAX - ELEMENT ANALYSIS

Listed at 11/8/2016 10:05:06 AM

Serial number:
Meas.date: 8/8/2016 11:34:17 AM
Live time: 153 s
Dead time: 0.0 %
Current: 40 µA
Filter: Ti/Al/Cu
Atmosphere: Air

Spectrum: BH6198
Method: gonca_Cu alloys (Bayes)
Count rate: 1672 cps
Voltage: 40 kV
Anode:
Optic:

Element	Line	Sigma/	Net area	Backgr.
Si	K12	0.00	579	3448
Cr	K12	0.00	138	412
Mn	K12	0.00	1366	376
Fe	K12	0.00	748	368
Ni	K12	0.00	385	369
Cu	K12	0.00	497	380
Sr	K12	0.00	145	362

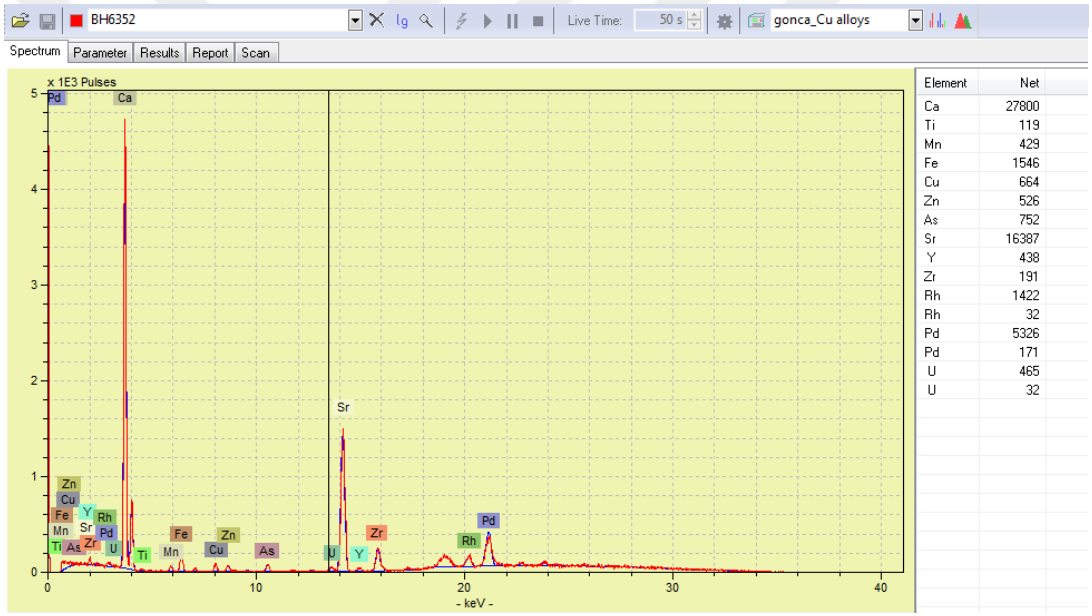

ARTAX - ELEMENT ANALYSIS

Listed at 11/8/2016 10:06:09 AM

Serial number:
Meas.date: 8/8/2016 9:35:57 AM
Live time: 181 s
Dead time: 0.0 %
Current: 40 µA
Filter: Ti/Al/Cu
Atmosphere: Air

Spectrum: BH6352
Method: gonca_Cu alloys (Bayes)
Count rate: 792 cps
Voltage: 40 kV
Anode:
Optic:

Element	Line	Sigma/	Net area	Backgr.
Ca	K12	0.00	27800	648
Ti	K12	0.00	119	210
Mn	K12	0.00	429	162
Fe	K12	0.00	1546	143
Cu	K12	0.00	664	157
Zn	K12	0.00	526	167
As	K12	0.00	752	128
Sr	K12	0.00	16387	319
Y	K12	0.00	438	278
Zr	K12	0.00	191	395
Rh	K12	0.00	1422	2001
Rh	L1	0.00	32	930
Pd	K12	0.00	5326	2306
Pd	L1	0.00	171	890
U	L1	0.00	465	268
U	M1	0.00	32	796

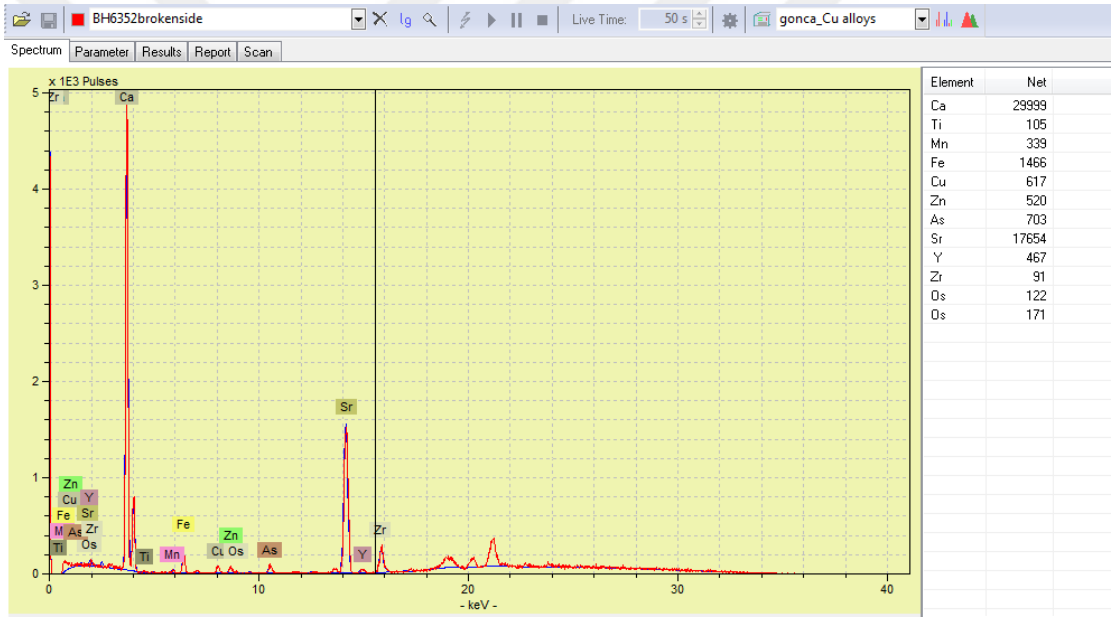

ARTAX - ELEMENT ANALYSIS

Listed at 11/8/2016 10:07:10 AM

Serial number:
Meas.date: 8/8/2016 9:39:58 AM
Live time: 181 s
Dead time: 0.0 %
Current: 40 µA
Filter: Ti/Al/Cu
Atmosphere: Air

Spectrum: BH6352brokenside
Method: gonca_Cu alloys (Bayes)
Count rate: 830 cps
Voltage: 40 kV
Anode:
Optic:

Element	Line	Sigma/	Net area	Backgr.
Ca	K12	0.00	29999	619
Ti	K12	0.00	105	230
Mn	K12	0.00	339	115
Fe	K12	0.00	1466	134
Cu	K12	0.00	617	166
Zn	K12	0.00	520	176
As	K12	0.00	703	168
Sr	K12	0.00	17654	305
Y	K12	0.00	467	272
Zr	K12	0.00	91	398
Os	L1	0.00	122	162
Os	M1	0.00	171	1087

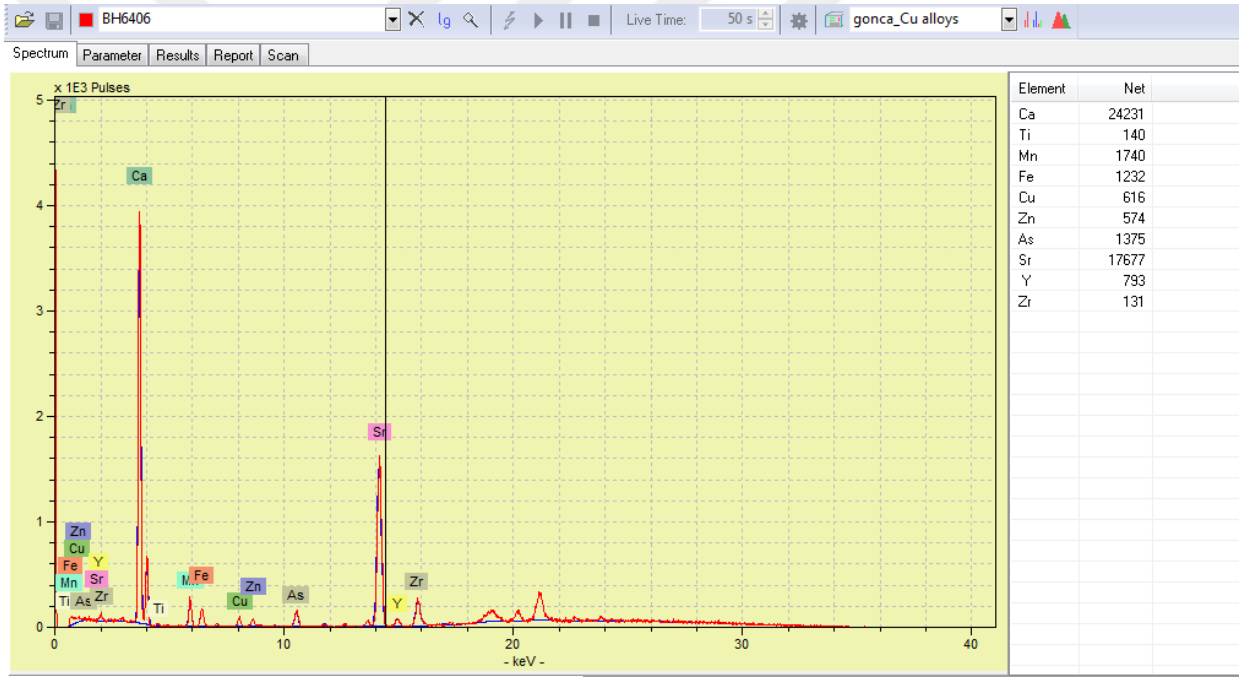

ARTAX - ELEMENT ANALYSIS

Listed at 11/8/2016 10:08:10 AM

Serial number:
Meas.date: 8/8/2016 10:21:43 AM
Live time: 181 s
Dead time: 0.0 %
Current: 40 µA
Filter: Ti/Al/Cu
Atmosphere: Air

Spectrum: BH6406
Method: gonca_Cu alloys (Bayes)
Count rate: 739 cps
Voltage: 40 kV
Anode:
Optic:

Element	Line	Sigma/	Net area	Backgr.
Ca	K12	0.00	24231	604
Ti	K12	0.00	140	189
Mn	K12	0.00	1740	148
Fe	K12	0.00	1232	126
Cu	K12	0.00	616	148
Zn	K12	0.00	574	149
As	K12	0.00	1375	130
Sr	K12	0.00	17677	299
Y	K12	0.00	793	277
Zr	K12	0.00	131	390

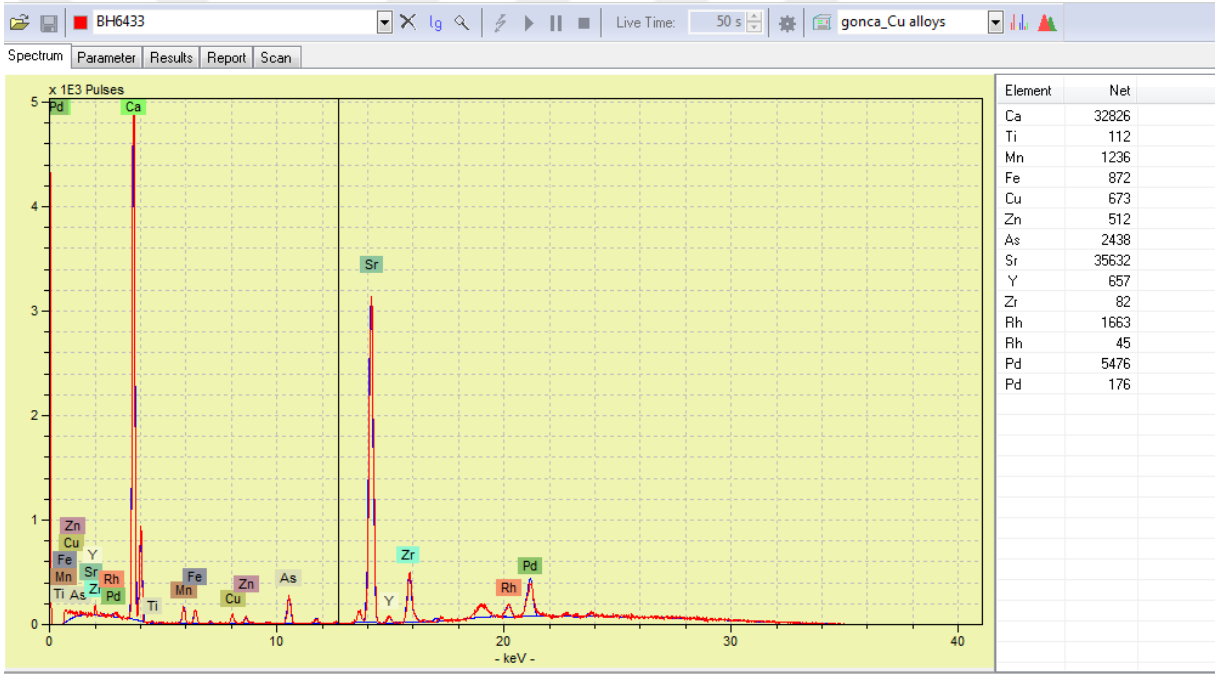

Element	Net
Ca	32826
Ti	112
Mn	1236
Fe	872
Cu	673
Zn	512
As	2438
Sr	35632
Y	657
Zr	82
Rh	1663
Rh	45
Pd	5476
Pd	176

ARTAX - ELEMENT ANALYSIS

Listed at 11/8/2016 10:09:07 AM

Serial number:
Meas.date: 8/8/2016 10:12:13 AM
Live time: 181 s
Dead time: 0.0 %
Current: 40 µA
Filter: Ti/Al/Cu
Atmosphere: Air

Spectrum: BH6433
Method: gonca_Cu alloys (Bayes)
Count rate: 1014 cps
Voltage: 40 kV
Anode:
Optic:

Element	Line	Sigma/	Net area	Backgr.
Ca	K12	0.00	32826	757
Ti	K12	0.00	112	227
Mn	K12	0.00	1236	212
Fe	K12	0.00	872	196
Cu	K12	0.00	673	183
Zn	K12	0.00	512	193
As	K12	0.00	2438	190
Sr	K12	0.00	35632	494
Y	K12	0.00	657	420
Zr	K12	0.00	82	572
Rh	K12	0.00	1663	2396
Rh	L1	0.00	45	1097
Pd	K12	0.00	5476	2759
Pd	L1	0.00	176	1054

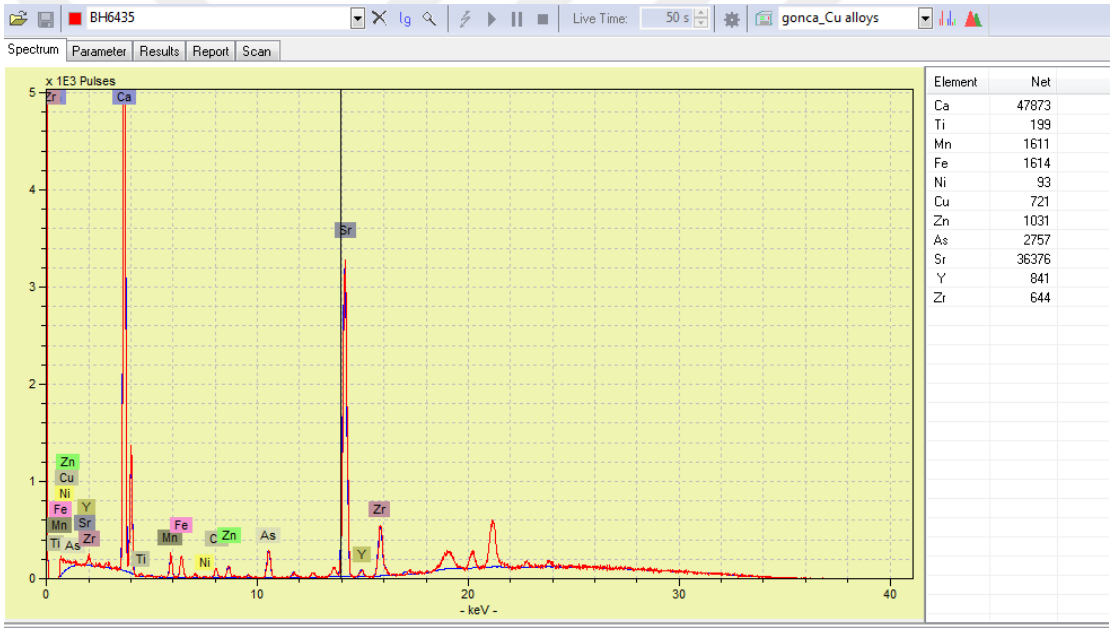

ARTAX - ELEMENT ANALYSIS

Listed at 11/8/2016 10:10:13 AM

Serial number:
Meas.date: 8/8/2016 8:40:01 AM
Live time: 197 s
Dead time: 0.0 %
Current: 40 µA
Filter: Ti/Al/Cu
Atmosphere: Air

Spectrum: BH6435
Method: gonca_Cu alloys (Bayes)
Count rate: 1289 cps
Voltage: 40 kV
Anode:
Optic:

Element	Line	Sigma/	Net area	Backgr.
Ca	K12	0.00	47873	1216
Ti	K12	0.00	199	384
Mn	K12	0.00	1611	254
Fe	K12	0.00	1614	249
Ni	K12	0.00	93	214
Cu	K12	0.00	721	275
Zn	K12	0.00	1031	311
As	K12	0.00	2757	281
Sr	K12	0.00	36376	561
Y	K12	0.00	841	475
Zr	K12	0.00	644	740

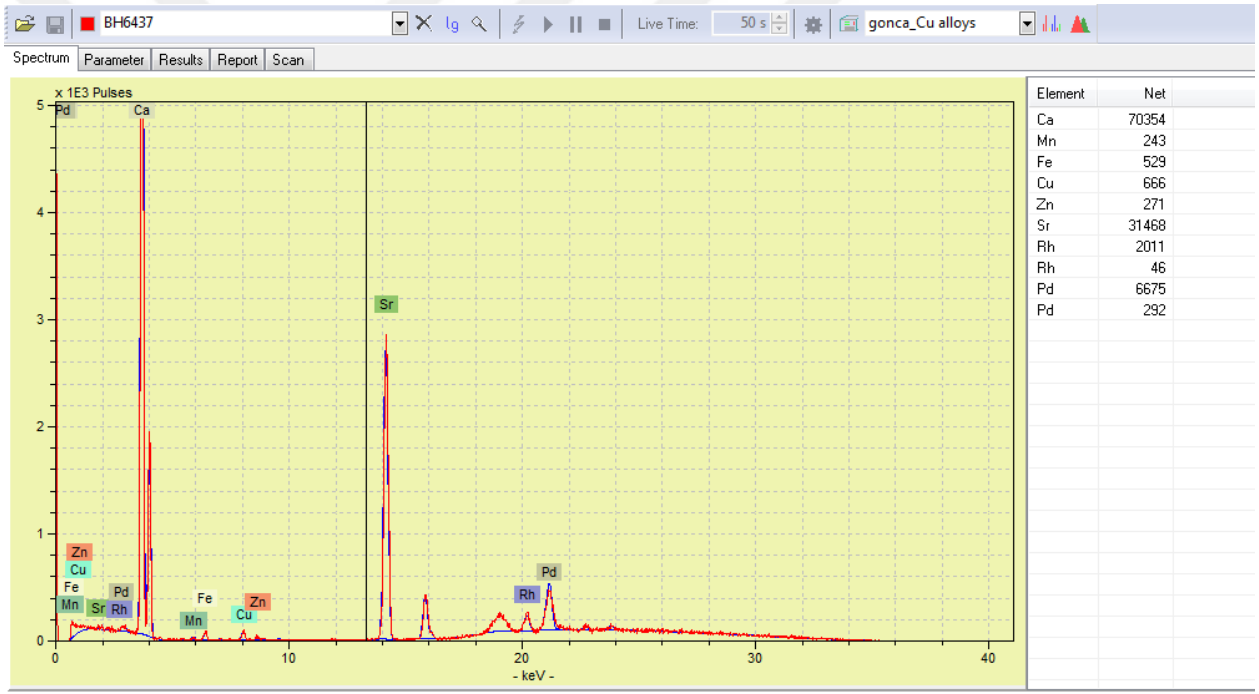

ARTAX - ELEMENT ANALYSIS

Listed at 11/8/2016 10:11:06 AM

Serial number:
Meas.date: 8/8/2016 9:44:08 AM
Live time: 181 s
Dead time: 0.0 %
Current: 40 µA
Filter: Ti/Al/Cu
Atmosphere: Air

Spectrum: BH6437
Method: gonca_Cu alloys (Bayes)
Count rate: 1305 cps
Voltage: 40 kV
Anode:
Optic:

Element	Line	Sigma/	Net area	Backgr.
Ca	K12	0.00	70354	983
Mn	K12	0.00	243	168
Fe	K12	0.00	529	154
Cu	K12	0.00	666	198
Zn	K12	0.00	271	189
Sr	K12	0.00	31468	450
Rh	K12	0.00	2011	3093
Rh	L1	0.00	46	1319
Pd	K12	0.00	6675	3510
Pd	L1	0.00	292	1284

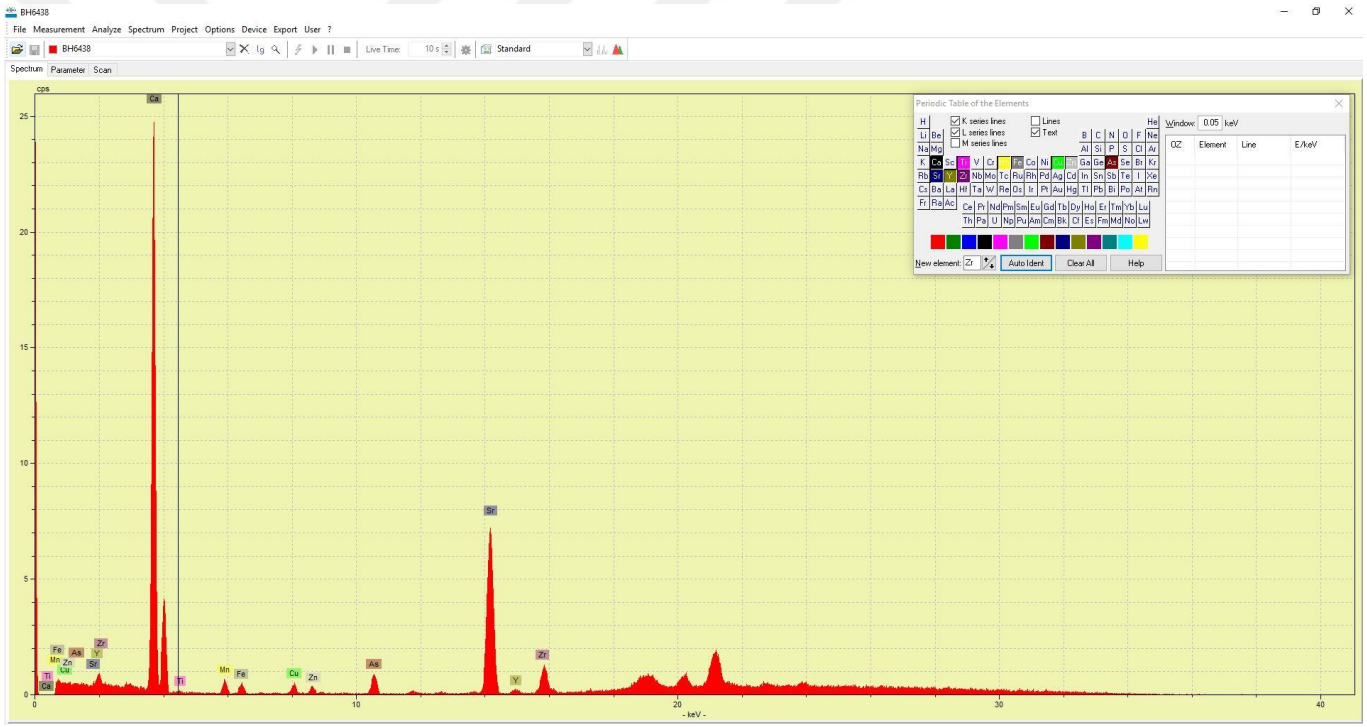

ARTAX - ELEMENT ANALYSIS

Listed at 11/8/2016 10:12:45 AM

Serial number:
Meas.date: 8/8/2016 10:07:21 AM
Live time: 181 s
Dead time: 0.0 %
Current: 40 µA
Filter: Ti/Al/Cu
Atmosphere: Air

Spectrum: BH6438
Method: gonca_Cu alloys (Bayes)
Count rate: 731 cps
Voltage: 40 kV
Anode:
Optic:

Element	Line	Sigma/	Net area	Backgr.
Ca	K12	0.00	27195	558
Ti	K12	0.00	124	187
Mn	K12	0.00	816	130
Fe	K12	0.00	522	111
Cu	K12	0.00	617	153
Zn	K12	0.00	412	173
As	K12	0.00	1425	139
Sr	K12	0.00	14582	270
Y	K12	0.00	317	267
Zr	K12	0.00	47	369

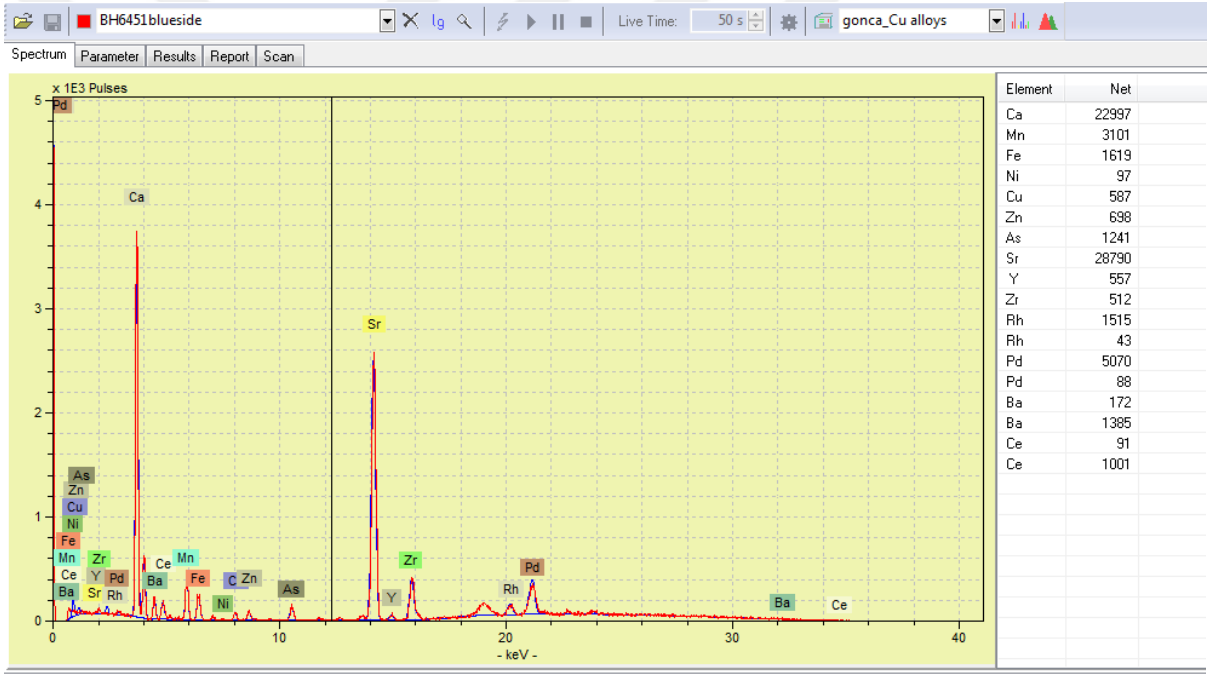

Element	Net
Ca	22997
Mn	3101
Fe	1619
Ni	97
Cu	587
Zn	698
As	1241
Sr	28790
Y	557
Zr	512
Rh	1515
Rh	43
Pd	5070
Pd	88
Ba	172
Ba	1385
Ce	91
Ce	1001

ARTAX - ELEMENT ANALYSIS

Listed at 11/8/2016 10:14:19 AM

Serial number:
Meas.date: 8/8/2016 9:11:20 AM
Live time: 180 s
Dead time: 0.0 %
Current: 40 µA
Filter: Ti/Al/Cu
Atmosphere: Air

Spectrum: BH6451blueside
Method: gonca_Cu alloys (Bayes)
Count rate: 862 cps
Voltage: 40 kV
Anode:
Optic:

Element	Line	Sigma/	Net area	Backgr.
Ca	K12	0.00	22997	600
Mn	K12	0.00	3101	213
Fe	K12	0.00	1619	168
Ni	K12	0.00	97	144
Cu	K12	0.00	587	174
Zn	K12	0.00	698	184
As	K12	0.00	1241	138
Sr	K12	0.00	28790	394
Y	K12	0.00	557	276
Zr	K12	0.00	512	387
Rh	K12	0.00	1515	1897
Rh	L1	0.00	43	880
Pd	K12	0.00	5070	2300
Pd	L1	0.00	88	845
Ba	K12	0.00	172	997
Ba	L1	0.00	1385	269
Ce	L1	0.00	91	269
Ce	M1	0.00	1001	464

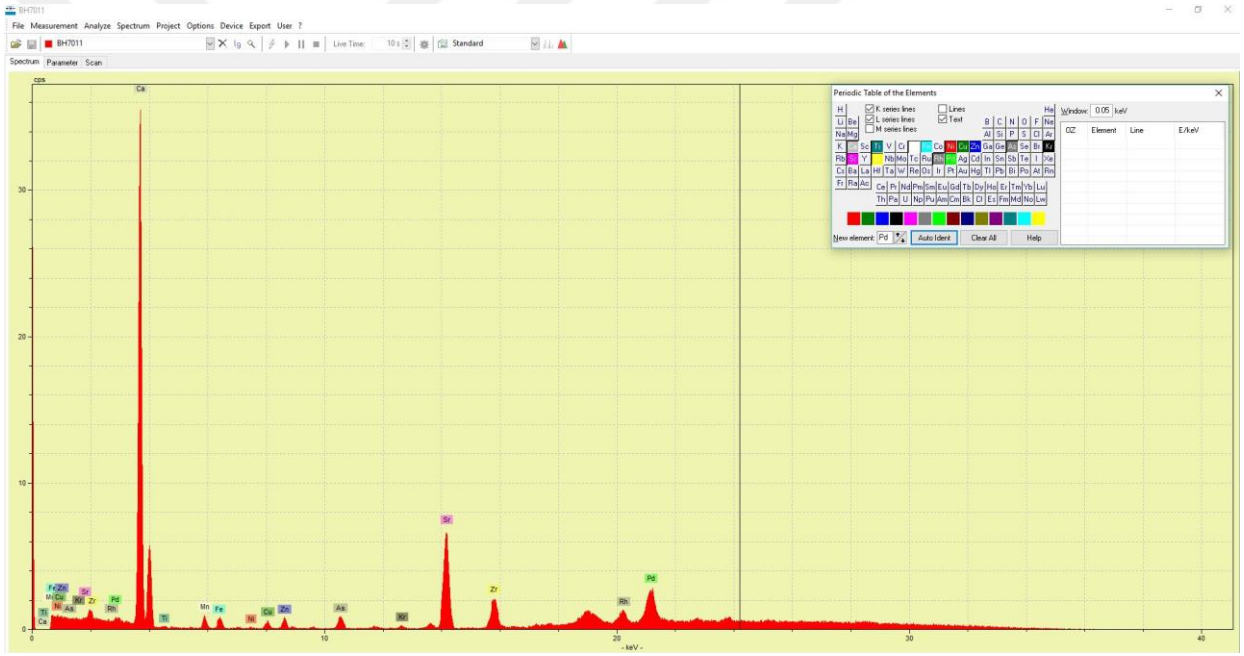

ARTAX - ELEMENT ANALYSIS

Listed at 11/8/2016 10:16:25 AM

Serial number:
Meas.date: 8/8/2016 8:55:12 AM
Live time: 182 s
Dead time: 0.0 %
Current: 40 µA
Filter: Ti/Al/Cu
Atmosphere: Air

Spectrum: BH7011
Method: gonca_Cu alloys (Bayes)
Count rate: 1045 cps
Voltage: 40 kV
Anode:
Optic:

Element	Line	Sigma/	Net area	Backgr.
Ca	K12	0.00	39146	958
Ti	K12	0.00	111	304
Mn	K12	0.00	1231	218
Fe	K12	0.00	928	214
Ni	K12	0.00	105	192
Cu	K12	0.00	716	206
Zn	K12	0.00	952	224
As	K12	0.00	1464	242
Sr	K12	0.00	13577	341
Zr	K12	0.00	2343	518
Rh	K12	0.00	2131	2730
Rh	L1	0.00	49	1398
Pd	K12	0.00	7058	3263
Pd	L1	0.00	239	1332

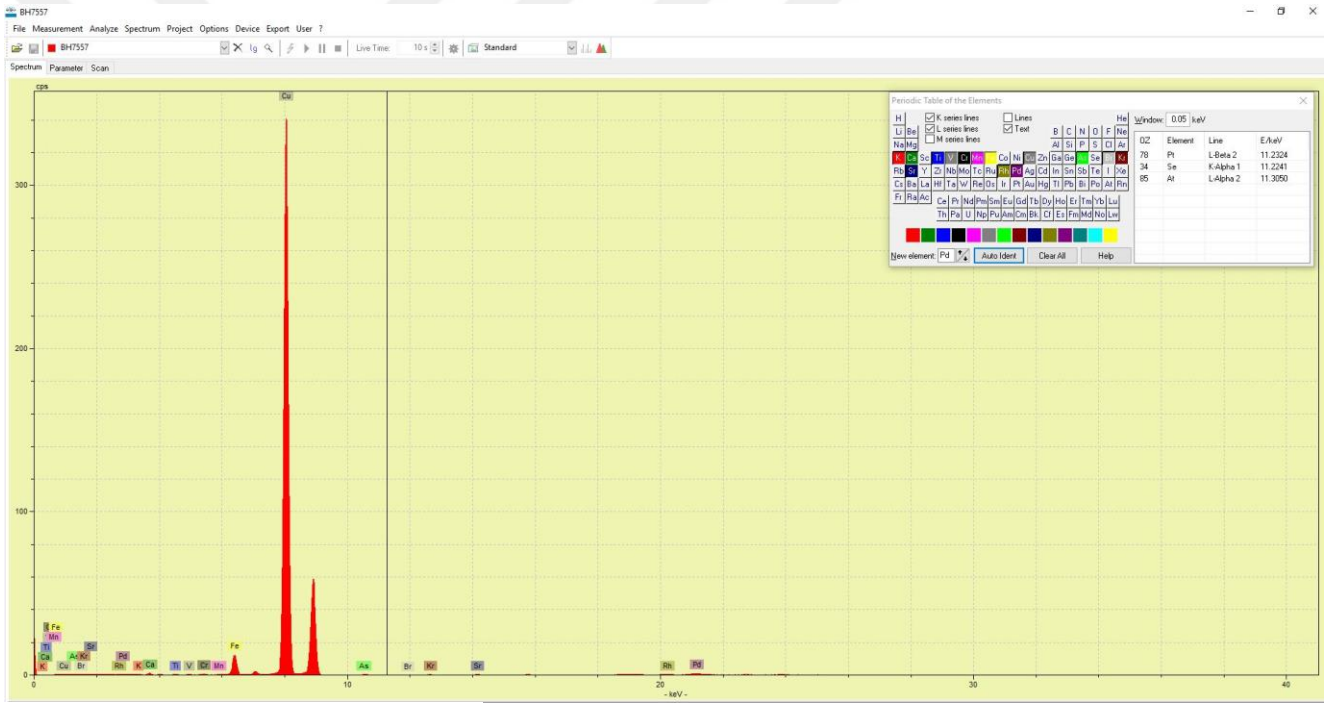

ARTAX - ELEMENT ANALYSIS

Listed at 11/8/2016 10:19:26 AM

Serial number:
Meas.date: 8/8/2016 10:40:32 AM
Live time: 239 s
Dead time: 0.0 %
Current: 40 µA
Filter: Ti/Al/Cu
Atmosphere: Air

Spectrum: BH7557
Method: gonca_Cu alloys (Bayes)
Count rate: 3831 cps
Voltage: 40 kV
Anode:
Optic:

Element	Line	Sigma/	Net area	Backgr.
K	K12	0.00	451	702
Ca	K12	0.00	1552	649
Ti	K12	0.00	442	528
V	K12	0.00	244	528
Cr	K12	0.00	669	680
Mn	K12	0.00	132	833
Fe	K12	0.00	21383	1152
Cu	K12	0.00	679713	3431
As	K12	0.00	851	96
Br	K12	0.00	218	85
Sr	K12	0.00	703	136
Rh	K12	0.00	925	1302
Rh	L1	0.00	17	832
Pd	K12	0.00	3711	1427
Pd	L1	0.00	340	816

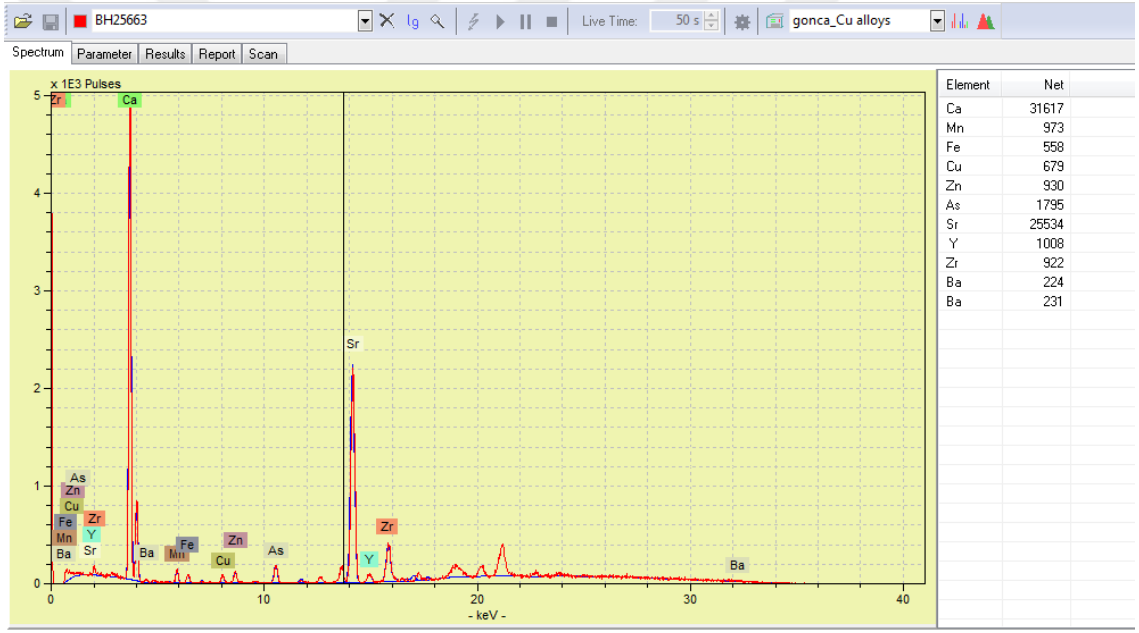

Element	Net
Ca	31617
Mn	973
Fe	558
Cu	679
Zn	930
As	1795
Sr	25534
Y	1008
Zr	922
Ba	224
Ba	231

ARTAX - ELEMENT ANALYSIS

Listed at 11/8/2016 10:21:20 AM

Serial number:
Meas.date: 8/8/2016 12:10:33 PM
Live time: 167 s
Dead time: 0.0 %
Current: 40 µA
Filter: Ti/Al/Cu
Atmosphere: Air

Spectrum: BH25663
Method: gonca_Cu alloys (Bayes)
Count rate: 1025 cps
Voltage: 40 kV
Anode:
Optic:

Element	Line	Sigma/	Net area	Backgr.
Ca	K12	0.00	31617	696
Mn	K12	0.00	973	193
Fe	K12	0.00	558	165
Cu	K12	0.00	679	173
Zn	K12	0.00	930	210
As	K12	0.00	1795	176
Sr	K12	0.00	25534	417
Y	K12	0.00	1008	391
Zr	K12	0.00	922	633
Ba	K12	0.00	224	1285
Ba	L1	0.00	231	225

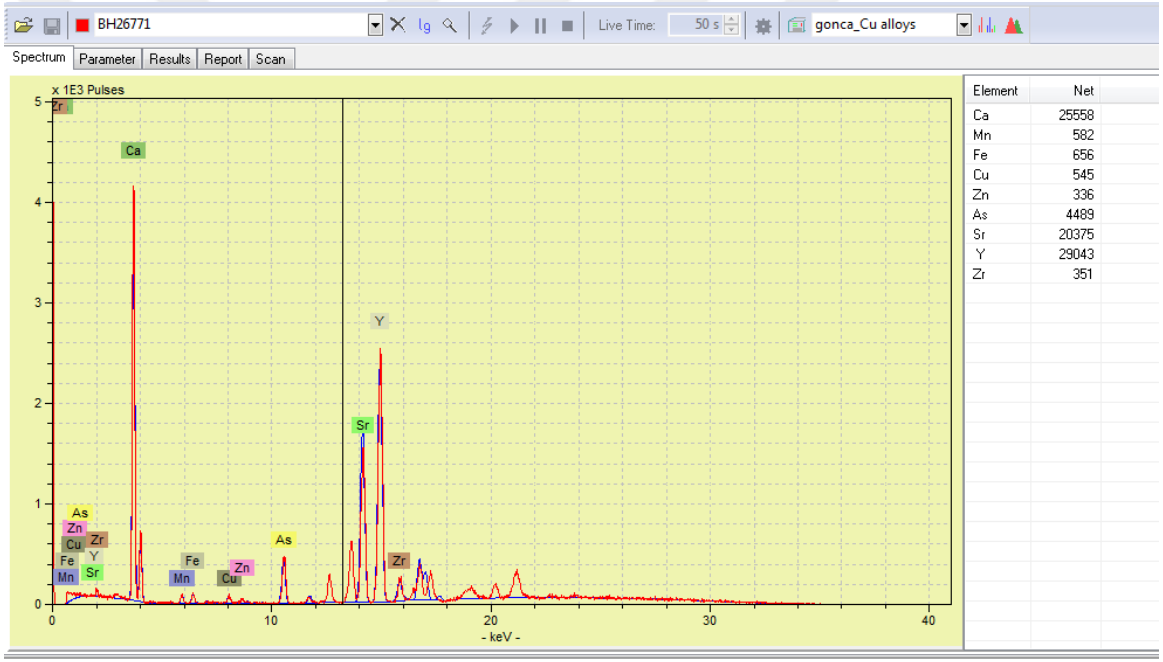

ARTAX - ELEMENT ANALYSIS

Listed at 11/8/2016 10:22:23 AM

Serial number:
Meas.date: 8/8/2016 2:17:23 PM
Live time: 181 s
Dead time: 0.0 %
Current: 40 µA
Filter: Ti/Al/Cu
Atmosphere: Air

Spectrum: BH26771
Method: gonca_Cu alloys (Bayes)
Count rate: 1070 cps
Voltage: 40 kV
Anode:
Optic:

Element	Line	Sigma/	Net area	Backgr.
Ca	K12	0.00	25558	574
Mn	K12	0.00	582	207
Fe	K12	0.00	656	234
Cu	K12	0.00	545	308
Zn	K12	0.00	336	304
As	K12	0.00	4489	218
Sr	K12	0.00	20375	620
Y	K12	0.00	29043	647
Zr	K12	0.00	351	863

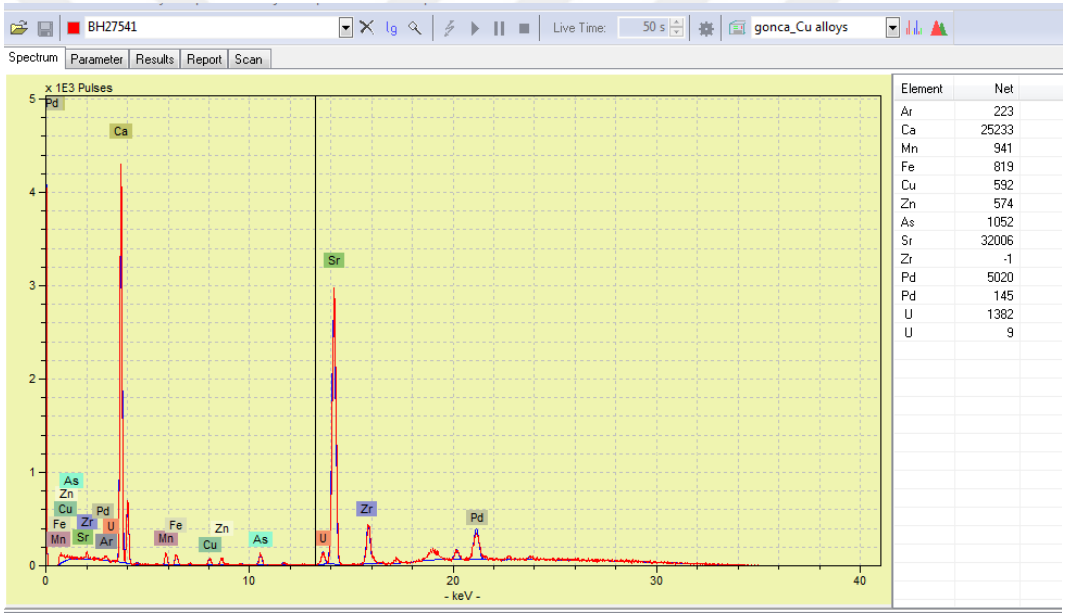

Element	Net
Ar	223
Ca	25233
Mn	941
Fe	819
Cu	592
Zn	574
As	1052
Sr	32006
Zr	-1
Pd	5020
Pd	145
U	1382
U	9

ARTAX - ELEMENT ANALYSIS

Listed at 11/8/2016 10:23:24 AM

Serial number:
Meas.date: 8/8/2016 12:30:17 PM
Live time: 182 s
Dead time: 0.0 %
Current: 40 µA
Filter: Ti/Al/Cu
Atmosphere: Air

Spectrum: BH27541
Method: gonca_Cu alloys (Bayes)
Count rate: 860 cps
Voltage: 40 kV
Anode:
Optic:

Element	Line	Sigma/	Net area	Backgr.
Ar	K12	0.00	223	789
Ca	K12	0.00	25233	571
Mn	K12	0.00	941	144
Fe	K12	0.00	819	145
Cu	K12	0.00	592	162
Zn	K12	0.00	574	164
As	K12	0.00	1052	163
Sr	K12	0.00	32006	463
Zr	K12	0.00		496
Pd	K12	0.00	5020	2348
Pd	L1	0.00	145	837
U	L1	0.00	1382	368
U	M1	0.00	9	704

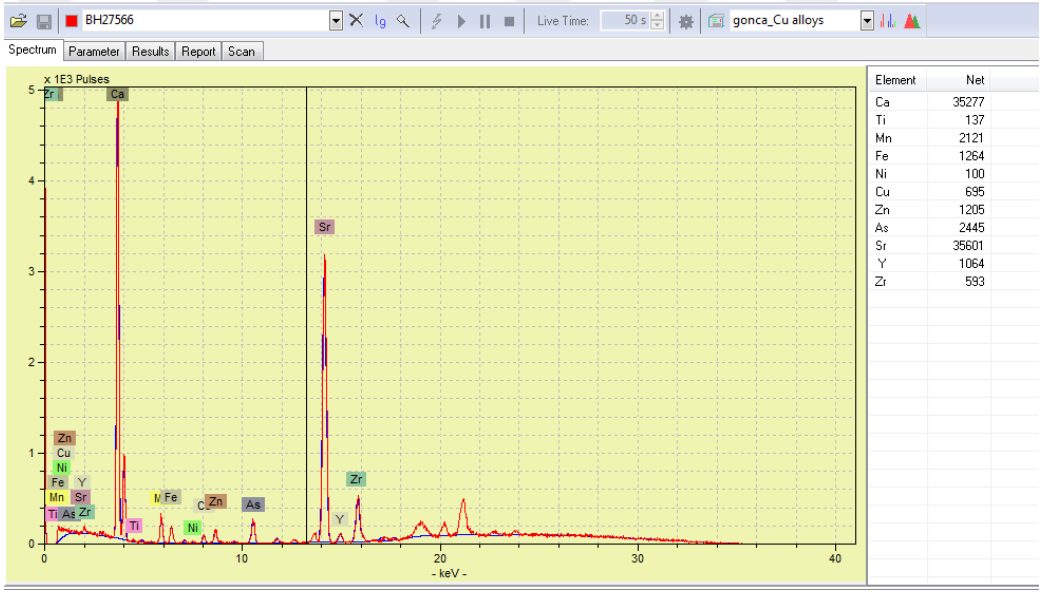

ARTAX - ELEMENT ANALYSIS

Listed at 11/8/2016 10:24:19 AM

Serial number:
Meas.date: 8/8/2016 12:34:25 PM
Live time: 181 s
Dead time: 0.0 %
Current: 40 µA
Filter: Ti/Al/Cu
Atmosphere: Air

Spectrum: BH27566
Method: gonca_Cu alloys (Bayes)
Count rate: 1189 cps
Voltage: 40 kV
Anode:
Optic:

Element	Line	Sigma/	Net area	Backgr.
Ca	K12	0.00	35277	972
Ti	K12	0.00	137	374
Mn	K12	0.00	2121	241
Fe	K12	0.00	1264	226
Ni	K12	0.00	100	210
Cu	K12	0.00	695	239
Zn	K12	0.00	1205	275
As	K12	0.00	2445	243
Sr	K12	0.00	35601	555
Y	K12	0.00	1064	492
Zr	K12	0.00	593	685

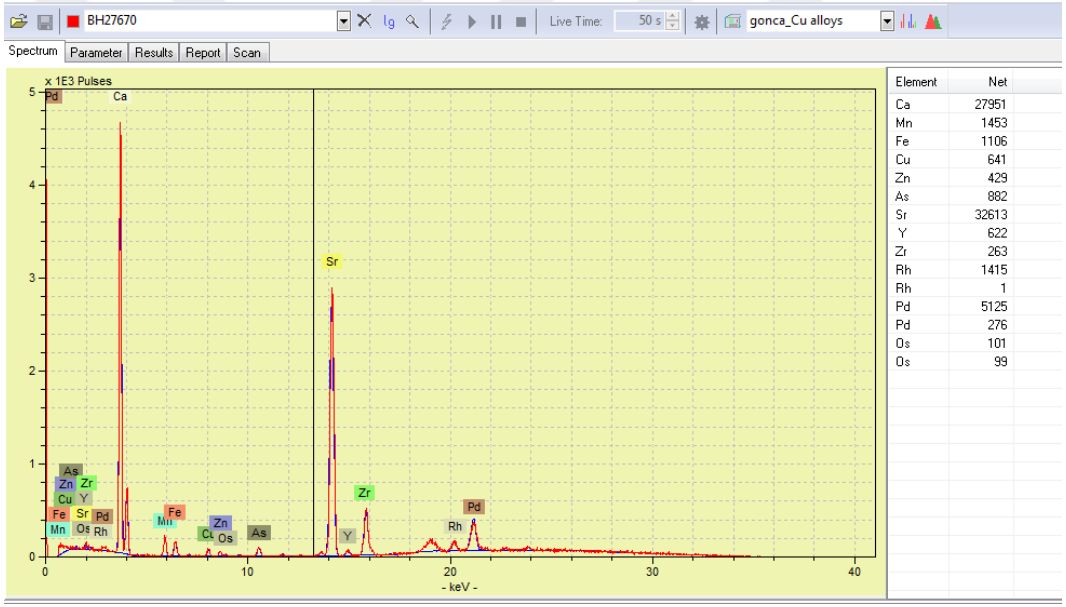

ARTAX - ELEMENT ANALYSIS

Listed at 11/8/2016 10:25:22 AM

Serial number:
Meas.date: 8/8/2016 12:25:59 PM
Live time: 182 s
Dead time: 0.0 %
Current: 40 µA
Filter: Ti/Al/Cu
Atmosphere: Air

Spectrum: BH27670
Method: gonca_Cu alloys (Bayes)
Count rate: 909 cps
Voltage: 40 kV
Anode:
Optic:

Element	Line	Sigma/	Net area	Backgr.
Ca	K12	0.00	27951	688
Mn	K12	0.00	1453	208
Fe	K12	0.00	1106	191
Cu	K12	0.00	641	164
Zn	K12	0.00	429	174
As	K12	0.00	882	169
Sr	K12	0.00	32613	413
Y	K12	0.00	622	369
Zr	K12	0.00	263	517
Rh	K12	0.00	1415	2100
Rh	L1	0.00	1	1004
Pd	K12	0.00	5125	2429
Pd	L1	0.00	276	959
Os	L1	0.00	101	158
Os	M1	0.00	99	1104

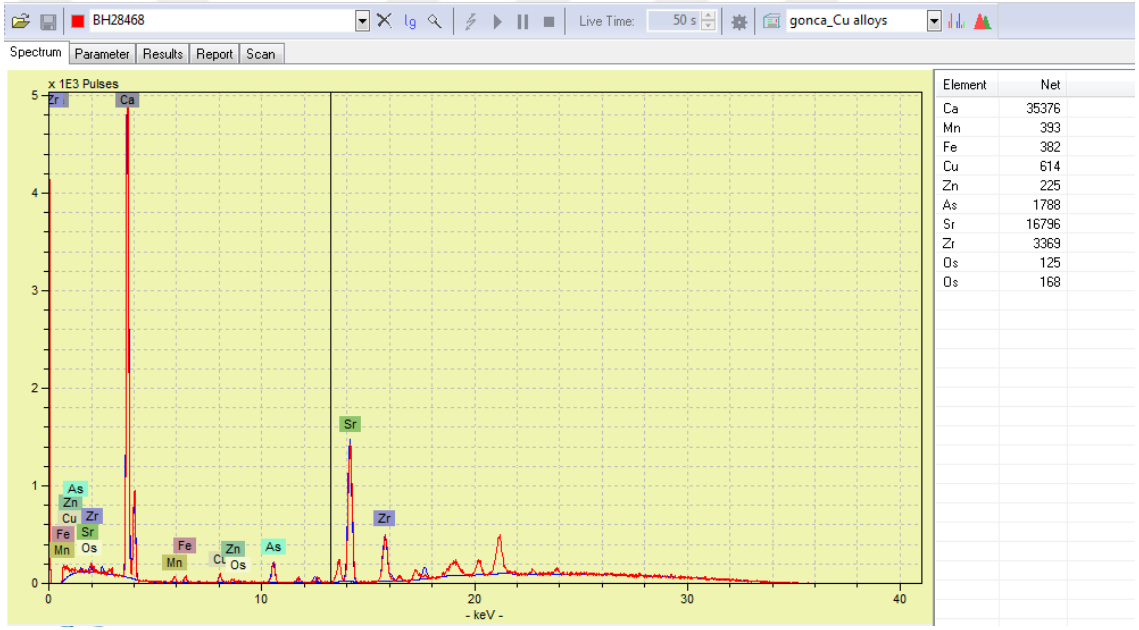

ARTAX - ELEMENT ANALYSIS

Listed at 11/8/2016 10:26:17 AM

Serial number:
Meas.date: 8/8/2016 12:06:24 PM
Live time: 181 s
Dead time: 0.0 %
Current: 40 µA
Filter: Ti/Al/Cu
Atmosphere: Air

Spectrum: BH28468
Method: gonca_Cu alloys (Bayes)
Count rate: 1042 cps
Voltage: 40 kV
Anode:
Optic:

Element	Line	Sigma/	Net area	Backgr.
Ca	K12	0.00	35376	934
Mn	K12	0.00	393	223
Fe	K12	0.00	382	220
Cu	K12	0.00	614	223
Zn	K12	0.00	225	253
As	K12	0.00	1788	225
Sr	K12	0.00	16796	455
Zr	K12	0.00	3369	604
Os	L1	0.00	125	237
Os	M1	0.00	168	1513

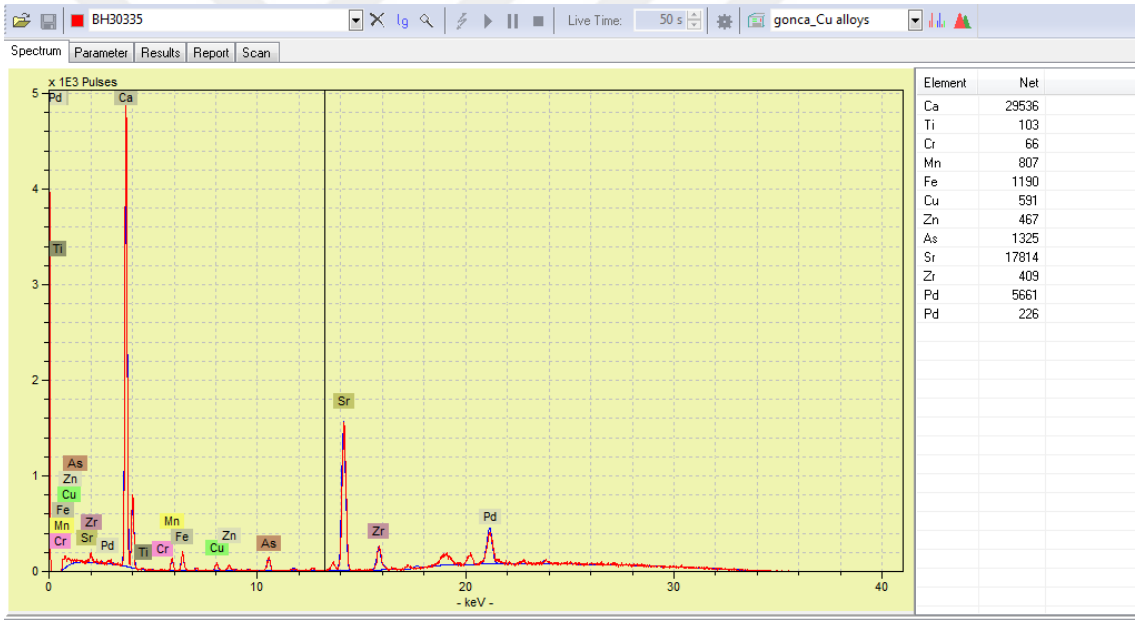

ARTAX - ELEMENT ANALYSIS

Listed at 11/8/2016 10:27:10 AM

Serial number:
Meas.date: 8/8/2016 2:22:08 PM
Live time: 180 s
Dead time: 0.0 %
Current: 40 µA
Filter: Ti/Al/Cu
Atmosphere: Air

Spectrum: BH30335
Method: gonca_Cu alloys (Bayes)
Count rate: 879 cps
Voltage: 40 kV
Anode:
Optic:

Element	Line	Sigma/	Net area	Backgr.
Ca	K12	0.00	29536	799
Ti	K12	0.00	103	273
Cr	K12	0.00	66	195
Mn	K12	0.00	807	191
Fe	K12	0.00	1190	198
Cu	K12	0.00	591	189
Zn	K12	0.00	467	207
As	K12	0.00	1325	154
Sr	K12	0.00	17814	337
Zr	K12	0.00	409	442
Pd	K12	0.00	5661	2841
Pd	L1	0.00	226	1108

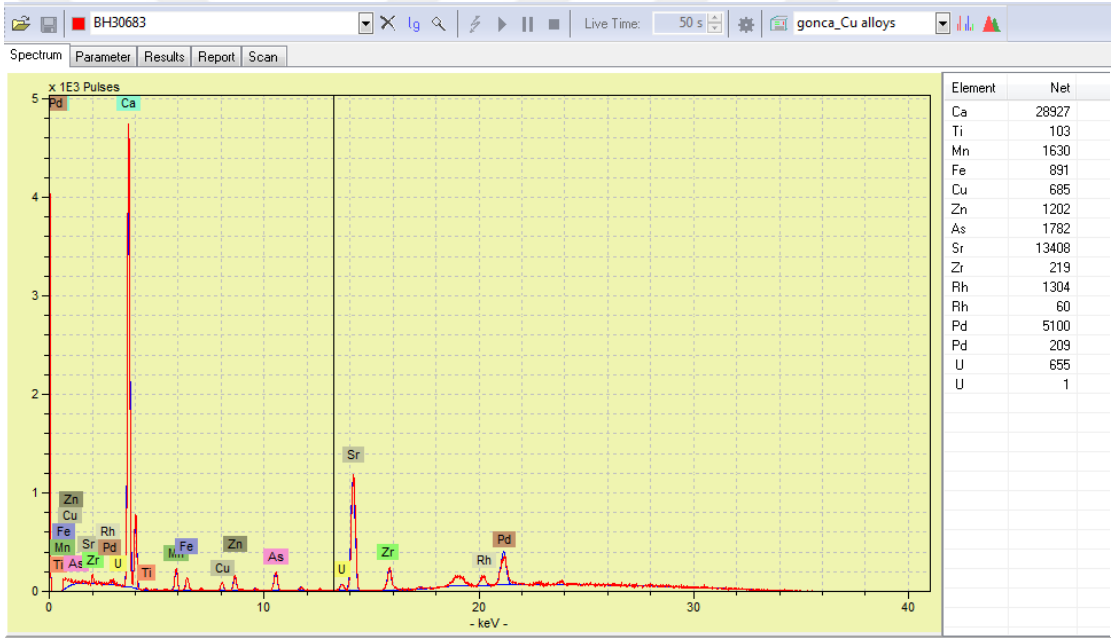

Element	Net
Ca	28927
Ti	103
Mn	1630
Fe	891
Cu	685
Zn	1202
As	1782
Sr	13408
Zr	219
Rh	1304
Rh	60
Pd	5100
Pd	209
U	655
U	1

ARTAX - ELEMENT ANALYSIS

Listed at 11/8/2016 10:27:56 AM

Serial number:
Meas.date: 8/8/2016 12:17:28 PM
Live time: 180 s
Dead time: 0.0 %
Current: 40 µA
Filter: Ti/Al/Cu
Atmosphere: Air

Spectrum: BH30683
Method: gonca_Cu alloys (Bayes)
Count rate: 796 cps
Voltage: 40 kV
Anode:
Optic:

Element	Line	Sigma/	Net area	Backgr.
Ca	K12	0.00	28927	696
Ti	K12	0.00	103	233
Mn	K12	0.00	1630	195
Fe	K12	0.00	891	185
Cu	K12	0.00	685	167
Zn	K12	0.00	1202	203
As	K12	0.00	1782	166
Sr	K12	0.00	13408	272
Zr	K12	0.00	219	372
Rh	K12	0.00	1304	1961
Rh	L1	0.00	60	1016
Pd	K12	0.00	5100	2302
Pd	L1	0.00	209	977
U	L1	0.00	655	223
U	M1	0.00	1	853

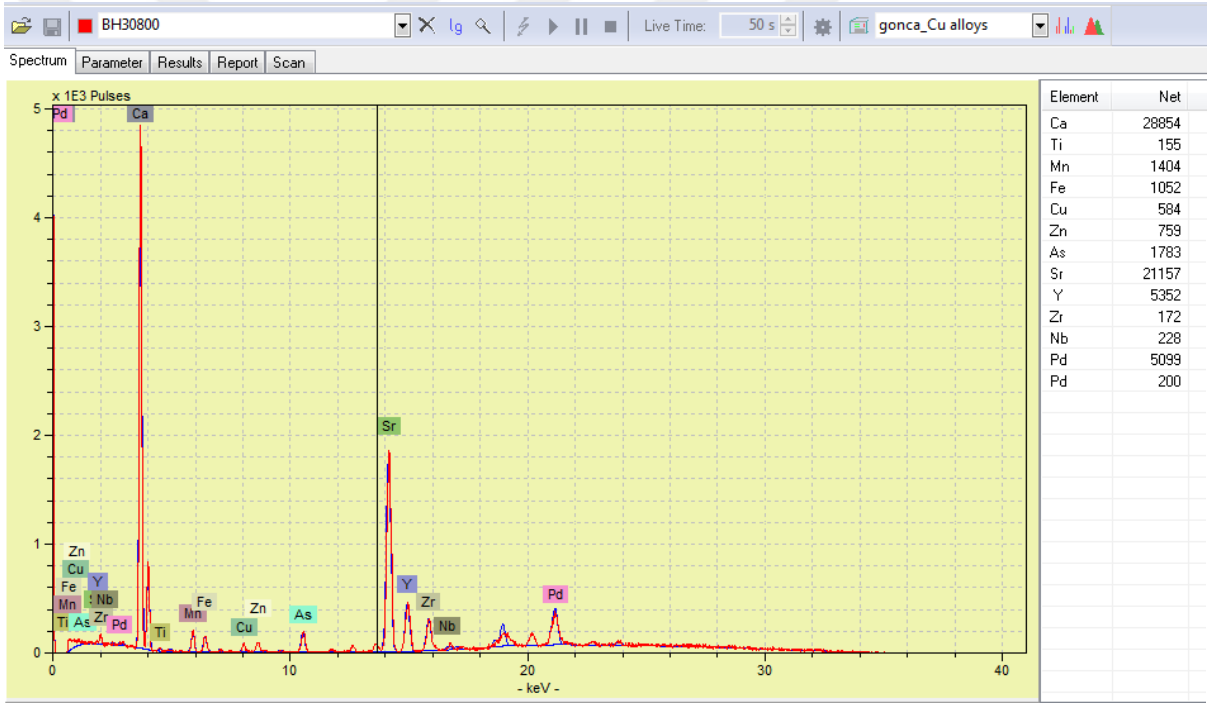

Element	Net
Ca	28854
Ti	155
Mn	1404
Fe	1052
Cu	584
Zn	759
As	1783
Sr	21157
Y	5352
Zr	172
Nb	228
Pd	5099
Pd	200

ARTAX - ELEMENT ANALYSIS

Listed at 11/8/2016 10:28:48 AM

Serial number:
Meas.date: 8/8/2016 12:47:33 PM
Live time: 181 s
Dead time: 0.0 %
Current: 40 µA
Filter: Ti/Al/Cu
Atmosphere: Air

Spectrum: BH30800
Method: gonca_Cu alloys (Bayes)
Count rate: 888 cps
Voltage: 40 kV
Anode:
Optic:

Element	Line	Sigma/	Net area	Backgr.
Ca	K12	0.00	28854	667
Ti	K12	0.00	155	261
Mn	K12	0.00	1404	192
Fe	K12	0.00	1052	172
Cu	K12	0.00	584	197
Zn	K12	0.00	759	252
As	K12	0.00	1783	180
Sr	K12	0.00	21157	383
Y	K12	0.00	5352	355
Zr	K12	0.00	172	552
Nb	K12	0.00	228	784
Pd	K12	0.00	5099	2558
Pd	L1	0.00	200	968

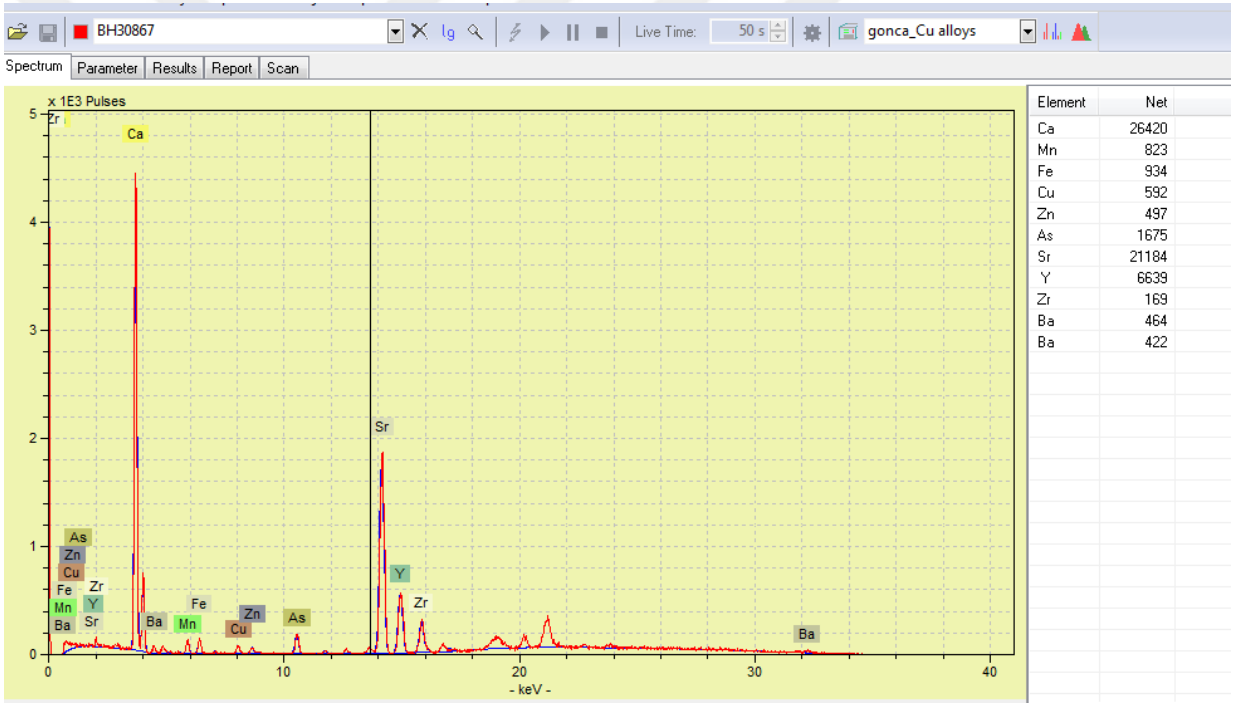

Element	Net
Ca	26420
Mn	823
Fe	934
Cu	592
Zn	497
As	1675
Sr	21184
Y	6639
Zr	169
Ba	464
Ba	422

ARTAX - ELEMENT ANALYSIS

Listed at 11/8/2016 10:30:04 AM

Serial number:
Meas.date: 8/8/2016 2:30:45 PM
Live time: 181 s
Dead time: 0.0 %
Current: 40 µA
Filter: Ti/Al/Cu
Atmosphere: Air

Spectrum: BH30867
Method: gonca_Cu alloys (Bayes)
Count rate: 831 cps
Voltage: 40 kV
Anode:
Optic:

Element	Line	Sigma/	Net area	Backgr.
Ca	K12	0.00	26420	616
Mn	K12	0.00	823	205
Fe	K12	0.00	934	177
Cu	K12	0.00	592	188
Zn	K12	0.00	497	195
As	K12	0.00	1675	170
Sr	K12	0.00	21184	396
Y	K12	0.00	6639	359
Zr	K12	0.00	169	495
Ba	K12	0.00	464	909
Ba	L1	0.00	422	248

ARTAX - ELEMENT ANALYSIS

Listed at 11/8/2016 10:31:15 AM

Serial number:
Meas.date: 8/8/2016 12:51:52 PM
Live time: 180 s
Dead time: 0.0 %
Current: 40 µA
Filter: Ti/Al/Cu
Atmosphere: Air

Spectrum: BH30872
Method: gonca_Cu alloys (Bayes)
Count rate: 1074 cps
Voltage: 40 kV
Anode:
Optic:

Element	Line	Sigma/	Net area	Backgr.
Ca	K12	0.00	37284	888
Mn	K12	0.00	269	194
Fe	K12	0.00	512	200
Cu	K12	0.00	629	222
Zn	K12	0.00	300	256
As	K12	0.00	2921	210
Sr	K12	0.00	24765	548
Y	K12	0.00	5039	515
Zr	K12	0.00	820	837
Rh	K12	0.00	1972	2742
Rh	L1	0.00	50	1208
Pd	K12	0.00	5909	3151
Pd	L1	0.00	245	1153

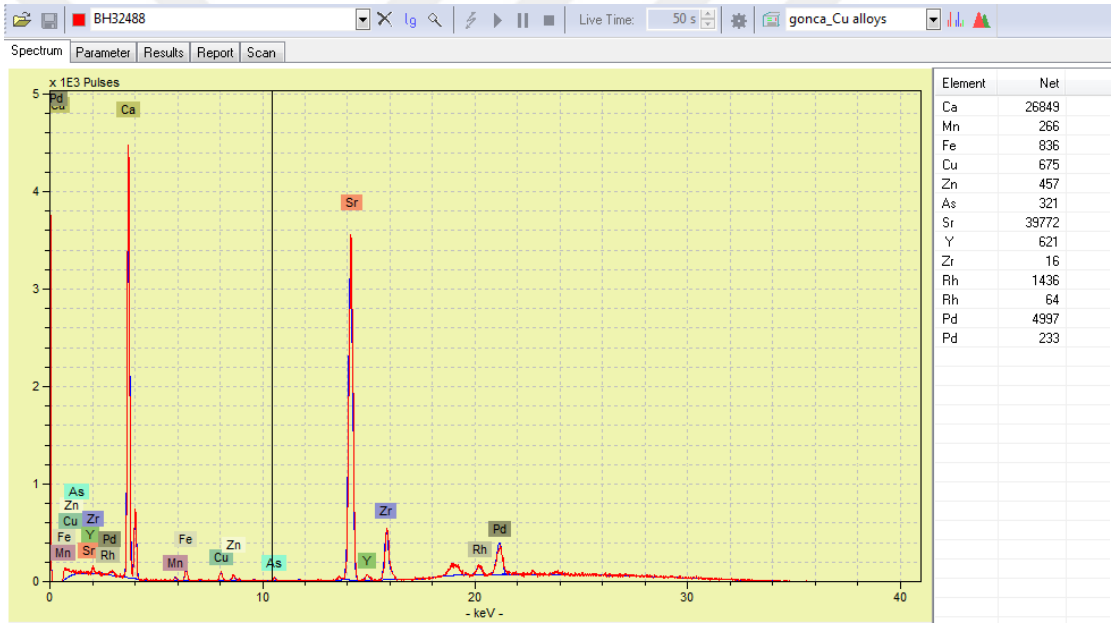

Element	Net
Ca	26849
Mn	266
Fe	836
Cu	675
Zn	457
As	321
Sr	39772
Y	621
Zr	16
Rh	1436
Rh	64
Pd	4997
Pd	233

ARTAX - ELEMENT ANALYSIS

Listed at 11/8/2016 10:32:25 AM

Serial number:
Meas.date: 8/8/2016 3:04:39 PM
Live time: 181 s
Dead time: 0.0 %
Current: 40 µA
Filter: Ti/Al/Cu
Atmosphere: Air

Spectrum: BH32488
Method: gonca_Cu alloys (Bayes)
Count rate: 927 cps
Voltage: 40 kV
Anode:
Optic:

Element	Line	Sigma/	Net area	Backgr.
Ca	K12	0.00	26849	562
Mn	K12	0.00	266	165
Fe	K12	0.00	836	155
Cu	K12	0.00	675	213
Zn	K12	0.00	457	202
As	K12	0.00	321	136
Sr	K12	0.00	39772	426
Y	K12	0.00	621	361
Zr	K12	0.00	16	476
Rh	K12	0.00	1436	2160
Rh	L1	0.00	64	969
Pd	K12	0.00	4997	2446
Pd	L1	0.00	233	919

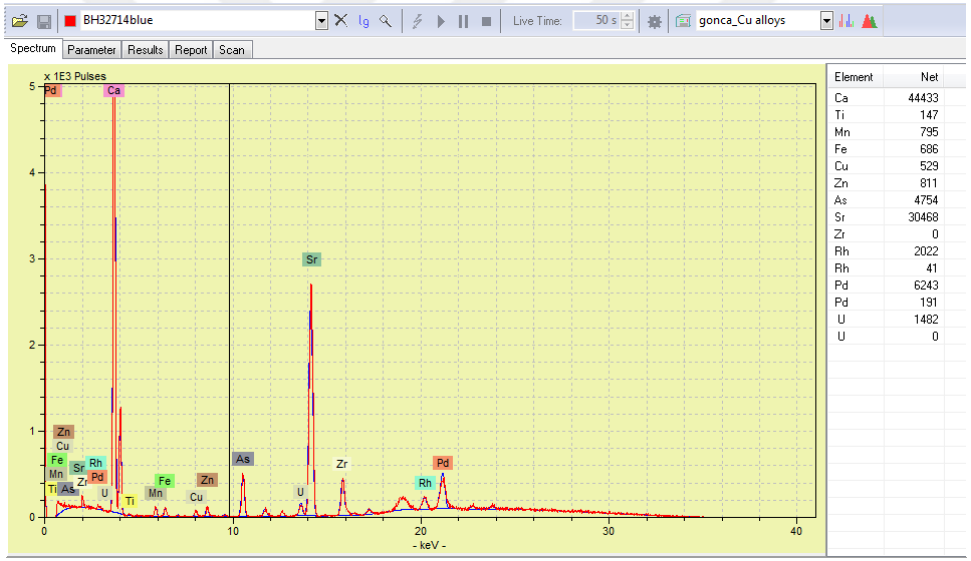

ARTAX - ELEMENT ANALYSIS

Listed at 11/8/2016 10:33:50 AM

Serial number:
Meas.date: 8/8/2016 2:51:55 PM
Live time: 181 s
Dead time: 0.0 %
Current: 40 µA
Filter: Ti/Al/Cu
Atmosphere: Air

Spectrum: BH32714blue
Method: gonca_Cu alloys (Bayes)
Count rate: 1180 cps
Voltage: 40 kV
Anode:
Optic:

Element	Line	Sigma/	Net area	Backgr.
Ca	K12	0.00	44433	858
Ti	K12	0.00	147	308
Mn	K12	0.00	795	223
Fe	K12	0.00	686	206
Cu	K12	0.00	529	260
Zn	K12	0.00	811	256
As	K12	0.00	4754	212
Sr	K12	0.00	30468	527
Zr	K12	0.00		646
Rh	K12	0.00	2022	3031
Rh	L1	0.00	41	1408
Pd	K12	0.00	6243	3438
Pd	L1	0.00	191	1338
U	L1	0.00	1482	460
U	M1	0.00		1132

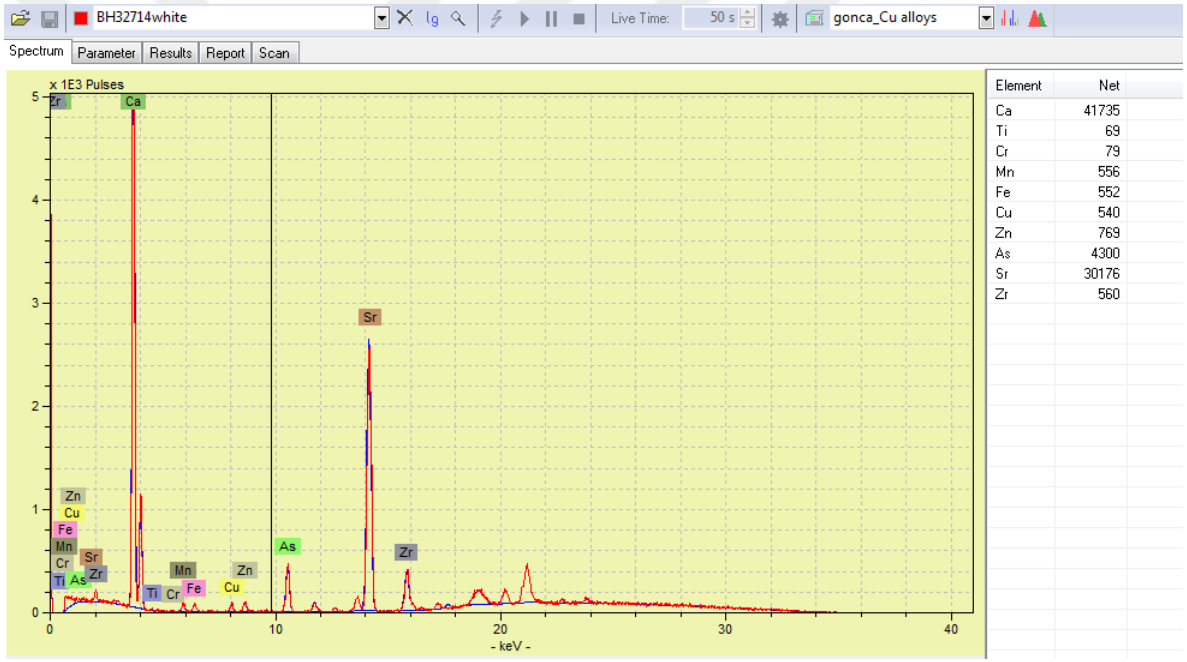

Element	Net
Ca	41735
Ti	69
Cr	79
Mn	556
Fe	552
Cu	540
Zn	769
As	4300
Sr	30176
Zr	560

ARTAX - ELEMENT ANALYSIS

Listed at 11/8/2016 10:35:00 AM

Serial number:
Meas.date: 8/8/2016 2:47:58 PM
Live time: 180 s
Dead time: 0.0 %
Current: 40 µA
Filter: Ti/Al/Cu
Atmosphere: Air

Spectrum: BH32714white
Method: gonca_Cu alloys (Bayes)
Count rate: 1131 cps
Voltage: 40 kV
Anode:
Optic:

Element	Line	Sigma/	Net area	Backgr.
Ca	K12	0.00	41735	804
Ti	K12	0.00	69	337
Cr	K12	0.00	79	233
Mn	K12	0.00	556	210
Fe	K12	0.00	552	200
Cu	K12	0.00	540	239
Zn	K12	0.00	769	240
As	K12	0.00	4300	222
Sr	K12	0.00	30176	501
Zr	K12	0.00	560	591

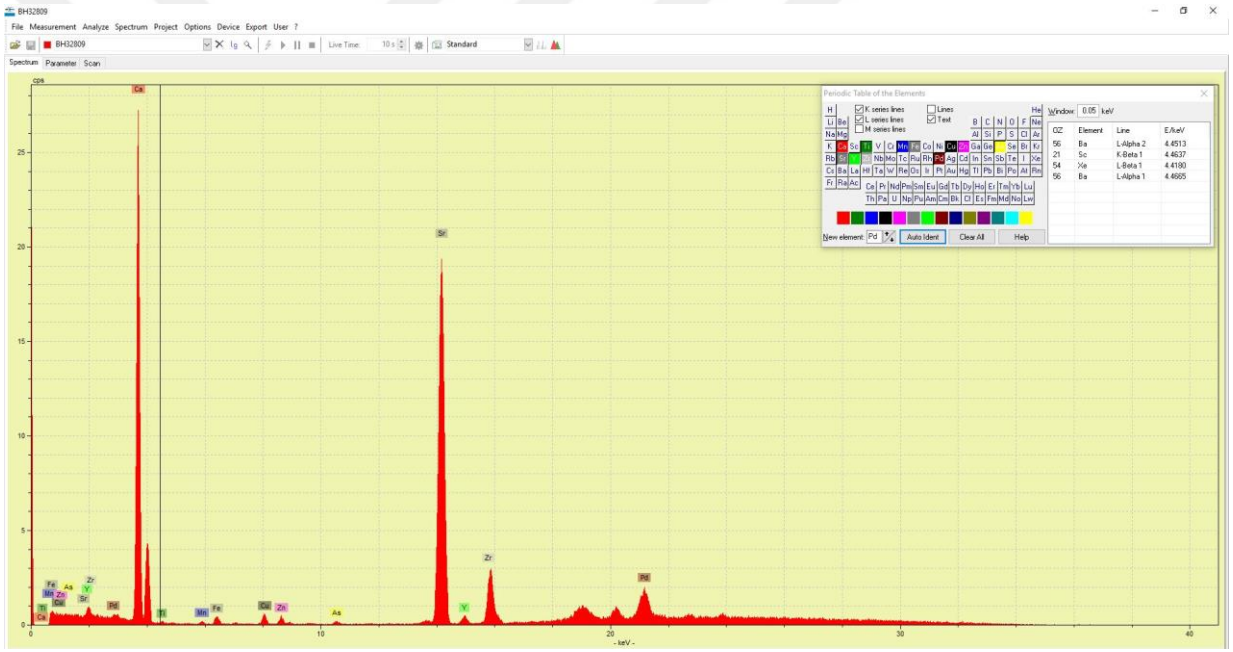

ARTAX - ELEMENT ANALYSIS

Listed at 11/8/2016 10:36:02 AM

Serial number:
Meas.date: 8/8/2016 3:00:35 PM
Live time: 181 s
Dead time: 0.0 %
Current: 40 µA
Filter: Ti/Al/Cu
Atmosphere: Air

Spectrum: BH32809
Method: gonca_Cu alloys (Bayes)
Count rate: 912 cps
Voltage: 40 kV
Anode:
Optic:

Element	Line	Sigma/	Net area	Backgr.
Ca	K12	0.00	29245	564
Ti	K12	0.00	100	256
Mn	K12	0.00	193	144
Fe	K12	0.00	575	144
Cu	K12	0.00	726	184
Zn	K12	0.00	460	195
As	K12	0.00	214	164
Sr	K12	0.00	39005	442
Y	K12	0.00	697	344
Zr	K12	0.00	84	400
Pd	K12	0.00	4854	2264
Pd	L1	0.00	258	889

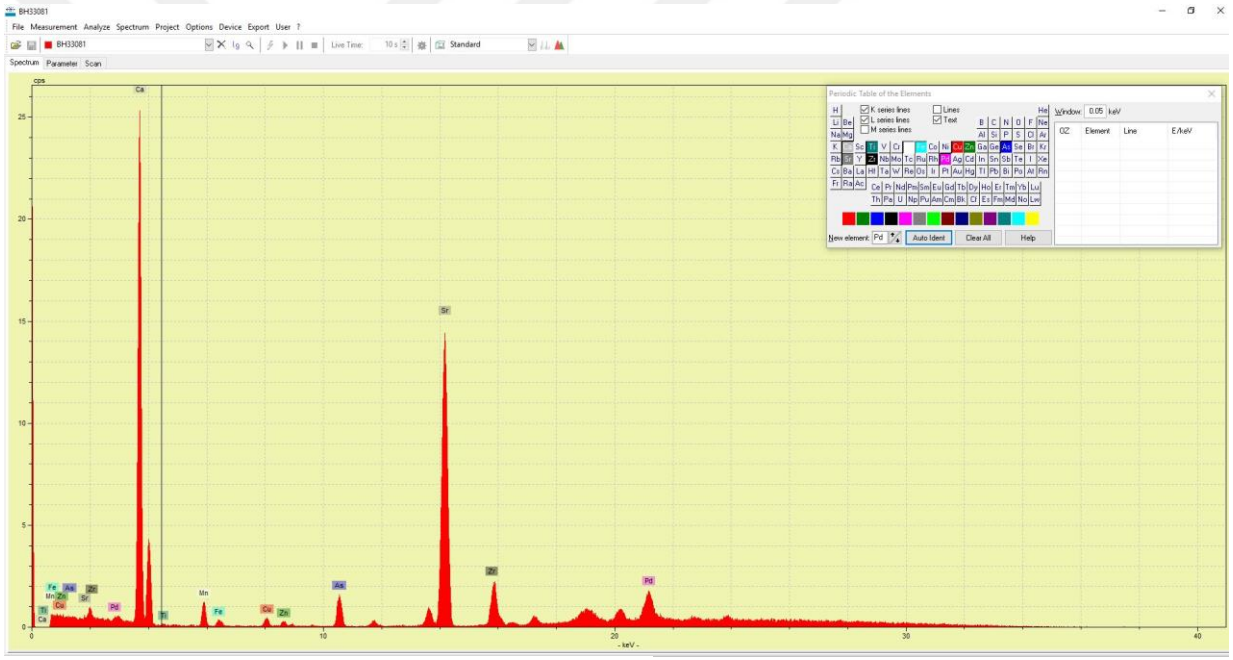

ARTAX - ELEMENT ANALYSIS

Listed at 11/8/2016 10:37:13 AM

Serial number:
Meas.date: 8/8/2016 3:13:53 PM
Live time: 181 s
Dead time: 0.0 %
Current: 40 µA
Filter: Ti/Al/Cu
Atmosphere: Air

Spectrum: BH33081
Method: gonca_Cu alloys (Bayes)
Count rate: 844 cps
Voltage: 40 kV
Anode:
Optic:

Element	Line	Sigma/	Net area	Backgr.
Ca	K12	0.00	28535	574
Ti	K12	0.00	77	242
Mn	K12	0.00	1672	122
Fe	K12	0.00	296	150
Cu	K12	0.00	624	173
Zn	K12	0.00	320	189
As	K12	0.00	2452	165
Sr	K12	0.00	29711	419
Zr	K12	0.00	717	450
Pd	K12	0.00	4341	2251
Pd	L1	0.00	238	791

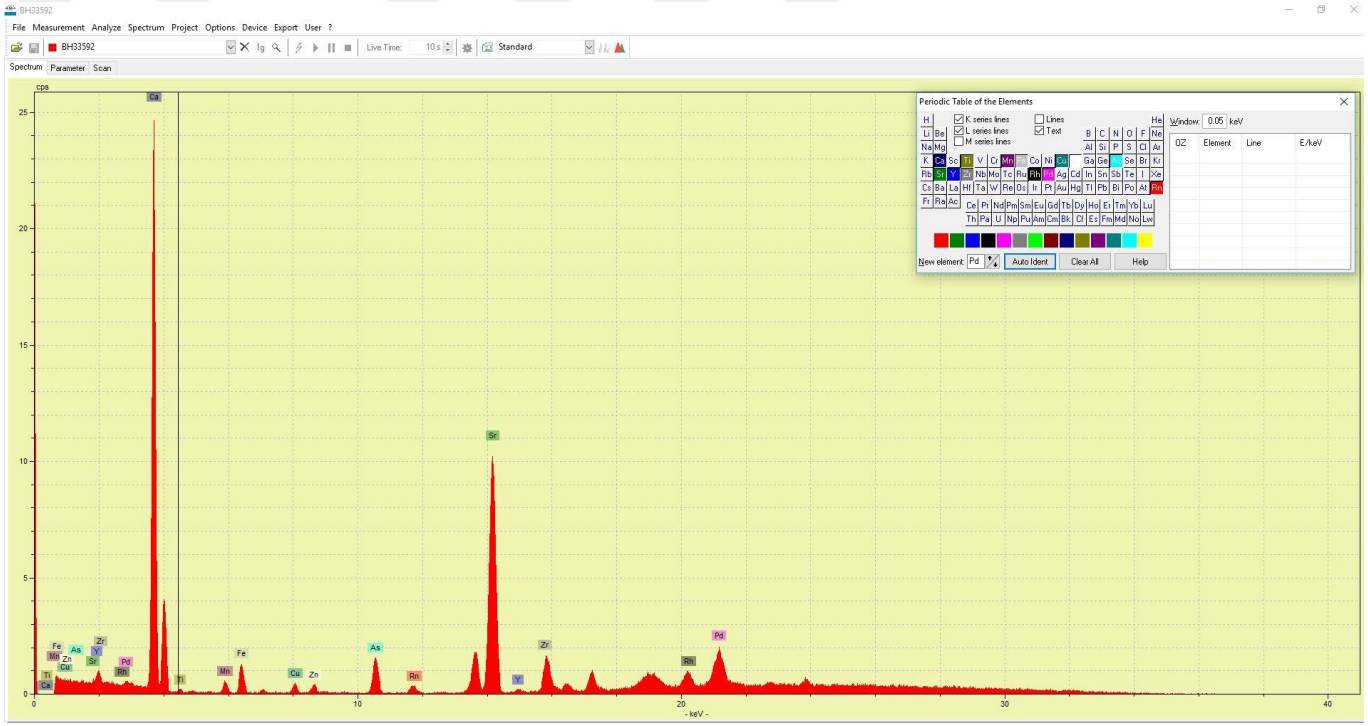

ARTAX - ELEMENT ANALYSIS

Listed at 11/8/2016 10:40:13 AM

Serial number:
Meas.date: 8/8/2016 3:09:48 PM
Live time: 180 s
Dead time: 0.0 %
Current: 40 µA
Filter: Ti/Al/Cu
Atmosphere: Air

Spectrum: BH33592
Method: gonca_Cu alloys (Bayes)
Count rate: 839 cps
Voltage: 40 kV
Anode:
Optic:

Element	Line	Sigma/	Net area	Backgr.
Ca	K12	0.00	26842	613
Ti	K12	0.00	147	226
Mn	K12	0.00	747	148
Fe	K12	0.00	1568	143
Cu	K12	0.00	555	194
Zn	K12	0.00	466	211
As	K12	0.00	2544	153
Sr	K12	0.00	23074	415
Y	K12	0.00	259	301
Zr	K12	0.00	463	492
Rh	K12	0.00	1372	2021
Rh	L1	0.00		1008
Pd	K12	0.00	4726	2298
Pd	L1	0.00	167	964

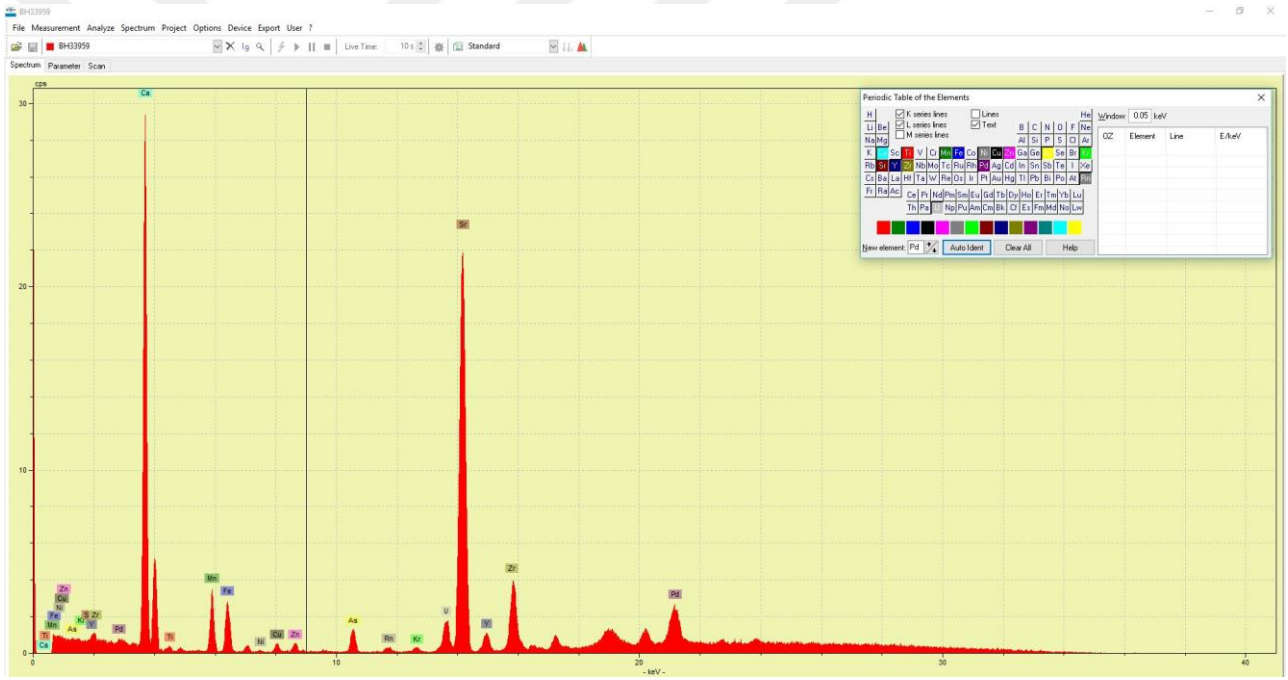

ARTAX - ELEMENT ANALYSIS

Listed at 11/8/2016 10:42:18 AM

Serial number:
Meas.date: 8/8/2016 1:13:02 PM
Live time: 189 s
Dead time: 0.0 %
Current: 40 µA
Filter: Ti/Al/Cu
Atmosphere: Air

Spectrum: BH33959
Method: gonca_Cu alloys (Bayes)
Count rate: 1264 cps
Voltage: 40 kV
Anode:
Optic:

Element	Line	Sigma/	Net area	Backgr.
Ca	K12	0.00	33989	1033
Ti	K12	0.00	287	382
Mn	K12	0.00	4314	281
Fe	K12	0.00	3447	273
Ni	K12	0.00	118	256
Cu	K12	0.00	689	269
Zn	K12	0.00	715	318
As	K12	0.00	2079	287
Sr	K12	0.00	46136	731
Y	K12	0.00	2071	596
Zr	K12	0.00	418	895
Pd	K12	0.00	6738	3573
Pd	L1	0.00	315	1355
U	L1	0.00	3525	601
U	M1	0.00	16	1234

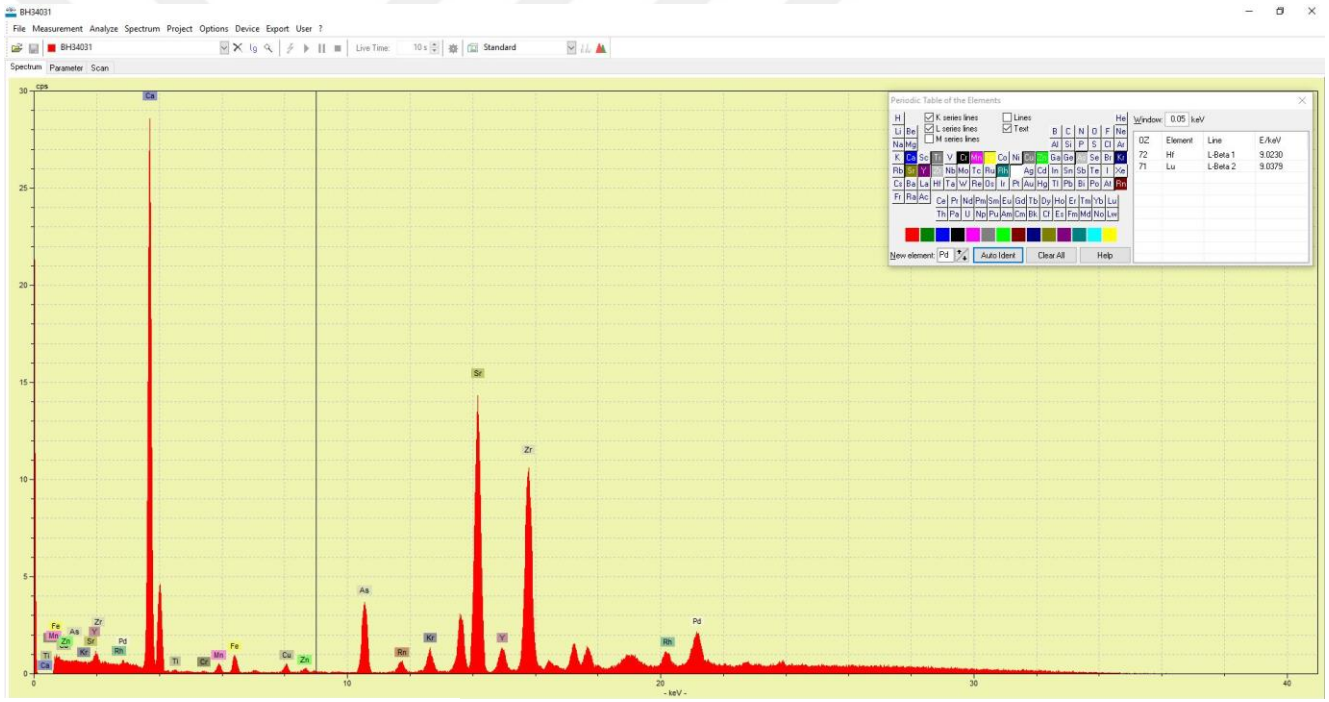

ARTAX - ELEMENT ANALYSIS

Listed at 11/8/2016 10:44:13 AM

Serial number:
Meas.date: 8/8/2016 2:43:48 PM
Live time: 181 s
Dead time: 0.0 %
Current: 40 µA
Filter: Ti/Al/Cu
Atmosphere: Air

Spectrum: BH34031
Method: gonca_Cu alloys (Bayes)
Count rate: 1169 cps
Voltage: 40 kV
Anode:
Optic:

Element	Line	Sigma/	Net area	Backgr.
Ca	K12	0.00	31262	683
Ti	K12	0.00	112	280
Cr	K12	0.00	74	202
Mn	K12	0.00	546	204
Fe	K12	0.00	1130	198
Cu	K12	0.00	579	245
Zn	K12	0.00	286	257
As	K12	0.00	6374	224
Sr	K12	0.00	31023	625
Y	K12	0.00	2677	669
Zr	K12	0.00	17489	1086
Rh	K12	0.00	1734	2250
Rh	L1	0.00		1183
Pd	K12	0.00	5308	2662
Pd	L1	0.00	240	1124

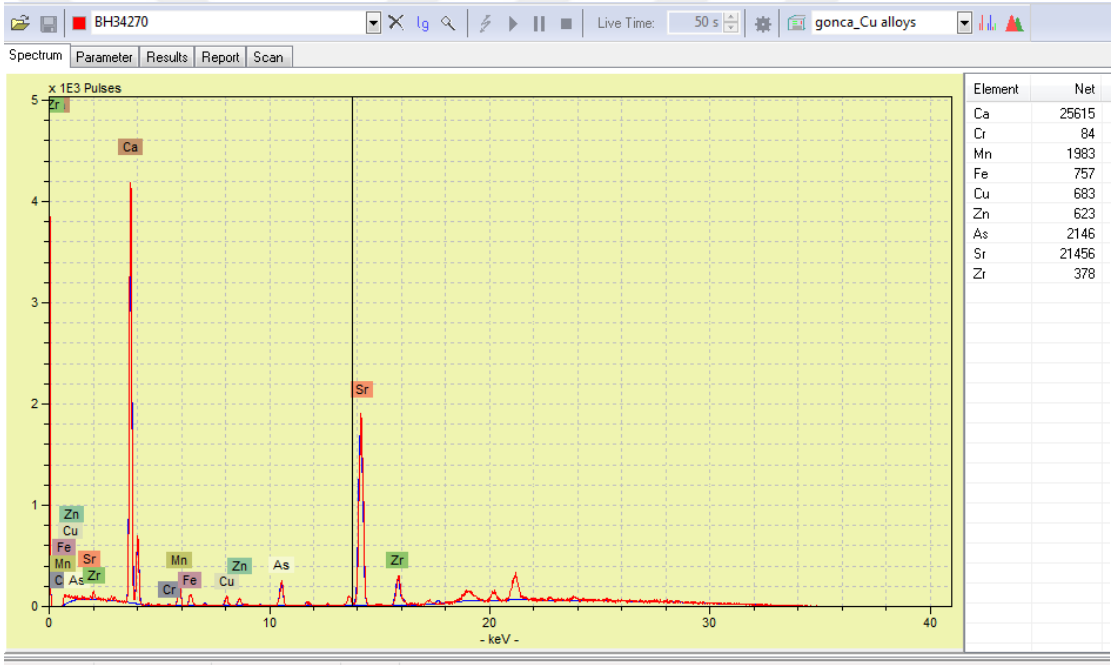

ARTAX - ELEMENT ANALYSIS

Listed at 11/8/2016 10:45:12 AM

Serial number:
Meas.date: 8/8/2016 2:56:22 PM
Live time: 182 s
Dead time: 0.0 %
Current: 40 µA
Filter: Ti/Al/Cu
Atmosphere: Air

Spectrum: BH34270
Method: gonca_Cu alloys (Bayes)
Count rate: 764 cps
Voltage: 40 kV
Anode:
Optic:

Element	Line	Sigma/	Net area	Backgr.
Ca	K12	0.00	25615	535
Cr	K12	0.00	84	137
Mn	K12	0.00	1983	135
Fe	K12	0.00	757	143
Cu	K12	0.00	683	146
Zn	K12	0.00	623	168
As	K12	0.00	2146	133
Sr	K12	0.00	21456	340
Zr	K12	0.00	378	379

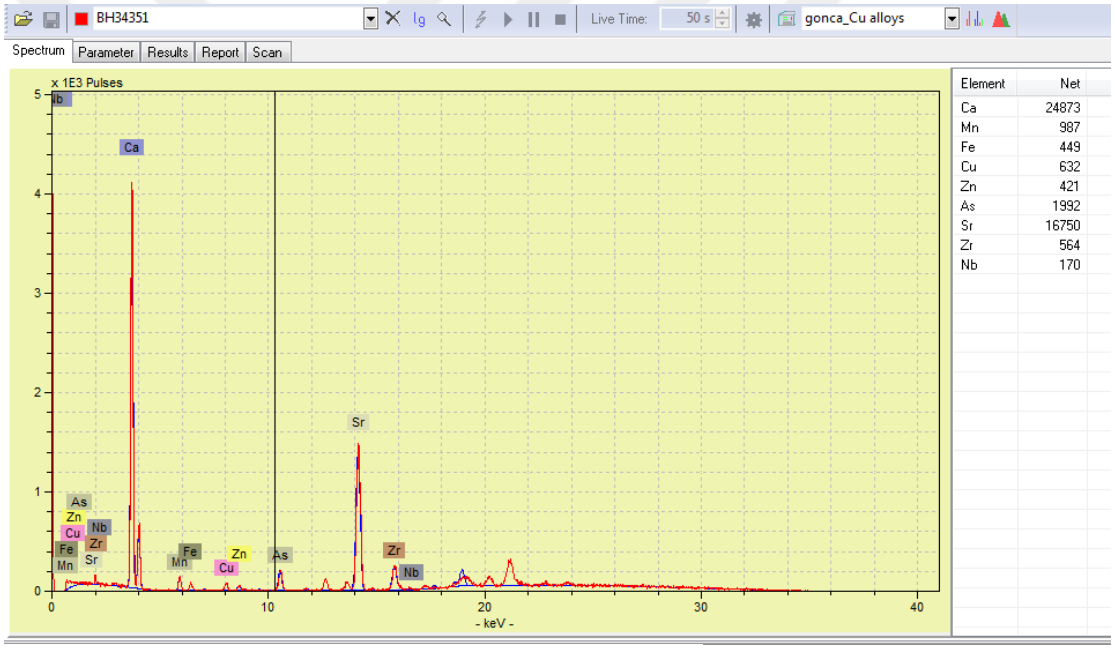

ARTAX - ELEMENT ANALYSIS

Listed at 11/8/2016 10:46:14 AM

Serial number:
Meas.date: 8/8/2016 2:13:07 PM
Live time: 180 s
Dead time: 0.0 %
Current: 40 µA
Filter: Ti/Al/Cu
Atmosphere: Air

Spectrum: BH34351
Method: gonca_Cu alloys (Bayes)
Count rate: 730 cps
Voltage: 40 kV
Anode:
Optic:

Element	Line	Sigma/	Net area	Backgr.
Ca	K12	0.00	24873	553
Mn	K12	0.00	987	131
Fe	K12	0.00	449	123
Cu	K12	0.00	632	121
Zn	K12	0.00	421	141
As	K12	0.00	1992	150
Sr	K12	0.00	16750	319
Zr	K12	0.00	564	433
Nb	K12	0.00	170	469

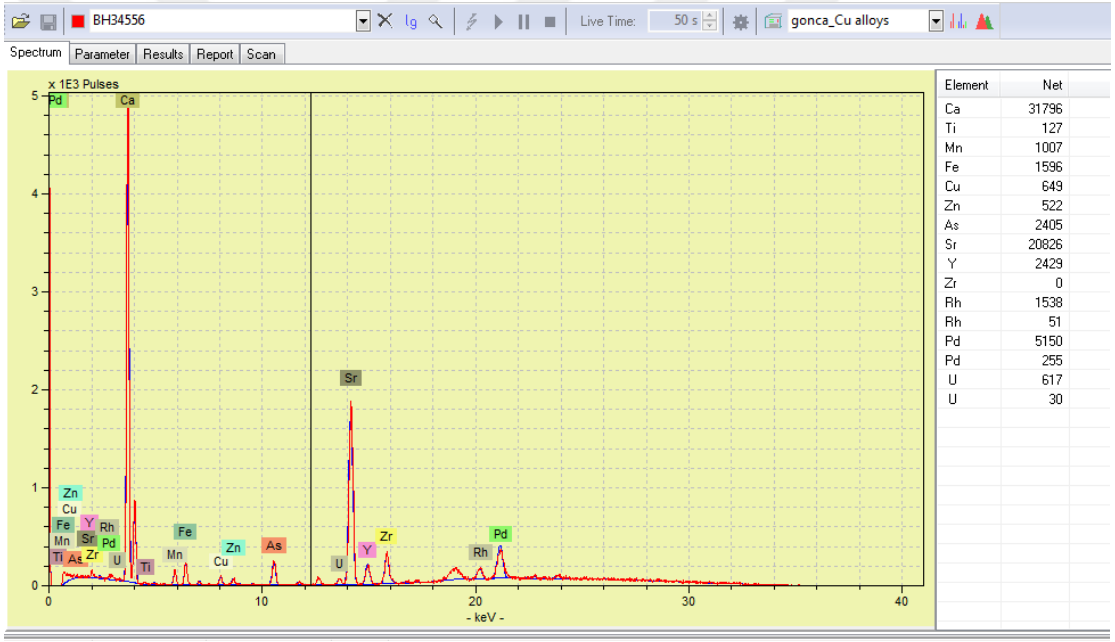

ARTAX - ELEMENT ANALYSIS

Listed at 11/8/2016 10:47:06 AM

Serial number:
Meas.date: 8/8/2016 2:08:22 PM
Live time: 181 s
Dead time: 0.0 %
Current: 40 µA
Filter: Ti/Al/Cu
Atmosphere: Air

Spectrum: BH34556
Method: gonca_Cu alloys (Bayes)
Count rate: 894 cps
Voltage: 40 kV
Anode:
Optic:

Element	Line	Sigma/	Net area	Backgr.
Ca	K12	0.00	31796	637
Ti	K12	0.00	127	239
Mn	K12	0.00	1007	204
Fe	K12	0.00	1596	200
Cu	K12	0.00	649	181
Zn	K12	0.00	522	222
As	K12	0.00	2405	162
Sr	K12	0.00	20826	339
Y	K12	0.00	2429	365
Zr	K12	0.00		537
Rh	K12	0.00	1538	2244
Rh	L1	0.00	51	920
Pd	K12	0.00	5150	2625
Pd	L1	0.00	255	889
U	L1	0.00	617	307
U	M1	0.00	30	784

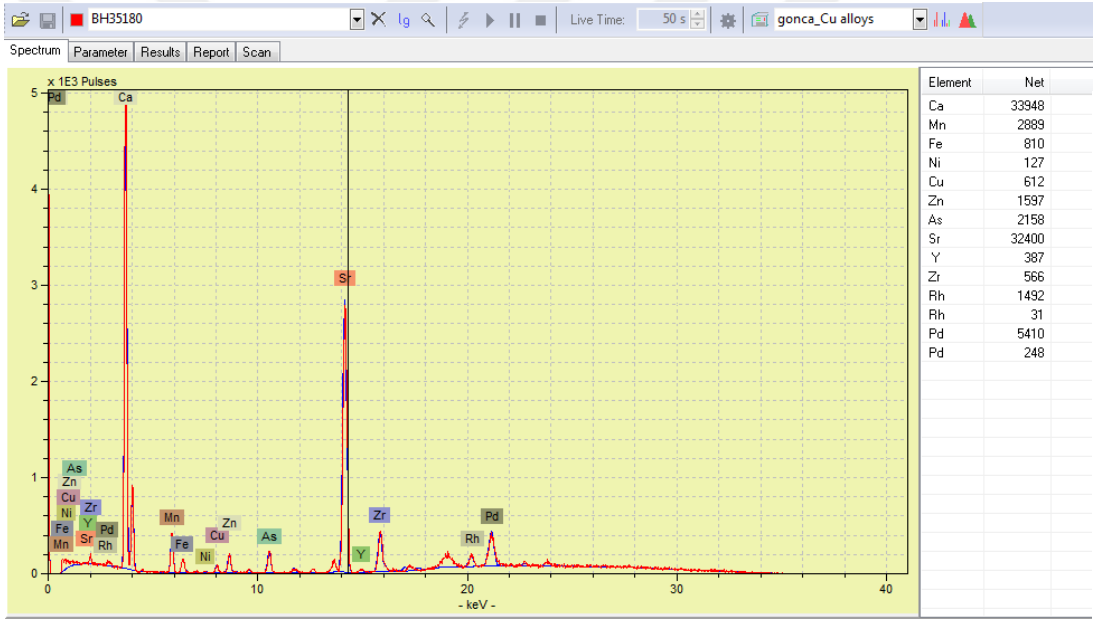

Element	Net
Ca	33948
Mn	2889
Fe	810
Ni	127
Cu	612
Zn	1597
As	2158
Sr	32400
Y	387
Zr	566
Rh	1492
Rh	31
Pd	5410
Pd	248

ARTAX - ELEMENT ANALYSIS

Listed at 11/8/2016 10:48:07 AM

Serial number:
Meas.date: 8/8/2016 12:42:46 PM
Live time: 180 s
Dead time: 0.0 %
Current: 40 µA
Filter: Ti/Al/Cu
Atmosphere: Air

Spectrum: BH35180
Method: gonca_Cu alloys (Bayes)
Count rate: 1043 cps
Voltage: 40 kV
Anode:
Optic:

Element	Line	Sigma/	Net area	Backgr.
Ca	K12	0.00	33948	820
Mn	K12	0.00	2889	224
Fe	K12	0.00	810	227
Ni	K12	0.00	127	184
Cu	K12	0.00	612	215
Zn	K12	0.00	1597	245
As	K12	0.00	2158	200
Sr	K12	0.00	32400	446
Y	K12	0.00	387	389
Zr	K12	0.00	566	588
Rh	K12	0.00	1492	2382
Rh	L1	0.00	31	1213
Pd	K12	0.00	5410	2848
Pd	L1	0.00	248	1145

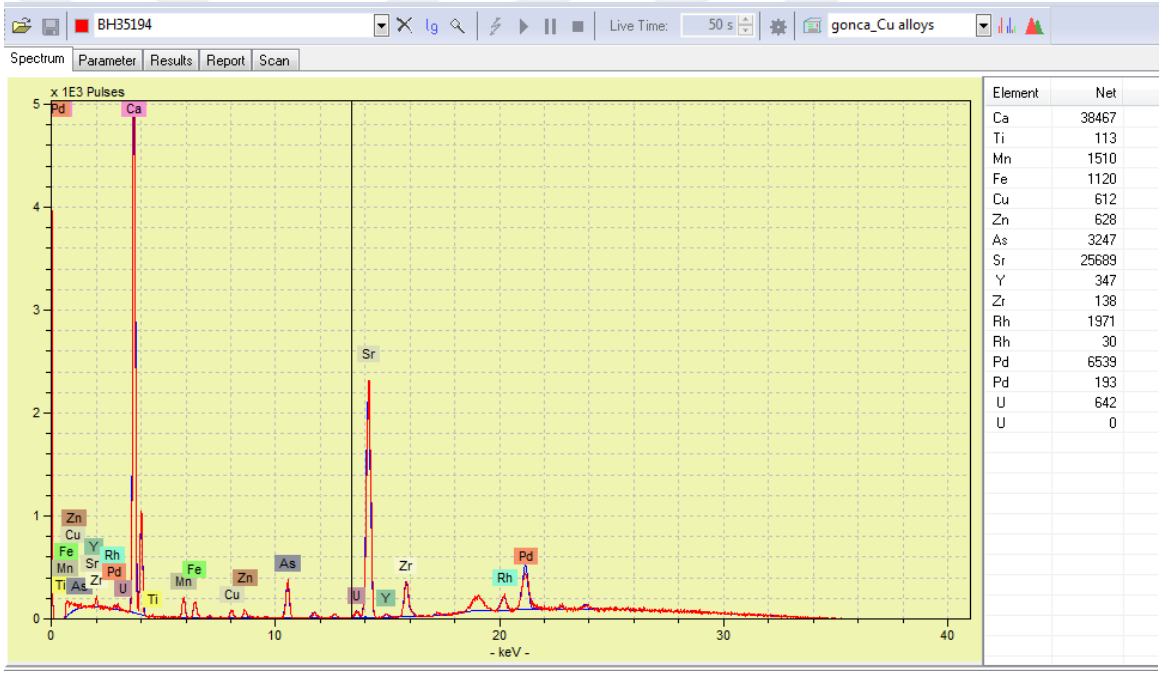

Element	Net
Ca	38467
Ti	113
Mn	1510
Fe	1120
Cu	612
Zn	628
As	3247
Sr	25689
Y	347
Zr	138
Rh	1971
Rh	30
Pd	6539
Pd	193
U	642
U	0

ARTAX - ELEMENT ANALYSIS

Listed at 11/8/2016 10:49:01 AM

Serial number:
Meas.date: 8/8/2016 12:38:37 PM
Live time: 181 s
Dead time: 0.0 %
Current: 40 µA
Filter: Ti/Al/Cu
Atmosphere: Air

Spectrum: BH35194
Method: gonca_Cu alloys (Bayes)
Count rate: 1079 cps
Voltage: 40 kV
Anode:
Optic:

Element	Line	Sigma/	Net area	Backgr.
Ca	K12	0.00	38467	892
Ti	K12	0.00	113	282
Mn	K12	0.00	1510	227
Fe	K12	0.00	1120	216
Cu	K12	0.00	612	208
Zn	K12	0.00	628	242
As	K12	0.00	3247	218
Sr	K12	0.00	25689	425
Y	K12	0.00	347	395
Zr	K12	0.00	138	558
Rh	K12	0.00	1971	2656
Rh	L1	0.00	30	1391
Pd	K12	0.00	6539	3216
Pd	L1	0.00	193	1329
U	L1	0.00	642	344
U	M1	0.00		1137

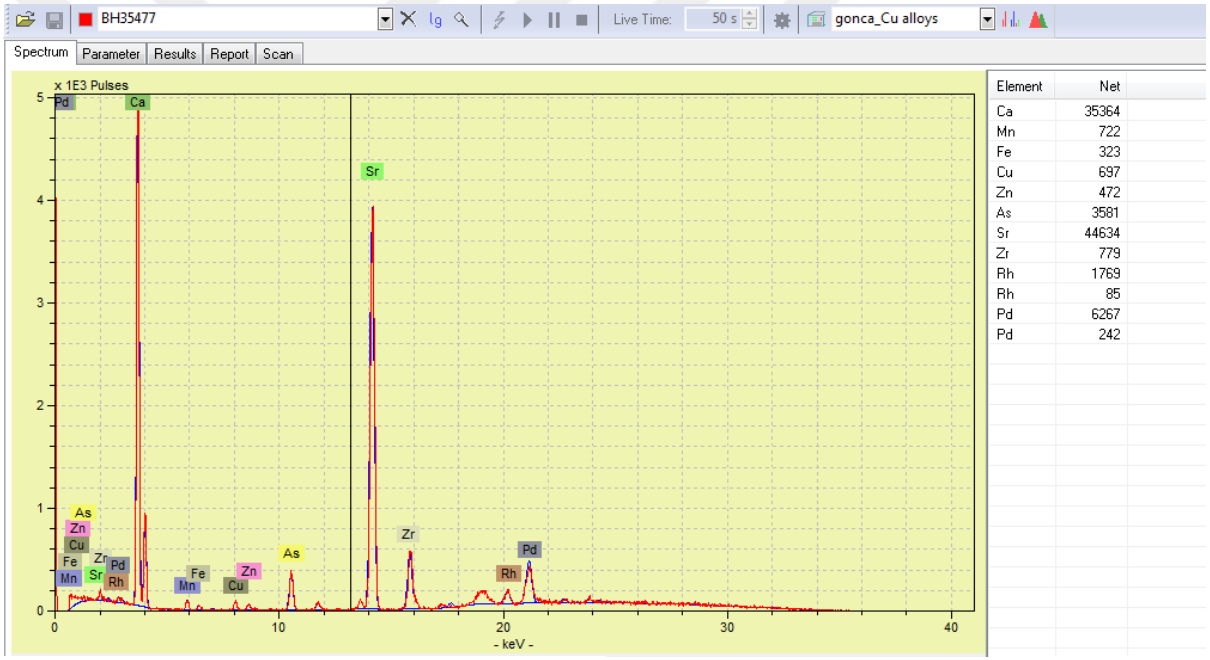

ARTAX - ELEMENT ANALYSIS

Listed at 11/8/2016 10:49:45 AM

Serial number:
Meas.date: 8/8/2016 12:21:38 PM
Live time: 181 s
Dead time: 0.0 %
Current: 40 µA
Filter: Ti/Al/Cu
Atmosphere: Air

Spectrum: BH35477
Method: gonca_Cu alloys (Bayes)
Count rate: 1122 cps
Voltage: 40 kV
Anode:
Optic:

Element	Line	Sigma/	Net area	Backgr.
Ca	K12	0.00	35364	828
Mn	K12	0.00	722	183
Fe	K12	0.00	323	156
Cu	K12	0.00	697	193
Zn	K12	0.00	472	205
As	K12	0.00	3581	249
Sr	K12	0.00	44634	537
Zr	K12	0.00	779	545
Rh	K12	0.00	1769	2269
Rh	L1	0.00	85	1183
Pd	K12	0.00	6267	2574
Pd	L1	0.00	242	1132

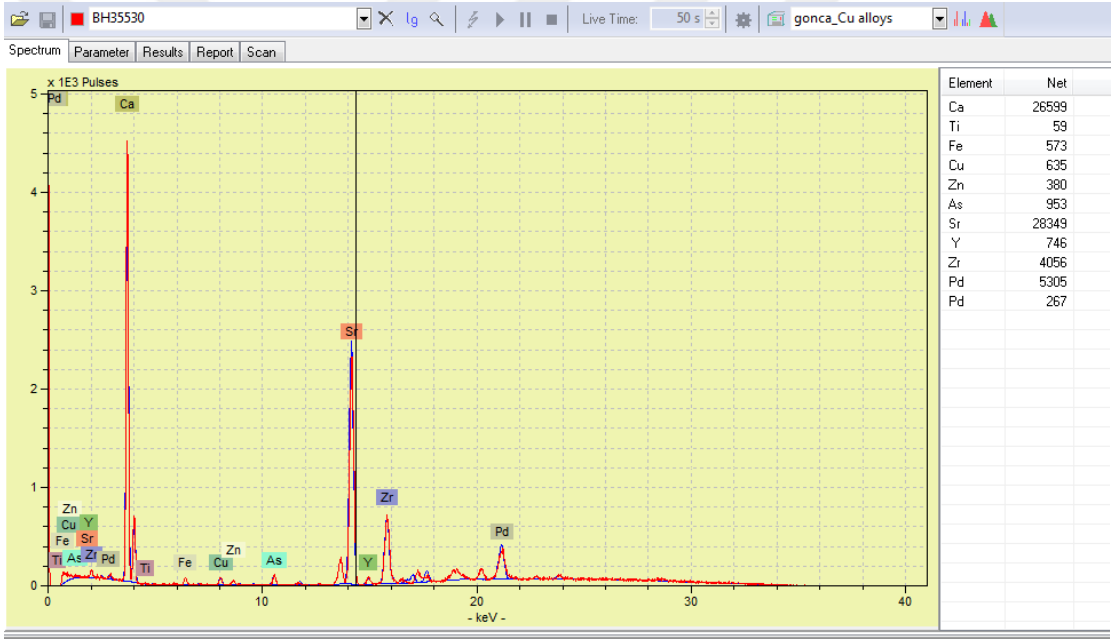

ARTAX - ELEMENT ANALYSIS

Listed at 11/8/2016 10:50:38 AM

Serial number:
Meas.date: 8/8/2016 2:04:12 PM
Live time: 181 s
Dead time: 0.0 %
Current: 40 µA
Filter: Ti/Al/Cu
Atmosphere: Air

Spectrum: BH35530
Method: gonca_Cu alloys (Bayes)
Count rate: 907 cps
Voltage: 40 kV
Anode:
Optic:

Element	Line	Sigma/	Net area	Backgr.
Ca	K12	0.00	26599	712
Ti	K12	0.00	59	256
Fe	K12	0.00	573	186
Cu	K12	0.00	635	172
Zn	K12	0.00	380	185
As	K12	0.00	953	146
Sr	K12	0.00	28349	450
Y	K12	0.00	746	364
Zr	K12	0.00	4056	650
Pd	K12	0.00	5305	2395
Pd	L1	0.00	267	958

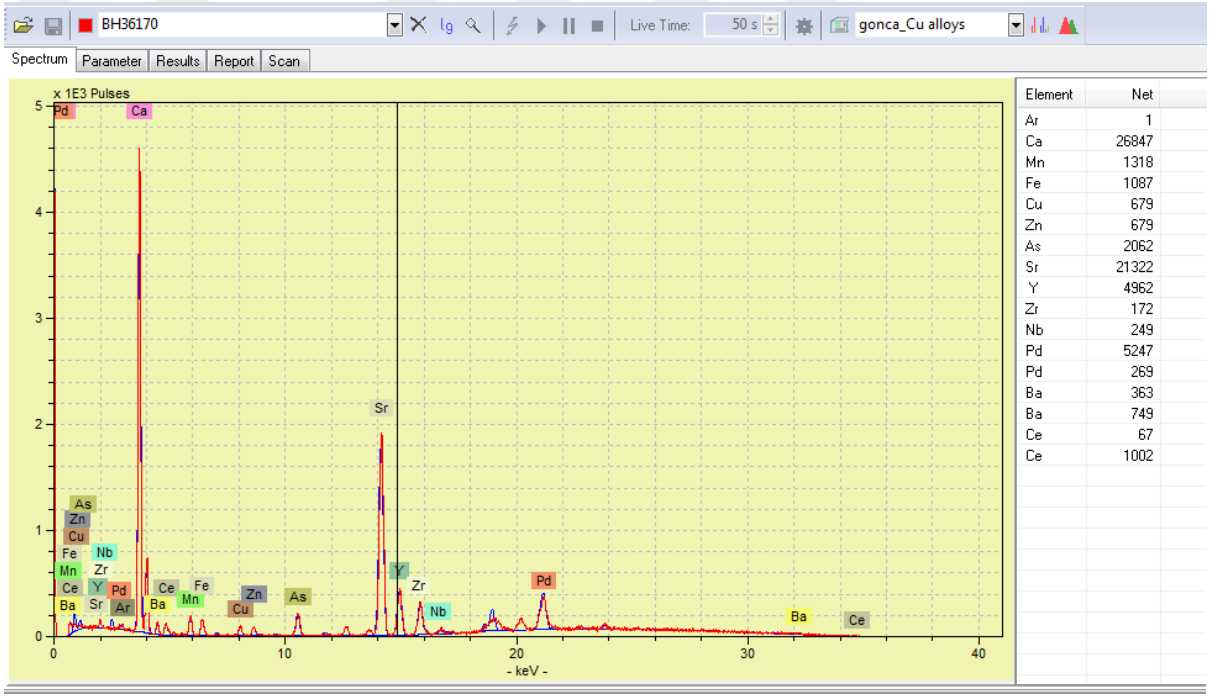

Element	Net
Ar	1
Ca	26847
Mn	1318
Fe	1087
Cu	679
Zn	679
As	2062
Sr	21322
Y	4962
Zr	172
Nb	249
Pd	5247
Pd	269
Ba	363
Ba	749
Ce	67
Ce	1002

ARTAX - ELEMENT ANALYSIS

Listed at 11/8/2016 10:51:32 AM

Serial number:
Meas.date: 8/8/2016 12:02:49 PM
Live time: 182 s
Dead time: 0.0 %
Current: 40 µA
Filter: Ti/Al/Cu
Atmosphere: Air

Spectrum: BH36170
Method: gonca_Cu alloys (Bayes)
Count rate: 878 cps
Voltage: 40 kV
Anode:
Optic:

Element	Line	Sigma/	Net area	Backgr.
Ar	K12	0.00	1	922
Ca	K12	0.00	26847	702
Mn	K12	0.00	1318	221
Fe	K12	0.00	1087	182
Cu	K12	0.00	679	217
Zn	K12	0.00	679	237
As	K12	0.00	2062	168
Sr	K12	0.00	21322	427
Y	K12	0.00	4962	359
Zr	K12	0.00	172	464
Nb	K12	0.00	249	691
Pd	K12	0.00	5247	2373
Pd	L1	0.00	269	953
Ba	K12	0.00	363	1154
Ba	L1	0.00	749	280
Ce	L1	0.00	67	265
Ce	M1	0.00	1002	527

The Element Analysis sheet for bead BH33086 could not be obtained at the time of this thesis.. Here we present the spectra for this bead.

The Element Analysis sheet for bead BH33660 could not be obtained at the time of this thesis.. Here we present the spectra for this bead.

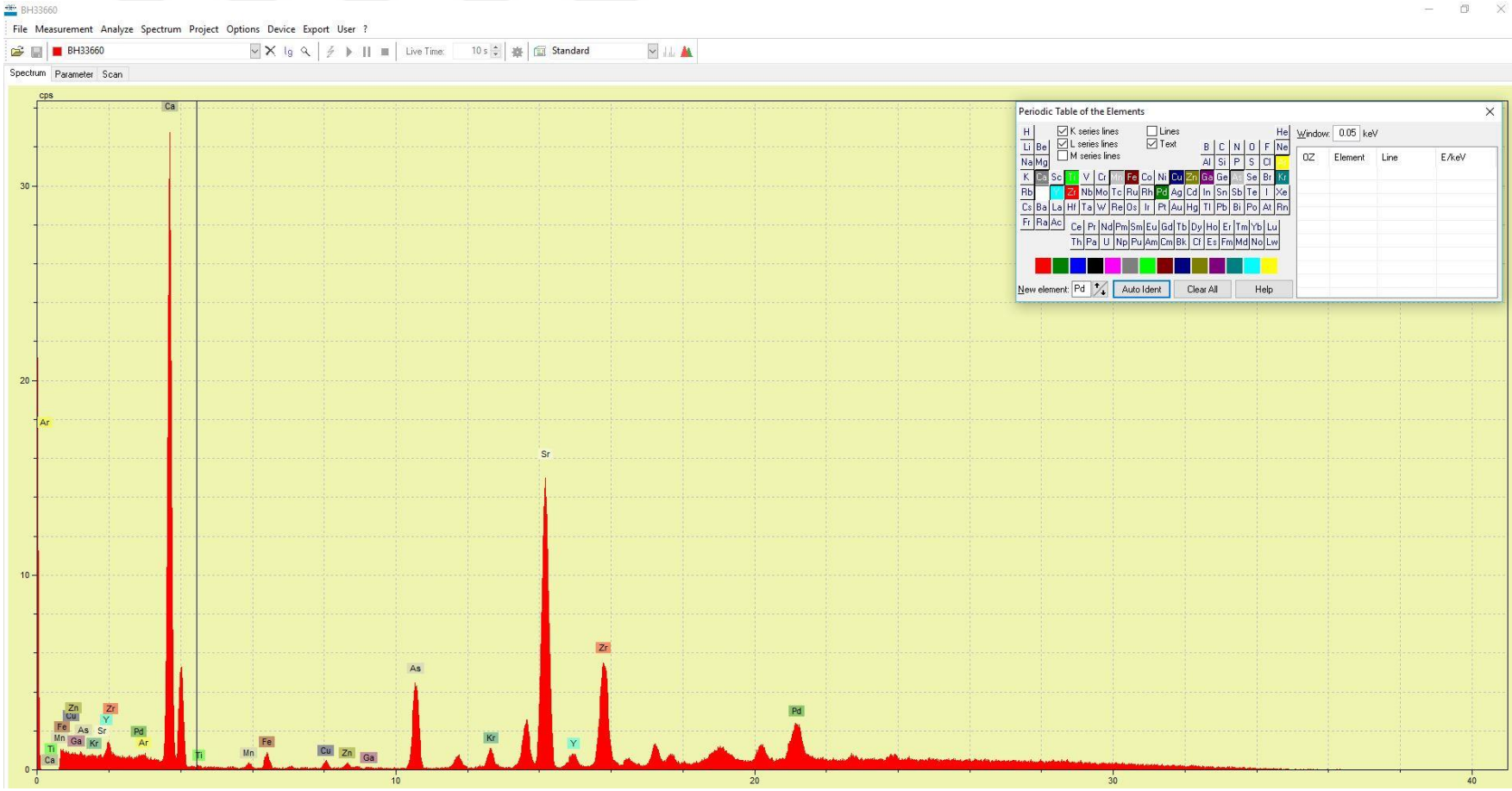

The Element Analysis sheet for bead BH33985 could not be obtained at the time of this thesis. Here we present the spectra for this bead.

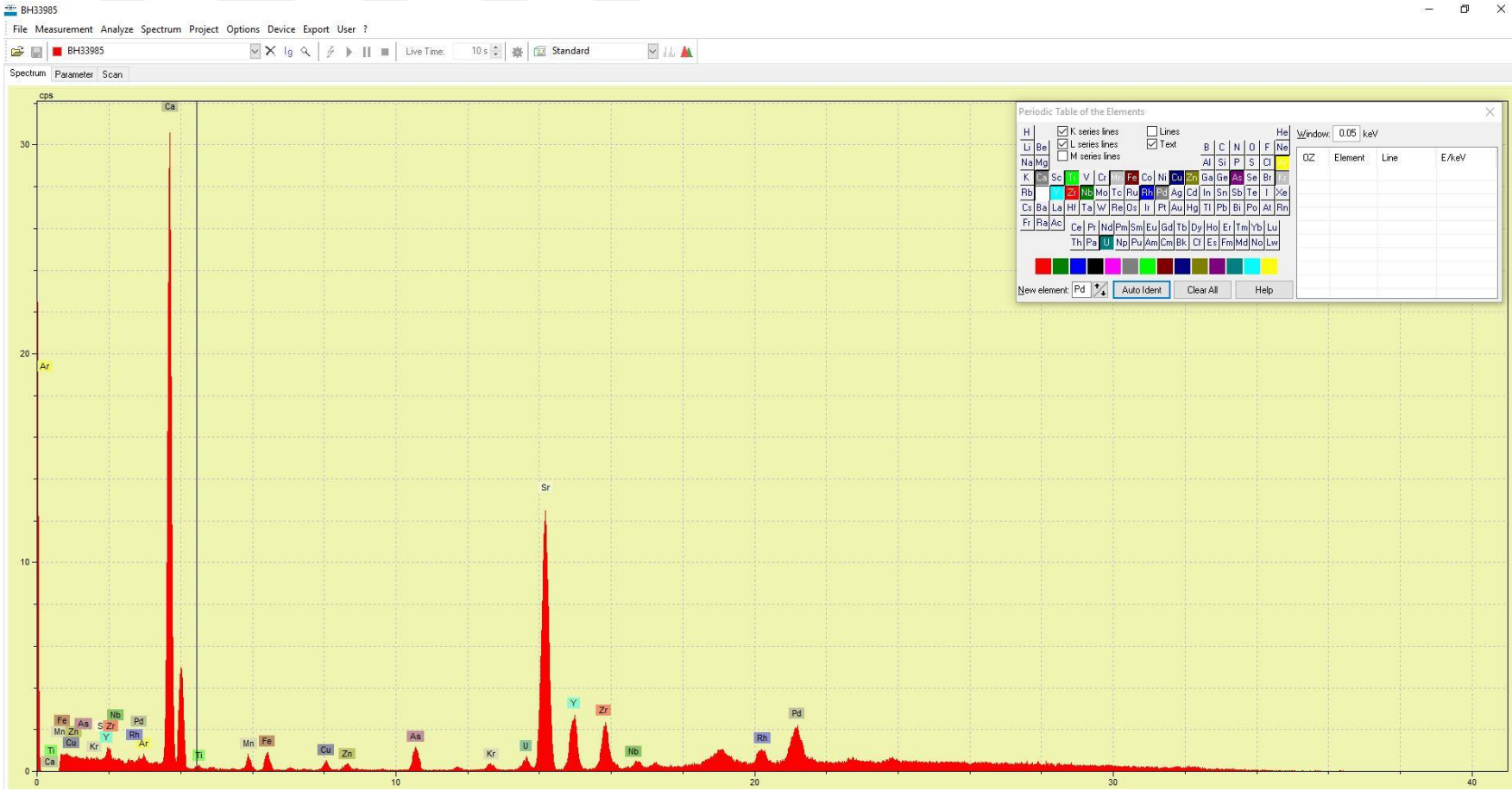

The Element Analysis sheet for bead BH7075 could not be obtained at the time of this thesis. Here we present the spectra for this bead.